

Microbial alteration of geochemical proxies in fine-grained carbonate sediments during early diagenesis

Within the framework of the DFG research unit 1644 "CHARON"

Dissertation

for the award of the degree

"Doctor rerum naturalium" (Dr.rer.nat.)

of the Georg-August University Göttingen

within the doctoral program "Geoscience"

of the Georg-August University School of Science (GAUSS)

submitted by

Dario Lambert Peter Fußmann

from Trier

Göttingen, 2021

Thesis Committee

Prof. Dr. Gernot Arp

Geoscience Center/Geobiology/Georg-August University Göttingen

Prof. Dr. Andreas Pack

Geoscience Center/Geochemistry and Isotope Geology/Georg-August University Göttingen

Members of the Examination Board

Reviewer: Prof. Dr. Gernot Arp

Geoscience Center/Geobiology/Georg-August University Göttingen

Second Reviewer: Prof. Dr. Andreas Pack

Geoscience Center/Geochemistry and Isotope Geology/Georg-August University Göttingen

Further members of the Examination Board

Prof. Dr. Volker Thiel

Geoscience Center/Geobiology/Georg-August University Göttingen

Prof. Dr. Thomas Müller

Geoscience Center/Mineralogy/Georg-August University Göttingen

Prof. Dr. Rolf Daniel

Dept. of Genomic and Applied Microbiology and Göttingen Genomics Lab./Georg-August University Göttingen

Dr. Andreas Reimer

Geoscience Center/Geobiology/Georg-August University Göttingen

Date of the oral examination: 05/17/2021

Contents

Acknowledgements	VIII
Preface	IX
Abstract	X
Kurzfassung	XII
1. Introduction	14
1.1 CaCO ₃ formation in the marine carbonate system, carbon cycling and -alteration	14
1.2 Environmental records in common carbonate minerals.....	17
1.3 Major diagenetic zones and their potential impacts on geochemical proxy records	18
1.4 Impact of microorganisms on CaCO ₃ precipitation and -alteration	20
1.5 Comparative pore water studies as biogeochemical and diagenetic tracers	21
1.6 Thesis objectives and study approaches	21
References.....	23
2. Authigenic formation of Ca-Mg carbonates in the shallow alkaline Lake Neusiedl, Austria	27
2.1 Introduction.....	28
2.2 Study Area	29
2.3 Material and Methods.....	31
2.3.1 Sampling and field measurements.....	31
2.3.2 Petrographic, mineralogical, and geochemical analyses.....	32
2.3.3 Pore water analysis	33
2.3.4 Bacterial 16S rRNA gene community profiling	33
2.4 Results	34
2.4.1 Sediment petrography and mineralogy	34
2.4.2 Pore water chemistry	41
2.4.3 Bacterial community composition	43
2.5 Discussion	46
2.5.1 Pore water gradients and their effect on Ca-Mg carbonate supersaturation	46
2.5.2 Microbial activity and carbonate saturation	47
2.5.3 Time and depth of carbonate formation.....	49
2.5.4 Potential pathways of authigenic Ca-Mg carbonate formation.....	50
2.6 Conclusions.....	51
Data availability	51
Acknowledgements.....	52
Financial support	52
References.....	53

3. Bacterial succession along a pore water gradient at Lake Neusiedl in Austria.....	60
3.1 Background and Summary	61
3.2 Methods	65
3.2.1 Sediment sampling at Lake Neusiedl, Austria.	65
3.2.2 DNA extraction and amplification of bacterial 16S rRNA genes.	65
3.2.3 Bioinformatic processing of 16S rRNA gene amplicons.	66
3.2.4 Bacterial community analysis.....	66
3.2.5 Water column and pore water analysis	67
Data records	67
Technical Validation	68
Acknowledgements.....	68
References.....	69
4. Tracing early diagenesis: Pore water gradients and bacterial communities within Holocene carbonate sediments in the lagoon of Aldabra (Seychelles)	73
4.1 Introduction.....	74
4.2 Study area and site description.....	75
4.3 Materials and Methods	78
4.3.1 Sampling and field measurements.....	78
4.3.2 Petrographic, mineralogical, and geochemical analyses.....	78
4.3.3 Pore water analysis	79
4.3.4 Bacterial community profiling	80
4.4 Results	81
4.4.1 Petrography and microfacies of sediments.....	81
4.4.2 Geochemistry of sediments.....	88
4.4.3 Pore water chemistry	92
4.4.4 Bacterial community composition of sediment cores.....	96
4.5 Discussion	98
4.5.1 Carbonate sediments within the lagoon of Aldabra	98
4.5.2 Physicochemical pore water gradients and microbial effects as indicators of early diagenesis	99
4.5.3 Diagenetic signatures within Holocene lagoon sediments of Aldabra.....	100
4.6 Conclusions.....	101
4.7 Acknowledgements	102
4.8 References.....	103
5. Decoupling of pore water chemistry, bacterial community profiles, and carbonate mud diagenesis in a land-locked pool on Aldabra (Seychelles, Indian Ocean)	108

5.1 Introduction.....	109
5.2 Study area.....	110
5.3 Material and Methods.....	112
5.3.1 Sampling and field measurements.....	112
5.3.2 Petrographic, mineralogical and geochemical analyses.....	112
5.3.3 Pore water analysis	113
5.3.4 Bacterial community profiling	114
5.4 Results	116
5.4.1 Petrography and geochemistry of sediments and organics.....	116
5.4.2 Pore water chemistry	124
5.4.3 Bacterial community composition	126
5.5 Discussion	129
5.5.1 Time and environment of carbonate deposition and diagenesis.....	129
5.5.2 Pore water gradients and their microbial and diagenetic implications	130
5.5.3 Bacterial abundance and its (partial) decoupling from current processes	134
5.6 Conclusions.....	135
5.7 Acknowledgements	135
References.....	136
6. Fine-grained carbonates exposed to changing pore water gradients.....	142
6.1 Boundary conditions of initial geochemical proxy values and their stability in modern, shallow marine carbonate sediments	142
6.2 Impacts of bacterial activity on sediment geochemistry	144
6.3 Bacterial gene data as additional diagenetic proxy	145
References.....	147
7. Summary, conclusions, and outlook.....	150
7.1 Summary and conclusions.....	150
7.2 Outlook.....	152
References.....	153
Appendices	154
Appendix A	154
Supplementary information for Chapters 2 and 3:	154
Appendix B	160
Supplementary information for Chapter 4:.....	160
Appendix C.....	166
Supplementary information for Chapter 5:.....	166
Curriculum Vitae	172

Acknowledgements

This thesis could not have been finished without the contribution and help of many people that I would like to credit here.

First of all, I would like to thank my supervisors and project leaders Gernot Arp and Andreas Reimer for giving me the opportunity to participate in this project. Thank you for your extraordinary guidance, insightful discussions, and for having my back at any time.

Furthermore, I would like to thank my second supervisor Andreas Pack for reviewing and evaluating this thesis.

Many thanks to Avril von Hoyningen-Huene, Dominik Schneider, and Rolf Daniel, from the department of genomics and applied microbiology for being extraordinary colleagues and project partners.

A huge thanks to all the members of the Geobiology working group. In particular, I would like to thank Manuel Reinhardt for being a very good colleague and having plenty of quality lunch breaks. Thank you Birgit Röhring, Wolfgang Dröse, and Axel Hackmann for your assistance during lab work.

Many thanks to my office members Yu Pei and Lin Qi Zheng, for creating a very thought- and respectful atmosphere in our shared working room.

I would also like to thank my thesis committee members Volker Thiel, Thomas Müller, Andreas Reimer, and Rolf Daniel for agreeing to evaluate this work.

I would like to express thanks to all the members of the DFG-research group CHARON, especially Chelsea Pederson for excellent project organization.

Much appreciated is Laura Ritterbach, my favorite person and “fellow sufferer”. Many thanks to my friends Nils Höche, Moritz Dandeck, Christian Hansen, Alexander Busch and the Fledermaus group for emotional support during everyday life. I would also like to thank the members of the Radsportclub Göttingen, especially Jonas Arlt and Tillmann Koch, for the offer to find productive distraction on the bike or track at almost any time.

Finally, I would like to thank my grandmother Marlene Schuster, my sister Linda and my parents Christa and Albert (Schuster-) Fußmann for unlimited support, faith, and motivation.

This thesis was financially supported by the DFG-Deutsche Forschungsgemeinschaft.

Preface

This is a cumulative thesis that includes four individual scientific studies in the form of published articles and manuscripts in preparation (Chapters 2-5). Furthermore, the thesis comprises an introduction (Chapter 1) and a synthesis, discussing the implications of the results for the (i) stability of initial geochemical proxy values in modern, shallow marine carbonate sediments, and (ii) the impacts of bacterial activity on sediment geochemistry (Chapter 6). A summary-, conclusion- and outlook- chapter (Chapter 7) finalizes the thesis.

The following published articles and manuscripts in preparation form the main part of this thesis (* = corresponding author):

Fussmann, D*, von Hoyningen-Huene, A. J. E., Reimer, A., Schneider, D., Babková, H., Peticzka, R., Maier, A., Arp, G., Daniel, R., and Meister, P.: Authigenic formation of Ca-Mg carbonates in the shallow alkaline lake Neusiedl, Austria, *Biogeosciences*, 17, <https://doi.org/10.5194/bg-17-2085-2020>, 2020 (Chapter 2).

Own contribution: investigation, analysis and curation of the hydro- and geochemical data, curation of the bacterial community data, and writing of the manuscript

von Hoyningen-Huene, A. J. E., Schneider, D., Fussmann, D., Reimer, A., Arp, G., and Daniel, R.*: Bacterial succession along a sediment porewater gradient at Lake Neusiedl in Austria, *Scientific data*, 6, 1-7, <https://doi.org/10.1038/s41597-019-0172-9>, 2019 (Chapter 3).

Own contribution: investigation, analysis and curation of the hydro- and geochemical data, and interpretation of the results

Fussmann D.*, von Hoyningen-Huene, A. J. E., Reimer, A., Schneider, D., Karius, V., Riechelmann, S., Liebetrau, V., Gentz, T., Daniel R., and Arp, G.: Tracing early diagenesis: Pore water gradients and bacterial communities within Holocene carbonate sediments in the lagoon of Aldabra (Seychelles), to be submitted to *The Depositional Record* (Chapter 4).

Own contribution: investigation, analysis and curation of the hydro- and geochemical data, curation of the bacterial community data, and writing of the manuscript

Fussmann D.*, von Hoyningen-Huene, A. J. E., Reimer, A., Schneider, D., Karius, V., Riechelmann, S., Pederson, C., Swart, P. K., Daniel R., and Arp, G.: Decoupling of pore water chemistry, bacterial community profiles, and carbonate mud diagenesis in a land-locked pool on Aldabra (Seychelles, Indian Ocean), submitted to *Geomicrobiology Journal* (Chapter 5).

Own contribution: investigation, analysis and curation of the hydro- and geochemical data, curation of the bacterial community data, and writing of the manuscript

Individual contributions were adapted to the overall style of this thesis.

Abstract

Fine-grained carbonate sediments play a crucial role in the global carbon cycle and are an exceptional record of past environmental conditions. Major paleoenvironmental constraints, derived from stable isotope and trace element records in these carbonate sediments, include ancient ocean temperatures, -seawater salinities and global elemental circulation patterns. Besides the inferences of past conditions at the Earth's surface, the understanding of these environmental archives enables the parameterization of models of future scenarios. Early diagenesis, involving carbonate phase dissolution and recrystallization, can potentially compromise these archives and, hence, distort the outcome of scientific models. For decades, the impact of changing physicochemical pore water gradients on contemporaneous carbonate phases during the earliest stages of diagenesis has been subject to controversial discussion. However, the role of specific bacterial communities within these processes is still not completely understood and bacterial genes are still not fully established as an additional proxy in descriptive diagenetic concepts. This thesis aims to track such bacterial effects on early diagenesis at shallow sediment depths. It shall provide a valuable feature for the evaluation of traditional isotope- and trace element signals in the fossil record. The primary objectives of this work include (i) assessment of the effects of changing physicochemical pore water gradients on contemporary fine-grained carbonate phases, (ii) the main impacts of the nearby environment on calcium carbonate alteration, (iii) the role of specific bacteria in the establishment of pore water gradients, and (iv) the potential use of multi-proxy studies, i. e. the combination of sediment geochemical-, pore water-, and bacterial 16S rRNA datasets, to trace complex diagenetic reaction paths.

The first and second case study focus on authigenic calcium-magnesium carbonate mud in the shallow alkaline Lake Neusiedl, located in eastern Austria. The cored sediments featured 20 cm of homogeneous greyish mud, containing 60 wt% carbonate, on top of dark laminated, semi-consolidated mud with 50 wt% carbonate and plant debris. The oxic water column with a pH of 9 changed to anoxic sediment pore water with a pH of 7.5. In addition, a decrease in sulfate, coinciding with an increase of total sulfur and ammonia between 0 and 15 cm core depth indicated an anaerobic heterotrophic decomposition of organic matter (including sulfate reduction) in the sediment. Saturation indices indicated supersaturation of disordered dolomite and calcite in the water column, compared to undersaturated conditions in the sediment. However, despite significant physicochemical changes in the pore water, the stoichiometric compositions and relative proportions of authigenic carbonate phases remained constant with increasing sediment depth. Hence, no evidence for calcium-magnesium carbonate formation or diagenetic alteration to more stable dolomite is apparent within the anoxic, sulfidic sediment of Lake Neusiedl. In contrast, the analytical data suggest authigenic carbonate formation in the supersaturated, well-mixed aerobic water column. These findings support an alternative concept to dolomite formation in anoxic sediments and potentially indicate low diagenetic reaction rates in such oxygen depleted deposits.

The third case study investigates shallow marine diagenetic environments on Aldabra, a remote coral atoll in the western Indian Ocean. The lagoon of Aldabra has previously been proposed to be a recent analogue of Jurassic lagoons that formed lithographic limestones. Thus, it should have represented a suitable setting to retrace diagenesis within fine-grained carbonate mud. Three different locations were sampled and analyzed within the 34 x 14.5 km sized lagoon. One each in the western- (WL), northern- (NL), and southern (SL) part. Overall, three different types of sediments and pore water environments were sampled by plexiglass push cores. The west lagoon cores consisted of intertidal, bioclastic carbonate sand with an oxygenated and porous pore space. Sediments in the north lagoon

occurred in supratidal karstic depressions and were characterized by anoxic shell detritus and a highly porous pore space. The cores from the south lagoon contained fine-grained, greyish carbonate mud with low porosity. Furthermore, the time scale for diagenetic processes was limited by a maximum radiocarbon age of 2357 ± 70 years. However, diagenetic alteration was solely noticeable in oxic sediments from the west lagoon and occurred in form of marine vadose, cryptocrystalline calcium carbonate cements. The exact reaction paths leading to this cement formation are not entirely clear. It may be either induced by abiogenic evaporation of pore waters during low tide, or biologically influenced by the presence of phototrophic and sulfate reducing bacteria. No significant traces of geochemical alteration were found in the sedimentary record of the north and south lagoon. Yet, pore water gradients indicate minor dissolution of metastable carbonate phases, possibly induced by acidifying sulfur oxidizing bacteria of the order Campylobacterales. The outcomes of this study suggest that diagenetic reactions are faster in oxygenated than in anoxic pore water environments. Moreover, sulfur oxidizing bacteria appear to play a fundamental role in the dissolution of metastable carbonates during early diagenesis.

The fourth case study includes a comparative pore water-sediment study of the Cinq Cases pool system, a shallow and saline water body in the southeast of Aldabra. The pools are characterized by occasional marine influx and short-time diagenetic reactions between sediment and pore water. However, the cored sediments provide radiocarbon ages of up to 3760 ± 30 years and indicated three environmental stages. An initial stage, characterized by least temporary anoxic conditions in a palustrine environment, with meteoric diagenesis (Unit III), a stage of slow marine flooding, including cyanobacteria and sponge blooms (Unit II), and a stage of lagoon flooding, with oxic conditions within the sediment (Unit I). These frequent changes in the depositional and diagenetic environments were retraced by three different proxies, which represent partially overlapping but different time scales. (i) Sediment data reflect ancient processes (ii) pore waters are influenced by recent processes, and (iii) bacterial communities mirror an overlay of ancient and recent processes. Hence, the decoupling of the different datasets used in this study exemplifies the feasibility and necessity of the application of such multiproxy studies in unstable depositional environments.

In summary, the results presented in this thesis indicate that only minor changes in the bulk geochemical record of fine-grained carbonate sediments can be expected during early diagenesis. If diagenetic changes occur in anoxic carbonate deposits, they are characterized by the dissolution of metastable phases, coupled to the activity of sulfur oxidizing bacteria of the order Campylobacterales. The final metabolic products of these organisms include sulfuric acid, which lowers the pH value and favors carbonate phase dissolution. However, diagenesis likely occurs faster in oxygenated pore water environments, but the exact reaction pathways and the involvement of microorganisms are still unclear. Future studies should focus on these oxic, cemented diagenetic zones. Furthermore, a precise evaluation and quantification of the influence of sulfur oxidizing bacteria on metastable carbonates during early diagenesis would be desirable. This could be achieved via cultivation experiments with bacteria of the order Campylobacterales.

Kurzfassung

Feinkörnige Karbonatsedimente enthalten zahlreiche Informationen über vergangene Umweltbedingungen und sind im globalen Kohlenstoffkreislauf von entscheidender Bedeutung. Diese Aufzeichnungen lassen sich mit Hilfe enthaltener Proxys (stabile Isotope und Spurenelemente) gewinnen und beinhalten Informationen über vergangene Ozean Temperaturen und -Salinitäten, sowie die Zirkulationsmechanismen bestimmter chemischer Elemente. Neben der Archivierung solcher Paläo-Umweltbedingungen lassen sich mit diesen Proxys ebenso zukünftige klimatische Entwicklungen simulieren. Die während der frühen Diagenese vonstattengehende Lösung und Rekristallisation von Karbonatphasen besitzt das Potential jene Archive zu verändern und damit getroffene Annahmen und Modelle zu verfälschen. Die Auswirkungen von sich verändernden physikochemischen Gradienten auf umgebende Karbonatphasen während der frühen Diagenese wurden bereits vielfach untersucht und kontrovers diskutiert. In den daraus gewonnenen Konzepten wurde jedoch die Rolle bakterieller Gemeinschaften sowie deren Eignung als zusätzlicher Proxy vernachlässigt. Die bakteriellen Auswirkungen auf frühdiagenetische Prozesse sollen dabei in dieser Arbeit untersucht werden, die darüber hinaus ein zusätzliches Werkzeug zur Evaluation traditioneller Isotopen- und Spurenelement-Proxys darstellen soll. Die Hauptfragestellung dieser Thesis beinhaltet (i) die Untersuchung sich verändernder physikochemischer Porenwassergradienten auf umgebende feinkörnige Karbonate, (ii) die Einflüsse der unmittelbaren Umwelt auf die Kalziumkarbonat Alteration, (iii) die Rolle bestimmter Bakterienstämme in der Errichtung von Porenwassergradienten und (iv) die Eignung von Multi-Proxy Studien, entsprechend die Kombination Sedimentgeochemischer-, Porenwasser- und bakterieller 16S rRNA Gendatensätze, um komplexe diagenetische Reaktionspfade auf zu decken.

Die ersten beiden Studien behandeln die Alteration und Fällung von authigenem Kalzium-Magnesium-Karbonatschlamm im flachen und alkalinen Neusiedlersee, der sich im Osten Österreichs erstreckt. Die aus dem See entnommenen Sedimente zeichneten sich durch eine Abfolge von 20 cm homogenem, gräulichem Schlamm mit einem Karbonatgehalt von 60 Gew% aus. Diese wurden von dunkel laminiertem, mit Pflanzenhäckseln durchsetztem und etwas kompaktiertem Schlamm mit einem Karbonatgehalt von 50 Gew% unterlagert. Die oxische Wassersäule des Sees wies einen pH-Wert von 9 auf, der sich im anoxischen Sediment auf Werte um 7.5 erniedrigte. Der anaerobe und von Sulfatreduktion gekennzeichnete, heterotrophe Abbau von organischem Material, wurde durch die Abnahme von Sulfat bei einem gleichzeitigen Anstieg der Gesamtschwefel- und Ammoniumkonzentrationen mit zunehmender Kerntiefe gekennzeichnet. Die Sättigungsindizes von Protodolomit und Kalzit lagen in der Wassersäule im übersättigten Bereich, wogegen sie im Sediment untersättigte Werte aufwiesen. Trotz jener beträchtlichen physikochemischen Änderungen im sedimentären Porenwasser, verblieben die Stöchiometrie sowie die relativen Anteile der authigenen Karbonatphasen mit zunehmender Kerntiefe konstant. Folglich ist damit kein Beweis für eine Fällung von Kalzium-Magnesium-Karbonaten oder eine Alteration zu thermodynamisch stabilerem Dolomit innerhalb des anoxischen, sulfidischen Sediments des Neusiedlersees erbracht. Die gewonnen Analysedaten favorisieren eher die Karbonatfällung in der übersättigten, gut durchmischten und aeroben Wassersäule. Entsprechend unterstützen die Ergebnisse dieser Studien ein alternatives Konzept der Dolomitfällung, entgegen jener in anoxischen Sedimenten. Darüber hinaus weisen sie auf langsame Diagenesereaktionen in solch sauerstoffarmen Ablagerungen hin.

Die dritte Studie befasst sich mit flachmarinen Diagenese- und Ablagerungsräumen auf Aldabra, einem abgelegenen Korallenatoll im westlichen indischen Ozean. Die Lagune dieses Atolls wurde in der Vergangenheit als rezentes Analogon jurassischer Lagunen bezeichnet, womit sie als prädestiniert für die Untersuchung von Diagenese in feinkörnigen Karbonatsedimenten erschien. Drei unterschiedliche

Lokalitäten wurden in der 34 x 14.5 km messenden Lagune untersucht. Diese umfassten jeweils eine in der West- (WL), Nord- (NL) und Südlagune (SL), die drei unterschiedliche Sediment- und Porenwassertypen zu Tage brachten, wobei die Beprobung mit Hilfe von Plexiglas Röhren erfolgte. Die Kerne der Westlagune beinhalteten intertidalen, bioklastischen Karbonatsand mit oxischem und porösem Porenraum. Die Sedimente der Nordlagune befanden sich im Wesentlichen in supratidalen Karstlöchern und bestanden aus hochporösem Bruchschill. Dagegen setzten sich die Kerne der Südlagune aus gräulichem, feinkörnigem Kalkschlamm mit entsprechend niedriger Porosität zusammen. Radiokarbonmessungen der Sedimente grenzten den zeitlichen Rahmen für Diagenesereaktionen auf 2357 ± 70 Jahre ein. Signifikante Alterationen wurden lediglich in den oxischen Kalksanden der Westlagune beobachtet. Diese zeichneten sich durch marin-vadose, kryptokristalline Kalziumkarbonat Zemente aus. Die genauen Reaktionspfade der Zementbildung waren dabei nicht gänzlich zu klären. Die Fällung jener diagenetischen Karbonate ist sowohl abiotisch, via Evaporation der Porenwässer während der Ebbe, oder mit Hilfe eines Konsortiums aus phototrophen und sulfatreduzierenden Bakterien möglich. Im Gegensatz dazu wurden keine diagenetischen Alterationen in den Sedimenten der Nord- und Südlagune festgestellt. Jedoch zeigten Porenwassergradienten eine Lösung metastabiler Karbonatminerale an, die mit einem verstärkten Auftretenden schwefeloxidierender Bakterien aus der Ordnung Campylobacteriales einher ging. Die Ergebnisse dieser Studie deuten an, dass frühdiagenetische Reaktionen in oxischen Sedimenten wesentlich schneller ablaufen als in anoxischen. Ergänzend dazu sind schwefeloxidierende Bakterien entscheidend an der Lösung metastabiler Karbonate während der frühen Diagenese beteiligt.

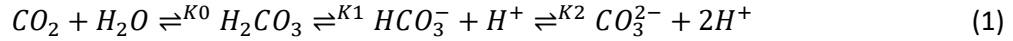
Die vierte Studie beinhaltet eine vergleichende Porenwasser-Sediment Studie des Cinq Cases Pool Systems, einem flachen und salinen Wasserkörper im Südosten Aldabras. Die dortigen Tümpel zeichnen sich durch gelegentliche marine Zuflüsse und damit verbundene, kurzzeitige Diagenesereaktionen aus. Die entnommenen Sedimente wurden mittels Radiokarbonmessungen auf 3760 ± 30 Jahre datiert und sind von drei vergangenen Umweltphasen gekennzeichnet. Einer ersten, die ein (zumindest temporär) anoxisches und palustrines Milieu mit meteorischer Diagenese einschließt („Unit III“). Einer weiteren, die eine langsame marine Überflutung sowie Cyanobakteria- und Schwammblüten beschreibt („Unit II“), sowie einer dritten, von lagunärer Überflutung inklusiver oxischer Sedimente gekennzeichneten Phase („Unit I“). Die Wechsel der Ablagerungs- und Diagenesebedingungen konnten mit Hilfe dreier verschiedener Proxys nachvollzogen werden, die zwar teils überlappende, doch unterschiedliche Zeitleisten repräsentieren. (i) Die Sedimentdaten stellen vergangene Prozesse dar, (ii) die Porenwasserdaten rezente und (iii) die bakteriellen Gemeinschaften spiegeln eine Überlagerung beider Zeitleisten wider. Folglich würde eine isolierte Betrachtung der einzelnen Parameter zu jeweils unterschiedlichen Schlussfolgerungen führen, was die Notwendigkeit solcher Multi-Proxy Studien aufzeigt.

Zusammengefasst deuten die Ergebnisse dieser Doktorarbeit darauf hin, dass nur geringe Änderungen der Geochemie feinkörniger Karbonatsedimente während der frühen Diagenese zu erwarten sind. Sofern diagenetische Prozesse innerhalb anoxischer Sedimente auftreten, zeichnen sie sich durch die Lösung metastabiler Mineralphasen aus. Diese geht mit der Aktivität schwefeloxidierender Bakterien der Ordnung Campylobacteriales einher. Die metabolischen Endprodukte dieser Organismen beinhalten Schwefelsäure, die sinkende pH-Werte- und entsprechend die Karbonatlösung begünstigt. Die frühe Diagenese zeigt sich dagegen in oxischen Sedimenten in Form kryptokristalliner Zemente. Die genauen Reaktionspfade dieser Zementfällung sind jedoch noch ungeklärt. Hochaufgelöste Studien dieser Zemente könnten weitere Aufschlüsse liefern. Kultivierungsexperimente mit Campylobacter würden zudem eine genauere Quantifizierung der Karbonatlösung durch deren metabolische Einflüsse ermöglichen.

1. Introduction

1.1 CaCO₃ formation in the marine carbonate system, carbon cycling and -alteration

Calcium carbonate (CaCO₃) precipitates under consumption of one calcium (Ca²⁺) and one carbonate (CO₃²⁻) ion to form two dominant mineralogical polymorphs. Calcite with a trigonal-, and aragonite with an orthorhombic lattice structure. Ca²⁺ is abundant in the oceans with an average concentration of 10 mmol·kg⁻¹ (Zeebe and Wolf-Gladrow, 2001). In contrast, dissolved inorganic carbon (DIC) exists in various forms and results from the transfer of atmospheric CO₂ into the hydrosphere (Figure 1.1a). The dissolution of CO₂ to form DIC can be simplified by equation (eq) 1:



Gaseous carbon dioxide (CO₂) dissolves in ocean waters to form carbonic acid (H₂CO₃), which dissociates into bicarbonate- (HCO₃⁻) and carbonate (CO₃²⁻) ions, as well as protons (H⁺). As only 1/1000 of dissolved CO₂ is present as H₂CO₃ (Butler, 1998; Dickson, 2010), K₀ can be neglected. The equilibrium constants K₁ and K₂ result from the activities of involved ions and can be defined in the following way:

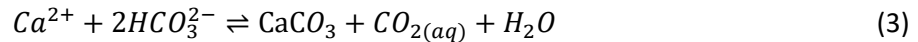
$$K_1 = \frac{[HCO_3^-][H^+]}{[H_2CO_3]} \quad (1.1)$$

$$K_2 = \frac{[CO_3^{2-}][H^+]}{[HCO_3^-]} \quad (1.2)$$

Overall, DIC is often expressed as:

$$DIC = CO_2 + HCO_3^- + CO_3^{2-} \quad (2)$$

Given oceanic surface conditions, K₁ measures nine times K₂ (Bach, 2015), which simplifies the precipitation of CaCO₃ according to the following equation (eq. 3):



To allow further statements about the preference of CaCO₃ to precipitate, the specific solubility product (K_{sp}) is needed. At standard conditions, it is defined by Mucci and Morse (1984) as follows:

$$K_{sp} = [Ca^{2+}] \cdot [CO_3^{2-}] \quad (4)$$

The saturation state Ω further describes the thermodynamic state of CaCO₃. It is defined by the ratio of the ion product of Ca²⁺ and CO₃²⁻ in sea water versus the solubility constant:

$$\Omega = \frac{[Ca^{2+}]_{sw} [CO_3^{2-}]_{sw}}{K_{sp}} \quad (5)$$

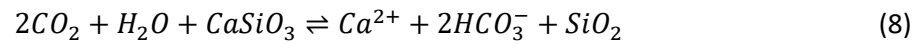
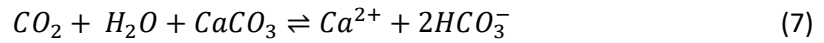
In the following chapters, the saturation index (SI) is used instead of the saturation state Ω, and is defined as:

$$SI = \log_{10} \Omega \quad (6)$$

A SI above zero (SI > 0) expresses the supersaturation of CaCO₃ and its preference to precipitate, whereas its undersaturation is reached at values below zero (SI < 0). Today, the surface of the ocean is supersaturated with respect to calcite (SI = 0.7) and aragonite (SI = 0.5), but their spontaneous precipitation is restricted to SI values greater than 1.3-1.4 (Morse, 2003). This is due to the fact that the initial step of crystal nucleation is kinetically unfavorable, which connects CaCO₃ precipitation in the ocean to the activity of carbonate forming organisms. Overall, CaCO₃ saturation is not sufficient to drive abiotic precipitation, but to preserve carbonates deposited in shallow water. Moreover, equations 1-3 indicate that CaCO₃ formation plays a fundamental role in global carbon cycling and influences atmospheric CO₂ levels. On the one hand, the sum of total DIC species is reduced, but on the other hand, the residual C is repartitioned in favor of CO₂. Over short time scales, this increases oceanic pCO₂ and eventually atmospheric CO₂ levels (Ridgwell and Zeebe, 2005).

In the ocean, pressure increases with depth, whereas the contemporary temperature decreases. This favors CaCO₃ undersaturation and its dissolution in the deep sea (Bach, 2015; Figure 1.1b). The depth at which significant amounts of carbonate dissolution are inevitable, is called carbonate compensation

depth (CCD), and lies at around 3500 m of depth (Ridgwell and Zeebe, 2005). Additionally, CaCO_3 can become undersaturated in pore waters of sediments in shallow waters, if it is exposed to organic matter (OM) oxidation during early diagenesis. However, not all carbonate deposits reach deeper waters. Certain portions are deposited on marine shelves or reef complexes. This Ca^{2+} removal from ocean waters is balanced by the weathering of surficial exposed CaCO_3 and silicate rocks, which completes the (surficial) carbon circle (Figure 1.1b).



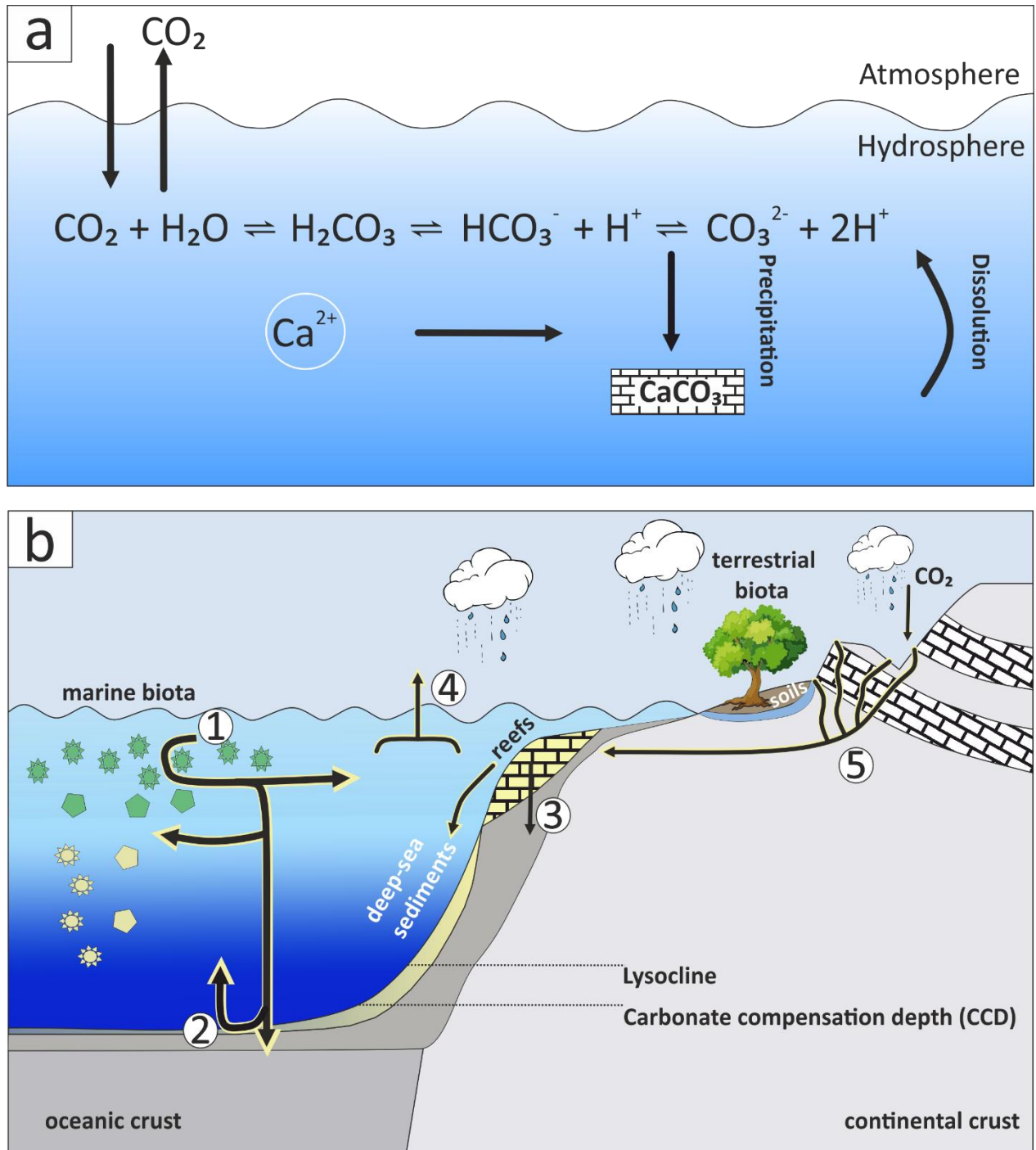


Figure 1.1a: Simplified scheme of the marine carbonate system and related CaCO_3 dissolution and precipitation (modified after Lange, 2017 and Kanwisher, 1960). b: The global (surficial) biogeochemical carbon cycling. 1 Precipitation of CaCO_3 by algae and foraminifera in the open ocean. $\text{Ca}^{2+} + 2\text{HCO}_3^- \rightleftharpoons \text{CaCO}_3 + \text{CO}_2(\text{aq}) + \text{H}_2\text{O}$. 2 Carbonate reaching deep sea sediments will dissolve during diagenesis if it is exposed to undersaturated bottom waters. 3 Precipitation of CaCO_3 by mollusks and corals in warm and shallow water, with possible build ups of reef structures. 4 Precipitation of CaCO_3 increases $p\text{CO}_2$ at the surface of the ocean and causes a net transfer of CO_2 to the atmosphere. 5 Tectonically uplifted CaCO_3 is exposed to erosion: $\text{CO}_2 + \text{H}_2\text{O} + \text{CaCO}_3 \rightleftharpoons \text{Ca}^{2+} + 2\text{HCO}_3^-$. Redrawn and modified after Ridgwell and Zeebe (2005.)

1.2 Environmental records in common carbonate minerals

A variety of elements and stable isotopes, derived from marine, lacustrine, and terrestrial carbonates, have been used as environmental proxies to obtain information about the Earth's surface conditions over geologic time scales. Well established proxies are the stable isotope contents of ^{18}O (Urey, 1947; Epstein and Mayeda, 1953) and ^{13}C (Craig, 1953; Park and Epstein, 1961). Both are recorded in the delta notation (δ) as $\delta^{18}\text{O}$ and $\delta^{13}\text{C}$, relative to a reference standard (Vienna Pee Dee Belemnite, VPDB) according to the following relationship:

$$\delta^{18}\text{O}_{\text{sample}} = 1000 \cdot \frac{[(\frac{^{18}\text{O}}{^{16}\text{O}})_{\text{Sample}} - (\frac{^{18}\text{O}}{^{16}\text{O}})_{\text{Standard}}]}{(\frac{^{18}\text{O}}{^{16}\text{O}})_{\text{Standard}}} \quad (9)$$

$\delta^{18}\text{O}$ values are frequently used in paleoclimate studies, because ^{18}O isotope fractionation depends on ambient temperatures. This connects the $\delta^{18}\text{O}$ value to various processes, such as global ice volume changes, external water input and evaporation (Katz et al., 2010). $\delta^{13}\text{C}$ values are determined similar to eq. 9 and depend on the ambient DIC reservoir. This reservoir responds to several physicochemical parameters (pH, temperature, pool of OM), which are coupled to climatic conditions (Mook, 1968; Zeebe and Wolf-Gladrow, 2001). Additionally, the initial values of trace elements and stable isotopes are determined by the mineralogy of the host phase. For instance, $\delta^{13}\text{C}$ values of aragonite are about 1 to 2 ‰ more positive than those of co-occurring calcite (Rubinson and Clayton, 1969; Emrich et al., 1970; Romanek et al., 1992). Furthermore, aragonite incorporates small portions of strontium (Sr) and calcite several amounts of magnesium (Mg). The latter causes the occurrence of high magnesium calcite (HMC) and low magnesium calcite (LMC), which are distinguished by a value of four mole % MgCO_3 .

Likewise, the Mg content of foraminiferal calcite tests represents an additional temperature proxy, as the amounts of incorporated Mg vary in correspondence to ambient temperatures. It is usually used to double check $\delta^{18}\text{O}$ data (Katz et al., 2010 and references therein). Strontium elemental and isotope concentrations of aragonite are used to study elemental cycling and diagenetic effects. It occurs in three stable isotopes (^{86}Sr , ^{87}Sr and ^{88}Sr), of which the measurements of the $^{87}\text{Sr}/^{86}\text{Sr}$ ratio are most common (Swart, 2015). Aragonite precipitating organisms do not fractionate against Sr isotopes, thus, the ^{87}Sr of the oceans can be retraced through time in unaltered carbonates. The ^{87}Sr content of the oceans is controlled by the weathering and erosion of continental crust, as the latter harbors relatively high $^{87}\text{Sr}/^{86}\text{Sr}$ ratios (Burke et al., 1982; DePaolo and Ingram, 1985; McArthur et al., 2001).

Additionally, Mg and Ca isotopes are frequently used in diagenetic studies (Raddatz et al., 2013; Wombacher et al., 2011; Higgins et al., 2018), as their amounts change with the respective CaCO_3 phase (calcite or aragonite). Summing up, the application of a certain proxy relies on (i) the individual research question, and (ii) the chemical and isotopic composition of the solution from which the proxy material (e.g. foraminifera tests) forms. Another important point is the degree of post depositional changes in initial chemistry due to diagenetic processes, which shall be discussed in the subsequent section 1.3.

1.3 Major diagenetic zones and their potential impacts on geochemical proxy records

The process of diagenesis comprises all physical, mineralogical, and chemical changes, which occur in sediments between their initial deposition and the time when they pass the temperature and pressure boundary to metamorphism (Murray and Pray, 1965). The focus of this section lies on early diagenesis, which includes OM degradation, CaCO_3 dissolution, re-precipitation, and compaction (Berner, 1980). Shallow marine, tropical carbonate predominantly consists of aragonite and HMC, whereas non-tropical carbonates harbor higher amounts of HMC and minor amounts of aragonite. The respective CaCO_3 polymorphs have different vulnerabilities to post-depositional alteration (diagenesis). Overall, aragonite and HMC are metastable, whereas LMC is the thermodynamically most favorable mineral phase (under ambient conditions; Wray and Daniels, 1957). Figure 1.2 depicts the major diagenetic zones, in which these minerals are prone to characteristic alteration patterns.

The meteoric zone involves freshwater as reacting fluid and extends from continental areas, over shelf margins and atolls (Figure 1.2). In general, it can be established anywhere, where carbonate sediments are subaerially exposed. Meteoric waters are usually enriched in dissolved CO_2 , but depleted in dissolved ions, which makes them corrosive to all carbonate minerals (Swart, 2015). Metastable phases (aragonite and HMC) are dissolved in contact with meteoric water and eventually, thermodynamically stable LMC is precipitated, after being sufficiently supersaturated. The precipitation of LMC can thereby occur before aragonite and HMC are completely dissolved (Budd, 1988). This process produces blocky pendant and meniscus cements in vadose pore spaces and isopachous equant cements in water saturated, phreatic pore spaces (Halley and Harris, 1979). The $\delta^{18}\text{O}$ values of these cements are controlled by the $\delta^{18}\text{O}$ of the meteoric fluid, which is predominantly fed by rainfall ($\delta^{18}\text{O} < 0$; Rozanski et al., 1993). Thus, $\delta^{18}\text{O}$ values of meteoric diagenetic carbonate are more negative than those of the primary phases. Moreover, temperature fractionation of ^{18}O can be neglected, as this meteoric diagenesis occurs at temperatures between 20 and 30 °C (Swart, 2015). The $\delta^{13}\text{C}$ value of the meteoric vadose environment is characterized by DIC derived from the soil zone, in which oxidation of OM occurs. Thus, the $\delta^{13}\text{C}$ is more negative than that of the respective host carbonate. However, photosynthetic activity in light exposed areas might enrich the meteoric fluid in $\delta^{13}\text{C}$. As light exposition decreases with depth, $\delta^{13}\text{C}$ values of the meteoric phreatic zone are more constant than those of the vadose zone (Swart, 2015). Additionally, when metastable carbonate host phases (aragonite and HMC) dissolve, Sr and Mg can be released into the pore space, because these elements are not incorporated into diagenetic LMC. If reducing conditions occur in the soil horizon, redox sensitive elements like manganese (Mn) and iron (Fe) are mobilized and eventually enriched in the diagenetic carbonate phase (Meyers, 1974; Frank and Lohmann, 1996).

The mixing zone of marine and meteoric waters is localized in the shallow subsurface of coastal settings (Figure 1.2). Mixtures of salt- and freshwater cause significant dissolution of carbonate rocks along coasts, hence, caves are often associated with these mixing zones (Sanford and Konikow, 1989). The dissolution processes are caused by a non-linear behaviour of activity coefficients of ions in fluids with varying salinity (Badiozamani, 1973). For example, the mixture of two waters with different salinity can create calcite dissolution, even though the two solutions are supersaturated with respect to this phase. However, carbonates exposed to mixed waters show a distinct covariation of $\delta^{18}\text{O}$ and $\delta^{13}\text{C}$ values. This is caused by the carbonate alteration in fluids with increasing stable isotope enrichment, as freshwater progresses to marine water through the mixing zone (Swart, 2015).

Marine vadose alteration occurs predominantly at beaches and tidal flats, marked by evaporation driven, rapid cementation of the pore space. The cements primarily consist of HMC and aragonite,

which harbor enriched stable isotope values compared to the host carbonate. This is due to evaporation, which causes a temperature fractionation of $\delta^{18}\text{O}$ and $\delta^{13}\text{C}$ (Swart, 2015).

The marine phreatic environment is localized at the shallow- to deep sea floor and immediately below (Figure 1.2). A constant pore flush with CaCO_3 saturated fluids causes the formation of aragonite and HMC cements, depending on the Mg/Ca ratio (Folk, 1974; Mucci and Morse, 1984). During phases of non-deposition, cementation extends even to the top of the sediments, resulting in the formation of firm- and hardgrounds (James and Choquette, 1983). Cementation in such hardgrounds is often difficult to assess, as the diagenetic crystals are too small to allow effective sampling without cross contamination (Swart, 2015). However, the $\delta^{18}\text{O}$ of cements formed in the marine phreatic pore space usually reflects the sea water value as no temperature fractionation occurs at shallow depths (Swart et al., 2002). Furthermore, the precipitation of cements from marine waters will possibly enrich the whole sample in $\delta^{13}\text{C}$ as inorganic aragonite and HMC have higher $\delta^{13}\text{C}$ values (Aissaoui, 1988). Braithwaite and Camoin (2011) confirm these assumptions.

The formation of aragonite and HMC cements also affects the concentrations of Sr and Mg in the pore space, as the former would incorporate Sr and the latter Mg. However, bulk stable isotope ($\delta^{13}\text{C}$ and $\delta^{18}\text{O}$) values show only minor deviations in the marine phreatic environment, despite the mentioned diagenetic reactions.

Marine burial diagenesis starts within the first meters of burial and is shaped by physical compaction and pressure solution of pristine carbonate phases, which produces the material for subsequent burial cementation. With increasing subsurface depth, pore fluids contain higher ion concentrations and are reducing, which causes the mobilization of Fe and Mn. These redox active elements can subsequently be incorporated into cements, typically consisting of coarse grained LMC or dolomite (Flügel, 2004). Within shallow areas of burial diagenesis, where temperature fractionation of stable isotopes is absent, only minor changes in the record are expectable, since the cement precipitating fluid originates from the host carbonates (Swart, 2015).

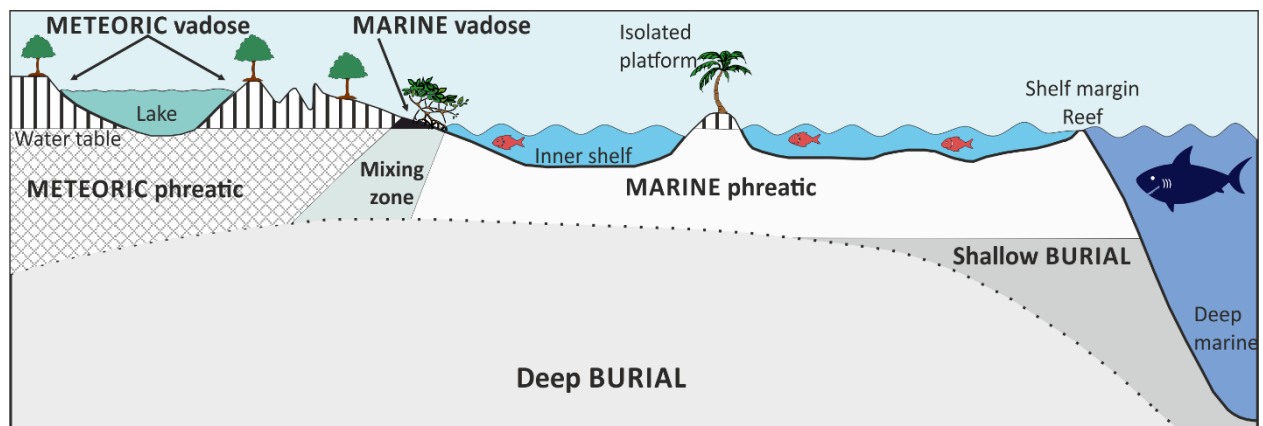


Figure 1.2: Major diagenetic zones, redrawn after Flügel (2004).

1.4 Impact of microorganisms on CaCO₃ precipitation and -alteration

Microbes play a key role in the primary production and biogeochemical transformation of OM, which affects the stability of carbonate phases. First, photosynthetic cyanobacteria use CO₂ as a primary source for the accumulation of OM. This depletes the surrounding fluid in dissolved CO₂, rises the pH and shifts the carbonate equilibrium (eq. 1; Figure 1.1a) towards CO₃²⁻. Thus, this metabolic process favors CaCO₃ supersaturation and, eventually, its precipitation (Castanier et al., 2000).

After the death of primary producers, their OM is deposited on the floor of water bodies. It is degraded by a variety of microorganisms that contribute to its gradual mineralization. Within this heterotrophic process, the microbes gain energy by oxidation of OM with an external electron acceptor (oxidant). The highest energy yield of all accessible oxidants is provided by oxygen, with 3190 kJ for every mole glucose oxidized (Froelich et al., 1979). After the depletion of this oxidant, other electron acceptors are needed, which are provided by nitrate (NO₃⁻, 3000 kJ mol⁻¹), manganese (II and IV) oxides (MnO, MnO₂, 2750 kJ mol⁻¹), iron (II and III) oxides (Fe₂O₃, FeOOH, FeO, 1400 kJ mol⁻¹) and sulfate (SO₄²⁻, 380 kJ mol⁻¹). This leads to a distinct physicochemical depth zonation in phreatic sediments (Figure 1.3). Sulfate is abundant in all marine and freshwater settings, with respective average concentrations of 29 mmol·L⁻¹ (Vairavamurthy et al., 1995) and 0.1 mmol·L⁻¹ (Bowen, 1979). This makes sulfate the most significant oxidant after oxygen is depleted, despite its comparably low energy yield (Henrichs and Reeburgh, 1987). If OM subsequently reaches the deeper subsurface, where SO₄²⁻ is finally exhausted, it is fermented to methane (CH₄) and CO₂. All those heterotrophic processes influence the physical and chemical parameters of pore water that surrounds carbonate sediments. An abundant metabolic end product is CO₂, which lowers the pH and shifts eq. 3 to the left, causing an eventual dissolution of carbonate phases. Especially dissimilatory, bacterial sulfate reduction (BSR) raised some attention in this context (Van Lith et al., 2002; Vasconcelos and McKenzie, 1997; Vasconcelos et al., 1995), as it may also contribute to carbonate precipitation via alkalinity increase, besides (dissolution favoring) CO₂ generation.

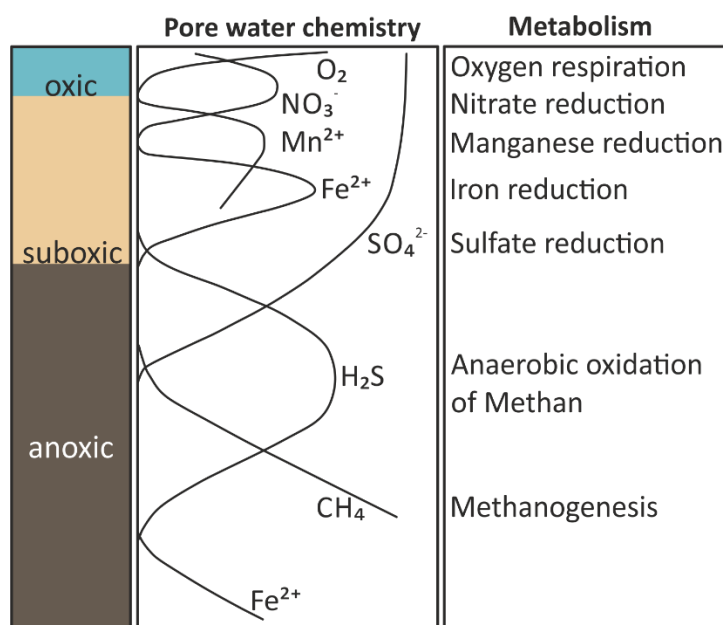


Figure 1.3: Typical biogeochemical zonation in phreatic sediments. The names of the main zones were proposed by Froelich et al. (1976) and Berner (1981). In general, the depth of each zone varies and increases from shelf to deep sea. Redrawn after Jørgensen and Kasten (2006).

1.5 Comparative pore water studies as biogeochemical and diagenetic tracers

Comparative pore water-solute profiles represent a powerful tool to investigate microbially driven geochemical reactions in sediments. This is due to the fact that pore water data are very sensitive to diagenetic changes, which are poorly observable in the bulk record of solids. Furthermore, they offer the opportunity to quantify sedimentary reactions in global marine geochemical cycles (Martin and Sayles, 2003).

The first ever recorded pore water study was conducted by Murray and Irvine (1895), who placed sea floor muds in a canvas bag and collected the drippings. In the following 20th century, pore water extraction methods were based on pressing pore fluids through a filter that holds back sediment particles. These pressing methods were gradually refined by inserting a piston into a coring cylinder, which forces the pore water from the bottom (Manheim, 1966). Another sophisticated invention was the “whole-core-squeezer” (Bender et al., 1987), which preserves the depth concentration relationships. This is accomplished by forcing the sediment towards a filter, placed at the top of the cored sample. A disadvantage of this method is the depth limitation of 2 to 4 cm (Martin and Sayles, 2003). Centrifugation represents another popular and practicable pore water extraction method and is the most common technique up to now. However, all these *ex-situ* methods include several biases (De Lange et al., 1992), such as oxygen contamination of reducing waters, degassing of CO₂ and CH₄, and miscellaneous concentration biases due to sediment compaction during squeezing. A detailed list of possible artifacts and their implications to certain pore water constituents can be found in Martin and Sayles (2003).

In-situ methods of pore water sampling are represented by suction methods. Suction samplers normally consist of vertically aligned sampling ports along a tube, which are covered by a nylon gauze (Bertolin et al., 1995; Van Der Loeff, 1980; Sayles et al., 1976; Watson and Frickers, 1990). Rhizon samplers represent another variation of such a suction *in-situ* method. A Rhizon sampler consists of a 10 cm long, porous polymer tube with a diameter of 2.5 mm, which is penetrated into the sediment. It is connected to a syringe, which creates a vacuum and eventually sucks the pore water out of the sediment. This method is well established in soil and agriculture science, as it offers the opportunity to nondestructively sample fluids from water unsaturated soils (Meijboom and van Noordwijk, 1991). Rhizon pore water sampling was introduced to geosciences by Seeberg-Elverfeldt et al. (2005), who applied this technique to aquatic sediments. Several geoscientific *in situ* pore water studies, using this non-destructive approach were conducted since then (Bontognali et al., 2010; Birgel et al., 2015; Steiner et al., 2018). However, despite the advantage of being a non-destructive technique and avoiding squeezing contaminations, CO₂ degassing and hence possible pH and alkalinity changes must be considered when sampling pore waters with this tool (Schrum et al., 2012).

1.6 Thesis objectives and study approaches

Microbial effects on the alteration of trace element- and stable isotope signals in carbonate muds are poorly understood. This is since combined datasets, consisting of depth-resolved sediment geochemistry-, pore water chemistry-, and bacterial gene data are scarce. However, this thesis merges such multi-proxy approaches, aiming to trace microbial effects on early diagenesis at shallow depths. It contains a first geomicrobiological multi-proxy study of sediments from Lake Neusiedl (LN) that is presented in [Chapters 2-3](#). Furthermore, this work includes the first detailed study of Holocene sediments and contemporaneous pore water from Aldabra, a raised coral atoll in the western Indian Ocean ([Chapters 4-5](#)). The following work shall provide a valuable feature to evaluate traditional

isotope- and trace element signals in the fossil record, which are used as proxies to reconstruct paleoenvironmental conditions. Specific questions that are addressed in this work include:

- i. What are the effects of hydrochemical pore water gradients on contemporary, fine-grained carbonate phases (mineralogy, stable isotope- and elemental concentrations) during the earliest stages of diagenesis?
- ii. What impacts does the nearby environment have on carbonate alteration?
- iii. Which role do specific bacteria play in the establishment of hydrochemical pore water gradients? How do they eventually affect the stability of carbonate phases?
- iv. Are geomicrobiological multi-proxy studies, consisting of sediment geochemical-, pore water-, and bacterial 16S rRNA datasets suitable to tackle these questions?

To successfully address these questions, three different studies, presented as individual chapters were conducted within the framework of phase II of the “DFG-Forschergruppe-1644 Charon (Teilprojekt-TP 7)”.

The studies in [chapters 2](#) and [3](#) focus on carbonate alteration in fine-grained sediments retrieved from Lake Neusiedl, which represents an extraordinary carbonate forming setting. This is since it is the only endorheic, evaporative water body in central Europe. Regional geologic effects constrain an alkaline water chemistry, and its shallowness contributes to fluctuating hydrochemical conditions according to the seasons. The sediments of LN consist of organic-rich carbonate mud, which is predominantly made up of authigenic HMC and protodolomite. Bulk sediment (Leco-CNS) and pore water (Ion Chromatography-IC; Inductively Coupled Plasma Mass Spectrometry-ICP-MS) analysis were combined with high resolution optics (Scanning Electron Microscopy-SEM) and 16S rRNA bacterial gene data, to trace potential diagenetic reaction paths within the upper sediment column (40 cm of depth from sediment top).

Early diagenetic effects on Holocene carbonate sediments from Aldabra are discussed in [Chapter 4](#). Three different sites (in the lagoon of the atoll), hosting different carbonate depositional environments, were sampled and evaluated with respect to diagenetic changes. Bulk sediment- and pore water stable isotope data ($\delta^{13}\text{C}$ and $\delta^{18}\text{O}$), were combined with thin section observations, state of the art geo- and hydrochemical analyses (Leco-CNS; IC; ICP-MS), and 16S rRNA bacterial gene data, to reveal microbial effects on early diagenetic proxy alterations.

A similar multi-proxy approach was applied to Cinq Cases, a landlocked pool system in the east of Aldabra. The study is presented in [Chapter 5](#) and incorporates analytical approaches similar to [Chapter 4](#), which are complemented with high resolution optical- and geochemical data by electron beam microprobe (EMP-WDX) analysis. [Chapter 5](#) reveals different time scales of individual parameters in this unstable depositional environment and emphasizes the necessity of multiproxy studies. Finally, the outcomes of [Chapters 2-5](#) are evaluated and discussed in [Chapter 6](#). It deals with the environmental impacts on carbonate sediments and early diagenetic effects of microbially induced pore water gradients on such deposits.

References

- Aissaoui, D. M.: Magnesian calcite cements and their diagenesis: dissolution and dolomitization, Mururoa Atoll, *Sedimentology*, 35, 821-841, <https://doi.org/10.1111/j.1365-3091.1988.tb01253.x>, 1988.
- Bach, L. T.: Reconsidering the role of carbonate ion concentration in calcification by marine organisms, *Biogeosciences*, 12, 4939-4951, <https://doi.org/10.5194/bg-12-4939-2015>, 2015.
- Badiozamani, K.: The dorag dolomitization model, application to the middle Ordovician of Wisconsin, *Journal of Sedimentary Research*, 43, 965-984, <https://doi.org/10.1306/74d728c9-2b21-11d7-8648000102c1865d>, 1973.
- Berner, R. A.: Early diagenesis: a theoretical approach, 1, Princeton University Press, <https://doi.org/10.1515/9780691209401>, 1980.
- Berner, R. A.: A new geochemical classification of sedimentary environments, *Journal of Sedimentary Research*, 51, 359-365, <https://doi.org/10.1306/212f7c7f-2b24-11d7-8648000102c1865d>, 1981.
- Bertolin, A., Rudello, D., and Ugo, P.: A new device for in-situ pore-water sampling, *Marine chemistry*, 49, 233-239, [https://doi.org/10.1016/0304-4203\(94\)00062-i](https://doi.org/10.1016/0304-4203(94)00062-i), 1995.
- Birgel, D., Meister, P., Lundberg, R., Horath, T., Bontognali, T. R., Bahniuk, A. M., de Rezende, C. E., Vásconcelos, C., and McKenzie, J. A.: Methanogenesis produces strong ¹³C enrichment in stromatolites of Lagoa Salgada, Brazil: a modern analogue for Palaeo-/Neoproterozoic stromatolites?, *Geobiology*, 13, 245-266, <https://doi.org/10.1111/gbi.12130>, 2015.
- Bontognali, T. R., Vasconcelos, C., Warthmann, R. J., Bernasconi, S. M., Dupraz, C., Strohmenger, C. J., and McKenzie, J. A.: Dolomite formation within microbial mats in the coastal sabkha of Abu Dhabi (United Arab Emirates), *Sedimentology*, 57, 824-844, <https://doi.org/10.1111/j.1365-3091.2009.01121.x>, 2010.
- Bowen, H. J. M.: Environmental chemistry of the elements, Academic Press., <https://doi.org/10.1039/9781847555991>, 1979.
- Braithwaite, C. J., and Camoin, G. F.: Diagenesis and sea-level change: lessons from Moruroa, French Polynesia, *Sedimentology*, 58, 259-284, <https://doi.org/10.1111/j.1365-3091.2010.01182.x>, 2011.
- Budd, D. A.: Aragonite-to-calcite transformation during fresh-water diagenesis of carbonates: Insights from pore-water chemistry, *Geological Society of America Bulletin*, 100, 1260-1270, [https://doi.org/10.1130/0016-7606\(1988\)100<1260:atctdf>2.3.co;2](https://doi.org/10.1130/0016-7606(1988)100<1260:atctdf>2.3.co;2), 1988.
- Burke, W., Denison, R., Hetherington, E., Koepnick, R., Nelson, H., and Otto, J.: Variation of seawater ⁸⁷Sr/⁸⁶Sr throughout Phanerozoic time, *Geology*, 10, 516-519, [https://doi.org/10.1130/0091-7613\(1982\)10<516:vosstp>2.0.co;2](https://doi.org/10.1130/0091-7613(1982)10<516:vosstp>2.0.co;2), 1982.
- Butler, J. N.: Ionic equilibrium: solubility and pH calculations, John Wiley & Sons, <https://doi.org/10.5860/choice.36-0965>, 1998.
- Castanier, S., Le Metayer-Levrel, G., and Perthuisot, J.-P.: Bacterial roles in the precipitation of carbonate minerals, in: *Microbial sediments*, Springer, 32-39, https://doi.org/10.1007/978-3-662-04036-2_5, 2000.
- Craig, H.: The geochemistry of the stable carbon isotopes, *Geochimica et cosmochimica acta*, 3, 53-92, [https://doi.org/10.1016/0016-7037\(53\)90001-5](https://doi.org/10.1016/0016-7037(53)90001-5), 1953.
- De Lange, G., Cranston, R., Hydes, D., and Boust, D.: Extraction of pore water from marine sediments: a review of possible artifacts with pertinent examples from the North Atlantic, *Marine Geology*, 109, 53-76, [https://doi.org/10.1016/0025-3227\(92\)90220-c](https://doi.org/10.1016/0025-3227(92)90220-c), 1992.

- DePaolo, D. J., and Ingram, B. L.: High-resolution stratigraphy with strontium isotopes, *Science*, 227, 938-941, <https://doi.org/10.1126/science.227.4689.938>, 1985.
- Dickson, A. G.: The carbon dioxide system in seawater: equilibrium chemistry and measurements, *Guide to best practices for ocean acidification research and data reporting*, 1, 17-40, 2010.
- Emrich, K., Ehhalt, D., and Vogel, J.: Carbon isotope fractionation during the precipitation of calcium carbonate, *Earth and Planetary Science Letters*, 8, 363-371, [https://doi.org/10.1016/0012-821x\(70\)90109-3](https://doi.org/10.1016/0012-821x(70)90109-3), 1970.
- Epstein, S., and Mayeda, T.: Variation of O18 content of waters from natural sources, *Geochimica et Cosmochimica Acta*, 4, 213-224, [https://doi.org/10.1016/0016-7037\(53\)90051-9](https://doi.org/10.1016/0016-7037(53)90051-9), 1953.
- Flügel, E.: *Microfacies of carbonate rocks: analysis, interpretation and application*, Springer Science & Business Media, <https://doi.org/10.1007/978-3-662-08726-8>, 2004.
- Folk, R. L.: The natural history of crystalline calcium carbonate; effect of magnesium content and salinity, *Journal of Sedimentary Research*, 44, 40-53, <https://doi.org/10.1306/74d72973-2b21-11d7-8648000102c1865d>, 1974.
- Frank, T. D., and Lohmann, K. C.: Diagenesis of fibrous magnesian calcite marine cement: Implications for the interpretation of $\delta^{18}\text{O}$ and $\delta^{13}\text{C}$ values of ancient equivalents, *Geochimica et Cosmochimica Acta*, 60, 2427-2436, [https://doi.org/10.1016/0016-7037\(96\)00097-x](https://doi.org/10.1016/0016-7037(96)00097-x), 1996.
- Froelich, P. N., Klinkhammer, G., Bender, M. L., Luedtke, N., Heath, G. R., Cullen, D., Dauphin, P., Hammond, D., Hartman, B., and Maynard, V.: Early oxidation of organic matter in pelagic sediments of the eastern equatorial Atlantic: suboxic diagenesis, *Geochimica et Cosmochimica Acta*, 43, 1075-1090, [https://doi.org/10.1016/0016-7037\(79\)90095-4](https://doi.org/10.1016/0016-7037(79)90095-4), 1979.
- Halley, R. B., and Harris, P. M.: Fresh-water cementation of a 1,000-year-old oolite, *Journal of Sedimentary Research*, 49, 969-987, <https://doi.org/10.1306/212f7892-2b24-11d7-8648000102c1865d>, 1979.
- Henrichs, S. M., and Reeburgh, W. S.: Anaerobic mineralization of marine sediment organic matter: rates and the role of anaerobic processes in the oceanic carbon economy, *Geomicrobiology Journal*, 5, 191-237, <https://doi.org/10.1080/01490458709385971>, 1987.
- Higgins, J. A., Blättler, C., Lundstrom, E., Santiago-Ramos, D., Akhtar, A., Ahm, A. C., Bialik, O., Holmden, C., Bradbury, H., and Murray, S.: Mineralogy, early marine diagenesis, and the chemistry of shallow-water carbonate sediments, *Geochimica et Cosmochimica Acta*, 220, 512-534, <https://doi.org/10.1016/j.gca.2017.09.046>, 2018.
- James, N. P., and Choquette, P. W.: Diagenesis 6. Limestones—the sea floor diagenetic environment, *Geoscience Canada*, <https://doi.org/10.1029/sc004p0045>, 1983.
- Jørgensen, B. B., and Kasten, S.: Sulfur cycling and methane oxidation, in: *Marine geochemistry*, Springer, 271-309, https://doi.org/10.1007/3-540-32144-6_8, 2006.
- Kanwisher, J.: pCO_2 in sea water and its effect on the movement of CO_2 in nature, *Tellus*, 12, 209-215, <https://doi.org/10.3402/tellusa.v12i2.9361>, 1960.
- Katz, M. E., Cramer, B. S., Franzese, A., Hönisch, B. r., Miller, K. G., Rosenthal, Y., and Wright, J. D.: Traditional and emerging geochemical proxies in foraminifera, *The Journal of Foraminiferal Research*, 40, 165-192, <https://doi.org/10.2113/gsjfr.40.2.165>, 2010.
- Lange, S.: *Microbial Alteration of Carbonate Archives*, Doctoral dissertation, 2017.
- Manheim, F. T.: A hydraulic squeezer for obtaining interstitial water from consolidated and unconsolidated sediments, *US Geol. Surv. Prof. Pap*, 550, 171-174, <https://doi.org/10.1306/74d71a23-2b21-11d7-8648000102c1865d>, 1966.
- Martin, W., and Sayles, F.: The recycling of biogenic material at the seafloor, 7, <https://doi.org/10.1016/b0-08-043751-6/07089-4>, 2003.

- McArthur, J. M., Howarth, R., and Bailey, T.: Strontium isotope stratigraphy: LOWESS version 3: best fit to the marine Sr-isotope curve for 0–509 Ma and accompanying look-up table for deriving numerical age, *The Journal of Geology*, 109, 155-170, <https://doi.org/10.1086/319243>, 2001.
- Meijboom, F., and van Noordwijk, M.: Rhizon soil solution samplers as artificial roots, *Root ecology and its practical application 3*. ISRR Symposium. Verein für Wurzelforschung, A-9020 Klagenfurt Austria, 793, 1991.
- Meyers, W. J.: Carbonate cement stratigraphy of the Lake Valley Formation (Mississippian) Sacramento Mountains, New Mexico, *Journal of Sedimentary Research*, 44, 837-861, <https://doi.org/10.1306/212f6bc2-2b24-11d7-8648000102c1865d>, 1974.
- Mook, W. G.: Geochemistry of the stable carbon and oxygen isotopes of natural waters in the Netherlands, *Rijksuniversiteit te Groningen*, [https://doi.org/10.1016/0031-0182\(71\)90002-2](https://doi.org/10.1016/0031-0182(71)90002-2), 1968.
- Morse, J. W.: Formation and diagenesis of carbonate sediments, <https://doi.org/10.1016/b0-08-043751-6/07093-6>, 2003.
- Mucci, A., and Morse, J. W.: The solubility of calcite in seawater solutions of various magnesium concentration, $I_t = 0.697$ m at 25 C and one atmosphere total pressure, *Geochimica et Cosmochimica Acta*, 48, 815-822, [https://doi.org/10.1016/0016-7037\(84\)90103-0](https://doi.org/10.1016/0016-7037(84)90103-0), 1984.
- Murray, J., and Irvine, R.: XXIII.—On the Chemical Changes which take place in the Composition of the Sea-Water associated with Blue Muds on the Floor of the Ocean, *Earth and Environmental Science Transactions of The Royal Society of Edinburgh*, 37, 481-507, <https://doi.org/10.1017/s0080456800032701>, 1895.
- Murray, R. C., and Pray, L. C.: Dolomitization and limestone diagenesis—an introduction, <https://doi.org/10.2110/pec.65.07.0001>, 1965.
- Park, R., and Epstein, S.: Metabolic fractionation of C13 & C12 in plants, *Plant Physiology*, 36, 133-138, <https://doi.org/10.1104/pp.36.2.133>, 1961.
- Raddatz, J., Liebetrau, V., Rüggeberg, A., Hathorne, E., Krabbenhöft, A., Eisenhauer, A., Böhm, F., Vollstaedt, H., Fietzke, J., and Correa, M. L.: Stable Sr-isotope, Sr/Ca, Mg/Ca, Li/Ca and Mg/Li ratios in the scleractinian cold-water coral *Lophelia pertusa*, *Chemical Geology*, 352, 143-152, <https://doi.org/10.1016/j.chemgeo.2013.06.013>, 2013.
- Ridgwell, A., and Zeebe, R. E.: The role of the global carbonate cycle in the regulation and evolution of the Earth system, *Earth and Planetary Science Letters*, 234, 299-315, <https://doi.org/10.1016/j.epsl.2005.03.006>, 2005.
- Romanek, C. S., Grossman, E. L., and Morse, J. W.: Carbon isotopic fractionation in synthetic aragonite and calcite: effects of temperature and precipitation rate, *Geochimica et cosmochimica acta*, 56, 419-430, [https://doi.org/10.1016/0016-7037\(92\)90142-6](https://doi.org/10.1016/0016-7037(92)90142-6), 1992.
- Rozanski, K., Araguás-Araguás, L., and Gonfiantini, R.: Isotopic patterns in modern global precipitation, *Climate change in continental isotopic records*, 78, 1-36, <https://doi.org/10.1029/gm078p0001>, 1993.
- Rubinson, M., and Clayton, R. N.: Carbon-13 fractionation between aragonite and calcite, *Geochimica et Cosmochimica Acta*, 33, 997-1002, [https://doi.org/10.1016/0016-7037\(69\)90109-4](https://doi.org/10.1016/0016-7037(69)90109-4), 1969.
- Sanford, W. E. and Konikow, L. F.: Simulation of calcite dissolution and porosity changes in saltwater mixing zones in coastal aquifers, *Water Resources Research*, 25, 655-667, <https://doi.org/10.1029/wr025i004p00655>, 1989.
- Sayles, F., Mangelsdorf Jr, P., Wilson, T., and Hume, D.: A sampler for the in situ collection of marine sedimentary pore waters, *Deep Sea Research and Oceanographic Abstracts*, 259-264, [https://doi.org/10.1016/0011-7471\(76\)91331-0](https://doi.org/10.1016/0011-7471(76)91331-0), 1976.

- Seeberg-Elverfeldt, J., Schlüter, M., Feseker, T. and Kölling, M.: Rhizon sampling of porewaters near the sediment-water interface of aquatic systems. *Limnology and oceanography: Methods*, 3, 361-371, <https://doi.org/10.4319/lom.2005.3.361>, 2005.
- Schrum, H. N., Murray, R. W., and Gribsholt, B.: Comparison of Rhizon sampling and whole round squeezing for marine sediment porewater, *Scientific Drilling*, 13, 47-50, <https://doi.org/10.5194/sd-13-47-2012>, 2012.
- Steiner, Z., Lazar, B., Erez, J., and Turchyn, A. V.: Comparing Rhizon samplers and centrifugation for pore-water separation in studies of the marine carbonate system in sediments, *Limnology and Oceanography: Methods*, 16, 828-839, <https://doi.org/10.1002/lom3.10286>, 2018.
- Swart, P. K., James, N. P., Mallinson, D., Malone, M. J., Matsuda, H., and Simo, T.: 10. Data Report: Carbonate Mineralogy of Sites Drilled during Leg 182, <https://doi.org/10.2973/odp.proc.sr.182.010.2002>, 2002.
- Swart, P. K.: The geochemistry of carbonate diagenesis: The past, present and future, *Sedimentology*, 62, 1233-1304, <https://doi.org/10.1111/sed.12205>, 2015.
- Urey, H. C.: The thermodynamic properties of isotopic substances, *Journal of the Chemical Society (Resumed)*, 562-581, <https://doi.org/10.1039/jr9470000562>, 1947.
- Vairavamurthy, M. A., Orr, W. L., and Manowitz, B.: Geochemical transformations of sedimentary sulfur: an introduction, 1-14, <https://doi.org/10.1021/bk-1995-0612.ch001>, 1995.
- Van Der Loeff, M. R.: Time variation in interstitial nutrient concentrations at an exposed subtidal station in the Dutch Wadden Sea, *Netherlands Journal of Sea Research*, 14, 123-143, [https://doi.org/10.1016/0077-7579\(80\)90018-6](https://doi.org/10.1016/0077-7579(80)90018-6), 1980.
- Van Lith, Y., Vasconcelos, C., Warthmann, R., Martins, J., and McKenzie, J.: Bacterial sulfate reduction and salinity: two controls on dolomite precipitation in Lagoa Vermelha and Brejo do Espinho (Brazil), *Hydrobiologia*, 485, 35-49, <https://doi.org/10.1023/a:1021323425591>, 2002.
- Vasconcelos, C., McKenzie, J. A., Bernasconi, S., Grujic, D., and Tiens, A. J.: Microbial mediation as a possible mechanism for natural dolomite formation at low temperatures, *Nature*, 377, 220-222, <https://doi.org/10.1038/377220a0>, 1995.
- Vasconcelos, C., and McKenzie, J. A.: Microbial mediation of modern dolomite precipitation and diagenesis under anoxic conditions (Lagoa Vermelha, Rio de Janeiro, Brazil), *Journal of sedimentary Research*, 67, 378-390, <https://doi.org/10.1306/d4268577-2b26-11d7-8648000102c1865d>, 1997.
- Watson, P. G., and Frickers, T. E.: A multilevel in situ pore-water sampler for use in intertidal sediments and laboratory microcosms, *Limnology and Oceanography*, 35, 1381-1389, <https://doi.org/10.4319/lo.1990.35.6.1381>, 1990.
- Wombacher, F., Eisenhauer, A., Böhm, F., Gussone, N., Regenber, M., Dullo, W.-C., and Rüggeberg, A.: Magnesium stable isotope fractionation in marine biogenic calcite and aragonite, *Geochimica et Cosmochimica Acta*, 75, 5797-5818, <https://doi.org/10.1016/j.gca.2011.07.017>, 2011.
- Wray, J. L., and Daniels, F.: Precipitation of calcite and aragonite, *Journal of the American Chemical Society*, 79, 2031-2034, <https://doi.org/10.1021/ja01566a001>, 1957.
- Zeebe, R. E., and Wolf-Gladrow, D.: CO₂ in seawater: equilibrium, kinetics, isotopes, 65, Gulf Professional Publishing, [https://doi.org/10.1016/s0422-9894\(01\)x8001-x](https://doi.org/10.1016/s0422-9894(01)x8001-x), 2001.

2. Authigenic formation of Ca-Mg carbonates in the shallow alkaline Lake Neusiedl, Austria

Dario Fussmann, Avril Jean Elisabeth von Hoyningen-Huene, Andreas Reimer, Dominik Schneider, Hana Babková, Robert Peticzka, Andreas Maier, Gernot Arp, Rolf Daniel, and Patrick Meister

Biogeosciences (2020), 17, 2085–2106

Abstract. Despite advances regarding the microbial and organic-molecular impact on nucleation, the formation of dolomite in sedimentary environments is still incompletely understood. Since 1960, apparent dolomite formation has been reported from mud sediments of the shallow, oligohaline and alkaline Lake Neusiedl, Austria. To trace potential dolomite formation or diagenetic alteration processes in its deposits, lake water samples and sediment cores were analyzed with respect to sediment composition, hydrochemistry and bacterial community composition. Sediments comprise 20 cm of homogenous mud with 60 wt% carbonate, which overlie dark-laminated consolidated mud containing 50 wt% carbonate and plant debris. Hydrochemical measurements reveal a shift from oxic lake water with pH 9.0 to anoxic sediment pore water with pH 7.5. A decrease in SO_4^{2-} with a concomitant increase of $\Sigma\text{H}_2\text{S}$ and NH_4^+ from 0-15 cm core depth, indicates anaerobic heterotrophic decomposition, including sulfate reduction. The bacterial community composition reflects the zonation indicated by the pore water chemistry, with a distinct increase of fermentative taxa below 15 cm core depth.

The water column is highly supersaturated with respect to (disordered) dolomite and calcite, whereas saturation indices of both minerals rapidly approach zero in the sediment. Notably, the relative proportions of different authigenic carbonate phases and their stoichiometric compositions remain constant with increasing core depth. Hence, evidence for Ca-Mg carbonate formation or ripening to dolomite is lacking within the sediment of Lake Neusiedl. As a consequence, precipitation of high-magnesium-calcite (HMC) and protodolomite does not occur in association with anoxic sediment and sulfate reducing conditions. Instead, analytical data for Lake Neusiedl suggest that authigenic HMC and protodolomite precipitate from the supersaturated, well-mixed aerobic water column. This observation supports an alternative concept to dolomite formation in anoxic sediments, comprising Ca-Mg carbonate precipitation in the water column under aerobic and alkaline conditions.

2.1 Introduction

Dolomite ($\text{CaMg}[\text{CO}_3]_2$) is the most abundant carbonate mineral in Earth's sedimentary record. It has rarely been observed forming in recent environments. Instead, most occurrences of large dolomite deposits in the geological record are the result of pervasive dolomitization of precursor carbonates by fluids with high Mg:Ca ratios and temperatures during burial (e.g. Machel, 2004). In contrast, the formation of dolomite near the sediment surface, so-called penecontemporaneous dolomite (Machel 2004 and references therein), or even primary precipitation in shallow aquatic environments, are often difficult to trace in the rock record and capture in modern environments. The difficulty in capturing ongoing dolomite formation is due to its peculiar kinetics, which are still incompletely understood, despite intense laboratory and field experiments. Dolomite does not form in sites where sufficient Ca, Mg, and carbonate ions are provided, which is generally explained by the high kinetic barrier of dolomite nucleation and growth (e.g. Lippmann, 1973).

Based on the presence of sulfate-reducing bacteria, Vasconcelos et al. (1995) proposed a microbial model, in which sulfate-reducing bacteria mediate carbonate precipitation, while Brady et al. (1996) consider sulfate ions as inhibitors for dolomite growth. Further experiments were performed with various organisms, such as denitrifiers (Rivadeneira et al., 2000), methanogenic archaea (Roberts et al., 2004) and aerobic halophilic bacteria (Sánchez-Román et al., 2009). All of these studies showed aggregate formation of carbonate minerals with the characteristic d_{104} -peak of dolomite under X-ray diffraction, hence, supporting a microbial factor in dolomite formation. It has been hypothesized that dolomite nucleation is mediated by microbial extracellular polymeric substances (EPS; Bontognali et al., 2014). However, Gregg et al. (2015) re-analyzed the X-ray diffraction data of many of the aforementioned microbial experiments, demonstrating that microbial dolomite products lack typical ordering reflections in XRD spectra and are in fact very high-magnesium-calcite (VHMC or "protodolomite"). In further studies sulfide (Zhang et al., 2013b), dissolved organic matter (Frisia et al., 2018) or clay minerals (Liu et al., 2019) were suggested to favor protodolomite nucleation in pore fluids. Nevertheless, it is not entirely clear, which of these factors play a fundamental role in natural environments and how the specific reaction mechanisms work.

While the concept that dolomite forms within sediments mediated by anaerobic microbial processes and their extracellular polymeric substances, is widely acknowledged, another aspect should be taken into account: the site of dolomite formation may not always coincide with the location where the mineral is found due to relocation after precipitation. Several studies describe unlithified dolomite precipitation in warm, arid and hypersaline marine environments, like coastal sabkhas (Illing et al., 1965; Bontognali et al., 2010; Court et al., 2017), coastal lakes, such as Lagoa Vermelha in Brazil (Vasconcelos and McKenzie, 1997; Van Lith et al., 2002; Sánchez-Román et al., 2009; Bahniuk et al., 2015) and ephemeral lakes along the Coorong Lagoon in South Australia (von der Borch, 1976; Rosen et al., 1989; Warren, 1990; Wright and Wacey, 2005). Dolomite precipitation is further reported in endorheic hypersaline lakes, e. g. Lake Qinghai in Tibet (Deng et al., 2010), Lake Acigöl (Turkey; Balci et al., 2016) and alkaline playa lakes such as Deep Springs Lake in California (Meister et al., 2011).

Another Ca-Mg carbonate forming location can be found in Turkey, where McCormack et al. (2018) describe dolomite in Quaternary sediments from Lake Van, which is suggested to have formed at the sediment-water interface characterized by varying salinities and low temperatures. These dolomite-bearing deposits have been related to the onset of a falling paleo lake-level and, hence, changing hydro-chemical conditions. Importantly, McCormack et al. (2018) locate the formation of dolomite near the sediment-water interface, where it is presumably related to microbial EPS. However, this area is also exposed to significant fluctuations in pH, temperature, and supersaturation. Precipitation-

experiments conducted by Deelman (1999) have shown that dolomite can form due to such fluctuations in pH and temperature. Hence, they agree with Ostwald's step rule, because dolomite formation happens via undersaturation of other metastable carbonate phases.

Lake Neusiedl is a Ca-Mg carbonate precipitating water body with exceptionally low salinity (1-2 g L⁻¹). It is a shallow and seasonally evaporative lake in the proximity of Vienna, Austria. Schroll and Wieden (1960) first reported the occurrence of poorly crystallized dolomite (notable by its broad XRD-reflections) at this locality and Müller et al. (1972) related its formation to diagenetic alteration of high-magnesium-calcite (HMC). The Mg:Ca ratios in Lake Neusiedl are unusually high (>7) compared to freshwater lakes, which favor the precipitation of HMC (Müller et al., 1972). Little is known about the crystallization paths of the Ca-Mg carbonate phases in this lake, in particular whether they form in the anoxic sediment or oxic water column and if early diagenetic alteration to dolomite ("ripening") takes place.

We revisit the formation of dolomite in Lake Neusiedl by comparing the sediment-geochemical and *in-situ* pore water data and critically evaluating the location of precipitation. This approach has been used to study dolomite formation in Lagoa Vermelha (Van Lith et al. 2002; Moreira et al., 2004) or in Deep Springs Lake (Meister et al., 2011). Since 2005, *in-situ* pore water extraction via rhizon samplers has been applied for geoscientific research questions (Seeberg-Elverfeldt et al., 2005) and several *in situ* pore water studies were conducted using this technique (e.g. Bontognali, 2010; Birgel et al., 2015; Steiner et al., 2018). Comparable *in-situ* pore water data from an oligohaline seasonally evaporative lake, which address the question of authigenic Ca-Mg carbonate precipitation, are absent so far. We further provide bacterial community analyses to address the potential role of microbes and their metabolisms in a carbonate mineral precipitation or alteration pathway. Hence, our study has three goals: (i) finding indications for the origin of Ca-Mg carbonate formation, (ii) evaluating the microbiological and geochemical conditions and their influence on carbonate saturation, and (iii) discussing which factors drive the formation of Ca-Mg carbonates in Lake Neusiedl.

2.2 Study Area

Lake Neusiedl, situated at the Austrian-Hungarian border, is the largest endorheic lake in Western Europe. It is located in the Little Hungarian Plain, a transition zone between the Eastern Alps and the Pannonian Basin in central Hungary. The region has been tectonically active since the early Miocene (Horváth, 1993) and is affected by NE-SW trending normal faults. This early Miocene tectonic activity included the closing of the Central Paratethys Sea and the formation of Lake Pannon about 11.6 million years ago. This ancient water body was characterized by highly fluctuating water levels that caused the deposition of local evaporite layers, which influence the salinity of today's deeper aquifers in the area (Piller et al., 2007; Krachler et al., 2018). The present topography of the Little Hungarian Plain is the result of ongoing local uplift and subsidence, which commenced in the latest Pliocene (Zámolyi et al., 2017). Elevated regions are represented by the Rust- and Leitha Hills, which are horst-like structures located west of Lake Neusiedl. Northward, the water body is separated from the Vienna basin by the raised Parndorf Plateau, which has a 25-45 m higher surface elevation than the lake area. South- and eastward, Lake Neusiedl is surrounded by flats, namely the Hansag- and Seewinkel Plain. Despite its proximity to the Alps, the region surrounding Lake Neusiedl did not have an ice cover during the last glacial maximum. Hence, its morphology is shaped by periglacial erosion and sedimentation (van Husen, 2004). Throughout the Seewinkel Plain, Pannonian marine to brackish sediments are largely covered by fluvio-glacial gravels. The gravels thin out westwards and are thus missing beneath parts of Lake Neusiedl, where fine-grained, unlithified lacustrine mud directly overlies compacted Pannonian strata (Loisl et al., 2018). The absence of a gravel layer has made the former lake area vulnerable to

aeolian erosion, favoring the formation of the present day flat trough over tectonic subsidence (Zámolyi et al., 2017).

The surface area of the water body spreads over 315 km² with a maximum depth of 1.8 m. With a salinity of 1-2 g·L⁻¹ and elevated pH values (>8.5), the water chemistry differs significantly from that of freshwater lakes (salinity: < 0.5 g·L⁻¹, pH: 6.5-7.5). Increased amounts of sodium- and bicarbonate ions mainly contribute to the lake's soda-like character (Herzig, 2014). Furthermore, the Mg:Ca ratio is unusually high in comparison to freshwater lakes (Krachler et al., 2012). Permanent surface water inflow is mainly provided by the Rákos and the Wulka streams, which drain a catchment area that is approximately 2.6 times the size of Lake Neusiedl (1.120 km²). Thus, their contribution to the lake's water balance is negligible compared to the significantly higher input from precipitation, providing 80 – 90% of the lake water (Herzig and Dokulil, 2001). As a result of its shallowness and the endorheic drainage system, the lake is very vulnerable to climatic changes, which highly influence the water level, water volume and, hence, the surface area of the lake throughout the year and over the centuries. In the past, Lake Neusiedl was characterized by highly fluctuating water levels and desiccation events (Moser, 1866), the last of which dates back between 1865 and 1870. Since 1910, the lake's water outflow can be regulated by the artificial Hanság- or Einser-Kanal in case of severe flooding events. The canal is located at the lake's southeastern shore (Figure 2.1).

More than half (178 km²) of Lake Neusiedl's surface area is covered with reed. Due to its wind exposure and shallowness, the water column of the open water area is well mixed and contains high amounts of suspended particles. The wind sheltering effect of *Phragmite* spears, in contrast, leads to clearer water in the reed belt. Clastic input into the water body is minor and reflects the mineralogical composition of the western neighboring Rust- and Leitha hills, which are characterized by crystalline rocks of the Eastern Alpine basement and Miocene marine carbonates ("Leithakalk", Figure 2.1). The deposits forming the present bed of Lake Neusiedl consist of fine-grained mud, which mainly contains typical authigenic carbonate phases such as Mg-calcite and protodolomite (Löffler, 1979). Those phases can clearly be distinguished from pure calcite, which is considered as allochthonous in the sedimentary environment of Lake Neusiedl (Müller et al., 1972). It is noteworthy that the mud volume has doubled in the time from 1963 to 1988, leading to an increase of the volumetric mud/water ratio from 36:64 in 1963, to 49:51 in 1988. This mud layer covers the whole lake area and would yield an average thickness of 64 cm, assuming an equal distribution across the lake basin (Bácsatyai, 1997). The thickness of soft sediment can increase up to 1 m at the border of the reed belt and open water, where *Phragmite* spears act as sediment traps for current driven, suspended particles (Löffler 1979).

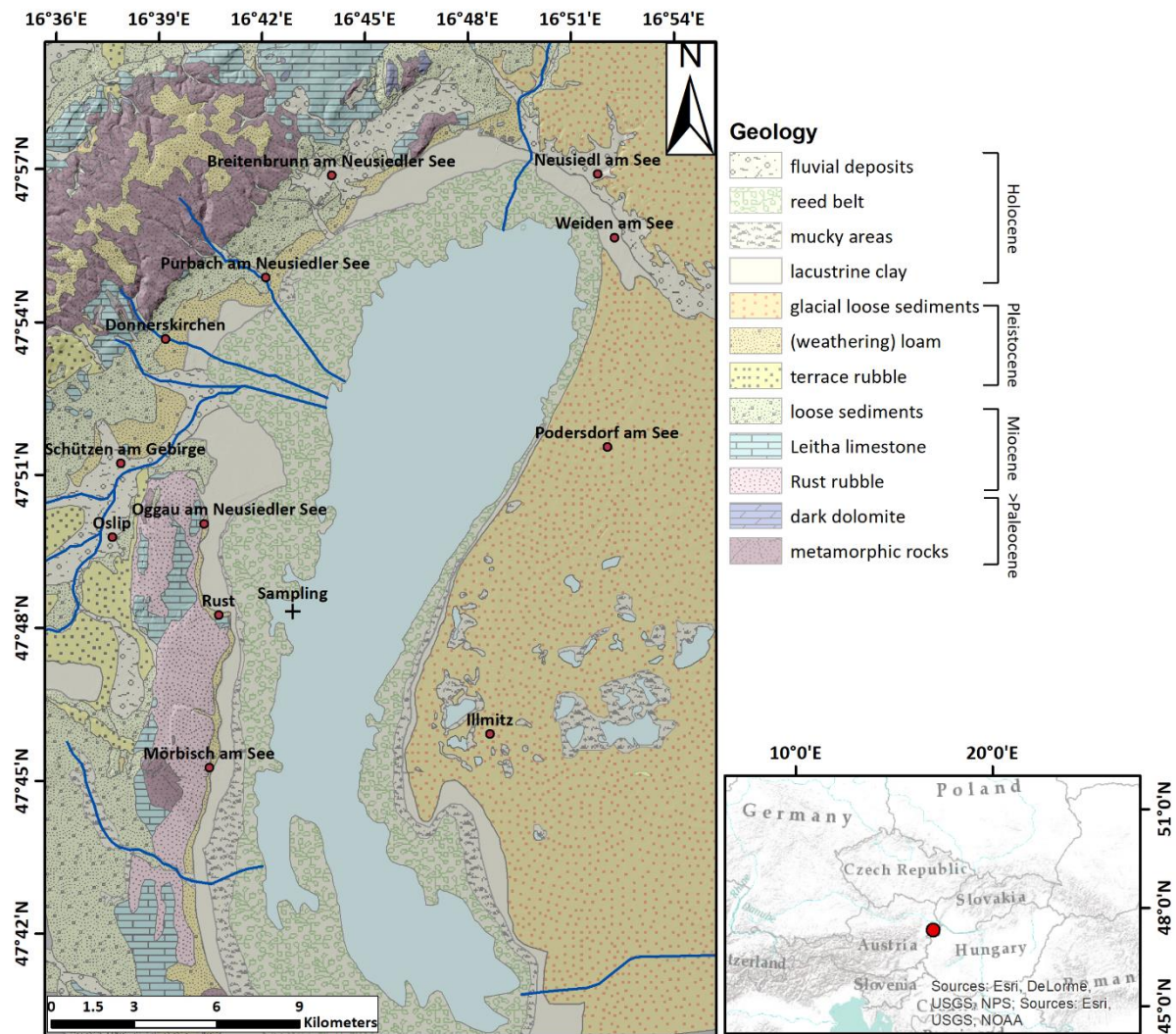


Figure 2.1: Lake Neusiedl and its surrounding geology, redrawn and simplified after Herrman et al. (1993).

2.3 Material and Methods

2.3.1 Sampling and field measurements

The sampling campaign at Lake Neusiedl was performed in August 2017 in the bay of Rust (16°42'33.635"E, 47°48'12.929"N) situated at the lake's central western shore. A pedalo boat was utilized to enable sampling approximately 500 m offshore. Physicochemical parameters of the lake water were measured directly in the field using a WTW Multi 3430 device equipped with a WTW Tetracon 925 conductivity probe, a WTW FDO 925 probe for dissolved O₂, and a WTW Sentix 940 electrode for temperature and pH (Xylem, Rye Brook, NY, USA), calibrated against standard pH-buffers 7.010 and 10.010 (HI6007 and HI6010, Hanna Instruments, Woonsocket, RI, USA; standard deviation ≤ 2%). Lake water was retrieved from a depth of 10 cm with a 500 ml Schott-Duran glass bottle without headspace from which subsamples for anion, nutrient and total alkalinity determination were distributed into 100 mL polyethylene (PE) and 250 mL Schott-Duran glass bottles (Schott, Mainz, Germany), respectively. For cation analysis, a 50 mL aliquot was filtered through membrane filters with a pore size of 0.7 μm (Merck, Darmstadt, Germany) into a PE-bottle and acidified with 100 μl HNO₃ (sub-boiled). Total alkalinity was determined via titration within 3 hours after sampling using a hand-held titration device and 1.6 N H₂SO₄ cartridges (Hach Lange, Düsseldorf, Germany; standard deviation ≤ 1.5%).

Five sediment cores, with the sample codes LN-K01, LN-K02, LN-K03, LN-K04 and LN-K05, were retrieved using PVC-tubes (6.3 cm diameter; Uwitec, Mondsee, Austria) in approximately 30 cm lateral distance. All cores were 30 to 40 cm in length and were used for sediment, pore water and bacterial community profiling. Cores LN-K01 and LN-K02 were subsampled and treated for bacterial community profiling as described in von Hoyningen-Huene et al. (2019) directly after recovery. Cores LN-K03, LN-K04 and LN-K05 were hermetically sealed after recovery and stored upright at temperatures close to their natural environment (22 ± 2 °C). Effects of pressure differences are neglectable in the present case, because the cores were sampled just below the lake floor.

2.3.2 Petrographic, mineralogical, and geochemical analyses

Two cores, labelled LN-K04 and LN-K05, were used for sediment geochemical and petrographic analyses. Sediment dry density and porosity were calculated from the corresponding sediment weights and volumes. For bulk organic and inorganic carbon content detection, sediment increments of 2.5 cm were subsampled from core LN-K04. They were freeze dried and powdered with a ball mill, before they were measured by a LECO RC612 (Leco, St Joseph, MI, USA) multi-phase carbon and water determination device. For calibration, Leco synthetic carbon (1 and 4.98 carbon%) and Leco calcium carbonate (12 carbon%) standards were used. The same increments were utilized for CNS elemental detection, which was operated with a Euro EA 3000 Elemental Analyzer (Hekatech, Wegberg, Germany). 2,5-Bis (5-tert-benzoxazol-2-yl) thiophene BBOT and atropine sulfate monohydrate (IVA Analysetechnik, Meerbusch, Germany) were provided as reference material. Analytical accuracy of all analyses was better than 3.3%.

XRD-analyses were conducted with identical increments at the Department of Geodynamics and Sedimentology in Vienna by a PANanalytical (Almelo, Netherlands) Xpert Pro device ($\text{CuK}\alpha$ radiation, 2θ refraction range of 2-70°, and a step size of 0.01°). Semi-quantitative phase composition analysis was performed with Rietveld refinement of peak intensities by using MAUD (version 2.8; Lutterotti et al., 2007). To ensure a better reproducibility of the semi-quantitative XRD-analysis, Rietveld refined results were compared and correlated with carbon data retrieved from the aforementioned LECO RC612 device.

In core LN-K05, sediment increments of 5 cm were subsampled for thin sectioning and light microscopic observations. To ensure a continuous section, rectangular steel meshes, 5 cm in length, were placed along the sediment column. These steel meshes, filled with soft sediment, were then embedded in LR White resin (London Resin Company, Reading, United Kingdom), after a dehydration procedure with ethanol. During dehydration, the sediments were treated with Sytox Green nucleic acid stain (Invitrogen, Carlsbad, CA, USA) to stain eukaryotic cell nuclei and prokaryotic cells for fluorescence microscopy. Samples were cured for 24 hours at 60°C before thin section preparation. The thin sections were ground down to a thickness of 40 to 50 μm and then capped with a glass cover. Petrographic observations were conducted with a petrographic and a laser-scanning microscope (Zeiss, Oberkochen, Germany, lsm excitation: 543 nm, 488 nm, 633 nm, laser unit: Argon/2, HeNe543, HeNe633).

For scanning electron microscopy, non-capped unpolished thin section fragments and freeze-dried loose sediment from cores LN-K05 and LN-K04 were placed on 12.5 mm plano carriers and sputtered with a platinum-palladium mixture. Field emission scanning electron microscopy was conducted with a Gemini Leo 1530 device (Zeiss, Oberkochen, Germany) with a coupled INCA x-act (Oxford Instruments, Abingdon, United Kingdom) EDX detector.

2.3.3 Pore water analysis

Redox potential and pH gradients were directly measured in the sediment of core LN-K03 one week after sampling with a portable WTW 340i pH meter, equipped with an Inlab Solids Pro pH-electrode (Mettler Toledo, Columbus, OH, USA) and a Pt 5900 A redox electrode (SI Analytics, Mainz, Germany) through boreholes (standard deviation $\leq 2\%$). Pore water was extracted from the core, using 5 cm CSS Rhizon samplers (Rhizosphere, Wageningen, Netherlands). Immediately after extraction, aliquots were fixed with Zn-acetate for determination of total sulfide ($\Sigma\text{H}_2\text{S}$). Pore water alkalinity was determined using a modified Hach titration method with self-prepared 0.01 N HCl cartridges as titrant. Major cation (Ca^{2+} , Mg^{2+} , Na^+ , K^+ and Li^+) and anion (Cl^- , F^- , Br^- , SO_4^{2-} and NO_3^-) concentrations of lake and pore water samples (including supernatants in the cores) were analyzed by ion chromatography with non-suppressed and suppressed conductivity detection, respectively (Metrohm 820 IC / Metrosep C3-250 analytical column, Metrohm 883 Basic IC/ Metrohm ASupp5-250 analytical column, Metrohm, Herisau, Switzerland; standard deviation $\leq 2\%$). Inductively coupled plasma mass spectrometry (ICP-MS; ICAP-Q, Thermo Fisher, Waltham, MA, USA) was used to determine Sr, Ba, Fe, Mn, Rb and B, as control for the cation determination by ion chromatography (standard deviation $\leq 3\%$).

Concentrations of NH_4^+ , NO_2^- , PO_4^{3-} , $\Sigma\text{H}_2\text{S}$ and dissolved silica ($\text{SiO}_{2(\text{aq})}$) were measured by photometric methods according to Grasshoff et al. (2009), using a SI Analytics Uviline 9400 spectrophotometer. In addition, methane and dissolved inorganic carbon (DIC) amounts were retrieved from a different core, sampled at the same locality in August 2017. Methane concentrations were determined from 5 cm^3 sediment samples stored upside down in gas-tight glass bottles containing 5 mL NaOH (5% w/v). Aliquots of 5 ml headspace methane were transferred to evacuated 10 ml vials. The aliquots were analyzed with an automated headspace gas chromatograph (GC Agilent 7697A coupled to an Agilent 7890B auto sampler) at the University of Vienna. Methane concentrations were quantified at a runtime of 1.798 min by a flame ionization detector and a methanizer. For linear calibration, a standard series with the concentrations 1001 ppb, 3013 ppb and 10003 ppb was used. DIC concentrations were retrieved by using a Shimadzu TOC-LCPH (Shimadzu, Kyoto, Japan) analyzer with an ASI-L autosampler and a reaction vessel containing a reaction solution of phosphoric acid (H_3PO_4 , 25%). The DIC was measured by conversion to carbon dioxide, which was detected by a NDIR detector.

All measured values were processed with the PHREEQC software package (version 3; Parkhurst and Appelo, 2013). The implemented phreeqc.dat and wateqf4.dat databases were used in order to calculate ion activities and $p\text{CO}_2$ (partial pressure of CO_2) of the water samples and mineral saturation states. The saturation indices of mineral phases are given as $\text{SI} = \log(\text{IAP}/K_{\text{so}})$.

2.3.4 Bacterial 16S rRNA gene community profiling

Two sediment cores labelled LN-K01 and LN-K02 were sampled for bacterial 16S rRNA gene-based community profiling. Each core was sampled in triplicate at every 2.5-5 cm of depth and the surface water filtered through a 2.7 (Merck, Darmstadt, Germany) and 0.2 μm (Sartorius, Göttingen, Germany) filter sandwich. RNAprotect Bacteria Reagent (Qiagen, Hilden, Germany) was immediately added to all samples, in order to preserve the nucleic acids. Before storage at -80°C , the samples were centrifuged for 15 min at $3.220 \times g$ and the RNAprotect Bacteria Reagent was decanted.

DNA was extracted and 16S rRNA genes were amplified and sequenced as described in detail by von Hoyningen-Huene et al. (2019). Briefly, DNA was extracted from 250 mg of each homogenized sediment sample or one third of each filter with the MoBio PowerSoil DNA isolation kit (MoBio, Carlsbad, CA, USA) according to manufacturer's instructions with an adjusted cell disruption step. Bacterial 16S rRNA genes were amplified in triplicate by PCR with the forward primer D-Bact-0341-b-S-17 and the reverse primer S-D-Bact-0785-a-A-21 (Klindworth et al., 2013) targeting the V3-V4

hypervariable regions. Primers included adapters for sequencing on an Illumina MiSeq platform. PCR triplicates were pooled equimolar and purified with MagSi-NGS^{Prep} magnetic beads (Steinbrenner, Wiesenbach, Germany) as recommended by the manufacturer and eluted in 30 µl elution buffer EB (Qiagen, Hilden, Germany).

PCR products were sequenced with the v3 Reagent kit on an Illumina MiSeq platform (San Diego, CA, USA) as described by Schneider et al. (2017). Sequencing yielded a total of 6,044,032 paired-end reads, which were quality-filtered (fastp, version 0.19.4; Chen et al., 2018), merged (PEAR, version 0.9.11; Zhang et al., 2013a) and processed. This comprised primer clipping (cutadapt, version 1.18; Martin, 2011), size-filtering, dereplication, denoising and chimera removal (VSEARCH, v2.9.1; Rognes et al., 2016). Taxonomy was assigned to the resulting amplicon sequence variants (ASVs; Callahan et al., 2017) via BLAST 2.7.1+ against the SILVA SSU 132 NR (Quast et al., 2012). After taxonomic assignment, 2,263,813 merged reads remained in the dataset. The resulting ASV abundance table was used for the visualization of community gradients along the cores (von Hoyningen-Huene et al., 2019). Data were analyzed using R (version 3.5.2; R Core Team, 2018) and RStudio (version 1.1.463; RStudio; R Team, 2016) using the base packages. Extrinsic domains, archaea and eukaryotes were removed from the ASV table for analysis. All ASVs with lower identity than 95% to database entries were assigned as unclassified. Replicates for each depth were merged, transformed into relative abundances and all ASVs with an abundance > 0.5% were summarized by their phylogenetic orders. Putative functions of all orders were assigned according to literature on cultured bacterial taxa and the closest cultured relatives of the ASVs present in our samples. For uncultured taxa, functions were inferred from literature on genomic and metagenomic sequencing data (Suppl. Material Tab. S6). The resulting table with relative abundances and functional assignments was used to generate bar charts in SigmaPlot (version 11; Systat Software, 2008).

2.4 Results

2.4.1 Sediment petrography and mineralogy

The cored sediment can be divided into three different lithological units, with depths presented as cm below sediment top. Unit I, in the first 15 cm, is characterized by homogenous, light to medium grey mud with very high water content and porosity (>65 weight%, 0,67). The mud consists of very fine-grained carbonate and siliciclastics, largely in the clay and silt size fraction. In the thin sections of embedded mud samples, carbonates make up most of the fine-grained matrix (Figure 2.2A and B). Remnants of diatoms and ostracods occur with random orientation. Detrital grains up to fine sand fraction, consisting of quartz, feldspar, mica, chlorite and carbonates make up as much as 20% of the sediment. The latter are distinguishable from authigenic carbonate phases by their bigger (up to mm measuring) size and fractured shape. The $C_{org}:N_{tot}$ ratio scatters around 10 (Figure 2.3) and plant detritus is evident in thin sections as opaque, up to several hundred µm in size, often elongated and randomly orientated particles (Figure 2.2A and B). These can be identified in the laser scan images, due to their chlorophyll related bright fluorescence (Figure 2.4A and B).

Unit II is located between 15 and 22 cm and appears as slightly darker, grey-colored mud without macrostructures. The microcrystalline matrix appearance is similar to Unit I, however, phytoclasts and detrital mineral grains are more abundant and up to mm in size, whereas the amount of bioclasts remains the same. Noticeably, detrital carbonate minerals and quartz grains occur layer-like or in defined lenses (Figure 2.2C and D). The component to matrix ratio slightly increases up to 25:75% and cubic, small (up to 10 µm), opaque minerals often occur intercalated with plant detritus. The $C_{org}:N_{tot}$ ratio also changes from 10 at 15 cm to 12 at 22 cm.

Unit III, occurs from 22 to 40 cm. It is distinctly darker than the units above and shows a significant decrease in water content and porosity to <50 weight% and <0.6, respectively. This decrease in porosity is also recognizable by a more cohesive sediment texture. Lamination is visible at the core's outer surface, but not in the cut section, in which plant detritus noticeably increases. Thin sections of this unit illustrate a rather compacted matrix, a horizontal orientation of elongated phytoclasts and a layered structure with detrital mineral grains (Figure 2.2E and F), further supported by the laser scan image (Figure 2.4C). Ostracod or diatom fragments still occur but are less abundant than in the units above. The particle to matrix ratio increases up to 35:65 % and the $C_{org}:N_{tot}$ ratio steadily increases from 12 to 14 through Unit III.

In SEM images, the matrix appears as microcrystalline aggregate of several nanometer-sized clotted crumbs (Figure 2.5). Locally, small, up to 1 μm in scale, irregularly shaped rhombohedral crystals are observable. With EDX measurements, these tiny crystals were identified as Ca-Mg carbonate phases. According to the XRD spectra, the bulk sediment mainly consists of carbonates and quartz with minor contributions of feldspar, clay, and mica (Figure 2.6). The d_{104} peak shift provides a suitable approach to estimate the Mg:Ca ratio in magnesium calcite and dolomite (Lumsden, 1979). Based on the d_{104} peak positions, three carbonate phases with different MgCO_3 -content are present: A calcite phase with minor amounts of MgCO_3 , a high-magnesium-calcite phase (HMC) with circa 18 mole% MgCO_3 and a very-high-magnesium-calcium-carbonate phase (protodolomite, Figure 2.6). The latter shows a 104 peak, shifted from $31^\circ 2\theta$ in ordered dolomite to ca. $30.8^\circ 2\theta$, indicating a MgCO_3 content of approx. 45 mole%. Due to the fact that typical dolomite ordering peaks (i.e. 01.5 and 10.1) could not be identified in the XRD spectra, we informally define the phase as "protodolomite", i. e. a carbonate phase with a nearly 1:1 stoichiometry of Ca and Mg, in which an incipient dolomite structure may or may not be present. Estimated relative mineral abundances vary between the three units (Figure 2.7): In Unit I the amount of authigenic carbonate minerals remains relatively constant at 55 weight%, whereas in Unit II a steep/large increase of detrital mineral phases (feldspar, quartz, calcite, mica) can be found. In Unit III the amount of Ca-Mg carbonate phases decreases and scatters around 40 weight%. Mica slightly increase with depth below 23 cm. Nevertheless, the authigenic HMC to protodolomite ratio does not change significantly throughout the section. Notably, neither authigenic Ca-Mg carbonate phase shows any down-core trend in stoichiometry. The $\text{Mg}/(\text{Ca}+\text{Mg})$ ratios of distinct solid phases remain largely constant with depth (Figure 2.8).

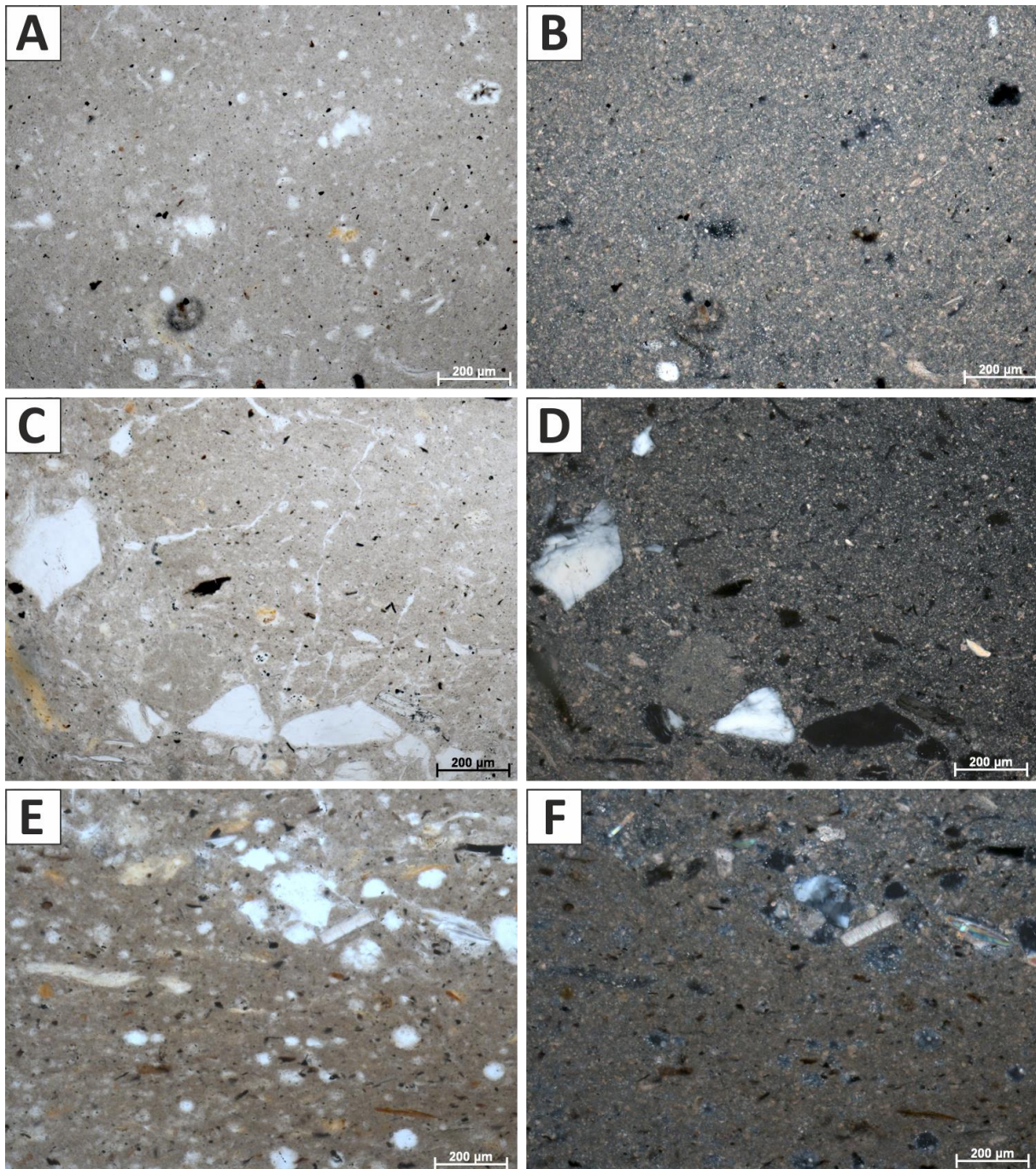


Figure 2.2: (A) Microfabric of Unit I at 5 cm depth in transmitted light. Note the randomly oriented, opaque and brownish plant particles. The microcrystalline matrix is more apparent under crossed polars (B). (C) Microfabric overview of Unit II at 17 cm depth. Large, up to fine sand-scale detrital feldspar grains occur in layers. (D) Same image section under crossed polars. (E) Microfabric of Unit III at 28 cm, illustrating the rather compacted shape of the matrix and the elongated appearance of plant detritus. The layering is evident by the occurrence of larger detrital grains in the upper image part. (F) Same section under crossed polars.

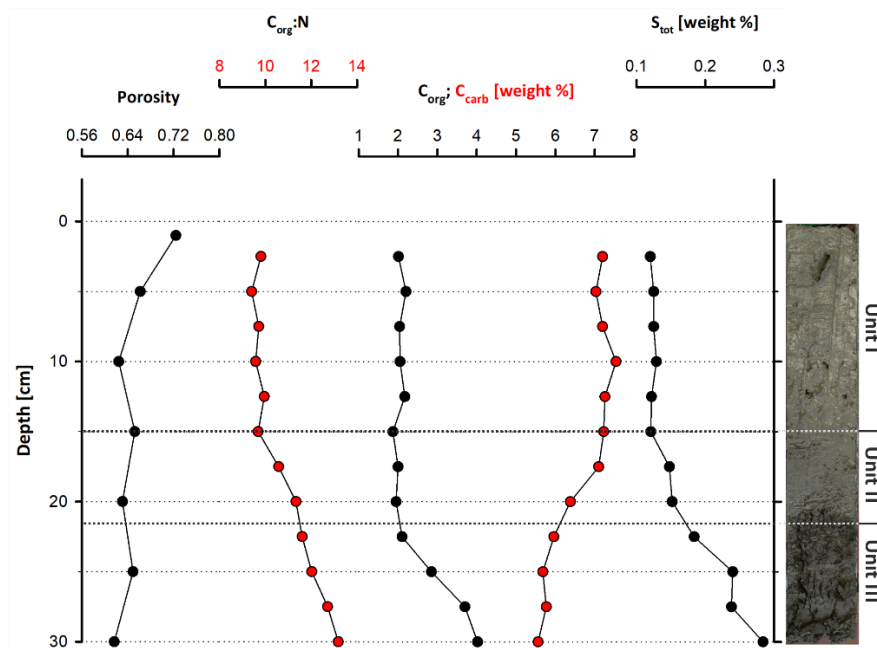


Figure 2.3: Geochemical parameters through Core LN-K04, showing an increasing amount of organic carbon, total sulfur and a decreasing porosity with depth.

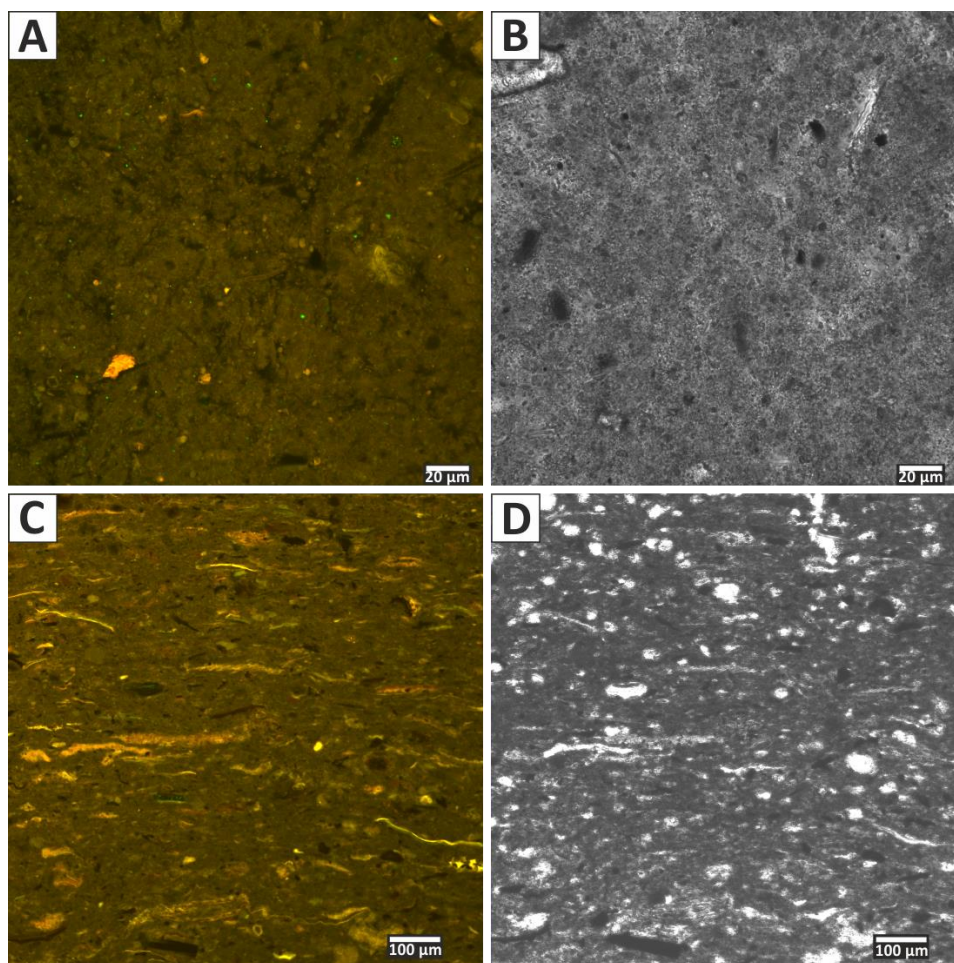


Figure 2.4: (A) Laser scanning micrograph (excitation 365 nm/emission 397-700 nm) of Unit I microfabric at 2 cm depth. The small, and randomly orientated plant particles show bright fluorescence due to their chlorophyll content. (B) Same section in transmitted light. (C) Fluorescent texture of Unit III (at 28 cm depth) is visible. The higher amount of plant detritus, particle layering and a compacted matrix are notable. Voids are resin embedding artefacts. (D) Same section as in (C) under transmitted light.

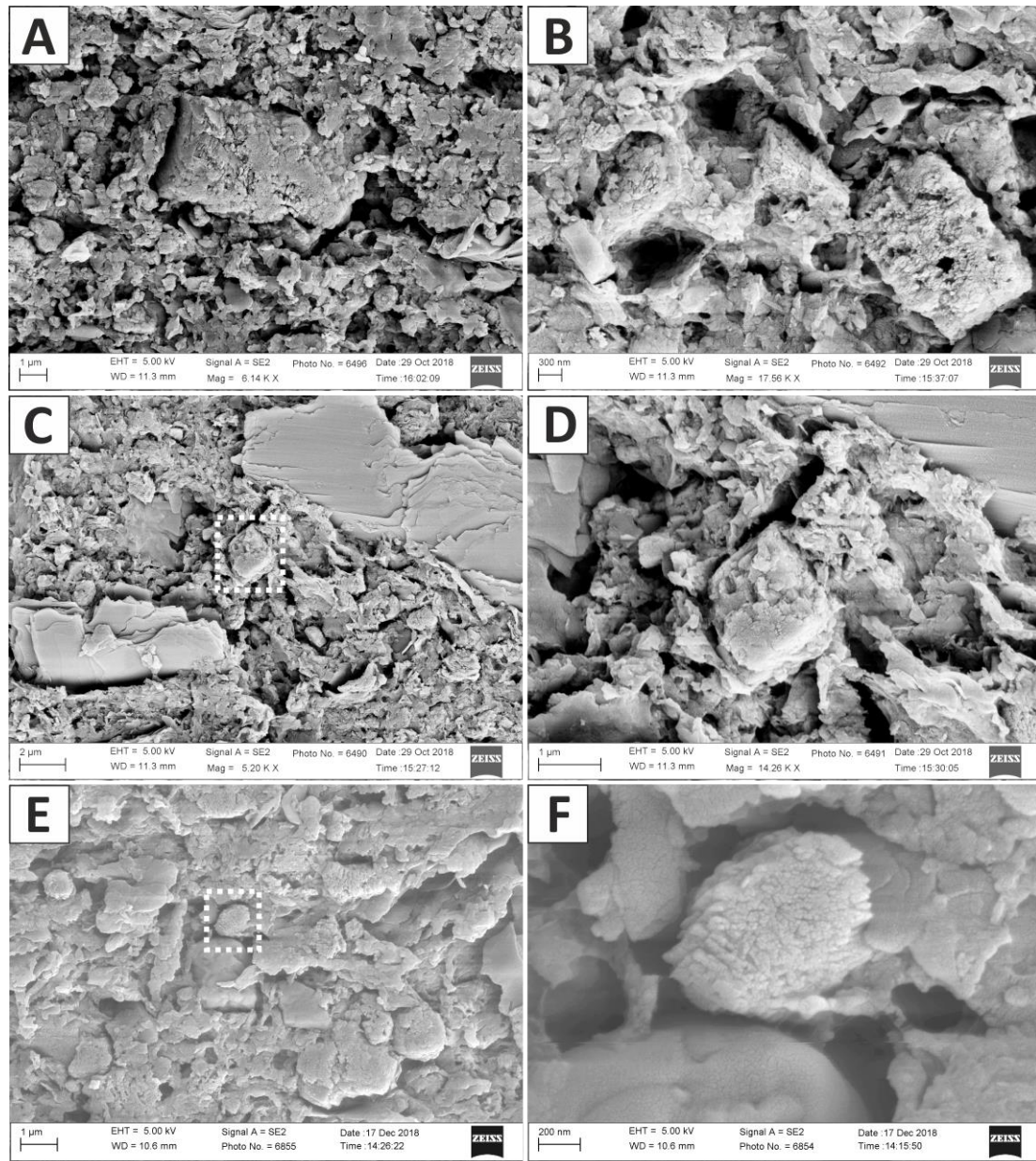


Figure 2.5: SEM images of Core LN-K 05, showing the crystal morphology of Ca-Mg phases with increasing depth. (A) HMC/protodolomite crystal in 9 cm depth. (B) Aggregate of 3 HMC/protodolomite crystals in 17 cm depth. (C) Matrix overview containing microcrystalline crumbs, layered mica crystals and a HMC/protodolomite rhombohedron (indicated by dashed rectangle) at 17 cm depth. (D) Detail of rhombohedron visible in C. (E) Matrix overview in 27 cm depth. HMC/protodolomite carbonate crystals appear rather xenomorphic (indicated by dashed rectangle). (F) Close up of HMC/protodolomite crystal accentuated in (E).

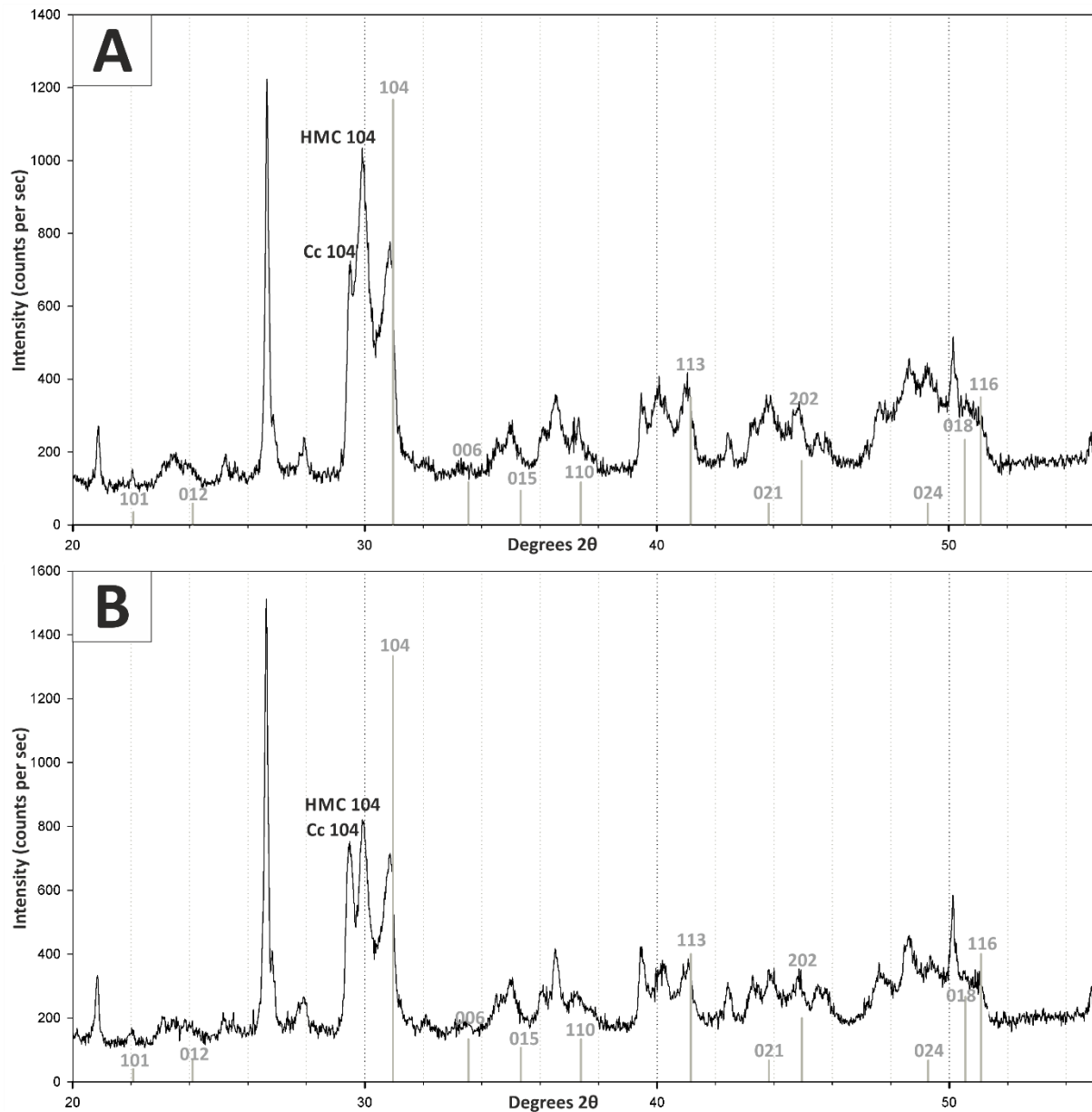


Figure 2.6: X-ray diffractograms of bulk Lake Neusiedl sediment (A) from 2 cm and (B) from 27.5 cm depth. Positions of dolomite peaks are marked in grey. Position of major calcite (Cc 104) and high-magnesium-calcite (HMC 104) peaks are also indicated. Note that typical dolomite ordering peaks could not be identified in the XRD-Spectra. Furthermore, a figure and a list containing major peaks of identified mineral phases is provided in the supplemental material.

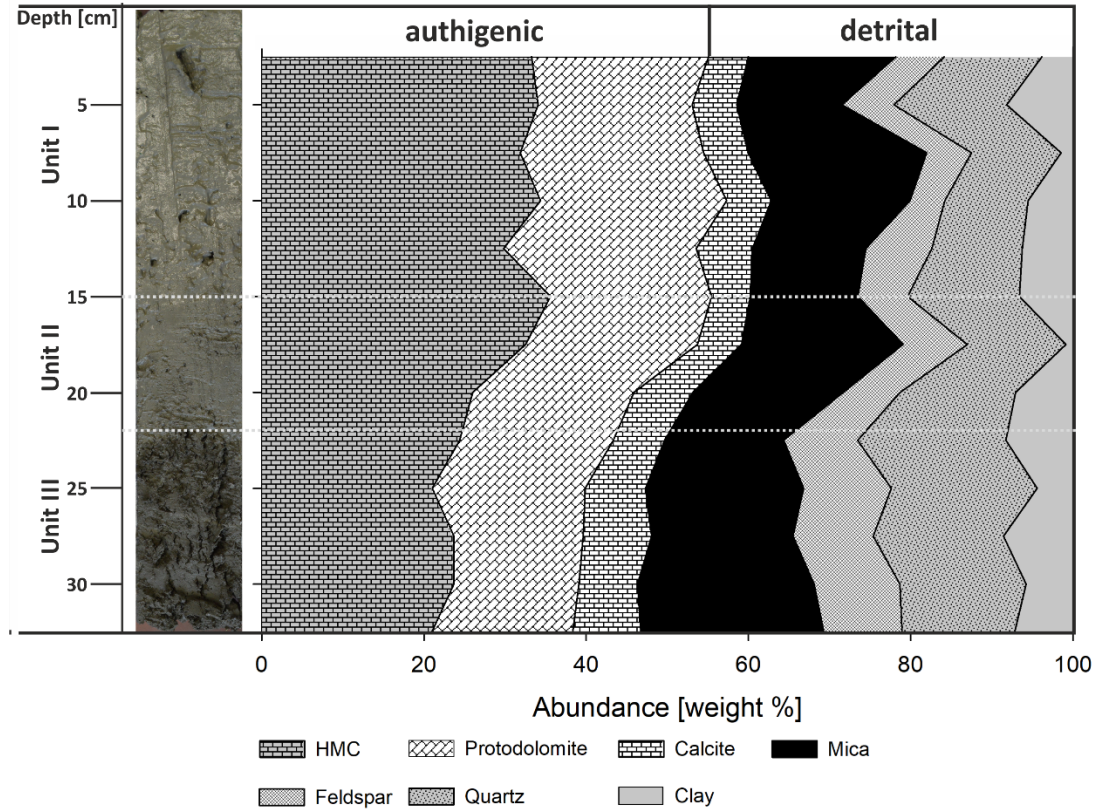


Figure 2.7: Core LN-K04 with the defined units I-III (left) and mineral quantities estimated from main peak heights (right; HMC: high-magnesium calcite,). The changes of mineral abundances coincide with unit boundaries

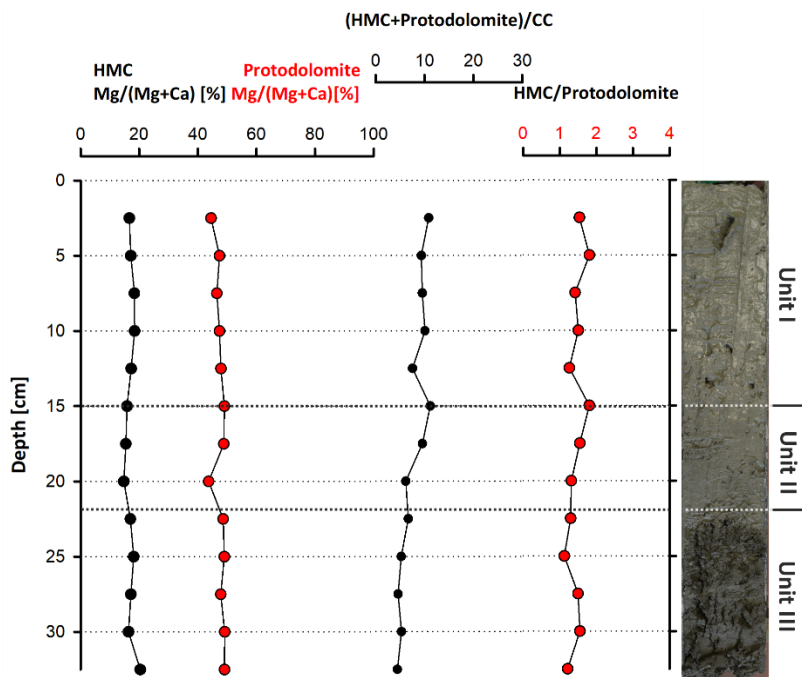


Figure 2.8: Stoichiometric compositions of authigenic carbonate phases (HMC and protodolomite), their abundance ratio, and their relation to detrital calcite.

2.4.2 Pore water chemistry

The water chemistry of Lake Neusiedl is characterized by high pH values (9.02) and moderate salinity (1.8‰). Sodium (Na^+) and magnesium (Mg^{2+}) are the major cations with concentrations of 14.3 and 5.1 $\text{mmol}\cdot\text{L}^{-1}$, respectively. Calcium (Ca^{2+}) concentration is considerably lower at 0.3 $\text{mmol}\cdot\text{L}^{-1}$. Total alkalinity (TA) measures 11.2 $\text{meq}\cdot\text{L}^{-1}$ whereas other major anions like chloride (Cl^-) and sulfate (SO_4^{2-}) hold a concentration of 7 and 4 $\text{mmol}\cdot\text{L}^{-1}$, respectively. Nutrient (NH_4^+ , NO_2^- , PO_4^{3-} , $\Sigma\text{H}_2\text{S}$, $\text{SiO}_{2(\text{aq})}$) concentrations lie below 0.004 $\text{mmol}\cdot\text{L}^{-1}$.

The pore water chemistry strongly differs between the sediment and the water column. The pH drops significantly at the water-sediment interface to a value around 7.5, which stays constant throughout the sediment core (Figure 2.9A). The entire section is anoxic with a redox potential of -234 mV at the top, which increases to -121 mV at the bottom (Figure 2.9B). Na^+ and Cl^- contents continuously increase with depth from 14 to 20 and from 7 to 8.8 $\text{mmol}\cdot\text{L}^{-1}$, respectively (Figure 2.9A). Mg^{2+} and Ca^{2+} show a different pattern: From 5 to 10 cm depth, the Mg^{2+} content decreases from 5 to 4 $\text{mmol}\cdot\text{L}^{-1}$, whereas the Ca^{2+} content increases from 0.5 to 0.6 $\text{mmol}\cdot\text{L}^{-1}$ in the same increment. From 10 cm downwards, the Mg^{2+} content scatters around 4 $\text{mmol}\cdot\text{L}^{-1}$ and the Ca^{2+} content decreases from 0.6 to below 0.5 $\text{mmol}\cdot\text{L}^{-1}$ (Figure 2.9A). Dissolved SO_4^{2-} and hydrogen sulfide ($\Sigma\text{H}_2\text{S}$) also show a noticeable trend: The $\Sigma\text{H}_2\text{S}$ content is close to zero in the top 5 cm of the sediment column, rapidly increases to 1 $\text{mmol}\cdot\text{L}^{-1}$ between 5 and 10 cm and remains constant to the bottom of the section. SO_4^{2-} follows an opposite trend. Its concentration decreases from 4 to 1 $\text{mmol}\cdot\text{L}^{-1}$ in the upper 10 cm and remains constant at 1 $\text{mmol}\cdot\text{L}^{-1}$ towards the section bottom. Total alkalinity also increases towards the lower part of the section, from 11.2 to 16.8 $\text{meq}\cdot\text{L}^{-1}$, with an increase between 5 and 15 cm depth.

NO_2^- is present in the upper 10 cm of the core and reaches its highest value (0.9 $\mu\text{mol}\cdot\text{L}^{-1}$) at 2 cm, while its concentration decreases to zero below 10 cm. Dissolved iron (Fe^{2+}) has a similar trend in the upper 10 cm, reaching its highest concentration at a depth of 2 cm (1.4 $\mu\text{mol}\cdot\text{L}^{-1}$). Below 10 cm core depth, iron concentrations lie below 0.3 $\mu\text{mol}\cdot\text{L}^{-1}$, with the exception of an outlier value of 0.5 $\mu\text{mol}\cdot\text{L}^{-1}$ at 13 cm. Concentrations of ammonia (NH_4^+) and phosphate (PO_4^{2-}) increase with depth. In the uppermost part of the sediment column, they are close to zero and increase to 0.37 and 0.02 $\text{mmol}\cdot\text{L}^{-1}$ at 13 cm. These values remain constant to the bottom of the core. Dissolved silica shows a curved profile with 0.3 $\text{mmol}\cdot\text{L}^{-1}$ at the top, reaching a maximum at 15 cm depth with 0.8 $\text{mmol}\cdot\text{L}^{-1}$ and declines to concentrations around 0.5 $\text{mmol}\cdot\text{L}^{-1}$. Methane (CH_4) concentration also shows a curved trend, reaching its highest value of 227 $\mu\text{mol}\cdot\text{L}^{-1}$ at a depth of 20 cm and concentrations between 14 and 64 $\mu\text{mol}\cdot\text{L}^{-1}$ close to the sediment surface (5 and 1 cm, respectively). Dissolved inorganic carbon (DIC) increases from 11.71 $\text{mmol}\cdot\text{L}^{-1}$ at the top to 18.01 $\text{mmol}\cdot\text{L}^{-1}$ at 30 cm depth. Only in the 15 to 20 cm increment, the amount of DIC slightly decreases from 15.37 to 14.94 $\text{mmol}\cdot\text{L}^{-1}$.

According to PHREEQC calculations, the water column at the sampling site (Bay of Rust) is supersaturated with respect to aragonite (SI = 0.92), calcite (SI = 1.07), protodolomite (SI = 2.92;) and dolomite (SI = 3.46; Figure 2.10). Sediment pore water is close to equilibrium throughout the whole section with respect to aragonite, whereas calcite is in equilibrium to slightly supersaturated between 10 and 27.5 cm depth. Protodolomite reaches equilibrium between 2.5 and 5 cm, while dolomite is supersaturated in the entire section. It should be noted that all saturation graphs reveal parallel trends, with their highest saturation at 17.5 cm and their lowest at 2.5 cm depth.

42 | Authigenic formation of Ca-Mg carbonates in the shallow alkaline Lake Neusiedl

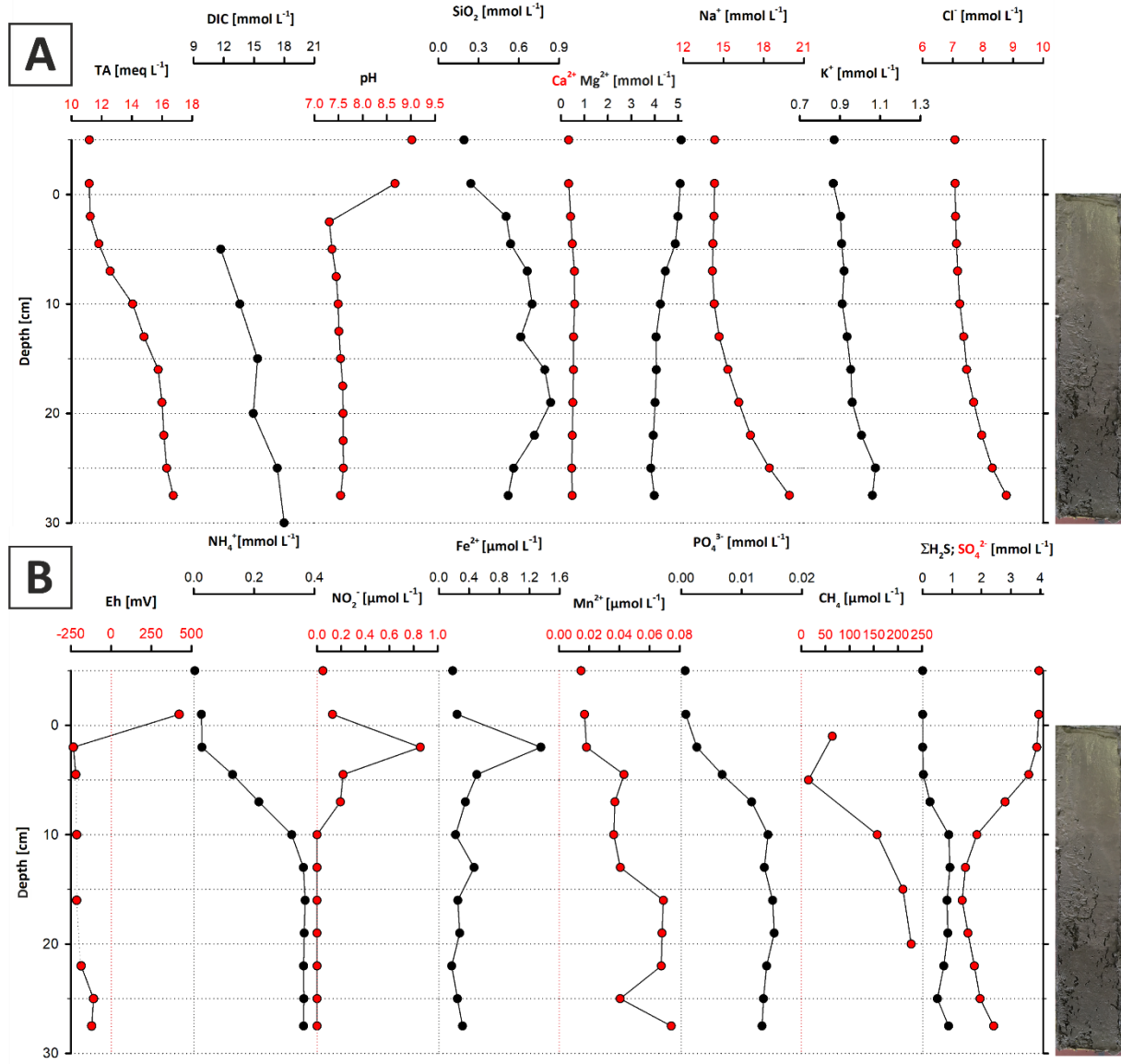


Figure 2.9: Major ion- (A) and metabolite concentrations (B) in the pore water of core LN-K03. Note that the sample slightly above 0 cm depth represents the supernatant water, and the top data points represent the water column (see text for explanations).

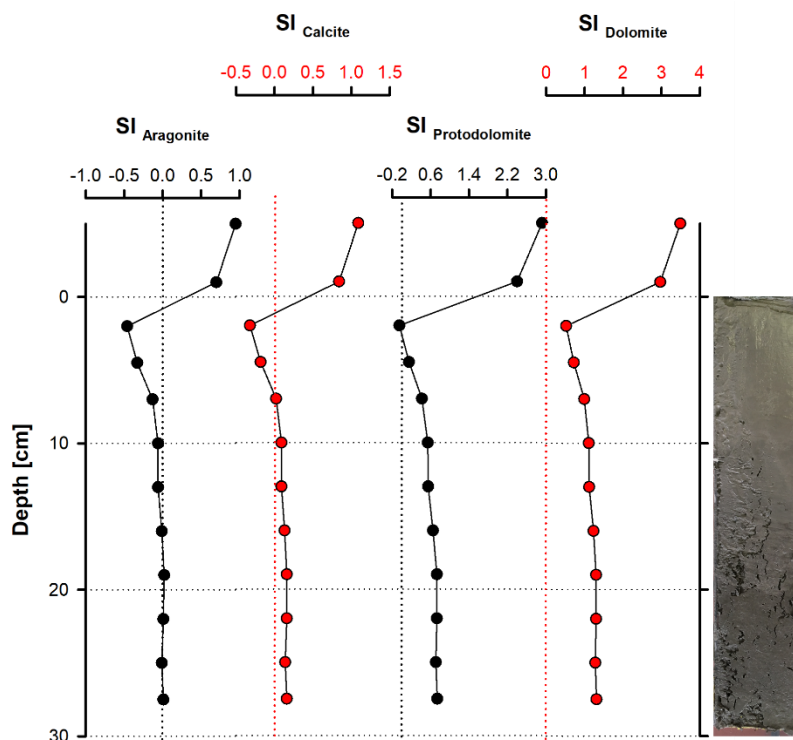


Figure 2.10: Saturation indices (SI) of selected carbonate mineral phases. Noteworthy, all phases are clearly supersaturated in the water column but close to saturation throughout most of the sediment column (except for the uppermost 10 cm).

2.4.3 Bacterial community composition

Bacterial 16S rRNA gene analysis revealed the presence of a diverse bacterial community with 1,226 amplicon sequence variants (ASVs) clustered at 100% sequence identity within the water column, 2,085 to 2,467 ASVs in the top 20 cm of the sediment core and 1,417 to 1,581 ASVs in the deeper sediment (20 - 35 cm core depth). The different bacterial taxa were grouped by known metabolic properties of characterized relatives, listed in Whitman (2015) and additional literature (see supplementary data). The distribution of the most abundant bacterial taxa differs between the water column and the sediment (Figure 2.11A and B).

The water column is dominated by aerobic heterotrophs, mainly *Alphaproteobacteria* and *Actinobacteria*, which are only of minor abundance in the sediment. Among the *Alphaproteobacteria*, the SAR 11 clade capable of oxidizing C1-compounds (Sun et al. 2011), is predominant. The nitrogen-fixing *Frankiales* are the most abundant representatives of the *Actinobacteria*. Furthermore, coccoid *Cyanobacteria* (*Synechococcales*) and *Bacteroidetes* are present in high relative abundances in the water column.

Within sediment Unit I (0-15 cm b. s.), the bacterial community composition changes to mainly anaerobic and facultatively anaerobic taxa. Only the uppermost 5 cm show increased relative abundances of *Cyanobacteria* (*Synechococcales*) and *Bacteroidetes* (aerobes and facultative anaerobes; Alderkamp et al., 2006, Flombaum et al., 2013), as well as *Verrucomicrobia* (mostly aerobic and facultative anaerobic heterotrophs, He et al. 2017), which include nitrogen-fixing members (Chiang et al. 2018). Besides these groups, *Gammaproteobacteria*, *Acidobacteria*, *Chloroflexi*, as well as sulfate-reducing *Deltaproteobacteria* are abundant. The latter mainly consist of *Desulfobacteraceae* and *Desulfarculales* (Figure 2.11C and D).

In sediment Unit II (15-22 cm b. s.), the relative proportions of these groups show a transition between sediment unit I and III. While *Gammaproteobacteria*, *Acidobacteria* and *Deltaproteobacteria* are still

abundant, the relative abundance of *Chloroflexi* increases strongly from 24.29 to 35.43%. Within the SRB, *Desulfobacteraceae* and *Desulfarculales* are successively replaced by *Deltaproteobacteria* of the Sva0485 clade. The *Syntrophobacterales* show their maximum relative abundance within sediment unit II.

In sediment unit III (22-40 cm b. s.), the abundance of *Chloroflexi* further increases to form the dominant bacterial phylum. The phylum consists of *Dehalococcoidia* and *Anaerolineae*. Other abundant groups in this unit are *Acidobacteria*, *Gammaproteobacteria*, and *Deltaproteobacteria* of the Sva0485 clade. Further details of the microbial community composition are given in von Hoyningen-Huene et al. (2019).

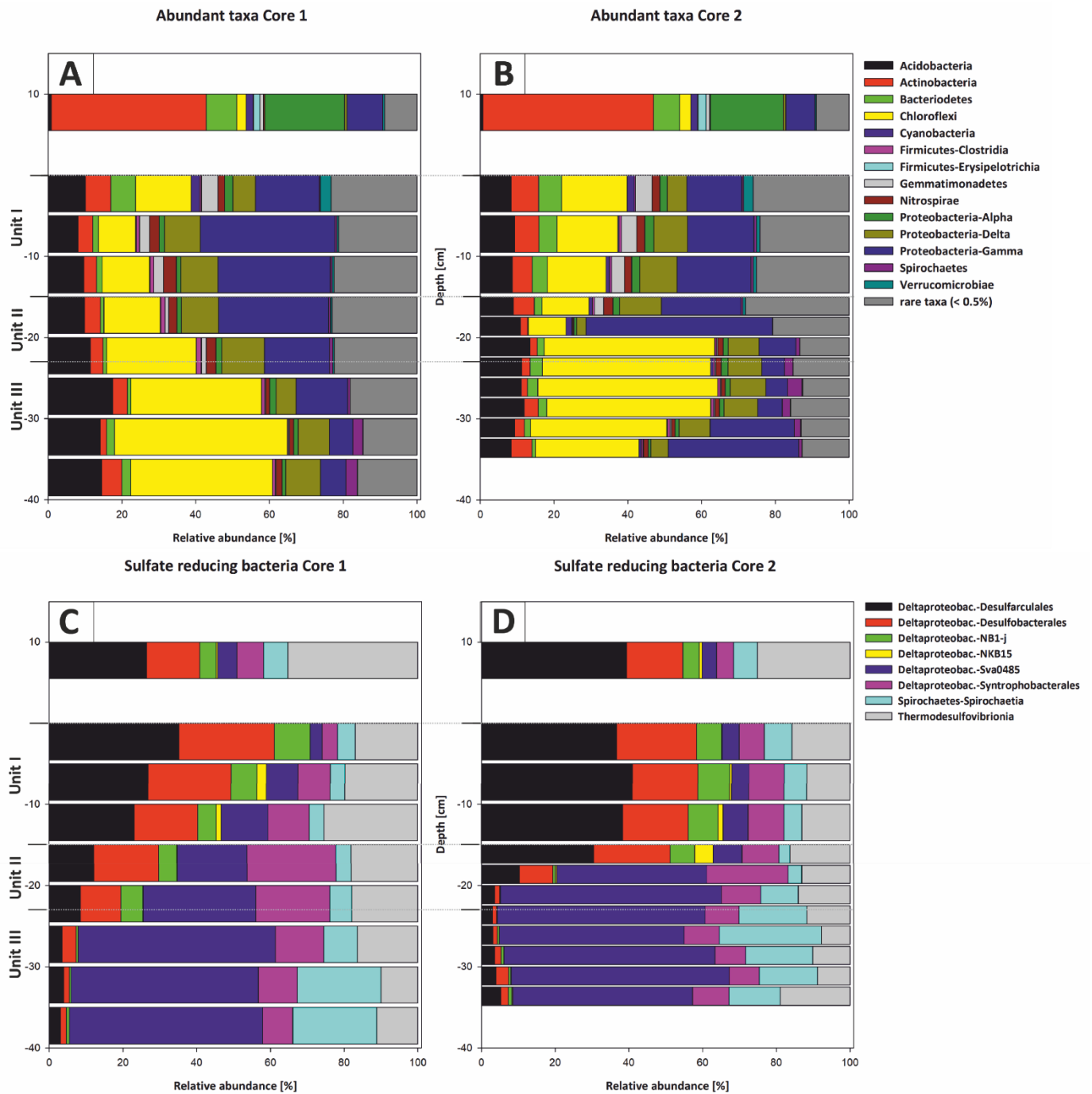


Figure 2.11: Most abundant taxa in Core 01 (A) and Core 02 (B). The legend indicates all abundant taxa on the phylum level, including the class level for Proteobacteria and Firmicutes. All orders below 0.5% relative abundance were summarized as rare taxa. The abundant taxa change at the transitions from water column to sediment and the lithological units (I-III). The taxonomic composition of sulfate reducers in Core 01 (C) and Core 02 (D) changes gradually from Unit I to II and more pronouncedly from Unit II to III. Sulfate reducers are shown on the class and order level. The column thickness relates to the sampled increments of either 5 or 2.5 cm. Sulfate reducers represent up to 15% of the total bacterial community and were normalized to 100% relative abundance to illustrate the changes within their composition.

2.5 Discussion

2.5.1 Pore water gradients and their effect on Ca-Mg carbonate supersaturation

Concentrations of the conservative trending ions Na^+ , K^+ , and Cl^- , steadily increase towards the bottom of the core section, reaching 19, 1, and 9 $\text{mmol}\cdot\text{L}^{-1}$, respectively. These concentrations are considerably higher than in the water column, where these ions measure 14, 0.9 and 7 $\text{mmol}\cdot\text{L}^{-1}$. Moreover, SO_4^{2-} shows an increase near the bottom of the core and is reported to further increase to values of 6.5 $\text{mmol}\cdot\text{L}^{-1}$ in a longer section from a different locality in the Bay of Rust (not shown in this study), which is higher than the overlying lake water (3.9 $\text{mmol}\cdot\text{L}^{-1}$). This rise in ion concentration indicates an ion source below the sampled interval. While saline deep ground waters are known to be present in deep aquifers (Neuhuber, 1971; Blohm, 1974; Wolfram, 2006), it is also possible that more highly concentrated brine exists in deeper mud layers due to more recent evaporation events (Figure 2.12). Lake Neusiedl dried out entirely between 1865 and 1875 (Moser, 1866) and high ion concentrations may relate to thin evaporite layers and brines that formed during this event.

The cause of the exceptionally high Mg:Ca ratio, which reaches values around 15 in the water column, is not yet entirely understood. The low Ca^{2+} concentrations in Lake Neusiedl can be linked to calcium carbonate formation (e.g. Wolfram and Herzig, 2013), but the high amounts of Mg^{2+} ions and their source remain elusive. Boros et al. (2014) describe similar phenomena in small alkaline lakes of the western Carpathian plain and relate the high magnesium levels to local hydrogeological conditions and the geological substrate of the lakes.

It should be noted that the Mg:Ca ratio reaches values around 7 in the 5-10 cm increment of the pore water section. This is caused by a considerable decrease of the Mg^{2+} ions in this increment (from 5 to 4 $\text{mmol}\cdot\text{L}^{-1}$) and an increase in Ca^{2+} concentration (from 0.3 to 0.5 $\text{mmol}\cdot\text{L}^{-1}$). This effect can be partly explained by a transition zone between lake and pore water in this section, in which the concentration gradient is balanced. Other factors contributing to this concentration shift may include ion exchange, e.g. with NH_4^+ generated in the pore water at clay minerals (von Breymann et al., 1990; Celik et al., 2001). However, in the case of Lake Neusiedl, the NH_4^+ concentration is not sufficient to explain this change within the Mg:Ca ratio. Another factor causing the decrease of Mg^{2+} concentrations may be the supply of dissolved silica for the precipitation of clay mineral precursor phases (Birsoy, 2002). Increasing SiO_2 concentration with depth indicates the dissolution of diatom frustules, which have been observed in thin sections of the present study. It is not entirely clear if this SiO_2 release into the pore water is related to hydrochemical or biogenic parameters. As the SiO_2 increase in the upper 20 cm of the pore water neither clearly correlates with alkalinity, nor with the salinity gradients (concentrations of conservative ions) and pH is not predictive (Ryves et al., 2006), diatom dissolution by an evident chemical undersaturation (saturation indices of amorphous SiO_2 lie between -1.35 and -0.65) may be not the only driver for the SiO_2 release. It is also conceivable that the enhanced silica release in the pore water is caused by bacteria, which attack the organic matrix of diatom frustules and, thus, expose the silica bearing skeletons to chemical undersaturation (Bidle and Azam, 1999). Bidle et al. (2003) have linked enhanced dissolution potential to uncultured *Gammmaproteobacteria*. This phylum showed increased abundances in the upper sediment column, supporting the hypothesis of a biogenic contribution to diatom dissolution and, hence, the provision of SiO_2 to sequester Mg^{2+} (Figure 2.12, eq. (5)) in Lake Neusiedl's pore waters.

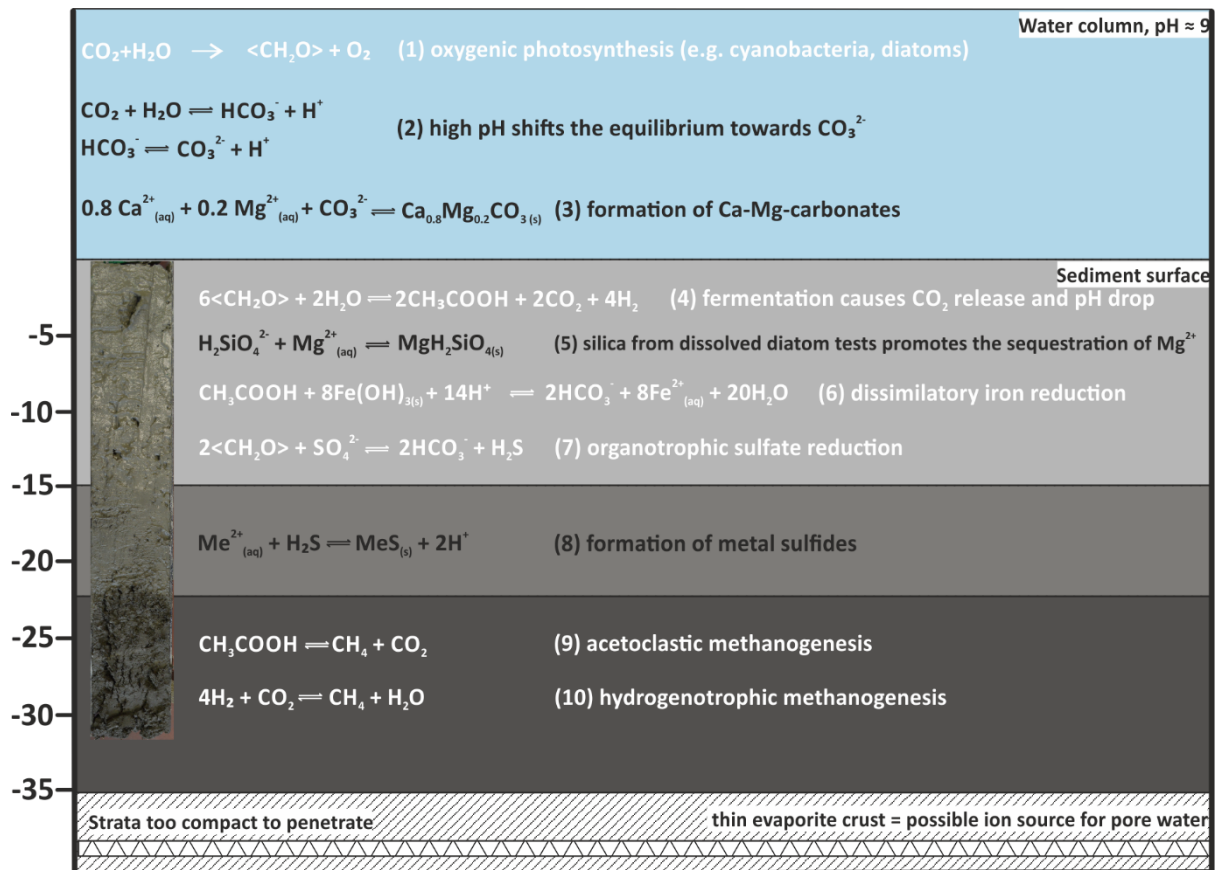


Figure 2.12: Suggested major microbial (simplified, indicated in white) and geochemical processes in water- and sediment column of Lake Neusiedl.

2.5.2 Microbial activity and carbonate saturation

Microbial metabolic reactions strongly affect pore water chemistry, particularly pH, alkalinity and hence carbonate mineral saturation state. In the present approach, the assessment of bacterial community composition is based on the metagenomic DNA within the sediment. This contains the active bacterial communities at their current depth as well as deposited, dormant or dead cells that originated in the water column or at shallower sediment depth (More et al., 2019). In the present study, a background of dormant or dead cells is evident through ASVs belonging to strict aerobes (e.g. *Rhizobiales*, *Gaiellales*) that were detected within deeper parts of the anaerobic mud core (Figure 2.11; Suppl. Material Tab. S5).

The water column is characterized by aerobic heterotrophs, including C1-oxidizers (SAR11 clade of the *Alphaproteobacteria*) and highly abundant freshwater *Actinobacteria*. These are common in most freshwater environments. An impact on carbonate mineral saturation or nucleation, however, is unknown as their role in the biogeochemical cycles remains largely undescribed (Neuenschwander, et al., 2018). A high abundance of *Cyanobacteria* of the *Synechococcales* is present in the water column. *Synechococcales* are known to create favorable conditions for carbonate nucleation in alkaline environments by raising the pH, photosynthetic metabolism and the complexation of cations at their cell envelopes (Thompson and Ferris, 1990). Further research is required to verify their potential role in HMC or protodolomite formation in Lake Neusiedl.

In sediment unit I (0-15 cm b. s.) *Synechococcales*, as well as aerobic *Bacteroidetes* are still abundant in the top 5 cm, likely due to the sedimentation of their cells from the water column. The uppermost measurement at 2.5 cm depth revealed reducing conditions and a low, close to neutral pH. This supports heterotrophic metabolisms and fermentation by *Gammaproteobacteria*, *Acidobacteria*,

Chloroflexi, and *Deltaproteobacteria*, which are the major taxa at this depth. At the very top of the sediment, a peak in NO_2^- and Fe^{2+} points to nitrate-reduction and Fe^{3+} -reduction (Kotlar et al., 1996; Jørgensen and Kasten, 2006). Farther below, the successive increase in NH_4^+ and PO_4^{3-} reflects anaerobic bacterial decomposition of organics, consistent e.g. with *Chloroflexi* capable of dissimilatory nitrate reduction to ammonium (DNRA).

Sulfate-reducers are present in unit I. Their increasing relative abundance coincides with a decrease in SO_4^{2-} and an increase in $\Sigma\text{H}_2\text{S}$ (Figure 2.9). Despite a concomitant increase in alkalinity, the bulk metabolic effect of the microbial community keeps the pH and carbonate saturation low (Figure 2.12, eq (7)). Model calculations in aquatic sediments have shown that sulfate reduction initially lowers the pH (e.g. Soetart et al., 2007) and as the alkalinity increases, the pH converges at values between 6 and 7. As a consequence, the saturation index for carbonate minerals concomitantly drops. If a sufficient amount of sulfate is reduced ($>10 \text{ mmol}\cdot\text{L}^{-1}$), the saturation level recovers and may slightly surpass initial conditions (Meister, 2013). Only when sulfate reduction is coupled to anaerobic oxidation of methane (AOM), the effect of both would raise the pH to higher values. However, as methane occurs below 10 cm (Figure 2.10), where SO_4^{2-} is still present, AOM is incomplete or absent.

In sediment unit II (15-22 cm b. s.) and unit III (22-40 cm b. s.), the bacterial community composition shifts towards a high abundance of *Chloroflexi* (*Dehalococcoidia* and *Anaerolineae*), known for their involvement in carbon cycling as organohalide respirers and hydrocarbon degraders (Hug et al., 2013). This change may reflect an increase in poorly degradable organic electron donors and hence plant debris in the laminated core unit III. The change in the relative composition of different orders within the SRB (i.e., change from *Desulfobacterales* and *Desulfarculales* to Sva0485 and *Spirochaetales*) may also be related to a change in available organic substrates. In total, sulfate reduction remains high, also recognizable by the occurrence of opaque (sulfide-) mineral spots and the increase of S_{tot} in the lower part of the section (Figure 2.2E; Figure 2.3). Fermentation as well as sulfate-reduction remain high with increasing depth, indicated by the near-neutral pH and raised alkalinity at low carbonate mineral saturation.

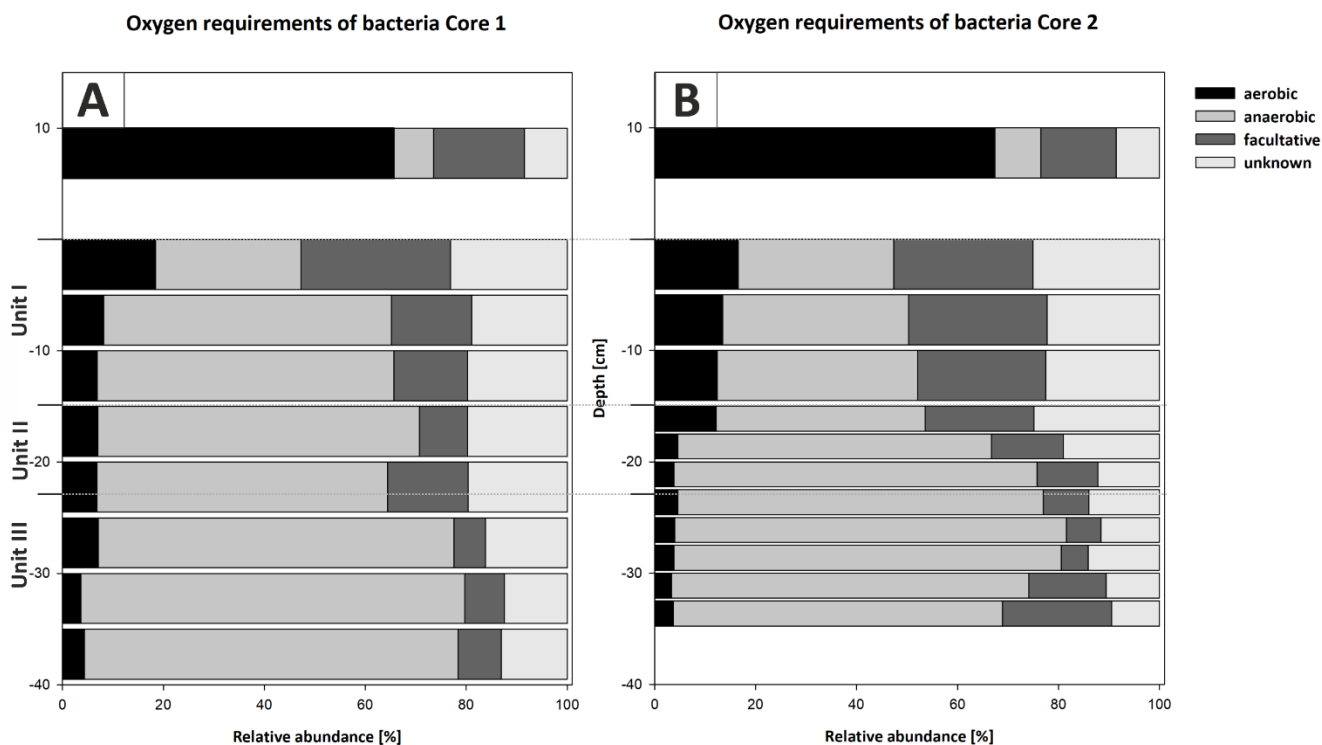


Figure 2.13: Oxygen utilization within the most abundant members of the bacterial community (A) and the potential energy metabolisms (B) plotted versus depth in Cores 01 and 02. The community in the water column indicates a predominantly aerobic regime. Rare taxa (< 0.5% relative abundance) were removed from the analysis and abundances normalized to 100%. Bacteria with an unknown metabolism were grouped as unknowns. The community inhabiting the sediment shows an early onset of sulfate reduction in the upper sediment layers and a shift to fermentation at the transition from Unit II to Unit III.

2.5.3 Time and depth of carbonate formation

A significant difference in saturation state between the water column and the sediment is evident. Whilst the water column is supersaturated with respect to aragonite, HMC, protodolomite and dolomite, they are close to equilibrium in the pore water. The down shift of saturation from the water column to the pore water is to be expected, due to the onset of anaerobic, heterotrophic metabolic activity (Figure 2.12, eq (4)).

The absence of aragonite at Lake Neusiedl is not entirely clear, as its formation is commonly linked to an interplay between high temperature, mineral supersaturation and Mg:Ca ratios (Fernández-Díaz et al., 1996; Given and Wilkinson, 1985). Based on precipitation experiments by De Choudens-Sanchez and Gonzalez (2009), which include temperatures of 19.98 °C and Mg:Ca ratios up to 5, aragonite would be the favored phase in Lake Neusiedl, as the lake's Mg:Ca ratio of 15 is too high and the concomitant calcite saturation not sufficient to provide calcite growth. However, the mentioned experiments were performed in a precipitation chamber with degassing conditions and hence reduced ρCO_2 , which makes them incomparable to the present study. In contrast, Niedermayr et al. (2013) observed the preferential formation of calcite at high Mg:Ca ratios when an amino acid (polyaspartic acid) is present. As the water column bears numerous bacterial species (Figure 2.11) and potentially comparable organic compounds, this is a likely scenario for Lake Neusiedl. Nevertheless, the precise evaluation why aragonite, is not present is impossible, as no related analytical data from the water column are available.

According to Löffler (1979), magnesium calcite forms first, which then alters to protodolomite. The alteration takes place from the inside, hence, resulting in a protodolomite core and a HMC rim.

However, the observation that ratios of HMC to protodolomite remain constant around 40 to 50% indicates no significant diagenetic alteration in the uppermost 30 cm of the sediment. Abrupt changes in these ratios, along with changing contributions of detrital mineral phases, such as mica and quartz, rather suggest changing sedimentation. Likewise, (low-Mg-) calcite essentially depends on the input of ostracod shells and transport of detrital carbonates delivered from the catchment area. Furthermore, no significant diagenetic overprint in form of recrystallization and/or cementation is apparent from the applied light- and electron-optical methods as well as the geochemical gradients. Most importantly, the stoichiometric ratio of each carbonate phase remains constant, confirming that no large-scale recrystallization of these phases occurs.

Considering that no signs of carbonate precipitation or diagenetic alteration were observed in the sediment column from the Bay of Rust, it can be concluded that carbonate minerals are unlikely to form in the pore water. Instead Ca-Mg carbonate crystals may precipitate in the water column and are deposited at the bottom of the lake (Figure 2.12, eq (3)). Age estimations for the mud sediments range from 150 years (Löffler, 1979) to 850-2300 years before present (radiocarbon ages from Neuhuber et al., 2015). Our dataset indicates that authigenic Ca-Mg Carbonate does not necessarily form in its present location, which is consistent with the large discrepancy between sediment- and authigenic carbonate age.

The observed detrital mineral spectrum reflects the mineral composition of the adjacent Leitha- (mica, feldspar, quartz, calcite) and Rust Hills (calcite) and are either windblown or transported by small, eastbound tributaries (Löffler, 1979). The layering in the lower part of the section (Unit III) reflects the lack of homogenization by wind driven wave action and indicates a higher water level. As this unit also contains higher amounts of plant particles and siliciclastics, possibly due to a higher water influx from vegetated surroundings, it is conceivable that the deposition of Unit III reflects environmental conditions before the installation of the water level regulating Einser-Kanal in 1909. The increase of C_{org} with depth further reflects this depositional change. It fits the increasing amount of plant particles with depth. The lignin bearing plant particles are difficult to degrade for heterotrophic organisms under the prevailing anoxic conditions (Benner et al., 1984). The higher amounts of plant material may reflect a lower salinity and thus higher primary production at their time of deposition, which can also be related to the stronger water level oscillations before regulations, including a larger lake surface and almost a magnitude higher catchment area (refer to a map in the supplementary data, provided by Hegedüs (1783)). Based on this consideration one might concur with the sediment age estimation of circa 150 years, as proposed by Löffler (1979). Nevertheless, it is important to distinguish between actual mineral formation and sediment deposition, including relocation: An unpublished sediment thickness map (GeNeSee project; unpubl.) suggests a current-driven relocation of mud deposits in the south-western lake area, where the bay of Rust is located. Thus, the radiocarbon data from Neuhuber et al. (2015) possibly reflect the date of precipitation, whereas Löffler's age estimation may refer to the date of local mud deposition.

2.5.4 Potential pathways of authigenic Ca-Mg carbonate formation

The precise formation pathway of authigenic Ca-Mg carbonate mineral precipitation in Lake Neusiedl has been controversially discussed. Some authors suggest a precipitation of HMC in the water column and subsequent alteration to protodolomite or dolomite within the anoxic pore water of the sediment (Müller et al., 1972). Others suggest the direct formation of protodolomite in the water column (Schiemer and Weisser, 1972). Our XRD and geochemical data support the latter hypothesis, as no diagenetic alteration is retraceable throughout the sediment section. While low saturation or even undersaturation in the sediment precludes a microbially induced precipitation in the pore water, high

supersaturation in the surface water body would support precipitation in the water column. Given the high alkalinity, CO₂ uptake by primary producers may have contributed to the high pH and high supersaturation in the surface water.

An alternative explanation to the controversially discussed microbial dolomite formation would be the ripening under fluctuating pH conditions in the water column. Deelman (1999) has demonstrated in his precipitation experiments that dolomite forms if the pH varies. At times of strong supersaturation, metastable carbonates (protodolomite) are formed, which ripen to ordered dolomite during subsequent phases of undersaturation of the metastable carbonate (while the stable phase remains supersaturated). This observation reflects Ostwald's step rule, according to which the metastable phase always forms first. Ostwald's step rule can also be demonstrated in the pore water, which is buffered by the metastable phase. Thereby the formation of the stable phase (dolomite) is inhibited despite its supersaturation. This observation is comparable with Land's (1998) "failure" to form dolomite for 30 years despite 1000-fold supersaturation.

In Lake Neusiedl, fluctuation of the pH in the overlying water column is likely to occur due to variations in meteoric water input and temperature, which may cause episodes of undersaturation. A fact, which is supported by Wolfram and Herzig (2013), who report an increase of Ca²⁺ concentration, depending on a dissolution of Ca-carbonates in Lake Neusiedl's open water during the winter months, when water levels rise and temperatures decrease. Such a seasonal dependent formation mechanism has recently been suggested to explain dolomite formation in a Triassic evaporative tidal flat setting (Meister and Frisia, 2019). Alternatively, Moreira et al. (2004) proposed that undersaturation of metastable phases occurs as a result of sulfide oxidation near the sediment surface. While we traced only small abundances of sulfate-oxidizing bacteria near the sediment-water interface (1%), fluctuating hydrochemical conditions are likely to occur in the diffusive boundary layer, where a pH drop is observed as a result of the biogeochemical processes discussed above. Dolomite formation in the diffusive boundary layer has been observed in Lake Van (McCormack et al., 2018), and was interpreted as a result of abundant microbial EPS, linked to a changing water level and hence -chemistry. In Lake Neusiedl, the amount of EPS in the diffusive boundary layer is difficult to estimate, but the potential Ca-Mg carbonate favoring change in hydrochemistry is granted.

2.6 Conclusions

Two phases of Ca-Mg carbonates (HMC, protodolomite) as well as calcite occur in form of fine-grained mud in Lake Neusiedl. Bacterial metabolic activity, including sulfate reduction and fermentation, leads to a decrease of pH within the sediment, leaving the Ca-Mg-carbonate phases at low/minor saturation in the pore water. In contrast, Ca-Mg carbonate phases are highly supersaturated in the alkaline water column. There, the carbonate formation mechanism may involve fluctuating hydrochemical conditions, leading to periods of undersaturation and ripening of HMC to protodolomite. Further, carbonate precipitation may be supported by phototrophic uptake of CO₂ by cyanobacteria, e.g. by *Synechococcus*. Precipitation of Ca-Mg carbonate, thus, most likely occurs in the open water. Based on the presented data set, precipitation or diagenetic alteration within the sediment is not indicated. The precise Ca-Mg carbonate reaction pathway needs further evaluation.

Data availability

All data required for the presented plots and supplementary, analytical data were submitted to PANGAEA (Data Publisher for Earth & Environmental Science) and are accessible via <https://doi.org/10.1594/PANGAEA.909663>. Microbiological datasets can be requested from Avril von Hoyningen-Huene.

Acknowledgements

We thank Wolfgang Dröse, Birgit Röring, and Axel Hackmann for their support during lab work. Furthermore, we thank Susanne Gier for support during XRD measurements and Beatrix Bethke, Caroline Haberhauer, and Barbara Hofbauer for help during sampling. We also thank Erich Draganits, Regina and Rudolf Krachler, and Stephanie Neuhuber for insightful discussions.

Financial support

The project was funded by the German Research Foundation DFG, research unit FOR-1644 "CHARON" (subproject TP7: AR 335/8-1, DA 374/11-1). Further support was provided by the Open Access Publication Funds of the Göttingen University. P.M. received funding by the European Commission (Marie-Curie IEF Project TRIADOL; no. 626025) and by the Department of Geodynamics and Sedimentology at the University of Vienna.

References

- Alderkamp, A.-C., Nejstgaard, J. C., Verity, P. G., Zirbel, M. J., Sazhin, A. F., and van Rijssel, M.: Dynamics in carbohydrate composition of *Phaeocystis pouchetii* colonies during spring blooms in mesocosms, *Journal of Sea Research*, 55, 169-181, <https://doi.org/10.1016/j.seares.2005.10.005>, 2006.
- Aloisi, G.: The calcium carbonate saturation state in cyanobacterial mats throughout Earth's history, *Geochimica et Cosmochimica Acta*, 72, 6037-6060, <https://doi.org/10.1016/j.gca.2008.10.007>, 2008.
- Bácsatyai, L., Csaplovics, E., Márkus, I. and Sindhuber, A.: Digitale Geländemodelle des Neusiedler See-Beckens, *Wissenschaftliche Arbeiten aus dem Burgenland*, 97, 1-53, 1997.
- Balci, N., Menekşe, M., Karagüler, N. G., Şeref Sönmez, M., and Meister, P.: Reproducing authigenic carbonate precipitation in the hypersaline Lake Acıgöl (Turkey) with microbial cultures, *Geomicrobiology Journal*, 33, 758-773, <https://doi.org/10.1080/01490451.2015.1099763>, 2016.
- Benner, R., Maccubbin, A., and Hodson, R. E.: Anaerobic biodegradation of the lignin and polysaccharide components of lignocellulose and synthetic lignin by sediment microflora, *Appl. Environ. Microbiol.*, 47, 998-1004, 1984.
- Bidle, K. D., and Azam, F.: Accelerated dissolution of diatom silica by marine bacterial assemblages, *Nature*, 397, 508-512, <https://doi.org/10.1038/17351>, 1999.
- Bidle, K. D., Brzezinski, M. A., Long, R. A., Jones, J. L., and Azam, F.: Diminished efficiency in the oceanic silica pump caused by bacteria-mediated silica dissolution, *Limnology and Oceanography*, 48, 1855-1868, <https://doi.org/10.4319/lo.2003.48.5.1855>, 2003.
- Birgel, D., Meister, P., Lundberg, R., Horath, T. D., Bontognali, T.R., Bahniuk, A. M., de Rezende, C. E., Váscnelos, C. and McKenzie, J. A.: Methanogenesis produces strong ¹³C enrichment in stromatolites of Lagoa Salgada, Brazil: a modern analogue for Palaeo-/Neoproterozoic stromatolites?, *Geobiology*, 13, 245-266, <https://doi.org/10.1111/gbi.12130>, 2015.
- Birsoy, R.: Formation of sepiolite-palygorskite and related minerals from solution, *Clays and Clay Minerals*, 50, 736-745, <https://doi.org/10.1346/000986002762090263>, 2002.
- Blohm, M.: Sedimentpetrographische Untersuchungen am Neusiedler See, Österreich, Dissertation, Ruprecht-Karl-Universität Heidelberg, 1974.
- Bontognali, T. R., Vasconcelos, C., Warthmann, R. J., Dupraz, C., Bernasconi, S. M., and McKenzie, J. A.: Microbes produce nanobacteria-like structures, avoiding cell entombment, *Geology*, 36, 663-666, <https://doi.org/10.1130/g24755a.1>, 2008.
- Bontognali, T. R., Vasconcelos, C., Warthmann, R. J., Bernasconi, S. M., Dupraz, C., Strohmenger, C. J., and McKenzie, J. A.: Dolomite formation within microbial mats in the coastal sabkha of Abu Dhabi (United Arab Emirates), *Sedimentology*, 57, 824-844, <https://doi.org/10.1111/j.1365-3091.2009.01121.x>, 2010.
- Bontognali, T. R., McKenzie, J. A., Warthmann, R. J., and Vasconcelos, C.: Microbially influenced formation of Mg-calcite and Ca-dolomite in the presence of exopolymeric substances produced by sulphate-reducing bacteria, *Terra Nova*, 26, 72-77, <https://doi.org/10.1111/ter.12072>, 2014.
- Boros, E., Horváth, Z., Wolfram, G., and Vörös, L.: Salinity and ionic composition of the shallow astatic soda pans in the Carpathian Basin, *International Journal of Limnology*, 50, 59-69, <https://doi.org/10.1051/limn/2013068>, 2014.

- Brady, P.V., Krumhansl, J. L. and Papenguth, H.W.: Surface complexation clues to dolomite growth, *Geochemica et Cosmochemica Acta*, 60, 727-731, [https://doi.org/10.1016/0016-7037\(95\)00436-x](https://doi.org/10.1016/0016-7037(95)00436-x), 1996.
- Callahan, B. J., McMurdie, P. J., and Holmes, S. P.: Exact sequence variants should replace operational taxonomic units in marker-gene data analysis, *The ISME journal*, 11, 2639-2643, <https://doi.org/10.1038/ismej.2017.119>, 2017.
- Celik, M., Özdemir, B., Turan, M., Koyuncu, I., Atesok, G., and Sarikaya, H.: Removal of ammonia by natural clay minerals using fixed and fluidised bed column reactors, *Water Science and Technology: Water Supply*, 1, 81-88, <https://doi.org/10.2166/ws.2001.0010>, 2001.
- Chen, S., Zhou, Y., Chen, Y., and Gu, J.: fastp: an ultra-fast all-in-one FASTQ preprocessor, *Bioinformatics*, 34, i884-i890, <https://doi.org/10.1093/bioinformatics/bty560>, 2018.
- Chiang, E., Schmidt, M. L., Berry, M. A., Biddanda, B. A., Burtner, A., Johengen, T. H., Palladino, D., and Deneff, V. J.: Verrucomicrobia are prevalent in north-temperate freshwater lakes and display class-level preferences between lake habitats, *PLoS One*, 13, e0195112, <https://doi.org/10.1371/journal.pone.0195112>, 2018.
- Court, W. M., Paul, A., and Lokier, S. W.: The preservation potential of environmentally diagnostic sedimentary structures from a coastal sabkha, *Marine Geology*, 386, 1-18, <https://doi.org/10.1016/j.margeo.2017.02.003>, 2017.
- Daye, M., Higgins J. and Bosak, T.: Formation of ordered dolomite in anaerobic photosynthetic biofilms. *Geology*, 47, 509-512, <https://doi.org/10.1130/g45821.1>, 2019.
- De Choudens-Sanchez, V. and Gonzalez, L. A.: Calcite and aragonite precipitation under controlled instantaneous supersaturation: elucidating the role of CaCO₃ saturation state and Mg/Ca ratio on calcium carbonate polymorphism. *Journal of Sedimentary Research*, 79, 363-376, <https://doi.org/10.2110/jsr.2009.043>, 2009.
- Deelman, J.: Low-temperature nucleation of magnesite and dolomite, *Neues Jahrbuch Für Mineralogie Monatshefte*, 289-302, 1999.
- Deng, S., Dong, H., Lv, G., Jiang, H., Yu, B., and Bishop, M. E.: Microbial dolomite precipitation using sulfate reducing and halophilic bacteria: Results from Qinghai Lake, Tibetan Plateau, NW China, *Chemical Geology*, 278, 151-159, <https://doi.org/10.1016/j.chemgeo.2010.09.008>, 2010.
- Flombaum, P., Gallegos, J. L., Gordillo, R. A., Rincón, J., Zabala, L. L., Jiao, N., Karl, D. M., Li, W. K., Lomas, M. W., and Veneziano, D.: Present and future global distributions of the marine Cyanobacteria *Prochlorococcus* and *Synechococcus*, *Proceedings of the National Academy of Sciences*, 110, 9824-9829, <https://doi.org/10.1073/pnas.1307701110>, 2013.
- Frisia, S., Borsato, A., and Hellstrom, J.: High spatial resolution investigation of nucleation, growth and early diagenesis in speleothems as exemplar for sedimentary carbonates, *Earth-Science Reviews*, 178, 68-91, <https://doi.org/10.1016/j.earscirev.2018.01.014>, 2018.
- Grasshoff, K., Kremling, K., and Ehrhardt, M.: *Methods of seawater analysis*, John Wiley & Sons, <https://doi.org/10.1002/9783527613984>, 2009.
- Gregg, J. M., Bish, D. L., Kaczmarek, S. E., and Machel, H. G.: Mineralogy, nucleation and growth of dolomite in the laboratory and sedimentary environment: a review, *Sedimentology*, 62, 1749-1769, <https://doi.org/10.1111/sed.12202>, 2015.
- Hahnke, R. L., Meier-Kolthoff, J. P., García-López, M., Mukherjee, S., Huntemann, M., Ivanova, N. N., Woyke, T., Kyrpides, N. C., Klenk, H.-P., and Göker, M.: Genome-based taxonomic classification of *Bacteroidetes*, *Frontiers in Microbiology*, 7, 2003, <https://doi.org/10.3389/fmicb.2016.02003>, 2016.

- He, S., Stevens, S. L., Chan, L.-K., Bertilsson, S., del Rio, T. G., Tringe, S. G., Malmstrom, R. R., and McMahon, K. D.: Ecophysiology of freshwater Verrucomicrobia inferred from metagenome-assembled genomes, *mSphere*, 2, e00277-17, <https://doi.org/10.1128/msphere.00277-17>, 2017.
- Hegedüs, J.N.: Lake Neusiedl and Hansag: Universal map of the County of Sopron, State archive of Sopron, 1783.
- Herrmann, P., Pascher, G., and Pistonik, J.: Geologische Karte der Republik Österreich. Geologische Bundesanstalt, Wien, 1993.
- Herzig, A.: Der Neusiedler See - Limnologie eines Steppensees, *Denisia* 33, zugleich Kataloge des oberösterreichischen Landesmuseums, 163, 101-114, 2014.
- Herzig, A., and Dokulil, M.: Neusiedler See - ein Steppensee in Europa, in: *Ökologie und Schutz von Seen.*, edited by: Dokulil, M., Hamm, A., and Kohl, J.-G., Facultas-Universitäts-Verlag, Wien, 401-415, 2001.
- Holmkvist, L., Kamyshny Jr, A., Bruechert, V., Ferdelman, T. G., and Jørgensen, B. B.: Sulfidization of lacustrine glacial clay upon Holocene marine transgression (Arkona Basin, Baltic Sea), *Geochimica et Cosmochimica Acta*, 142, 75-94, <https://doi.org/10.1016/j.gca.2014.07.030>, 2014.
- Horváth, F.: Towards a mechanical model for the formation of the Pannonian basin, *Tectonophysics*, 226, 333-357, [https://doi.org/10.1016/0040-1951\(93\)90126-5](https://doi.org/10.1016/0040-1951(93)90126-5), 1993.
- Hug, L. A., Castelle, C. J., Wrighton, K. C., Thomas, B. C., Sharon, I., Frischkorn, K. R., Williams, K. H., Tringe, S. G., and Banfield, J. F.: Community genomic analyses constrain the distribution of metabolic traits across the Chloroflexi phylum and indicate roles in sediment carbon cycling, *Microbiome*, 1, 22, <https://doi.org/10.1186/2049-2618-1-22>, 2013.
- Illing, L., Wells, A., and Taylor, J.: Penecontemporary dolomite in the Persian Gulp, *SEPM Special Publication*, 13, 89-111, 1965.
- Jørgensen, B. B., and Kasten, S.: Sulfur cycling and methane oxidation, in: *Marine Geochemistry*, edited by Schulz, H. D. and Zabel, M., Springer, Berlin, 271-309, https://doi.org/10.1007/3-540-32144-6_8, 2006.
- Kampbell, D., Wilson, J. T., and Vandegrift, S.: Dissolved oxygen and methane in water by a GC headspace equilibration technique, *International Journal of Environmental Analytical Chemistry*, 36, 249-257, <https://doi.org/10.1080/03067318908026878>, 1989.
- Klindworth, A., Pruesse, E., Schweer, T., Peplies, J., Quast, C., Horn, M., and Glöckner, F. O.: Evaluation of general 16S ribosomal RNA gene PCR primers for classical and next-generation sequencing-based diversity studies, *Nucleic Acids Research*, 41, e1, <https://doi.org/10.1093/nar/gks808>, 2013.
- Kotlar, E., Tartakovsky, B., Argaman, Y., and Sheintuch, M.: The nature of interaction between immobilized nitrification and denitrification bacteria, *Journal of Biotechnology*, 51, 251-258, [https://doi.org/10.1016/s0168-1656\(96\)01603-3](https://doi.org/10.1016/s0168-1656(96)01603-3), 1996.
- Krachler, R., Korner, I., Dvorak, M., Milazowszky, N., Rabitsch, W., Werba, F., Zulka, P., and Kirschner, A.: Die Salzlacken des Seewinkels: Erhebung des aktuellen ökologischen Zustandes sowie Entwicklung individueller Lackenerhaltungskonzepte für die Salzlacken des Seewinkels (2008–2011), *Österreichischer Naturschutzbund, Eisenstadt, Österreich*, 2012.
- Krachler, R., Krachler, R., Gülce, F., Keppler, B. K., and Wallner, G.: Uranium concentrations in sediment pore waters of Lake Neusiedl, Austria, *Science of the Total Environment*, 633, 981-988, <https://doi.org/10.1016/j.scitotenv.2018.03.259>, 2018.

- Land, L. S.: Failure to Precipitate Dolomite at 25 C from dilute solution despite 1000-fold oversaturation after 32 years, *Aquatic Geochemistry*, 4, 361-368, 1998.
- Lippmann, F.: The System CaCO₃-MgCO₃, in: *Sedimentary Carbonate Minerals*, edited by Lippmann, F., Springer, Berlin, 148-190, https://doi.org/10.1007/978-3-642-65474-9_4, 1973.
- Loisl, J., Tari, G., Draganits, E., Zámolyi, A. and Gjerazi, I.: High-resolution seismic reflection data acquisition and interpretation, Lake Neusiedl, Austria, northwest Pannonian Basin, *Interpretation*, 6, SB77-SB974, <https://doi.org/10.1190/int-2017-0086.1>, 2018.
- Liu, D., Xu, Y., Papineau, D., Yu, N., Fan, Q., Qiu, X., and Wang, H.: Experimental evidence for abiotic formation of low-temperature proto-dolomite facilitated by clay minerals, *Geochimica et Cosmochimica Acta*, 247, 83-95, <https://doi.org/10.1016/j.gca.2018.12.036>, 2019.
- Löffler, H.: Neusiedlersee: The limnology of a shallow lake in central Europe, in: *Monographiae Biologicae*, 37, Dr. W. Junk bv Publishers, The Hague, 543pp., <https://doi.org/10.1007/978-94-009-9168-2>, 1979.
- Lutterotti, L., Bortolotti, M., Ischia, G., Lonardelli, I., and Wenk, H.: Rietveld texture analysis from diffraction images, *Zeitschrift für Kristallographie, Supplements*, 26, 125-130, https://doi.org/10.1524/zksu.2007.2007.suppl_26.125, 2007.
- Machel, H. G.: Concepts and models of dolomitization: a critical reappraisal, Geological Society, London, Special Publications, 235, 7-63, <https://doi.org/10.1144/gsl.sp.2004.235.01.02>, 2004.
- Martin, M.: Cutadapt removes adapter sequences from high-throughput sequencing reads, *EMBnet journal*, 17, 10-12, <https://doi.org/10.14806/ej.17.1.200>, 2011.
- McCormack, J., Bontognali, T. R., Immenhauser, A., and Kwiecien, O.: Controls on cyclic formation of Quaternary early diagenetic dolomite, *Geophysical Research Letters*, 45, 3625-3634, <https://doi.org/10.1002/2018gl077344>, 2018.
- Meister, P., Reyes, C., Beaumont, W., Rincon, M., Collins, L., Berelson, W., Stott, L., Corsetti, F., and Nealson, K.H.: Calcium- and magnesium-limited dolomite precipitation at Deep Springs Lake, California, *Sedimentology*, 58, 1810-1830, <https://doi.org/10.1111/j.1365-3091.2011.01240.x>, 2011.
- Meister, P.: Two opposing effects of sulfate reduction on carbonate precipitation in normal marine, hypersaline, and alkaline environments, *Geology*, 41, 499-502, <https://doi.org/10.1130/g34185.1>, 2013.
- Meister, P. and Frisia, S.: Dolomite formation by nano-crystal aggregation in the Dolomia Principale of the Brenta Dolomites (Northern Italy). *Rivista Italiana di Paleontologia e Stratigrafia*, 125, 183-196, 2019.
- More, K. D., Giosan, L., Grice, K., and Coolen, M. J.: Holocene paleodepositional changes reflected in the sedimentary microbiome of the Black Sea, *Geobiology*, 17, 436-448, <https://doi.org/10.1111/gbi.12338>, 2019.
- Moreira, N., Walter, L. M., Vasconcelos, C., McKenzie, J. A. and McCall, P.: Role of sulfide oxidation in dolomitization: Sediments and pore-water geochemistry of a modern hypersaline lagoon system. *Geology*, 32, 701-704, <https://doi.org/10.1130/g20353.1>, 2004.
- Moser, I.: Der abgetrocknete Boden des Neusiedler Sees, *Jahrbuch der Kaiserlich-Königlichen Geologischen Reichsanstalt Wien*, 16, 338-344, 1866.
- Müller, G., Irion, G., and Förstner, U.: Formation and diagenesis of inorganic Ca-Mg carbonates in the lacustrine environment, *Naturwissenschaften*, 59, 158-164, <https://doi.org/10.1007/bf00637354>, 1972.

- Neuenschwander, S. M., Ghai, R., Pernthaler, J., and Salcher, M. M.: Microdiversification in genome streamlined ubiquitous freshwater Actinobacteria, *The ISME Journal*, 12, 185-198, <https://doi.org/10.1038/ismej.2017.156>, 2018.
- Neuhuber, F.: Ein Beitrag zum Chemismus des Neusiedler Sees, *Sitzungsberichte der Akademie der Wissenschaften in Wien, mathematisch-naturwissenschaftliche Klasse, Abteilung 1*, 179, 225-231, 1971.
- Neuhuber, S., Steier, P., Gier, S., Draganits, E., and Kogelbauer, I.: Radiogenic Carbon Isotopes in Authigenic Carbonate from Lake Neusiedl, Austria, *EGU General Assembly Conference Abstracts*, 2015.
- Niedermayr, A., Köhler, S. J., and Dietzel, M.: Impacts of aqueous carbonate accumulation rate, magnesium and polyaspartic acid on calcium carbonate formation (6–40 °C), *Chemical Geology*, 340, 105-120, <https://doi.org/10.1016/j.chemgeo.2012.12.014>, 2013.
- Parkhurst, D. L., and Appelo, C.: Description of input and examples for PHREEQC version 3: a computer program for speciation, batch-reaction, one-dimensional transport, and inverse geochemical calculations, *US Geological Survey*, 2328-7055, <https://doi.org/10.3133/tm6a43>, 2013.
- Pau, M., and Hammer, Ø.: Sediment mapping and long-term monitoring of currents and sediment fluxes in pockmarks in the Oslofjord, Norway, *Marine Geology*, 346, 262-273, <https://doi.org/10.1016/j.margeo.2013.09.012>, 2013.
- Piller, W. E., Harzhauser, M., and Mandic, O.: Miocene Central Paratethys stratigraphy—current status and future directions, *Stratigraphy*, 4, 151-168, 2007.
- Quast, C., Pruesse, E., Yilmaz, P., Gerken, J., Schweer, T., Yarza, P., Peplies, J., and Glöckner, F. O.: The SILVA ribosomal RNA gene database project: improved data processing and web-based tools, *Nucleic acids research*, 41, D590, <https://doi.org/10.1093/nar/gks1219>, 2012.
- Rivadeneira, M. a. A., Delgado, G., Soriano, M., Ramos-Cormenzana, A., and Delgado, R.: Precipitation of carbonates by *Nesterenkonia halobia* in liquid media, *Chemosphere*, 41, 617-624, [https://doi.org/10.1016/s0045-6535\(99\)00496-8](https://doi.org/10.1016/s0045-6535(99)00496-8), 2000.
- Roberts, J. A., Bennett, P. C., González, L. A., Macpherson, G., and Milliken, K. L.: Microbial precipitation of dolomite in methanogenic groundwater, *Geology*, 32, 277-280, <https://doi.org/10.1130/g20246.2>, 2004.
- Rognes, T., Flouri, T., Nichols, B., Quince, C., and Mahé, F.: VSEARCH: a versatile open source tool for metagenomics, *PeerJ*, 4, e2584, <https://doi.org/10.7717/peerj.2584>, 2016.
- Rosen, M. R., Miser, D. E., Starcher, M. A., and Warren, J. K.: Formation of dolomite in the Coorong region, South Australia, *Geochimica et Cosmochimica Acta*, 53, 661-669, [https://doi.org/10.1016/0016-7037\(89\)90009-4](https://doi.org/10.1016/0016-7037(89)90009-4), 1989.
- Ryves, D. B., Battarbee, R. W., Juggins, S., Fritz, S. C., and Anderson, N. J.: Physical and chemical predictors of diatom dissolution in freshwater and saline lake sediments in North America and West Greenland, *Limnology and Oceanography*, 51, 1355-1368, <https://doi.org/10.4319/lo.2006.51.3.1355>, 2006.
- Sánchez-Román, M., Vasconcelos, C., Warthmann, R., Rivadeneira, M., McKenzie, J. A., and Swart, P.: Microbial dolomite precipitation under aerobic conditions: results from Brejo do Espinho Lagoon (Brazil) and culture experiments, in: *Perspectives in Carbonate Geology: A Tribute to the Career of Robert Nathan Ginsburg*, edited by: Swart, P. K., Eberli, G. P., McKenzie, J. A., Jarvis, I. and Stevens, T., *IAS Special Publication*, 41, 167-178, <https://doi.org/10.1002/9781444312065>, 2009.

- Schiemer, F., and Weisser, P.: Zur Verteilung der submersen Makrophyten in der schilffreien Zone des Neusiedler Sees, Sitzungsberichte der Akademie der Wissenschaften in Wien, mathematische-naturwissenschaftliche Klasse, Abteilung 1., 180, 87-97, 1972.
- Schmidt, F., Koch, B. P., Goldhammer, T., Elvert, M., Witt, M., Lin, Y.-S., Wendt, J., Zabel, M., Heuer, V. B., and Hinrichs, K.-U.: Unraveling signatures of biogeochemical processes and the depositional setting in the molecular composition of pore water DOM across different marine environments, *Geochimica et Cosmochimica Acta*, 207, 57-80, <https://doi.org/10.1016/j.gca.2017.03.005>, 2017.
- Schmidt, M., Xeflide, S., Botz, R., and Mann, S.: Oxygen isotope fractionation during synthesis of CaMg-carbonate and implications for sedimentary dolomite formation, *Geochimica et Cosmochimica Acta*, 69, 4665-4674, <https://doi.org/10.1016/j.gca.2005.06.025>, 2005.
- Schneider, D., Thürmer, A., Gollnow, K., Lugert, R., Gunka, K., Groß, U., and Daniel, R.: Gut bacterial communities of diarrheic patients with indications of *Clostridioides difficile* infection, *Scientific Data*, 4, 170152, <https://doi.org/10.1038/sdata.2017.152>, 2017.
- Schneider, D., Wemheuer, F., Pfeiffer, B., and Wemheuer, B.: Extraction of total DNA and RNA from marine filter samples and generation of a cDNA as universal template for marker gene studies, in: *Metagenomics*, edited by: Streit, W. and Daniel, R., Springer, Berlin, 13-22, https://doi.org/10.1007/978-1-4939-6691-2_2, 2017.
- Schroll, E., and Wieden, P.: Eine rezente Bildung von Dolomit im Schlamm des Neusiedler Sees, *Tschermaks mineralogische und petrographische Mitteilungen*, 7, 286-289, <https://doi.org/10.1007/bf01127917>, 1960.
- Seeberg-Elverfeldt, J., Schlüter, M., Feseker, T. and Kölling, M.: Rhizon sampling of porewaters near the sediment-water interface of aquatic systems. *Limnology and oceanography: Methods*, 3, 361-371, <https://doi.org/10.4319/lom.2005.3.361>, 2005
- Shotbolt, L.: Pore water sampling from lake and estuary sediments using Rhizon samplers. *Journal of Paleolimnology*, 44, 695-700, <https://doi.org/10.1007/s10933-008-9301-8>, 2010.
- Soetaert, K., Hofmann, A. F., Middelburg, J. J., Meysman, F.J. and Greenwood, J.: The effect of biogeochemical processes on pH, *Marine Chemistry*, 105, 30-51, <https://doi.org/10.1016/j.marchem.2007.06.008>, 2007.
- Steiner, Z., Lazar, B., Erez, J., and Turchyn, A. V.: Comparing Rhizon samplers and centrifugation for pore-water separation in studies of the marine carbonate system in sediments, *Limnology and Oceanography: Methods*, 16, 828-839, <https://doi.org/10.1002/lom3.10286>, 2018.
- Systat Software: SigmaPlot for Windows, version 11.0, 2008.
- Team, R.: RStudio: integrated development for R. (RStudio, Inc., Boston, MA, USA), 2016.
- Team, R. C.: R: A language and environment for statistical computing, 2018.
- Thompson, J., and Ferris, F.: Cyanobacterial precipitation of gypsum, calcite, and magnesite from natural alkaline lake water, *Geology*, 18, 995-998, [https://doi.org/10.1130/00917613\(1990\)018<0995:cpogca>2.3.co;2](https://doi.org/10.1130/00917613(1990)018<0995:cpogca>2.3.co;2), 1990.
- van Husen, D.: Quaternary glaciations in Austria, in: *Quaternary Glaciations – Extent and Chronology, Part I, Europe*, *Developments in Quaternary Science*, 2, Elsevier, Amsterdam, 1-13, [https://doi.org/10.1016/s1571-0866\(04\)80051-4](https://doi.org/10.1016/s1571-0866(04)80051-4), 2004.
- Van Lith, Y., Vasconcelos, C., Warthmann, R., Martins, J., and McKenzie, J.: Bacterial sulfate reduction and salinity: Two controls on dolomite precipitation in lagoa vermelha and brejo do espinho (brazil), *Hydrobiologia*, 485, 35-49, <https://doi.org/10.1007/s00792-005-0441-8>, 2002.
- van Tuyl, F.M.: The origin of dolomite, *Iowa Geological Survey Annual Report*, 25, 251-421, <https://doi.org/10.17077/2160-5270.1180>, 1914.

- Vasconcelos, C., McKenzie, J. A., Bernasconi, S., Grujic, D., and Tiens, A. J.: Microbial mediation as a possible mechanism for natural dolomite formation at low temperatures, *Nature*, 377, 220-222, <https://doi.org/10.1038/377220a0>, 1995.
- Vasconcelos, C., and McKenzie, J. A.: Microbial mediation of modern dolomite precipitation and diagenesis under anoxic conditions (Lagoa Vermelha, Rio de Janeiro, Brazil), *Journal of Sedimentary Research*, 67, 378-390, <https://doi.org/10.1306/d4268577-2b26-11d7-8648000102c1865d>, 1997.
- von Breyman, M. T., Collier, R., and Suess, E.: Magnesium adsorption and ion exchange in marine sediments: A multi-component model, *Geochimica et Cosmochimica Acta*, 54, 3295-3313, [https://doi.org/10.1016/0016-7037\(90\)90286-t](https://doi.org/10.1016/0016-7037(90)90286-t), 1990.
- von der Borch, C. C., Lock, D. E., and Schwebel, D.: Ground-water formation of dolomite in the Coorong region of South Australia, *Geology*, 3, 283-285, [https://doi.org/10.1130/0091-7613\(1975\)3<283:gfdit>2.0.co;2](https://doi.org/10.1130/0091-7613(1975)3<283:gfdit>2.0.co;2), 1975.
- von Hoyningen-Huene, A. J. E., Schneider, D., Fussmann, D., Reimer, A., Arp, G., and Daniel, R.: Bacterial succession along a sediment porewater gradient at Lake Neusiedl in Austria, *Scientific Data*, 6, 1-7, <https://doi.org/10.1038/s41597-019-0172-9>, 2019.
- Warren, J. K.: Sedimentology and mineralogy of dolomitic Coorong lakes, South Australia, *Journal of Sedimentary Research*, 60, 843-858, <https://doi.org/10.1306/212f929b-2b24-11d7-8648000102c1865d>, 1990.
- Wenk, H.-R., Hu, M., and Frisia, S.: Partially disordered dolomite: microstructural characterization of Abu Dhabi sabkha carbonates, *American Mineralogist*, 78, 769-774, 1993.
- Whitman, W. B.: *Bergey's manual of systematics of Archaea and Bacteria*, Wiley Online Library, 2015.
- Wickham, H.: *ggplot2: elegant graphics for data analysis*, Springer, https://doi.org/10.1007/978-3-319-24277-4_12, 2016.
- Wolfram, G.: Bedeutung und Vorkommen von Salzlebensräumen, in: *Salzlebensräume in Österreich*, edited by Wolfram, G., Zülka, K. P., Albert, R., Danihelka, J., Eder, E., Fröhlich, W., Holzer, T., Holzinger, W. E., Huber, H.-J., Korner, I., Lang, A., Mazzucco, K., Milasowszky, N., Oberleitner, I., Rabitsch, W., Sauberer, N., Schagerl, M., Schlick-Steiner, B. C., Steiner, F. M. and Steiner, K.-H., Umweltbundesamt, Wien, 13-26, 2006.
- Wright, D. T., and Wacey, D.: Precipitation of dolomite using sulphate-reducing bacteria from the Coorong Region, South Australia: significance and implications, *Sedimentology*, 52, 987-1008, <https://doi.org/10.1111/j.1365-3091.2005.00732.x>, 2005.
- Wolfram, G. and Herzig, A.: Nährstoffbilanz Neusiedler See, *Wiener Mitteilungen*, 228, 317-338, 2013.
- Zámolyi, A., Salcher, B., Draganits, E., Exner, U., Wagreich, M., Gier, S., Fiebig, M., Lomax, J., Surányi, G., and Diel, M.: Latest Pannonian and Quaternary evolution at the transition between Eastern Alps and Pannonian Basin: new insights from geophysical, sedimentological and geochronological data, *International Journal of Earth Sciences*, 106, 1695-1721, <https://doi.org/10.1007/s00531-016-1383-3>, 2017.
- Zhang, J., Kobert, K., Flouri, T., and Stamatakis, A.: PEAR: a fast and accurate Illumina Paired-End read mergeR, *Bioinformatics*, 30, 614-620, <https://doi.org/10.1093/bioinformatics/btt593>, 2013a.
- Zhang, F., Yan, C., Teng, H.H., Roden, E.E. and Xu, H.: In situ AFM observations of Ca-Mg carbonate crystallization catalyzed by dissolved sulfide: Implications for sedimentary dolomite formation, *Geochimica et Cosmochimica Acta*, 105, 44-55, <https://doi.org/10.1016/j.gca.2012.11.010>, 2013b.

3. Bacterial succession along a pore water gradient at Lake Neusiedl in Austria

Avril Jean Elisabeth von Hoyningen-Huene, Dominik Schneider, Dario Fussmann, Andreas Reimer, Gernot Arp, and Rolf Daniel

Scientific Data (2019), 6, 1-7

Abstract. We provide bacterial 16S rRNA community and hydrochemical data from water and sediments of Lake Neusiedl, Austria. The sediments were retrieved at 5 cm intervals from 30–40 cm push cores. The lake water community was recovered by filtration through a 3.0/0.2 µm filter sandwich. For 16S rRNA gene amplicon-based community profiling, DNA was extracted from the sediment and filters and the bacterial V3-V4 regions were amplified and sequenced using a MiSeq instrument (Illumina). The reads were quality-filtered and processed using open source bioinformatic tools, such as PEAR, cutadapt and VSEARCH. The taxonomy was assigned against the SILVA SSU NR 132 database. The bacterial community structure was visualised in relation to water and porewater chemistry data. The bacterial community in the water column is distinct from the sediment. The most abundant phyla in the sediment shift from Proteobacteria to Chloroflexota (formerly Chloroflexi). Ammonium and total alkalinity increase while sulphate concentrations in the porewater decrease. The provided data are of interest for studies targeting biogeochemical cycling in lake sediments.

3.1 Background and Summary

Lake Neusiedl is the largest, seasonally evaporative lake in western Europe covering an area of approximately 315 km. Its sediments show high contents of authigenic high magnesium calcite and poorly ordered dolomite, which have been the focus of multiple studies on sediment formation, geochemistry and water level (Soja et al., 2013; Kogelbauer and Loiskandl, 2015; Müller et al., 1972; Schroll and Wieden, 1960). There is a strong economic interest in the lake and the surrounding national parks due to their recreational value. Thus, the lake's water quality, including potential pathogenic microbes, is monitored on a regular basis (Hatvani et al., 2018; Magyar et al., 2013; Jirsa et al., 2014; Pretzer et al., 2017). Nevertheless, the bacterial community composition of water and sediment remains largely unexplored, particularly in relation to the lakes' hydrochemistry.

Soft sediment push-cores were taken in the bay of Rust in August 2017 (Figure 3.1a). Two 30–40 cm cores were used for bacterial community analysis and one for porewater extraction and analysis. The water (core supernatant) was filtered through a 3.0 and 0.2 µm filter sandwich. All samples for bacterial community analysis were stored in RNAprotect Bacteria Reagent (Qiagen, Hilden, Germany) for transport. The reagent was removed by centrifugation from the samples prior to storage at -80 °C. Metagenomic DNA was extracted from 0.25 g of sediment or one third of a filter. Subsequently, the V3-V4 region of bacterial 16S rRNA genes were amplified using primers described by Klindworth et al. (2013). After purification with magnetic beads, the amplicons were sequenced, yielding a total of 6,044,032 raw paired-end reads. Bioinformatic processing of the data included quality-filtering and base pair correction of overlapping regions (fastp), read-merging (PEAR), primer clipping (cutadapt), size-selection, dereplication, denoising and chimera removal (VSEARCH). After taxonomic assignment 2,263,812 high-quality 16S rRNA gene sequences remained in the dataset. Amplicon sequence variants (Callahan et al., 2017; ASVs) with 100 % sequence identity were screened with BLASTn against the SILVA SSU 132 NR database for taxonomic assignment. The ASV abundance table was used for visualization of the bacterial community. Total alkalinity (TA) was determined by titration. Major cations and anions were measured by ion-chromatography and ICP-MS was used to determine trace element content. Nutrient concentrations and total sulphide were assessed photometrically (Grasshoff et al., 2009). Porewater chemistry and bacterial community composition were analysed in intervals of 5 cm (Figure 3.1c).

The bacterial community composition and diversity as well as the porewater chemistry of the sediment are distinct from the water column and change gradually with depth (Figure 3.1b). The water column has a lower phylogenetic diversity than the top sediment layers (Figure 3.1c) and is dominated by aquatic *Actinobacteria* (hgcl clade; Aguilar et al., 2018; Warnecke et al., 2004; Tandon et al., 2018; Newton et al., 2011; Neuenschwander et al., 2018) and freshwater *Alphaproteobacteria* (SAR11 clade III; Aguilar et al., 2018; Herlemann et al., 2014; Brown et al., 2012; Zhang et al., 2014b; Llíros et al., 2014; Eiler et al., 2016) with relative abundances of more than 40 % and up to 20 % (Figure 3.1c and 3.2). The uppermost sediment layer is the most diverse and harbours the largest number of associated genera (Figure 3.2). It shares community members of water and sediment, such as *Synechococcus* or the algae-associated *Phaeodactylibacter* (Flombaum et al., 2013; Lei et al., 2015). The phylogenetic diversity (Figure 3.1c) and associated genera (Figure 3.2) in the sediment decrease gradually with depth until approximately 20 cm. Members of the *Proteobacteria* and *Chloroflexota* (Parks et al., 2018) are dominant in the sediment community, which shifts from 15-35 % *Gammaproteobacteria* in the top 15 cm to approximately 40 % *Chloroflexota* below 15 cm. Notably, the upper sediment layers harbour sulphate-reducing bacteria, such

as *Desulfobacteraceae* and *Desulfarculaceae* (Schneider et al., 2013; Diaz et al., 2014; Broman et al., 2017; Reyes et al., 2016; Figure 3.2). The decline in sulphate, increase in total sulphide ($\Sigma\text{H}_2\text{S}$) and low redox potential also indicate sulphate reduction (Figure 3.1c). Below 15 cm the bacterial community is associated with *Anaerolineae*, *Aminicenantales* and *Dehalococcoidia* (Figure 3.2). Members of these taxa are known fermenters, organohalide respirators and hydrocarbon degraders (Hug et al., 2013; Dombrowski et al., 2017; Kadnikov et al., 2019). Increasing degradative processes are indicated by the increase in ammonium and total alkalinity (Figure 3.1c).

The bacterial community of Lake Neusiedl has mainly been studied with regard to potential pathogens (Hatvani et al., 2018; Pretzer et al., 2017). Here, *Enterobacteriaceae*, more specifically *Escherichia/Shigella*, but not *Vibrionaceae* were detected with a relative abundance of up to 10 % at almost all depths in the sediment, but not in the water column. While they indicate an anthropogenic impact on the sediment, the bacteria detected are based on DNA amplification and may not be metabolically active. This data may contribute to studies identifying the sampling site as hotspot for faecal pollution (Hatvani et al., 2018; Magyar et al., 2013; Figure 3.1a). Further, this survey forms a basis for studies targeting biogeochemical cycling in alkaline lakes.

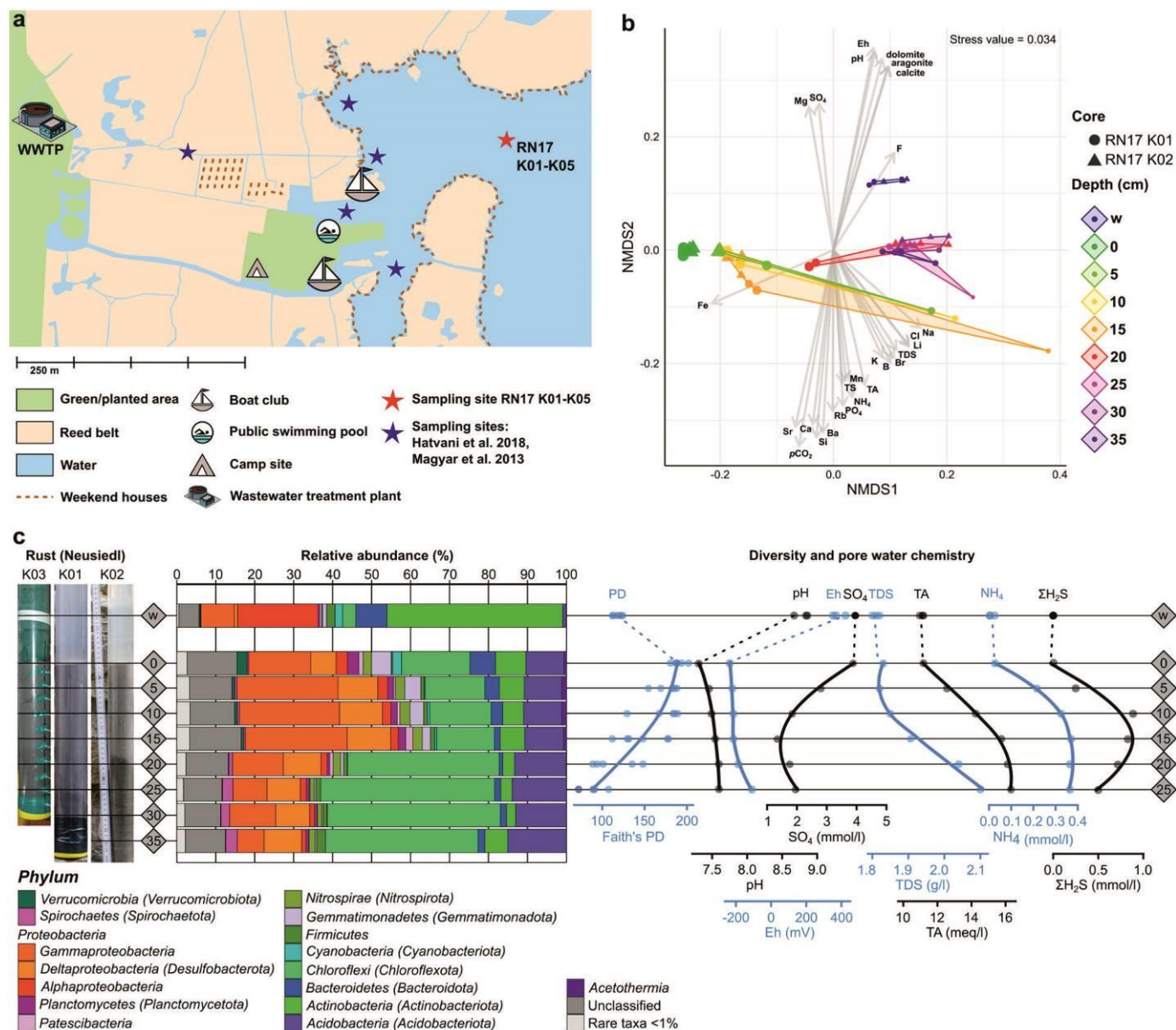


Figure 3.1: Sampling site in the bay of Rust, NMDS and depth profiles of the bacterial community composition and porewater properties. (a) Sampling site of this study (red star) and previous studies (blue stars). Markers for anthropogenic influences, such as a wastewater treatment, holiday houses (brown dashed lines) and recreational sites (pool, boat club, camp site) are indicated by pictograms or dashed lines. (b) Non-metric multidimensional scaling (NMDS) of bacterial communities ($n = 47$) with the environmental fit ($p < 0.01$) of porewater properties (grey arrows) based on a weighted generalized UniFrac analysis using the vegan package incorporated into ampvis2 (Andersen et al., 2018; Oksanen et al., 2013). Depths are indicated in cm or w (water column) and triangles or circles indicate the sediment core. (c) Sampling depths of the sediment cores (Rust Neusiedl RN-K01 and RN-K02) for bacterial community analysis. Each bacterial phylum depicted here comprises more than 1% relative abundance of the bacterial community in at least one sample. All other amplicon sequence variants (ASVs) are summarized as rare taxa and those with a taxonomic match below 95% sequence identity were summarized as "Unclassified". The phylum Proteobacteria is shown at class level (Alpha-, Gamma-, Deltaproteobacteria). Names in brackets indicate revised phylum classifications according to Parks et al. (2018). The phylogenetic diversity (Faith's PD) was calculated based on the rarefied community (5,873 reads per sample) and a midpoint-rooted phylogenetic tree. Indicators for microbial activity in the porewater chemistry were selected and depicted as profiles of up to 25 cm depth.

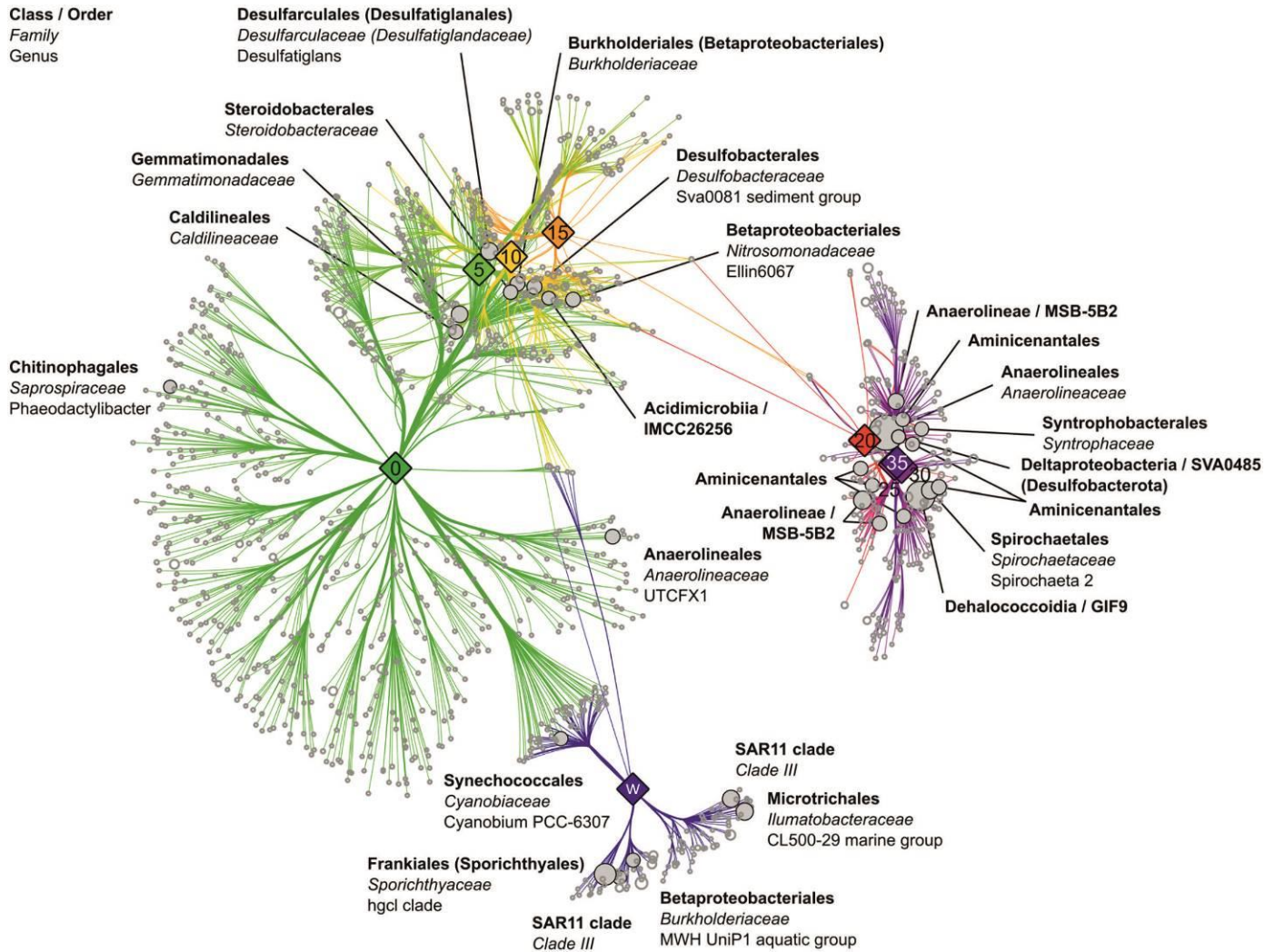


Figure 3.2: Bacterial genera associated with the different depths of the sediment cores and water column. The association network was calculated with the indicpecies (Cáceres and Legendre, 2009) package in R and visualised in Cytoscape with an edge-weighted spring embedded layout. Branch lengths indicate the phi correlation coefficient. Each light grey circle indicates a bacterial genus associated ($p < 0.001$) with the depth it is connected to. The 30 most abundant genera are indicated by filled circles and named up to the point where the classification turns to uncultured. Revised names according to Parks et al. (2018) are indicated in brackets. Average relative abundance of each genus among all samples is indicated by the circle size. Each sampling depth is indicated by a filled diamond shape containing the depth in cm or w (water column).

3.2 Methods

3.2.1 Sediment sampling at Lake Neusiedl, Austria.

Three soft sediment push-cores (RN-K01/K02/K03) covering 30 to 40 cm depth were sampled in close lateral distance to each other at the bay of Rust (16°42′33.635″E, 47°48′12.929″N) at Lake Neusiedl, Austria in August of 2017. PVC coring tubes (Uwitec, Mondsee, Austria) of 60 cm length and 63 mm diameter (RN-K01/K03) or 100 cm and 50 mm diameter (RN-K02) were manually pushed into the sediment at the sampling site. A rubber plug was applied to the top of the coring tube to create a partial vacuum, which allowed retrieval of the sediment. After allowing the sediment to settle on cores RN-K01 and K02, 600 ml core supernatant (water column) was filtered through a 3.0 µm polycarbonate (Merck, Darmstadt, Germany) and 0.2 µm polyethersulfone (Sartorius, Göttingen, Germany) filter sandwich. Subsequently, filters were immediately stored in RNeasy Protect Bacteria Reagent (Qiagen, Hilden, Germany). Sampling of the sediment for community analysis occurred under exclusion of the outer 1 cm of sediment, which is in contact with the walls of the coring tubes. RN-K01/K02 were sampled in triplicate at every 5 cm of depth. RN-K02 was sampled at a higher resolution (every 2.5) as the sediment showed finer lamination. Every triplicate was immediately mixed with RNeasy Protect Bacteria Reagent (Qiagen, Hilden, Germany) and kept at ambient temperature in a cool box with freezer elements for transport. Before storage, samples were centrifuged at 3,220 × g for 15 min and the clear supernatant containing the RNeasy Protect Bacteria Reagent discarded. Samples were stored at -80 °C. Core RN-K03 and the core supernatant were stored in the cool and dark until analytical chemical analysis.

3.2.2 DNA extraction and amplification of bacterial 16S rRNA genes.

DNA was extracted from 0.25 mg of sediment from each sample of RN-K01/K02 using the MoBio Power Soil Kit (MoBio, CA, USA) with minor modifications. For this purpose, sediments were thawed on ice and homogenized to disrupt any layering caused by the previous centrifugation step. Subsequently, 0.25 mg were transferred into bead-beating tubes supplied by the manufacturer. DNA from the water column (core supernatant) was extracted by cutting one third of the frozen filter sandwiches into small pieces in the bead-beating tubes. After the addition of SDS-containing Solution C1, cells were mechanically disrupted with a FastPrep (MP Biomedicals, Eschwege, Germany) at 6.5 m/s for 20 s. After disruption, the DNA was extracted according to manufacturer's instructions. Subsequently, DNA was eluted twice in 50 µl of prewarmed DEPC-treated water (Schneider et al., 2017b). Bacterial 16 S rRNA genes were amplified by PCR with forward and reverse primers published by (Klindworth et al., 2013) and added adapters for MiSeq sequencing (underlined) (D-Bact-0341-b-S-17, TCGTCGGCAGCGTCAGATGTGTATAAGAGACAG CCTACGGGNGGCWGCAG; S-D-Bact-0785-a-A-21, GTCTCGTGGGCTCGGAGATGTGTATAAGA GACAGGACTACHVGGGTATCTAATCC). PCR reactions were performed in a total volume of 50 µl containing 10 µl of five-fold GC Buffer (Thermo Scientific, Waltham, MA, USA), 5 % DMSO, 0.2 mM of forward and reverse primer, 200 µM dNTPs, 0.2 mM MgCl₂, 1 U Phusion High-Fidelity DNA polymerase (Thermo Scientific, Waltham, MA, USA) and 20–25 ng template DNA. The PCR mixture was denatured for 1 min at 98 °C and then subjected to 25 cycles at 98 °C for 45 s, 45 s at 60 °C, and 30 s at 72 °C, followed by a final extension at 72 °C for 5 min. Negative controls were prepared without template and positive controls with genomic *E. coli* DH5α DNA as template. PCR reactions for each sample were performed in triplicate. PCR triplicates were pooled in equal amounts in order to minimize amplification bias, concentrated and purified with MagSi-NGS_{Prep} magnetic beads as recommended by the manufacturer (Steinbrenner, Wiesenbach,

Germany). After the final washing step, the beads were air-dried and DNA eluted in 30 µl of elution buffer EB (Qiagen, Hilden, Germany). Purified PCR products were quantified and sequenced as described by (Schneider et al., 2017a) using a MiSeq instrument and v3 chemistry (Illumina, San Diego, CA, USA).

3.2.3 Bioinformatic processing of 16S rRNA gene amplicons.

Paired-end sequencing data from the Illumina MiSeq were quality-filtered with fastp (Chen et al., 2018; version 0.19.4) using default settings with the addition of an increased per base phred score of 20, base pair corrections by overlap (-c), as well as 5'- and 3'-end read trimming with a sliding window of 4, a mean quality of 20 and minimum sequence size of 50 bp. After quality control, the paired-end reads were merged using PEAR (Zhang et al., 2014a; version 0.9.11) and primers clipped using cutadapt (Martin, 2011; version 1.18) with default settings. Sequences were then processed using VSEARCH (Rognes et al., 2016; v2.9.1). This included sorting and size-filtering of the paired reads to ≥ 300 bp (--sortbylength --minseqlength 300), dereplication (--derep_full length). Dereplicated amplicon sequence variants (ASVs) were denoised with UNOISE3 using default settings (--cluster_unoise - minsize 8) and chimeras were removed (--uchime3_denovo). An additional reference-based chimera removal was performed (--uchime_ref) against the SILVA SSU NR database (version 132). Raw reads were mapped to ASVs (--usearch_global-id 0.97). The taxonomy was assigned using BLAST 2.7.1+ (Altschul et al., 1990) against the SILVA SSU 132 NR database with an identity of at least 95 % to the query sequence resulting in a total of 21,009 ASVs.

3.2.4 Bacterial community analysis

For data evaluation all samples from the 5 cm intervals were analysed. Additional samples taken due to the finer lamination of one core were not considered in the presented analysis but are available in the dataset (NCBI Sequence Read Archive). Sequences comprising extrinsic domains, eukaryotes and archaea were removed from the ASV table using grepl, a base R function (version 3.4.4). A phylogenetic tree was generated by aligning all sequences of the filtered dataset with MAFFT (Katoh and Standley, 2013) at a maximum of 100 iterations. The tree was calculated using FastTree 2.1.7 (OpenMP; Price et al., 2010), saved in newick format and midpoint rooted using FigTree (Rambaut and Drummond, 2012; version 1.4.4). The dataset was analysed in R (R Core Team, 2018; version 3.5.2) and RStudio (Rstudio Team, 2016; version 1.1.456). Depth profiles in the form of bar and line charts were generated with ggplot2 (Wickham, 2016; version 3.1.0) using standard R packages. Alphadiversity indices and species richness were calculated with the ampvis2 (Andersen et al., 2018) package (version 2.4.1) and Faith's phylogenetic diversity with picante (Kembel et al., 2010; version 1.7) and the midpoint-rooted tree. For this purpose, 16 samples with a read count below 5,000 were excluded from the diversity analysis (RN17_K1_DNA_Bac_2a, 3a, 5a, 6a, RN17_K2_DNA_Bac_5a-c, 7a-c, 9a-c, 11a-c). All other samples were rarefied in ampvis2 to 5,873 reads. For the visualisation in bar charts, the mean of all replicates from both cores was used to account for the variance at the sampling sites. The non-metric multidimensional scaling (NMDS) matrix was calculated using the ASV table and phylogenetic tree in a weighted generalized UniFrac analysis using the ampvis2 package (version 2.4.1) including the package GUniFrac (Chen et al., 2012; version 1.1). Environmental fit of the metadata were also calculated and plotted onto the NMDS if $p < 0.01$. An association network of the bacterial community was calculated using the indicpecies (Cáceres and Legendre, 2009) package (version 1.7.6) with the multipatt function and the r.g species-site group association function for calculation of the association strength. The significance cut-off for the phi coefficient was set to $p < 0.001$.

The network was visualised in Cytoscape (version 3.5.1) with an edge-weighted spring-embedded layout using weight as the force and average abundance as the circle size.

3.2.5 Water column and pore water analysis

For hydrochemical analysis, capped and tightly sealed sediment cores, including the supernatant water column above, were stored upright in the cool and dark until analytical investigation 5 days after sampling. Core supernatants were collected in 250 ml polyethylene (PE) bottles for anion, nutrient, and total alkalinity (TA) determination. For cation analysis, a 50 ml aliquot of the supernatants was filtered through 0.7 μm diameter membrane filters (Merck, Darmstadt, Germany) into a PE-bottle and acidified with 100 μl HNO_3 (suprapure, Merck, Darmstadt, Germany). Physicochemical parameters of the core supernatants were measured using a WTW Multi 3430 device equipped with a WTW Tetracon 925 conductivity probe, a WTW FDO 925 probe for dissolved O_2 , a Schott Pt 61 redox electrode, and a WTW Sentix 940 electrode for temperature and pH, which was calibrated against standard pH-buffers 7.010 and 10.010 (HI6007 and HI6010, Hanna Instruments, Vöhringen, Germany). Total alkalinity was determined via titration using a hand-held titration device and 1.6 N H_2SO_4 cartridges (Hach, Loveland, CO, USA).

Redox potential (Eh) and pH gradients were measured through boreholes directly in the sediment core using a portable WTW 340i pH meter equipped with an Inlab Solids Pro pH-electrode (Mettler Toledo, Gießen, Germany) and a Pt 5900A redox electrode (SI Analytics, Mainz, Germany). Porewater was extracted from core RN-K03 using 5 cm CSS Rhizon samplers (Rhizosphere, Wageningen, Netherlands). Immediately after extraction, aliquots were fixed with Zn-acetate for determination of total sulphide or acidified with suprapure HNO_3 for analysis of main cations and trace elements. Porewater alkalinity was immediately determined by titration with cartridges (Hach, Loveland, CO, USA) containing self-prepared 0.01 n HCl as titrant. An aliquot for determination of nutrients and anions was stored in the cool and dark until subsequent analysis. Total sulphide ($\Sigma\text{H}_2\text{S}$) and nutrient concentrations (NH_4 , NO_2 , PO_4 , SiO_2) were measured by photometric methods according to Grasshoff et al. (2009), using an SI Analytics Uviline 9400 spectrophotometer within a few days after extraction.

Major cation (Ca, Mg, Na, K and Li) and anion (Cl, F, Br and SO_4) concentrations of all water samples (porewaters, water column) were analysed by ion chromatography with non-suppressed and suppressed conductivity detection, respectively (Metrohm 820 IC/Metrosep C3-250 analytical column, Metrohm 883 Basic IC/Metrohm ASupp5-250 analytical column). ICP-MS (ICAP-Q, Thermo Fisher, Waltham, MA, USA) was used to determine Sr, Ba, Fe, Mn, Rb and B, as well as control for the cation determination by ion chromatography. Total dissolved salts (TDS) were calculated as the sum of all measured cations and anions. The chemical analysis was completed within two weeks after extraction with the analytical accuracy of all methods exceeding 1.5 %.

All measured values were processed by the PHREEQC software package, version 3 (Parkhurst and Appelo, 2013), using the phreeqc.dat and wateqf4.dat databases in order to calculate ion activities and pCO_2 (partial pressure of CO_2) of the water samples and mineral saturation states. The saturation indices of all mineral phases are given as $\log(\text{IAP}/K_{\text{SO}})$ where IAP denotes the ion activity product and K_{SO} is the solubility product of the corresponding mineral (solid phase).

Data records

The 16S rRNA gene paired-end raw reads were deposited to the National Center for Biotechnology Information Sequence Read Archive (SRA) and can be found under the accession number PRJNA507590

(Bio Project 507590/SRP171602). This BioProject contains 63 samples and 126 zipped FASTQ files, which were processed using the CASAVA software (Illumina, San Diego, CA, USA). The processing included demultiplexing and adapter removal from the sequences. The following files have been deposited at figshare: a FASTA file with the assigned ASV sequences after bioinformatic processing; the ASV count table with taxonomic assignments, the read statistics before, during and after bioinformatic processing; the metadata, porewater chemical data and alphadiversity metrics of each sample. The individual files may also be accessed through a figshare collection.

Technical Validation

For microbial community analysis the layers (2.5–5 cm) of both soft sediment push-cores were sampled in three technical replicates to allow for the microbial heterogeneity at each depth. The PCR reactions were run in three technical replicates per sample and PCR products were pooled equimolar. Negative controls without DNA template and positive controls with genomic *E. coli* DH5 α DNA as template were also performed. Correct amplicon size was determined on a 0.8 % agarose gel. PCR triplicates per sample were pooled in equimolar amounts for amplicon sequencing to minimize possible PCR bias. Physiochemical data were measured with calibrated probes and ions and nutrients were measured against IC and nutrient standards from Merck (Darmstadt, Germany) and Honeywell Fluka (Charlotte, NC, USA). The analytical accuracy of all methods exceeded 1.5 %.

Acknowledgements

This study was funded by the German research foundation (DFG) in the framework of the research unit “CHARON” (subproject TP7: DA 374/11-1, AR 335/8-1). We thank Prof. Dr. Patrick Meister, University of Vienna, for his support during the field work and his feedback. Anja Poehlein and Melanie Heinemann are hereby gratefully acknowledged for performing the amplicon sequencing and initial sequence processing after the MiSeq run. We acknowledge support by the Open Access Publication Funds of the University of Göttingen.

References

- Aguilar, P., Dorador, C., Vila, I., and Sommaruga, R.: Bacterioplankton composition in tropical high-elevation lakes of the Andean plateau, *FEMS microbiology ecology*, 94, fiy004, <https://doi.org/10.1093/femsec/fiy004>, 2018.
- Altschul, S. F., Gish, W., Miller, W., Myers, E. W., and Lipman, D. J.: Basic local alignment search tool, *Journal of molecular biology*, 215, 403-410, [https://doi.org/10.1016/s0022-2836\(05\)80360-2](https://doi.org/10.1016/s0022-2836(05)80360-2), 1990.
- Andersen, K. S., Kirkegaard, R. H., Karst, S. M., and Albertsen, M.: ampvis2: an R package to analyse and visualise 16S rRNA amplicon data, *BioRxiv*, 299537, <https://doi.org/10.1101/299537>, 2018.
- Broman, E., Sjöstedt, J., Pinhassi, J., and Dopson, M.: Shifts in coastal sediment oxygenation cause pronounced changes in microbial community composition and associated metabolism, *Microbiome*, 5, 1-18, <https://doi.org/10.1186/s40168-017-0311-5>, 2017.
- Brown, M. V., Lauro, F. M., DeMaere, M. Z., Muir, L., Wilkins, D., Thomas, T., Riddle, M. J., Fuhrman, J. A., Andrews-Pfannkoch, C., and Hoffman, J. M.: Global biogeography of SAR11 marine bacteria, *Molecular systems biology*, 8, 595, <https://doi.org/10.1038/msb.2012.28>, 2012.
- Cáceres, M. D., and Legendre, P.: Associations between species and groups of sites: indices and statistical inference, *Ecology*, 90, 3566-3574, <https://doi.org/10.1890/08-1823.1>, 2009.
- Callahan, B. J., McMurdie, P. J., and Holmes, S. P.: Exact sequence variants should replace operational taxonomic units in marker-gene data analysis, *The ISME journal*, 11, 2639-2643, <https://doi.org/10.1038/ismej.2017.119>, 2017.
- Chen, J., Bittinger, K., Charlson, E. S., Hoffmann, C., Lewis, J., Wu, G. D., Collman, R. G., Bushman, F. D., and Li, H.: Associating microbiome composition with environmental covariates using generalized UniFrac distances, *Bioinformatics*, 28, 2106-2113, <https://doi.org/10.1093/bioinformatics/bts342>, 2012.
- Chen, S., Zhou, Y., Chen, Y., and Gu, J.: fastp: an ultra-fast all-in-one FASTQ preprocessor, *Bioinformatics*, 34, i884-i890, <https://doi.org/10.1093/bioinformatics/bty560>, 2018.
- Diaz, M., Van Norstrand, J., Eberli, G., Piggot, A., Zhou, J., and Klaus, J.: Functional gene diversity of oolitic sands from Great Bahama Bank, *Geobiology*, 12, 231-249, <https://doi.org/10.1111/gbi.12079>, 2014.
- Dombrowski, N., Seitz, K. W., Teske, A. P., and Baker, B. J.: Genomic insights into potential interdependencies in microbial hydrocarbon and nutrient cycling in hydrothermal sediments, *Microbiome*, 5, 1-13, <https://doi.org/10.1186/s40168-017-0322-2>, 2017.
- Eiler, A., Mondav, R., Sinclair, L., Fernandez-Vidal, L., Scofield, D. G., Schwientek, P., Martinez-Garcia, M., Torrents, D., McMahon, K. D., and Andersson, S. G.: Tuning fresh: radiation through rewiring of central metabolism in streamlined bacteria, *The ISME journal*, 10, 1902-1914, <https://doi.org/10.1038/ismej.2015.260>, 2016.
- Flombaum, P., Gallegos, J. L., Gordillo, R. A., Rincón, J., Zabala, L. L., Jiao, N., Karl, D. M., Li, W. K., Lomas, M. W., and Veneziano, D.: Present and future global distributions of the marine Cyanobacteria *Prochlorococcus* and *Synechococcus*, *Proceedings of the National Academy of Sciences*, 110, 9824-9829, <https://doi.org/10.1073/pnas.1307701110>, 2013.
- Grasshoff, K., Kremling, K., and Ehrhardt, M.: *Methods of seawater analysis*, John Wiley & Sons, <https://doi.org/10.1002/9783527613984>, 2009.

- Hatvani, I. G., Kirschner, A. K., Farnleitner, A. H., Tanos, P., and Herzig, A.: Hotspots and main drivers of fecal pollution in Neusiedler See, a large shallow lake in Central Europe, *Environmental Science and Pollution Research*, 25, 28884-28898, <https://doi.org/10.1007/s11356-018-2783-7>, 2018.
- Herlemann, D. P., Woelk, J., Labrenz, M., and Jürgens, K.: Diversity and abundance of "Pelagibacterales" (SAR11) in the Baltic Sea salinity gradient, *Systematic and applied microbiology*, 37, 601-604, <https://doi.org/10.1016/j.syapm.2014.09.002>, 2014.
- Hug, L. A., Castelle, C. J., Wrighton, K. C., Thomas, B. C., Sharon, I., Frischkorn, K. R., Williams, K. H., Tringe, S. G., and Banfield, J. F.: Community genomic analyses constrain the distribution of metabolic traits across the Chloroflexi phylum and indicate roles in sediment carbon cycling, *Microbiome*, 1, 1-17, <https://doi.org/10.1186/2049-2618-1-22>, 2013.
- Jirsa, F., Pirker, D., Krachler, R., and Keppler, B. K.: Total mercury in sediments, macrophytes, and fish from a shallow steppe lake in eastern Austria, *Chemistry & biodiversity*, 11, 1263-1275, <https://doi.org/10.1002/cbdv.201400172>, 2014.
- Kadnikov, V. V., Mardanov, A. V., Beletsky, A. V., Karnachuk, O. V., and Ravin, N. V.: Genome of the candidate phylum Aminicenantes bacterium from a deep subsurface thermal aquifer revealed its fermentative saccharolytic lifestyle, *Extremophiles*, 23, 189-200, <https://doi.org/10.1007/s00792-018-01073-5>, 2019.
- Katoh, K., and Standley, D. M.: MAFFT multiple sequence alignment software version 7: improvements in performance and usability, *Molecular biology and evolution*, 30, 772-780, <https://doi.org/10.1093/molbev/mst010>, 2013.
- Kembel, S. W., Cowan, P. D., Helmus, M. R., Cornwell, W. K., Morlon, H., Ackerly, D. D., Blomberg, S. P., and Webb, C. O.: Picante: R tools for integrating phylogenies and ecology, *Bioinformatics*, 26, 1463-1464, <https://doi.org/10.1093/bioinformatics/btq166>, 2010.
- Klindworth, A., Pruesse, E., Schweer, T., Peplies, J., Quast, C., Horn, M., and Glöckner, F. O.: Evaluation of general 16S ribosomal RNA gene PCR primers for classical and next-generation sequencing-based diversity studies, *Nucleic acids research*, 41, e1-e1, <https://doi.org/10.1093/nar/gks808>, 2013.
- Kogelbauer, I., and Loiskandl, W.: Characterization of sediment layer composition in a shallow lake: from open water zones to reed belt areas, *Hydrology & Earth System Sciences*, 19, 1427-1438, <https://doi.org/10.5194/hess-19-1427-2015>, 2015.
- Lei, X., Li, Y., Wang, G., Chen, Y., Lai, Q., Chen, Z., Zhang, J., Liao, P., Zhu, H., and Zheng, W.: *Phaeodactylibacter luteus* sp. nov., isolated from the oleaginous microalga *Picochlorum* sp, *International journal of systematic and evolutionary microbiology*, 65, 2666-2670, <https://doi.org/10.1099/ijs.0.000321>, 2015.
- Llirós, M., Inceoğlu, Ö., García-Armisen, T., Anzil, A., Leporcq, B., Pigneur, L.-M., Viroux, L., Darchambeau, F., Descy, J.-P., and Servais, P.: Bacterial community composition in three freshwater reservoirs of different alkalinity and trophic status, *PLoS One*, 9, e116145, <https://doi.org/10.1371/journal.pone.0116145>, 2014.
- Magyar, N., Hatvani, I. G., Székely, I. K., Herzig, A., Dinka, M., and Kovács, J.: Application of multivariate statistical methods in determining spatial changes in water quality in the Austrian part of Neusiedler See, *Ecological Engineering*, 55, 82-92, <https://doi.org/10.1016/j.ecoleng.2013.02.005>, 2013.
- Martin, M.: Cutadapt removes adapter sequences from high-throughput sequencing reads, *EMBnet journal*, 17, 10-12, <https://doi.org/10.14806/ej.17.1.200>, 2011.

- Müller, G., Irion, G., and Förstner, U.: Formation and diagenesis of inorganic Ca– Mg carbonates in the lacustrine environment, *Naturwissenschaften*, 59, 158-164, <https://doi.org/10.1007/bf00637354>, 1972.
- Neuenschwander, S. M., Ghai, R., Pernthaler, J., and Salcher, M. M.: Microdiversification in genome-streamlined ubiquitous freshwater Actinobacteria, *The ISME journal*, 12, 185-198, <https://doi.org/10.1038/ismej.2017.156>, 2018.
- Newton, R. J., Jones, S. E., Eiler, A., McMahon, K. D., and Bertilsson, S.: A guide to the natural history of freshwater lake bacteria, *Microbiology and molecular biology reviews*, 75, 14-49, <https://doi.org/10.1128/mnbr.00028-10>, 2011.
- Oksanen, J., Blanchet, F., Kindt, R., Legendre, P., Minchin, P., O'Hara, R., Simpson, G., Solymos, P., Stevens, M., and Wagner, H.: *Vegan: community ecology package* <http://CRAN.R-project.org/package=vegan>, 2013.
- Parkhurst, D. L., and Appelo, C.: Description of input and examples for PHREEQC version 3: a computer program for speciation, batch-reaction, one-dimensional transport, and inverse geochemical calculations, US Geological Survey, 2328-7055, <https://doi.org/10.3133/tm6a43>, 2013.
- Parks, D. H., Chuvochina, M., Waite, D. W., Rinke, C., Skarshewski, A., Chaumeil, P.-A., and Hugenholtz, P.: A standardized bacterial taxonomy based on genome phylogeny substantially revises the tree of life, *Nature biotechnology*, 36, 996-1004, <https://doi.org/10.1038/nbt.4229>, 2018.
- Pretzer, C., Druzhinina, I. S., Amaro, C., Benediktsdóttir, E., Hedenström, I., Hervio-Heath, D., Huhulescu, S., Schets, F. M., Farnleitner, A. H., and Kirschner, A. K.: High genetic diversity of *Vibrio cholerae* in the European lake Neusiedler See is associated with intensive recombination in the reed habitat and the long-distance transfer of strains, *Environmental microbiology*, 19, 328-344, <https://doi.org/10.1111/1462-2920.13612>, 2017.
- Price, M. N., Dehal, P. S., and Arkin, A. P.: FastTree 2—approximately maximum-likelihood trees for large alignments, *PLoS One*, 5, e9490, <https://doi.org/10.1371/journal.pone.0009490>, 2010.
- Rambaut, A., and Drummond, A.: *FigTree: Tree figure drawing tool*, v1. 4.2, Institute of Evolutionary Biology, University of Edinburgh, 2012.
- Reyes, C., Dellwig, O., Dähnke, K., Gehre, M., Noriega-Ortega, B. E., Böttcher, M. E., Meister, P., and Friedrich, M. W.: Bacterial communities potentially involved in iron-cycling in Baltic Sea and North Sea sediments revealed by pyrosequencing, *FEMS microbiology ecology*, 92, fiw054, <https://doi.org/10.1093/femsec/fiw054>, 2016.
- Rognes, T., Flouri, T., Nichols, B., Quince, C., and Mahé, F.: VSEARCH: a versatile open source tool for metagenomics, *PeerJ*, 4, e2584, <https://doi.org/10.7717/peerj.2584>, 2016.
- R Core Team. R: A language and environment for statistical computing. R Foundation for Statistical Computing, <https://www.Rproject.org>, 2019.
- RStudio Team. RStudio: integrated development for R. RStudio Inc., <http://www.rstudio.com>, 2016.
- Schneider, D., Arp, G., Reimer, A., Reitner, J., and Daniel, R.: Phylogenetic analysis of a microbialite-forming microbial mat from a hypersaline lake of the Kiritimati Atoll, Central Pacific, *PLoS One*, 8, e66662, <https://doi.org/10.1371/journal.pone.0066662>, 2013.
- Schneider, D., Thürmer, A., Gollnow, K., Lugert, R., Gunka, K., Groß, U., and Daniel, R.: Gut bacterial communities of diarrheic patients with indications of *Clostridioides difficile* infection, *Scientific data*, 4, 1-6, 170152, <https://doi.org/10.1038/sdata.2017.152>, 2017a.

- Schneider, D., Wemheuer, F., Pfeiffer, B., and Wemheuer, B.: Extraction of total DNA and RNA from marine filter samples and generation of a cDNA as universal template for marker gene studies, in: *Metagenomics*, Springer, 13-22, https://doi.org/10.1007/978-1-4939-6691-2_2, 2017b.
- Schroll, E., and Wieden, P.: Eine rezente Bildung von Dolomit im Schlamm des Neusiedler Sees, *Tschermaks mineralogische und petrographische Mitteilungen*, 7, 286-289, <https://doi.org/10.1007/bf01127917>, 1960.
- Soja, G., Züger, J., Knoflacher, M., Kinner, P., and Soja, A.-M.: Climate impacts on water balance of a shallow steppe lake in Eastern Austria (Lake Neusiedl), *Journal of Hydrology*, 480, 115-124, <https://doi.org/10.1016/j.jhydrol.2012.12.013>, 2013.
- Tandon, K., Yang, S.-H., Wan, M.-T., Yang, C.-C., Baatar, B., Chiu, C.-Y., Tsai, J.-W., Liu, W.-C., and Tang, S.-L.: Bacterial community in water and air of two sub-alpine lakes in Taiwan, *Microbes and environments*, ME17148, <https://doi.org/10.1264/jsme2.me17148>, 2018.
- Warnecke, F., Amann, R., and Pernthaler, J.: Actinobacterial 16S rRNA genes from freshwater habitats cluster in four distinct lineages, *Environmental microbiology*, 6, 242-253, <https://doi.org/10.1111/j.1462-2920.2004.00561.x>, 2004.
- Wickham, H.: *ggplot2: elegant graphics for data analysis*, springer, <https://doi.org/10.1111/j.1541-0420.2011.01616.x>, 2016.
- Zhang, J., Kobert, K., Flouri, T., and Stamatakis, A.: PEAR: a fast and accurate Illumina Paired-End read mergeR, *Bioinformatics*, 30, 614-620, <https://doi.org/10.1093/bioinformatics/btt593>, 2014a.
- Zhang, Y., Zhao, Z., Dai, M., Jiao, N., and Herndl, G. J.: Drivers shaping the diversity and biogeography of total and active bacterial communities in the South China Sea, *Molecular Ecology*, 23, 2260-2274, <https://doi.org/10.1111/mec.12739>, 2014b

4. Tracing early diagenesis: Pore water gradients and bacterial communities within Holocene carbonate sediments in the lagoon of Aldabra (Seychelles)

Dario Fussmann, Avril Jean Elisabeth von Hoyningen-Huene, Andreas Reimer, Dominik Schneider, Volker Karius, Sylvia Riechelmann, Volker Liebetrau, Torben Gentz, Rolf Daniel, and Gernot Arp

Manuscript in preparation for submission to *The Depositional Record*

Abstract. Comparative sediment pore water studies are crucial to unravel the effects of early diagenesis on geochemical proxies of shallow-marine carbonate sediments. The lagoon of Aldabra, located in the western Indian Ocean, was suggested to be a suitable setting to retrace such reactions. It has been proposed to be a recent analogue of Jurassic lagoons, which are characterized by the deposition of thick, fine-grained carbonate mud successions. Within the 34·14.5 km large lagoon, we analyzed three different locations. One in the western- (WL), northern- (NL), and southern-(SL) part, respectively. Unconsolidated sediments were sampled by using push cores, exhibiting different types of deposits and pore water environments. The west lagoon cores consist of intertidal, bioclastic carbonate sand, characterized by an oxic and porous pore space. North lagoon sediments occur preferentially in supratidal karstic depressions and consist of coarse-grained shell detritus. The pore space is entirely anoxic and marked by high porosities. Cores from the south lagoon contain fine-grained, greyish carbonate mud, traversed by mangrove roots. The anoxic pore space harbors low porosities, due to small sized sediment particles. Radiocarbon data of WL and SL represent a timespan < 2,500 a, which limits the time scale for diagenetic processes in the present study. Considerable alterations were solely found in WL sediments, in form of marine vadose, cryptocrystalline calcite cements. The precise pathway of cement formation is not entirely clear. It may be either induced abiogenic by evaporation of pore waters during low tide, or biologically influenced by the presence of thin microbial mats. Deposits from NL and SL do not show significant traces of geochemical alteration. Yet, pore water gradients indicate dissolution of metastable carbonate, induced by acidifying sulfur oxidizing bacteria of the order Campylobacterales. These findings indicate that early diagenesis possibly occurs faster in oxygenated than in anoxic environments.

4.1 Introduction

Geochemical proxies of fine-grained carbonate sediments are commonly used to retrace past environmental conditions, including temperature, salinity, oxygenation, water mass exchange, and primary productivity (Elderfield et al., 2006; Groeneveld et al., 2018; Zachos et al., 2001; Xu et al., 2006). However, proxies like stable isotopes or trace elements can be strongly influenced by early diagenesis, i. e. by the dissolution, alteration, and re-precipitation of carbonate phases (Allan and Matthews, 1982; Banner and Hanson, 1990; Bathurst, 1976; Higgins et al., 2018; Swart and Eberli, 2005).

Early diagenesis is described in oxic and anoxic depositional environments, e. g. during fast encrusting hardground and beachrock formation (Ge et al., 2020; Gischler and Lomando, 1997; Christ et al., 2015) or alteration of primary minerals in restricted, oxygen limited environments (Suess, 1979; Talbot and Kelts, 1986; Ni et al., 2020). Early diagenesis in both settings is closely related to the decomposition of organic matter (OM), which changes the physicochemical properties of the contemporaneous pore water, e. g. through the release of HCO_3^- and coupled alkalinity increase in the surrounding pore space.

For instance, (Burdige et al., 2010) report an oxygen driven heterotrophic decay of OM, resulting in the dissolution and re-precipitation of carbonate minerals in Bahamian sediments. Likewise, anoxic sulfate reduction (SR) has raised some attention in the last decades with respect to the mineralization of OM. Some studies propose SR to enhance carbonate precipitation by the consumption of protons during sulfide formation (Mucci et al., 2000; Mackenzie et al., 1995; Burdige, 2011), while others suggest only minor or even dissolution effects on carbonate minerals (Meister, 2013; Jourabchi et al., 2005). In any case, the study of physicochemical gradients in contemporaneous pore waters is crucial to retrace the biogeochemical influences on early diagenetic alteration.

The lagoon of Aldabra offers promising conditions to study both, anoxic and oxic variations of diagenetic processes, as it is renowned for its sandy beaches and shores, as well as its protected inner lagoon bays, which include fine-grained carbonate mud accumulations (Hamyilton et al., 2012; Hamylton et al., 2018). Gaillard et al. (1994) refer to the latter as thick and rich in organic carbon, which makes these mud deposits possible environments for oxic and anoxic decomposition of organic matter. The authors suggest that the fine-grained sediments are recent analogues of lithographic limestones, formed in the Jurassic lagoons of Cerin and Solnhofen, and well known for their excellent preservation of fossils (Schweigert, 2011 and references therein; Bernier, 1994).

In this study, we present the first dataset of pore waters, hosted within Holocene carbonate deposits from three different sites on the Aldabra Atoll. The data include oxic pore waters from carbonate sand deposits in the west lagoon (WL), anoxic pore waters within organic rich mud and shell detritus from the north lagoon (NL), and anoxic pore waters in greyish carbonate mud from the south lagoon (SL). Furthermore, we focus on the biogeochemical processes between carbonate and fluid phases, and their effects on early diagenesis in oxic and anoxic depositional environments. In addition, these physicochemical datasets are correlated with the local bacterial community composition (16S rRNA gene-based) to determine the role within these diagenetic processes.

4.2 Study area and site description

The raised coral atoll of Aldabra (Figure 4.1; 46°29'42.569"E, 9°25'46.338"S), is located in the western Indian Ocean, ca. 420 km northwest of Madagascar and ca. 620 km east of the African continent. It belongs to the Outer Islands of the Seychelles and measures 34 km east to west and 14.5 km north to south. Aldabra is situated in the most arid sector of the western Indian Ocean and marked by an exceptional seasonality of rainfall (Farrow, 1971). Most precipitation is recorded from December to April during the north-west monsoon, with an average of 970 mm/yr (mean of the past 50 years; rain gauge data provided by the Seychelles Islands Foundation, SIF). The south-east monsoon, occurring from May to December, is characterized by minor rainfall. Aldabra is hardly ever affected by severe storms, as it is located northwest of the Indian Ocean belt of tropical cyclones (Walsh, 1984).

The atoll rim is formed by Pleistocene rocks, namely Takamaka- ("Marine Isotope Stage"-MIS 7) and Aldabra (MIS 5) limestone, which rise (at most) 8 m above sea level. They frame a shallow (up to 5 m in depth) lagoon, which is filled with unconsolidated Holocene sediment (Braithwaite, 2020). Tidal channels divide the rim into 4 islands, namely Picard-, Polymnie-, Middle- (Île Malabar) and South Island (Grande Terre), which vary between 0.25 and 5 km in width. Three main channels connect the lagoon with the open ocean: Grande Passe (between Polymnie and Île Picard), Passe Houareau (between Grande Terre and Île Malabar) and Passe Gionnet (between Polymnie and Île Malabar). Additionally, a network of shallower channels exists between Picard and Grand Terre, as well as Picard and Polymnie (Figure 4.1a).

Braithwaite et al. (1973) provided a detailed depositional history of Aldabra, which includes phases of both, emergence and submergence during the Pleistocene. Remarkable sea level lowstands during glacial phases caused today's highly karstified and rugged atoll rim (e. g. in MIS 6, sea level is considered to be 90 ± 15 m lower than today; Siddall et al., 2003; Rohling et al., 2009). Fine grained and locally organic-rich, unconsolidated carbonate deposits were described from protected inner lagoon embayment areas (Hamylton et al., 2012; Hamylton et al., 2018; Gaillard et al., 1994), three of which were approached in this study (Figure 4.1). One at the inner shore of Île Malabar in the north lagoon, characterized by fine- and coarse-grained sediment accumulations in karstic depressions and high input of feces from adjacent seabird colonies (Figure 4.2a and b). Another in a protected embayment of Grande Terre, in the south of the Lagoon, with bioturbated, greyish carbonate mud accumulations, adjacent to mangrove shrubs (Figure 4.2c). The mud deposits decrease lagoon ward and become restricted to holes within the karstic limestone basement (Figure 4.2d). The third site was sampled at the shore of the west lagoon, close to Île Moustique, an inner lagoon island. The latter differs from the previous ones, as it is not marked by locally restricted carbonate mud deposits, but vast, superficially encrusted, intertidal sand flats (Figure 4.2e and f).

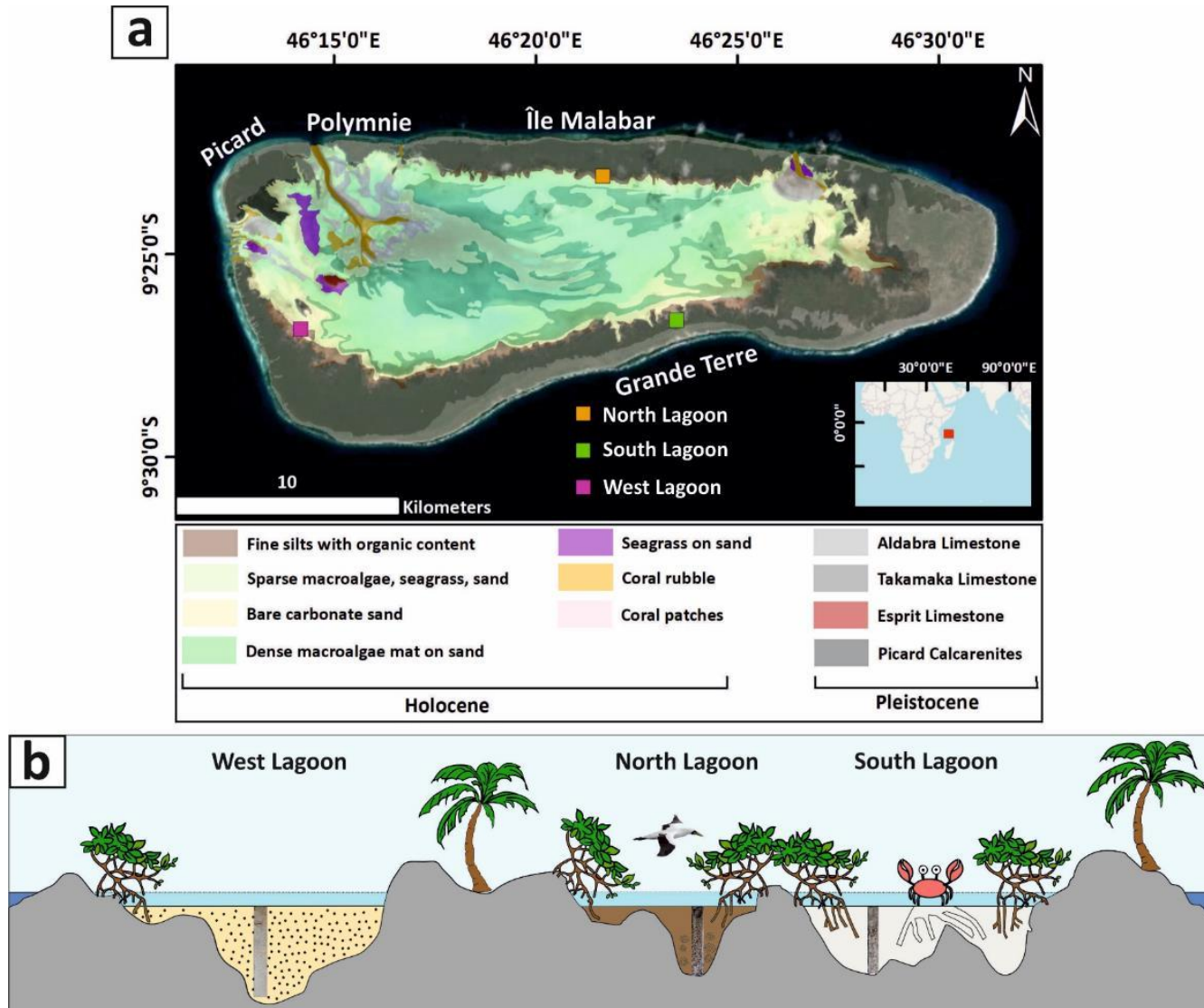


Figure 4.1: (a) shows the distribution of abundant unconsolidated sediment within the lagoon-, and Pleistocene Limestones at the rim of Aldabra (changed after Fussmann et al. 2021, in review). (b) illustrates a schematic cross section of the three different sampling sites, simplified after von Hoyningen-Huene et al. (2021, under review)



Figure 4.2: (a) shows the sampling site in the north lagoon, view direction south-southwest (SSW). (b) illustrates the identical site, view direction southeast (SE). (c) depicts the sampling in the south lagoon, view direction north (N). (d) shows the sampling site from a distance of ca. 50 m, view direction south (S). Mud accumulations decrease lagoon wards. (e) illustrates the sampled, intertidal and slightly encrusted sandflat in the west lagoon, of which (f) depicts an overview. View direction is northeast (NE).

4.3 Materials and Methods

4.3.1 Sampling and field measurements

The sampling campaign on Aldabra took place in November 2017, at the end of the dry season. Sampling was conducted at three different sites, with one in the west-, north-, and south lagoon, respectively. In the field, physicochemical parameters of the respective water columns were measured with a WTW Multi 3630 device equipped with a WTW Tetracon conductivity probe, a WTW FDO 925 probe for dissolved oxygen (O₂), and a WTW Sentix 940 electrode for temperature and pH (Xylem, Rye Brook, NY, USA). The pH probe was calibrated against standard pH-buffers 7.010 and 10.010 (HI6007 and HI6010, Hanna Instruments, Woonsocket, RI, USA; standard deviation ≤ 2 %), prior to each sampling trip. At each locality, lagoon water samples were taken from depths greater 10 cm with a pre-rinsed 500 mL bottle made of polyethylene (PE) without headspace. From the PE bottle, subsamples for anion, nutrient, and total alkalinity (TA) measurements were distributed into 100 mL PE and 250 mL Schott-Duran Glas bottles (Schott, Mainz, Germany), respectively.

To prepare selected subsamples for cation analysis, 50 mL aliquots were filtered through membrane filters (pore size 0.8 µm; Roth, Karlsruhe, Germany) into a PE bottle and acidified with 100 µL HNO₃ (suprapur; Merck, Darmstadt, Germany). Titration was applied to determine total alkalinity within 24 hours after sampling. The procedure was conducted with a hand-held titration device and 0.16 N H₂SO₄ cartridges (Hach Lange, Düsseldorf, Germany, standard deviation ≤ 1.5 %).

At the west-, north- and south lagoon sampling sites, two individual cores (WL-K04, WL-K05, NL-K04, NL-K06; SL-K04, SL-K07) were retrieved by PVC tubes (6.3 cm inside diameter) in approximately 30 cm lateral distance. The cores measured up to 50 cm in length and were used for sediment and pore water analysis. The cores were hermetically sealed after recovery and stored upright at temperatures close to their natural environment (30 ± 2 °C) for 24 hours, before they were opened and subsampled for hydro- and geochemical analyses.

4.3.2 Petrographic, mineralogical, and geochemical analyses

Subsamples from west (WL-K04), north (NL-K04) and south lagoon (SL-K04) cores were taken in increments of 2.5 to 5 cm for sediment geochemical and petrographic analyses. A total of 32 freeze dried, powdered subsamples was used for bulk organic and inorganic carbon detection. The measurements were performed with a LECO RC612 (Leco, St Joseph, MI, USA) multi-phase carbon and water determination device, which was calibrated with Leco synthetic carbon (1 and 4.98 carbon%) and Leco calcium carbonate (12 carbon%). Subsample duplicates were utilized for CNS elemental detection, which was conducted with an Euro EA 3000 Elemental Analyzer (Hekatech, Wegberg, Germany). Reference material was provided by 2.5-Bis (5-tert-benzoxazol-2-yl) thiophene BBOT and atropine sulfate monohydrate (IVA Analysetechnik, Meerbusch, Germany). Analytical accuracy of all analyses was better than 3 %.

Powdered subsamples were rinsed with ultra-pure water to remove salts, before they were analyzed for bulk carbonate δ¹⁸O and δ¹³C values at the Ruhr-University-Bochum. A Continuous-Flow- Isotope-Ratio-Mass-Spectrometer (CF-IRMS) of the type MAT 253, connected to a ConFloIV and a GasBenchII (all ThermoFisherScientific, Waltham, MA, USA) was used to determine δ¹⁸O_{carb} and δ¹³C_{carb}. Isotope data are reported in ‰ relative to Vienna Pee Dee Belemnite (VPDB). A two-point correction was applied with the certified standards IAEA-603 and NBS 18. The 1σ-reproducibility of the in-house standard is 0.05 ‰ for δ¹³C and 0.06 ‰ for δ¹⁸O. Radiocarbon measurements were conducted at three gastropod shells

subsampled at different depths from core SL-K04 and one gastropod shell subsampled from core WL-K04. The measurements were performed at the Mini Carbon Dating System (MICADAS; Wacker et al., 2010a; Synal et al., 2007) lab of the Alfred Wegener Institute (AWI; Bremerhaven, Germany). Radiocarbon content of the samples was determined alongside reference standards (oxalic acid II; NIST 4990c) and size matched preparations of IAEA-C1 were used for blank corrections. Blank correction (including sample processing blank) and standard normalization was performed using the BATS software (Wacker et al., 2010b). Powdered sediment duplicate portions from the identical 32 increments as used for the bulk carbon detections were utilized for XRD analyses. The measurements were conducted at the Department of Sedimentology and Environmental Geology in Göttingen with a PANalytical (Almelo, Netherlands) Xpert MPD device (CuK α radiation, 2 Θ refraction range of 4-69.5°, step size 0.02°). Reference Intensity Ratio (RIR) of peaks by PANalytical's HighScore software (version 3.0.5), was used for semi-quantitative phase composition. RIR results were normalized to inorganic carbon data, retrieved from the LECO RC612 device, to correct for unidentifiable microcrystalline and amorphous phases.

Another fraction from each sample increment was subsampled for thin sectioning and light microscopic observations. To ensure a continuous section, rectangular steel meshes, 5 cm in length, were placed along the sediment column. These sediment filled steel meshes, were embedded in LR White resin (London Resin Company, Reading, United Kingdom), after a dehydration procedure with ethanol. The hardened samples were cut, ground down to a thickness of 40 to 50 μm and capped with a glass cover. Petrographic observations were conducted with a petrographic microscope (Zeiss, Oberkochen, Germany). To ensure a simplified facies description, the individual cores were divided into three lithological units, based on characteristic petrographic observations.

4.3.3 Pore water analysis

A portable WTW 340i pH meter, equipped with an Inlab Solids Pro pH-electrode (Mettler Toledo, Columbus, OH, USA) and a Pt 5900 A redox electrode (SI Analytics, Mainz, Germany) was used to measure redox potential and pH gradients. The measurements were performed within 24 hours after sampling through boreholes directly in the sediment of the cores (standard deviation $\leq 2\%$). Subsequently, 5 cm CSS Rhizon samplers (Rhizosphere, Wageningen, Netherlands) were used to extract pore water. For determination of total sulfide ($\Sigma\text{H}_2\text{S}$), 10 mL aliquots were fixed with Zn-acetate immediately after extraction. Pore water alkalinity was analyzed by a modified Hach titration method with 0.01 N HCl cartridges (Hach-Lange, Düsseldorf, Germany) as titrant. Ion chromatography with suppressed and non-suppressed conductivity detection was used for the detection of major cation (Ca^{2+} , Mg^{2+} , Na^+ , K^+ and Li^+) and anion (Cl^- , F^- , Br^- and SO_4^{2-}) concentrations of lagoon and pore water samples (including the core supernatant; Metrohm 820 IC/Metrosep C3-250 analytical column, Metrohm 883 Basic IC/Metrohm ASupp5-250 analytical column, Metrohm, Herisau, Switzerland; standard deviation $\leq 1.5\%$). Trace elements (Sr^{2+} , Ba^{2+} , Fe^{2+} , Mn^{2+} , Rb^+ and B^{3+}) were measured by inductively coupled plasma mass spectrometry (ICP-MS; ICAP-Q, ThermoFisherScientific, Waltham, MA, USA; standard deviation $\leq 2\%$). Concentrations of NH_4^+ , PO_4^{3-} , $\Sigma\text{H}_2\text{S}$ and dissolved silica ($\text{SiO}_{2(\text{aq})}$) were measured by photometric methods according to (Grasshoff et al., 2009), using a SI Analytics Uviline 9400 spectrophotometer. Carbon isotope values of pore water DIC (dissolved inorganic carbon) were determined with a MAT 253 at the Ruhr-University Bochum. For details on the mass spectrometer and equipment please refer to section 3.2. The 1σ -reproducibility of the in-house standard is $\leq 0.19\text{‰}$ and values are given relative to VPDB. Pore water $\delta^{18}\text{O}$ was measured by the Thermo Fisher Scientific GmbH in Bremen, with a Thermo Fisher™ Delta Ray™

Isotope Ratio Infrared Spectrometer (IRIS) coupled to an Universal Reference Interface (URI) Connect and Teledyne CETAC™ ASX-7100 Autosampler. Certified USGS 48 reference material was used to correct internal standards (standard deviation $\leq 0.07\%$). Pore water related $\delta^{18}\text{O}$ values are reported relative to Vienna Standard Mean Ocean Water (VSMOW).

Measured data were processed with the PHREEQC software package (version 3; (Parkhurst and Appelo, 2013)). The implemented phreeqc.dat and wateqf4.dat databases were used to calculate ion activities and ρCO_2 (partial pressure of CO_2) of the water samples and compute mineral saturation states. The saturation indices are given as $\text{SI} = \log(\text{IAP}/K_{sp})$. Excess Ca^{2+} and reduced SO_4^{2-} were calculated from ocean water (ow) and pore fluid (pf) compositions according to Walter and Burton (1990).

$$\text{Excess}[\text{Ca}_{pf}^{2+}] = [\text{Ca}_{pf}^{2+}] - [\text{Cl}_{pf}^-] \cdot \frac{[\text{Ca}_{ow}^{2+}]}{[\text{Cl}_{ow}^-]} \quad (10)$$

The amount of SO_4^{2-} reduced is derived from pore fluid SO_4^{2-} and Cl^- concentrations:

$$[\text{SO}_4^{2-}]_{\text{reduced}} = \frac{[\text{SO}_4^{2-}]_{ow}}{[\text{Cl}_{ow}^-]} \cdot [\text{Cl}_{pf}^-] - [\text{SO}_4^{2-}]_{pf} \quad (11)$$

With a molar $\text{SO}_4^{2-}/\text{Cl}^-$ ratio of overlying seawater of 0.0517, taken from Millero (1974).

4.3.4 Bacterial community profiling

Samples for bacterial community analysis were taken from cores K01-K03 at each sampling site. The cores were subsampled at 2.5-5 cm intervals. The overlying water column was sampled in three independent 200 mL replicates. The water was filtered through a 3.0 μm polycarbonate (Merck, Darmstadt, Germany) and 0.2 μm polyethersulfone (Sartorius, Göttingen, Germany) filter sandwich using reusable filter holders with receivers and manually operated PVC vacuum pumps from NALGENE (Thermo Fisher Scientific, Waltham, MA, USA). All samples were immediately fixed in RNAprotect Bacteria Reagent (Qiagen, Hilden, Germany) for transport. Before long-term storage, the conservation reagent was decanted after centrifugation of each sample for 1 hour at 3,150 x g. The samples were subsequently stored at -20°C . DNA for 16S rRNA gene amplification was extracted from all samples with the RNeasy PowerSoil Total RNA Extraction kit and RNeasy PowerSoil DNA Elution kit (Qiagen) according to the manufacturers' instructions. Half of a filter or 1 g of sediment were used in each extraction. The final elution volume was adjusted to 50 μL of nuclease-free water. Bacterial 16S rRNA genes were amplified by PCR using a Phusion Polymerase and V3-V4 primers SD-Bact-0341-b-S-17 and S-D-Bact-0785-a-A-21 (Klindworth et al., 2013). The 50 μL master mix and PCR-cycling conditions were used as described in von Hoyningen-Huene et al. (2019). Approximately 20-25 ng of DNA template were used in each reaction. Each sample was amplified in triplicate. Successful PCR reactions were pooled equimolar and purified using MagSi magnetic beads (Steinbrenner, Wiesenbach, Germany) and a Janus automated workstation (PerkinElmer, Downers Grove, IL, USA) according to manufacturer's instructions. Samples were eluted in 30 μL of EB (Qiagen) and submitted for sequencing at the Göttingen Genomics Laboratory. Sequencing was performed by a MiSeq sequencer (Illumina, San Diego, CA, USA) in paired-end mode and v3 chemistry (Illumina). Sequenced samples were demultiplexed and adapters trimmed using the CASAVA analysis software (Illumina). The resulting raw reads were quality filtered and processed using an in-house pipeline described in detail by von Hoyningen-Huene et al. (2019). Briefly, samples were quality filtered with fastp v0.20.0 (Chen et al., 2018b) and paired reads merged with PEAR v0.9.11 (Zhang et al., 2014). Remaining primers were clipped with cutadapt 2.5 (Martin, 2011). Sequences were clustered into amplicon sequence variants (ASVs) at 100% sequence identity with VSEARCH v.2.14.1 (Rognes et al., 2016). This included size-sorting, de-replication, denoising with the UNOISE3 algorithm (Edgar, 2016), chimera removal and ASV clustering.

ASVs were taxonomically assigned by using BLAST against the SILVA SSU 138 Ref NR 99 database (Quast et al., 2012). For further analysis, ASV tables were generated using the biom tools in QIIME version 1.9.1 (Caporaso et al., 2010). All hits below 95% BLAST identity and a hit quality below 93%, according to the SILVA NGS user guide, were regarded as unclassified taxa. All chloroplast, mitochondria and Archaea hits were removed from the dataset. The final ASV table was subset using ampvis2 (Andersen et al., 2018), normalized with gmp (Chen et al., 2018a) and transformed into relative abundances using base (R Core Team, 2018), R Version 4.0.0 and RStudio Version 1.3.959 (RStudio Team, 2016). All taxa which are present in at least one sample with a relative abundance of $\geq 5\%$ (order level) were included in the study. Diversity and species richness were calculated from the non-normalized ASV table, which was rarefied to 19,906 reads, using ampvis2 and the included vegan package (Jari Oksanen et al., 2018). Sequences are accessible at the NCBI Sequence Read Archive within the BioProject PRJNA611521 and under the accession numbers SRR11295008-501. All samples with a relative abundance of $\geq 5\%$ in at least one sample were used as a basis for bar charts and plotted in SigmaPlot (version 11; Systat Software, San Jose, CA). Abundant taxa were grouped according to their metabolisms, which were inferred from known respiratory processes of characterized relatives listed in Whitman (2015) and additional literature (see supplementary data).

4.4 Results

4.4.1 Petrography and microfacies of sediments

4.4.1.1 West Lagoon

Core WL-K04 is divided into three different units, based on the respective lithology. The units are presented as depth (cm) below surface. “West Lagoon Unit I” (WLU I) extends from 0 to 15 cm, WLU II from 15 to 40 cm, and WLU III from 40 to 50 cm. Figure 4.3 illustrates the lithological units of core WL-K04 in detail. Unit III (40-50 cm) is characterized by a medium to well sorted carbonate sand, consisting of micritized and detrital grains, locally encrusted with cryptocrystalline cement. In contrast, Unit II (15-40 cm) is made up of poorly sorted carbonate sand, with large (up to 2 mm) bioclasts. Unit I (0-15 cm) consists of medium sorted carbonate sand, with layers encrusted with cryptocrystalline cement. Microfacies close ups are shown in Figure 4.4.

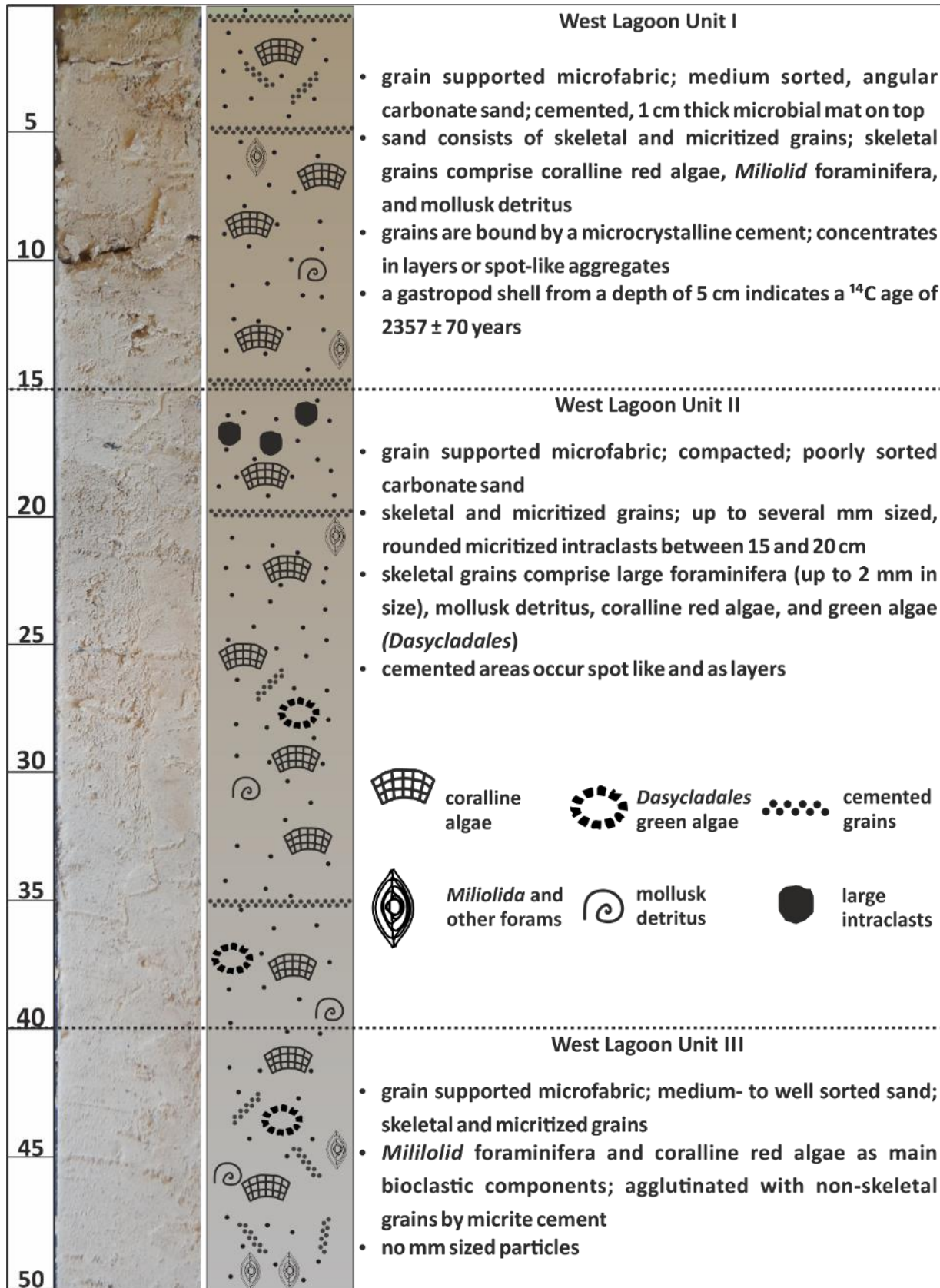


Figure 4.3: Petrography and microfacies of core WL-K04. Dashed lines mark different lithological Units.

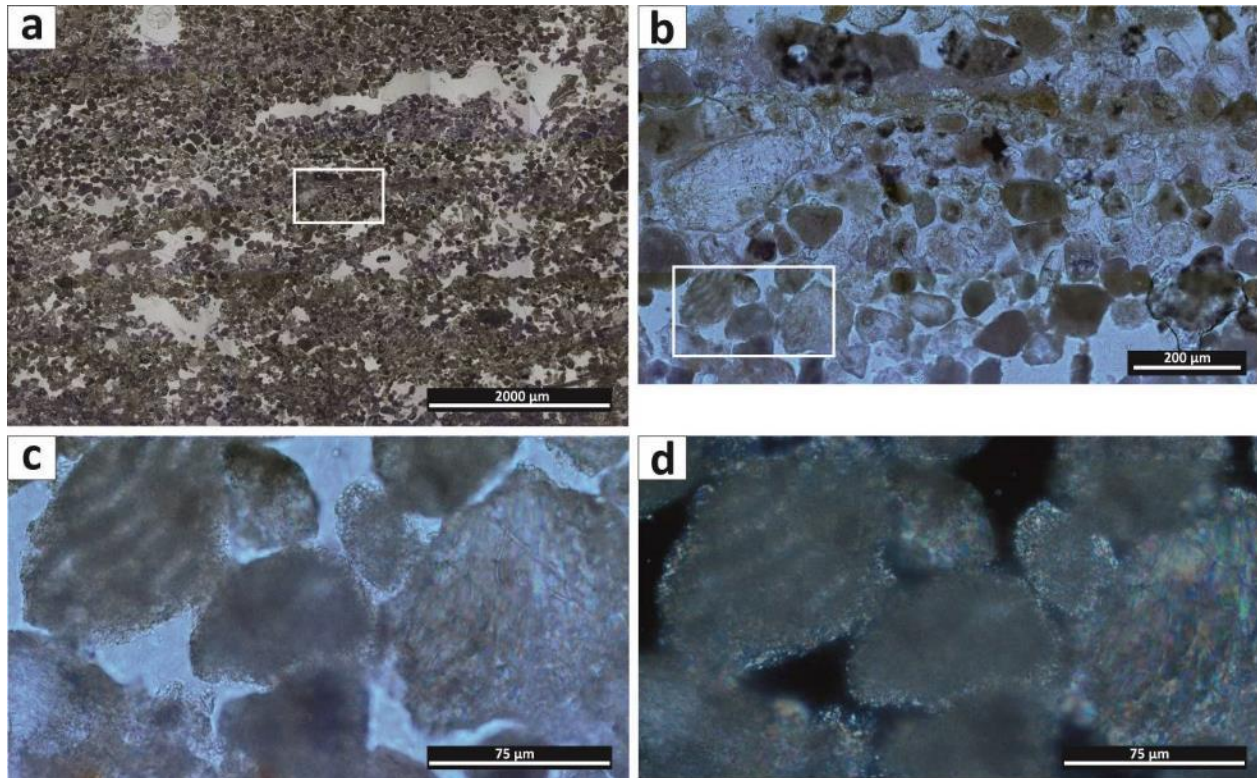


Figure 4.4: (a) shows a thin section of the microfacies of WLU I, embedded in LR White. Encrusted layers can be distinguished from those without cements. The area indicated by a white rectangle is depicted in image (b) and shows cements, which connect two grains with each other. A closer cutout with these cements is illustrated in (c) (transmitted light) and (d) (crossed polars).

4.4.1.2 North Lagoon

Core NL-K04 can also be divided into three different lithological units. “North Lagoon Unit I” (NLU I) extends from 0 to 10 cm, NLU II from 10 to 42.5 cm, and NLU III from 42.5 to 49.5 cm. Figure 4.5 shows an overview of the microfacies of core NL-K04. In summary, the core is characterized by an equal mixture of light brown mud and shell detritus in Unit III (42.5-49 cm), which is covered by a thick succession of shell detritus (Unit II, 20-42.5 cm). Unit III (0-10 cm) is made up of dark brown mud with intercalated plant detritus and bioclasts. Microfacies images are illustrated in Figure 4.7a-d.

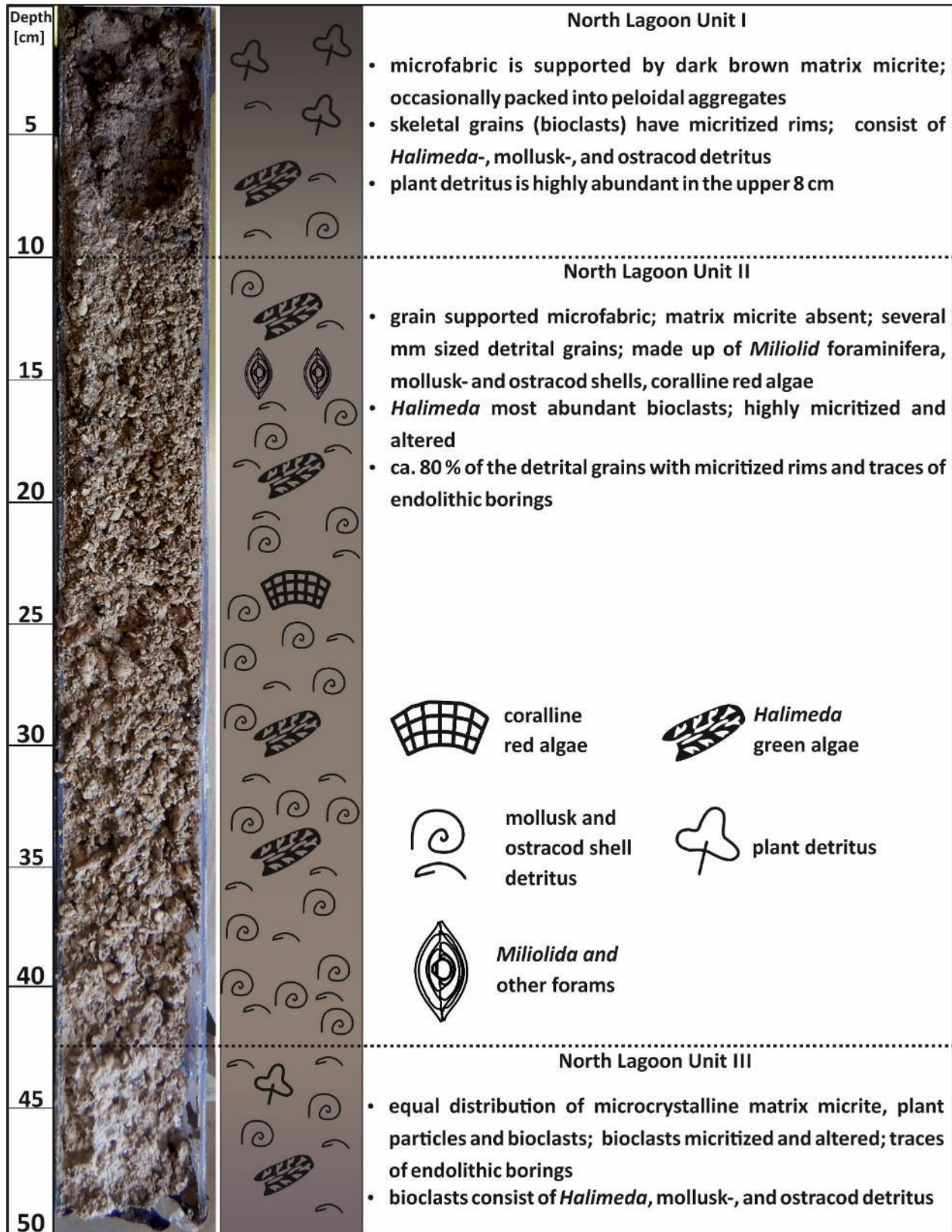


Figure 4.5: Petrography and microfacies of core NL-K04. Dashed lines mark different lithological Units.

4.4.1.3 South Lagoon

Core SL-K04 is also dissected into three lithological units. “South Lagoon Unit I” (SLU I) extends from 0 to 20 cm, SLU II from 20 to 35 cm, and SLU III from 35 to 44 cm. The microfacies of core SL-K04 is illustrated in Figure 4.6. Briefly, Unit III (35-44 cm) consists of a mixture of grey micrite with embedded peloids and bioclasts in a 60:40 ratio. It is overlain by Unit II (20-35 cm), which is traversed extensively by mangrove rootage. At the top, Unit I (0-20 cm) represents a mixture of bioclasts, peloids, plant detritus, and grey micrite. Microfacies images are depicted in Figure 4.7e and f.

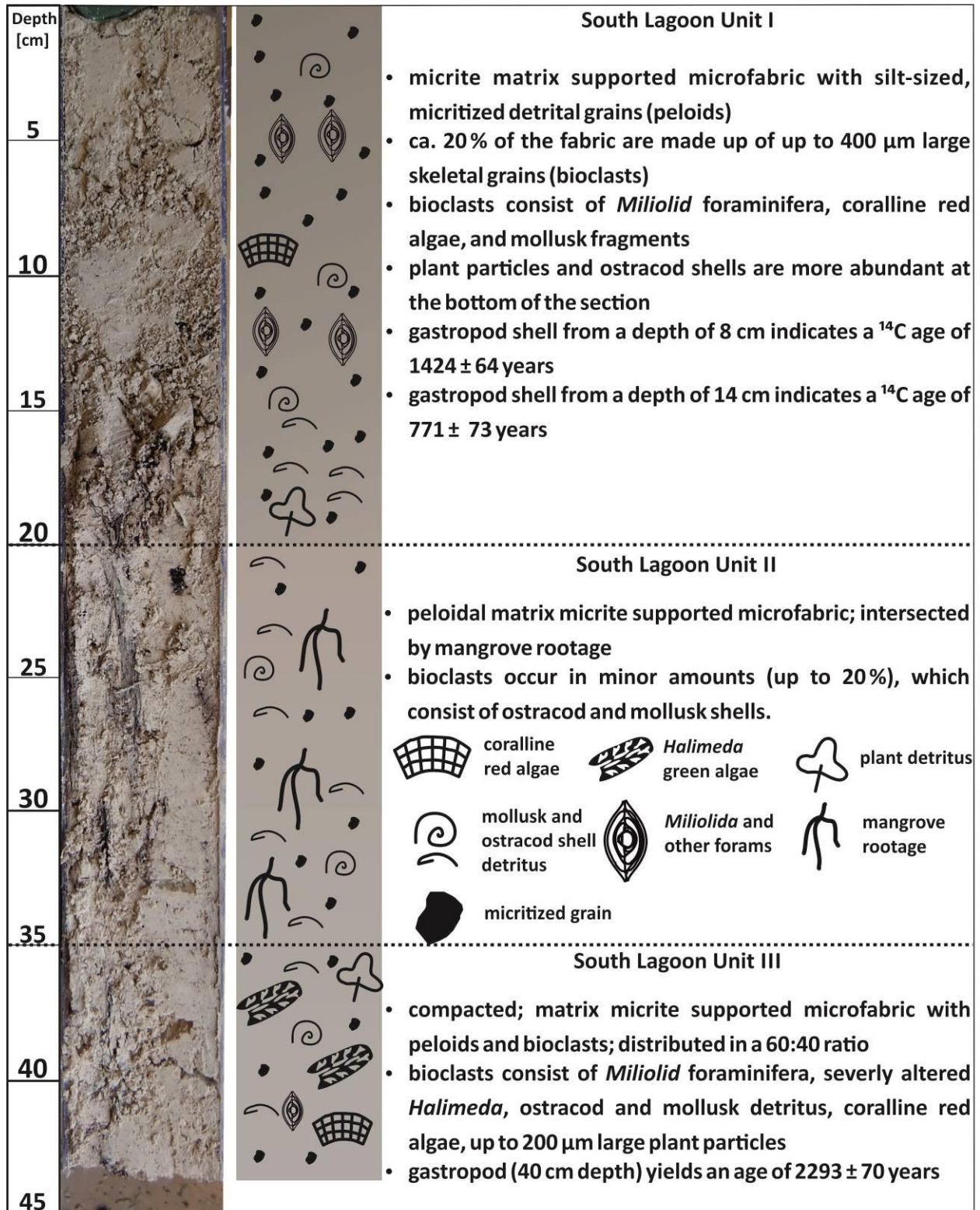


Figure 4.6: Petrography and microfacies of core SL-K04. Dashed lines mark different lithological Units.

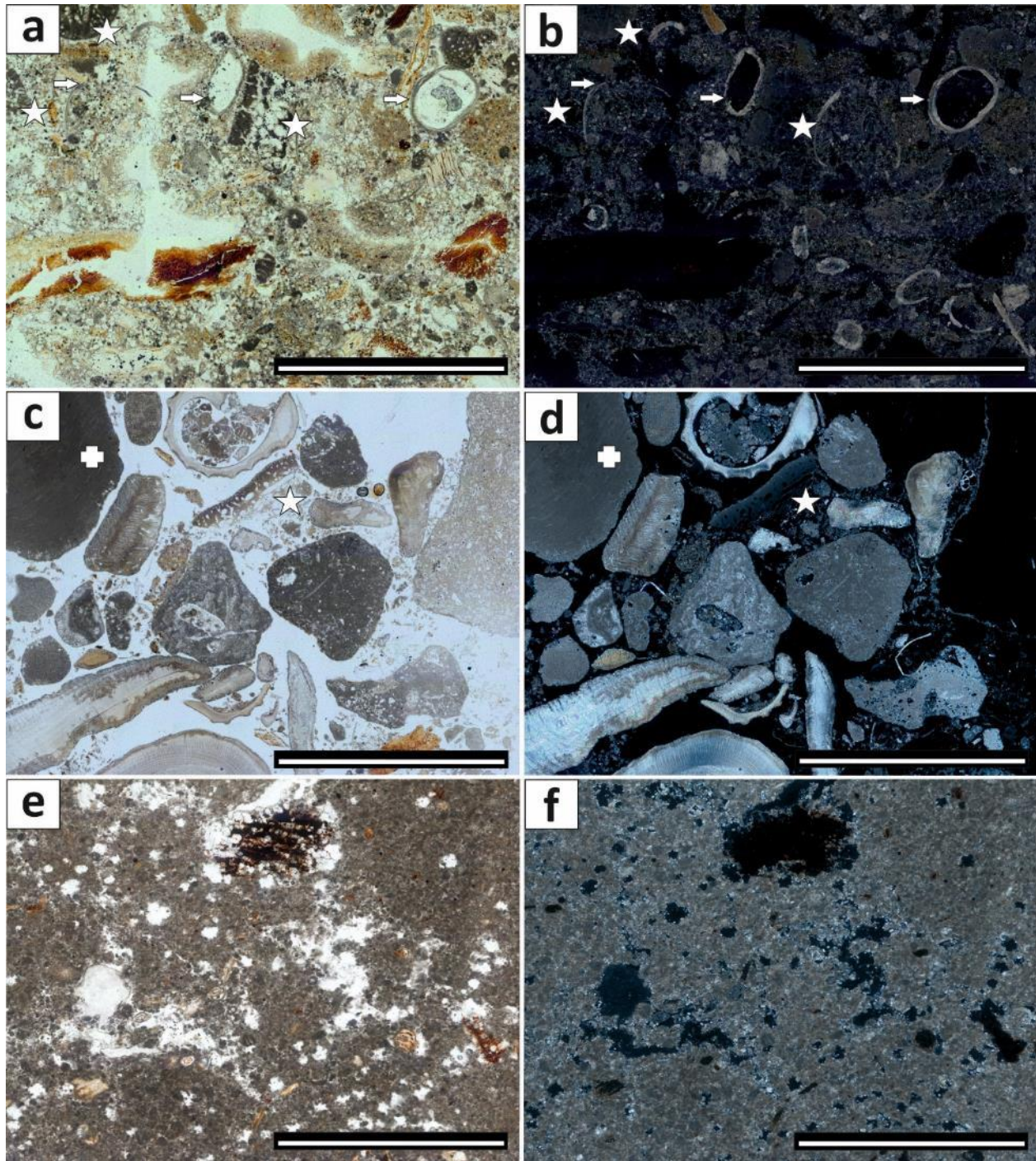


Figure 4.7: Close up images of thin sections. Sediments are embedded in LR White. NLU I is depicted in transmitted light (a) and crossed polars (b) Notable are ostracod shells (arrows) and highly altered, dark appearing Halimeda fragments (stars). (c) shows a close-up of NLU-II in transmitted light, while (d) shows the same area under crossed polars. A grain supported fabric in this Unit is evident. Main components in the image are red algae (upper left, crosses), Halimeda and shell fragments. (e) shows the microfabric of SLU-I, characterized by micritized grains, micrite and occasional plant detritus. (f) shows the identical image under crossed polars. The scale bars measure 2 mm.

4.4.2 Geochemistry of sediments

4.4.2.1 West Lagoon

In WLU III (40-50 cm), bulk CaCO_3 consists of 9-20 wt% low magnesium calcite (LMC), 62-73 wt% aragonite (Ar), and 13 wt% high magnesium calcite (HMC; Figure 4.8). Respective C_{org} and N_{tot} values range from 0.4 to 0.35, and 0.04 to 0.03 wt%, whereas S_{tot} remains constant at 0.1 wt%. Isotope values measure +2.0 for $\delta^{13}\text{C}_{\text{carb}}$, and -2.1 for $\delta^{18}\text{O}_{\text{carb}}$, respectively (Figure 4.9).

WLU II (15-40 cm) is made up of 16-23 wt% LMC, 57-68 wt% Ar, and 12-16 wt% HMC. C_{org} , N_{tot} and S_{tot} show values between 0.4 and 0.5, around 0.04, and between 0.1 and 0.15 wt%, respectively. Bulk $\delta^{13}\text{C}_{\text{carb}}$ values vary between +1.4 and 1.6 ‰. $\delta^{18}\text{O}_{\text{carb}}$ range from -2.4 to -2.2 ‰.

The carbonate content of WLU I (0-15 cm) comprises 96 wt%, of which 20 wt% are LMC, 63 wt% Ar, and 13 wt% HMC. C_{org} , N_{tot} and S_{tot} show constant values of 0.4, 0.04, and 0.1 wt%, respectively. Bulk $\delta^{13}\text{C}_{\text{carb}}$ values increase from +0.8 ‰ to +1.3 ‰ towards the top of WLU I, whereas $\delta^{18}\text{O}_{\text{carb}}$ values stay constant (-2.4 to -2.3 ‰). In addition, ^{14}C age data indicate a radiocarbon age of 2357 ± 70 a for a gastropod shell, sampled at a depth of 5 cm (WLU I).

4.4.2.2 North Lagoon

Within NLU III (42.5-49.5 cm), CaCO_3 scatters from 88 to 94 wt% and is made up of 30 % LMC, 55 wt% Ar and 5 wt% HMC (Figure 4.8). The respective C_{org} , N_{tot} and S_{tot} levels decrease from 3.2 to 1.2, 0.2 to 0.1 and 0.4 to 0.3 wt %, including a concomitant increase of the $C_{\text{org}}/N_{\text{tot}}$ ratio from 17 to 18.5, towards the top of the unit. Bulk $\delta^{13}\text{C}_{\text{carb}}$ values lie between -0.4 and -1.0 ‰ and $\delta^{18}\text{O}_{\text{carb}}$ varies between -2.0 and -2.8 ‰ (Figure 4.9).

In NLU II (10-42.5 cm), the carbonate fraction varies between 87 and 96 wt% and subdivides into 30 wt% LMC, 60 wt% Ar, and 5 wt % HMC. C_{org} , N_{tot} and S_{tot} rise from 0.6 to 3.0, 0.04 to 0.2 and 0.1 to 0.4, respectively. The individual bulk $\delta^{13}\text{C}_{\text{carb}}$ and $\delta^{18}\text{O}_{\text{carb}}$ lie between -1.0 and -2.0 ‰ and -2.0 and -2.9 ‰. An outlier is observed at a depth of 31 cm, where $\delta^{13}\text{C}_{\text{carb}}$ measures -2.75 ‰.

Bulk CaCO_3 of NLU I (0-10 cm) varies between 70 and 76 wt% and consists of ca. 22 wt% LMC, 45 wt% Ar and 5 wt% HMC. An outlier is notable at 3-6 cm of depth, where Ar rises to 52 wt%. C_{org} varies between 7 and 11 wt%, N_{tot} between 0.4 and 0.6 wt%, and S_{tot} between 0.7 and 1 wt%. Bulk isotope values in NLU I are -0.8 ‰ ($\delta^{13}\text{C}_{\text{carb}}$) and -3.2 ‰ ($\delta^{18}\text{O}_{\text{carb}}$).

4.4.2.3 South Lagoon

The CaCO_3 content of SLU III (35-44 cm) lies between 94 and 95 wt%, which distribute into 28 wt% LMC, 59 wt% Ar and 7 wt% HMC (Figure 4.8). C_{org} , N_{tot} , and S_{tot} range from 0.7 to 1 wt%, 0.05 to 0.06 wt%, and 0.14 to 0.15 wt%, respectively. Bulk $\delta^{13}\text{C}_{\text{carb}}$ and $\delta^{18}\text{O}_{\text{carb}}$ decrease from -0.4 to -0.6 ‰ and -2.4 to -2.7 ‰ towards the top of the unit (Figure 4.9). ^{14}C age data from a gastropod shell, sampled at a depth of 40 cm, determine a radiocarbon age of 2293 ± 70 a.

Bulk CaCO_3 of SLU II (20-35 cm) measure 92-93 wt%, which distribute into 29 wt% LMC, 58 wt% Ar and 6 wt% HMC. However, at 30-35 cm, LMC and Ar mark outliers with 38 wt% and 48 wt%. C_{org} , N_{tot} , and S_{tot} individually increase from 1.0 to 1.5 wt%, 0.06 to 0.09 wt%, and 0.16 to 0.25 wt% towards the upper part of the unit. In SLU II, bulk $\delta^{13}\text{C}_{\text{carb}}$ and $\delta^{18}\text{O}_{\text{carb}}$ show little variation (+0.1 to -0.2 ‰; -2.8 to -2.7 ‰).

Within SLU I (0-20 cm), CaCO_3 varies between 92 and 93 wt%, and divides into 31 wt% LMC, 57 wt% Ar, and 5 wt% HMC. In SLU I, C_{org} decreases top ward, from 1.6 to 1.2 wt%, whereas N_{tot} remains stable at 0.09 wt%. This trend is mirrored by the $C_{\text{org}}/N_{\text{tot}}$ ratio, which decreases from 17 to 12. Additionally, S_{tot} also decreases towards the top from 0.25 to 0.2 wt%.

Bulk $\delta^{13}\text{C}_{\text{carb}}$ values show little variation (+0.1 to +0.2 ‰), which is also valid for $\delta^{18}\text{O}_{\text{carb}}$ (-2.7 to -2.8 ‰). Furthermore, ^{14}C age data, obtained from gastropod shells at depths of 8 and 17 cm, indicate respective radiocarbon ages of 1424 ± 64 a and 771 ± 73 a.

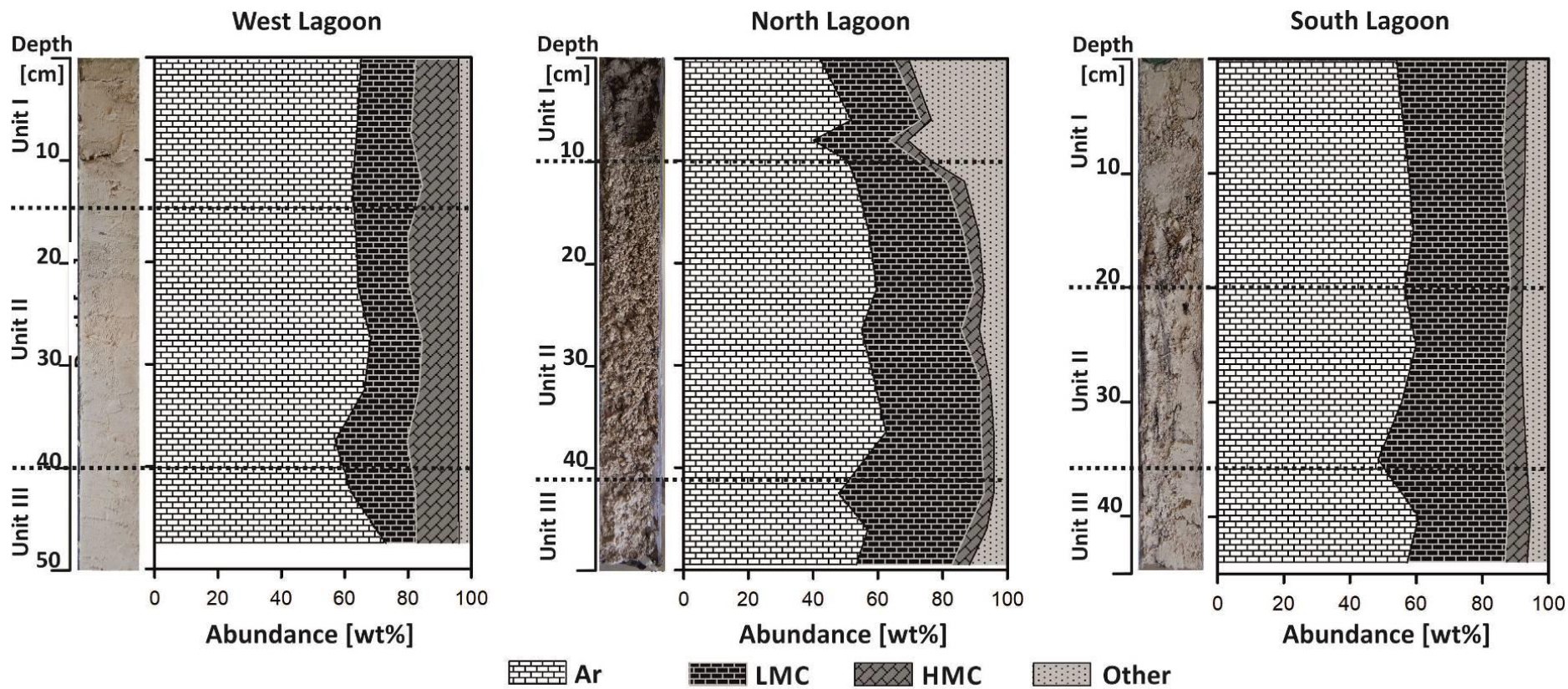


Figure 4.8: Mineralogical distribution of the core sediments based on the XRD results. Dashed lines mark the borders of the lithological units. “Other” refers to amorphous, non-crystalline phases.

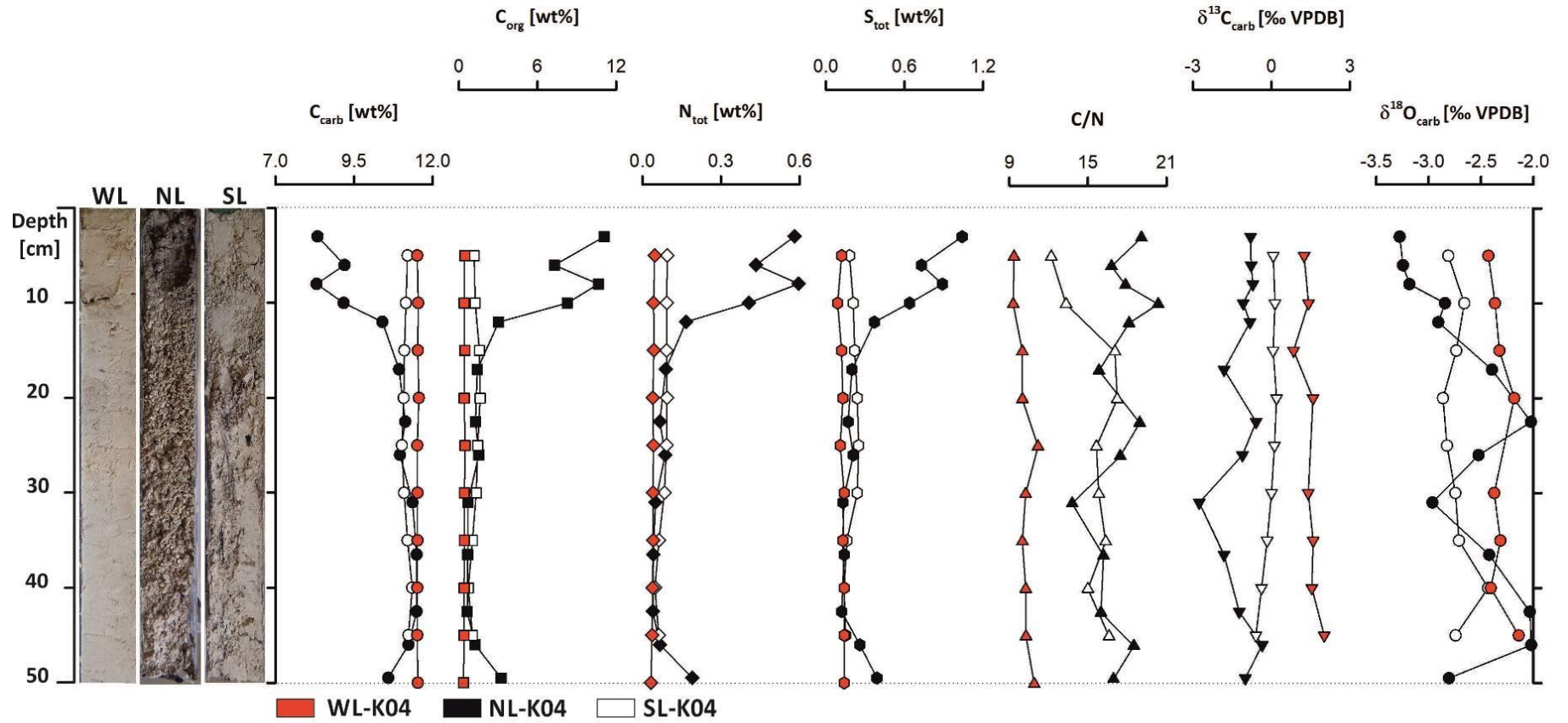


Figure 4.9: Bulk geochemistry of the sampling sites.

4.4.3 Pore water chemistry

4.4.3.1 West Lagoon

The core from the west lagoon is characterized by an elevated salinity value at the top ($41.5 \text{ g}\cdot\text{kg}^{-1}$), which is notably higher than in the overlying water column ($36 \text{ g}\cdot\text{kg}^{-1}$; Figure 4.10a). Subsequently, salinity decreases to $36.8 \text{ g}\cdot\text{kg}^{-1}$ at a depth of 25 cm, before it increases again to $40.8 \text{ g}\cdot\text{kg}^{-1}$ at the bottom of the core (47.5 cm). The pH drops from 7.9 in the water column to 7.2 at the top of the core. It then continuously rises to 7.5 at a depth of 47.5 cm. The cored section is completely oxic, with redox potentials between +238 mV at the top and +318 mV at the bottom. Total alkalinity (TA) rises from $2.6 \text{ mmol}\cdot\text{kg}^{-1}$ in the water column to $5.1 \text{ mmol}\cdot\text{kg}^{-1}$ at the top of the core. It remains stable to a depth of 17 cm, before it lowers to $4 \text{ mmol}\cdot\text{kg}^{-1}$ at 47.5 cm. Total dissolved sulfide is not detected in the present section, however, reduced SO_4^{2-} (SO_4^{2-} -red) peaks at $0.2 \text{ mmol}\cdot\text{kg}^{-1}$ at a depth of 6 cm, before it returns to values around 0 until 25 cm of depth. It then increases up to $0.2 \text{ mmol}\cdot\text{kg}^{-1}$ towards the bottom of the core. $\delta^{13}\text{C}_{\text{DIC}}$ measures -4.7 ‰ at a depth of 6 cm, it then decreases to -6.4 ‰ at a depth of 38.5 cm, before it increases to -2.2 ‰ at 43 cm (Figure 4.10c). At the bottom of the core, $\delta^{13}\text{C}_{\text{DIC}}$ holds a value of -4 ‰ . $\delta^{18}\text{O}_{\text{VSMOW}}$ is at $+0.9 \text{ ‰}$ at 6 cm and decreases to $+0.6 \text{ ‰}$ at a depth of 25 cm. Subsequently, it increases to $+0.9 \text{ ‰}$ at 47.5 cm. The amount of excess Ca^{2+} drops to $-0.5 \text{ mmol}\cdot\text{kg}^{-1}$ at 6 cm, returns to $0.1 \text{ mmol}\cdot\text{kg}^{-1}$ and decreases to 0.3 up to the bottom of the core. SI_{Ar} decreases from 0.7 in the water column to values around 0.2 in the sediment section. Crossplots of the molar ratios of elements sensitive to diagenesis ($\text{Sr}^{2+}/\text{Ca}^{2+}$, $\text{Ca}^{2+}/\text{Cl}^-$, and $\text{Mg}^{2+}/\text{Cl}^-$) are illustrated in Figure 4.11. The $\text{Sr}^{2+}/\text{Ca}^{2+}$ ratio increases within the core, compared to lagoon water (from 8.8 to values > 9.2). In contrast $\text{Ca}^{2+}/\text{Cl}^-$ decreases within WL-K04/05 (18.2-18.8) compared to the lagoon water value of 18.8, which indicates small amounts of LMC formation (Figure 4.11a). $\text{Mg}^{2+}/\text{Cl}^-$ also increases from 97.3 in the water column, to values between 97.4 and 97.5 within the core, confirming the LMC precipitation trend (Figure 4.11b).

4.4.3.2 North Lagoon

The pore water of core NL-K04 is characterized by an almost constant salinity, which slightly increases from $36.3 \text{ g}\cdot\text{kg}^{-1}$ in the water column to $36.8 \text{ g}\cdot\text{kg}^{-1}$ at the bottom of the core (44 cm; Figure 4.10b). The pH values drop from 7.7 in the open water to 7.0 at the core's surface, before slightly rising to 7.2 at the bottom. Core NL-K04 is entirely anoxic, with a maximum redox potential of -157 mV in the deeper sediment. Total alkalinity rises to $9.4 \text{ mmol}\cdot\text{kg}^{-1}$ at a depth of 7 cm, before stabilizing at $7.0 \text{ mmol}\cdot\text{kg}^{-1}$ at 15 cm and decreasing to concentrations below $6 \text{ mmol}\cdot\text{kg}^{-1}$ at 34 cm. Total dissolved sulfide ($\Sigma\text{H}_2\text{S}$) is absent in the water column. In the sediment, it peaks at $2.8 \text{ mmol}\cdot\text{kg}^{-1}$ at a depth of 15 cm, and then slowly decreases to $0.6 \text{ mmol}\cdot\text{kg}^{-1}$ at 44 cm. The values of SO_4^{2-} -red reach a maximum of $2.4 \text{ mmol}\cdot\text{kg}^{-1}$ at a depth of 7 cm, and then decrease to 0 at the bottom of the core. Stable isotope data (Figure 4.10a) are recorded in core NL-K06 up to a depth of 19 cm, where $\delta^{13}\text{C}$ of dissolved inorganic carbon ($\delta^{13}\text{C}_{\text{DIC}}$) reaches its lowest value (-11.1 ‰). In the water column, $\delta^{13}\text{C}_{\text{DIC}}$ measures -3.5 ‰ , which decreases to -8.4 ‰ at a depth of 2 cm. In the water column, $\delta^{18}\text{O}_{\text{VSMOW}}$ measures $+1 \text{ ‰}$ and remains constant in the sediment. Excess Ca^{2+} is above 0 throughout the core and reaches its highest value with $0.2 \text{ mmol}\cdot\text{kg}^{-1}$ at a depth of 11 cm. SI_{Ar} decreases from 0.2 in the water column to values between 0.0 and 0.1 within the sediment. $\text{Sr}^{2+}/\text{Ca}^{2+}$ shows only minor variation within NL-K04 compared to the water column. The $\text{Ca}^{2+}/\text{Cl}^-$ ratio (Figure 4.11a) slightly rises from 18.9 in the water column up to 19.2 within the core, indicating small amounts of CaCO_3 dissolution.

The $\text{Mg}^{2+}/\text{Cl}^-$ ratio further confirms this trend by increasing from 97.5 in the water column to values from 97.6 to 97.8 within NL-K04 (Figure 4.11b).

4.4.3.3 South Lagoon

Core SL-K07 shows elevated salinities ($40.2 \text{ g}\cdot\text{kg}^{-1}$) at the top, which decrease to $38.2 \text{ g}\cdot\text{kg}^{-1}$ at the bottom of the core (37.5 cm; Figure 4.10c). The overlying low tide salinity is higher ($41.3 \text{ g}\cdot\text{kg}^{-1}$) than the high tide value ($38 \text{ g}\cdot\text{kg}^{-1}$). The pH decreases from 8.0 in the water column to 7.0 at the top of the core. It then increases up to 7.2 at a depth of 29 cm and remains stable between 7.1 and 7.2 until 37.5 cm. The entire core is anoxic, with Eh values between -243 mV at the top and -309 mV at the bottom of the core. Total alkalinity is highest in the upper part of the core, with $7.1 \text{ mmol}\cdot\text{kg}^{-1}$ at the top, which decreases to $4.7 \text{ mmol}\cdot\text{kg}^{-1}$ at 30 cm, before increasing again to $5.8 \text{ mmol}\cdot\text{kg}^{-1}$ at the bottom. Total dissolved sulfide is absent in the water column but increases in the core from $0.1 \text{ mmol}\cdot\text{kg}^{-1}$ at the top to $0.6 \text{ mmol}\cdot\text{kg}^{-1}$ at 7.5 cm. $\Sigma\text{H}_2\text{S}$ then decreases to $0.2 \text{ mmol}\cdot\text{kg}^{-1}$ at 22 cm, before it rises again to $0.5 \text{ mmol}\cdot\text{kg}^{-1}$ at 37.5 cm. SO_4^{2-} red is below 0 within the water column and reaches its lowest value within the core (-0.6) at 2.5 cm. Subsequently, it rises to $1.3 \text{ mmol}\cdot\text{kg}^{-1}$ at a depth of 7.5 cm, before it decreases to values around $0.5 \text{ mmol}\cdot\text{kg}^{-1}$ towards the bottom of the core. $\delta^{13}\text{C}_{\text{DIC}}$ is highest at a depth of 2.5 cm, with a value of -5.3 ‰ (Figure 4.10c). It decreases to -9.2 ‰ at a depth of 10 cm, before increasing again to -7.9 ‰ at 34 cm. $\delta^{18}\text{O}_{\text{VSMOW}}$ measures +1.7 ‰ at the top of SL-K07. It lowers to 1.4 ‰ at a depth of 34 cm, before it increases to 1.5 ‰ at 37.5 cm. Excess Ca^{2+} is slightly negative in the water column ($-0.2 \text{ mmol}\cdot\text{kg}^{-1}$), before it increases to $1.1 \text{ mmol}\cdot\text{kg}^{-1}$ at a depth of 2.5 cm. The values stabilize close to 0 towards the bottom of the core. SI_{Ar} decreases from 0.6 in the water column, to values between 0.0 and 0.1 throughout the core. The $\text{Sr}^{2+}/\text{Ca}^{2+}$ ratio shows minor variation (Figure 4.11). It is highest in the water column (8.9) and reaches values between 8.8 and 8.9 throughout the core. $\text{Ca}^{2+}/\text{Cl}^-$ measures 18.9 in the water column and shows a distinct increase to 20.6 at the top of the core, which indicates CaCO_3 dissolution (Figure 4.11a). The rest of SL-K07 is characterized by values between 18.9 and 19.0. $\text{Mg}^{2+}/\text{Cl}^-$ rises from 97.5 in the water column to 97.9 at the top of the core, which confirms the aforementioned dissolution trend. The rest of SL-K07 is marked by values between 97.6 and 97.8 (Figure 4.11b).

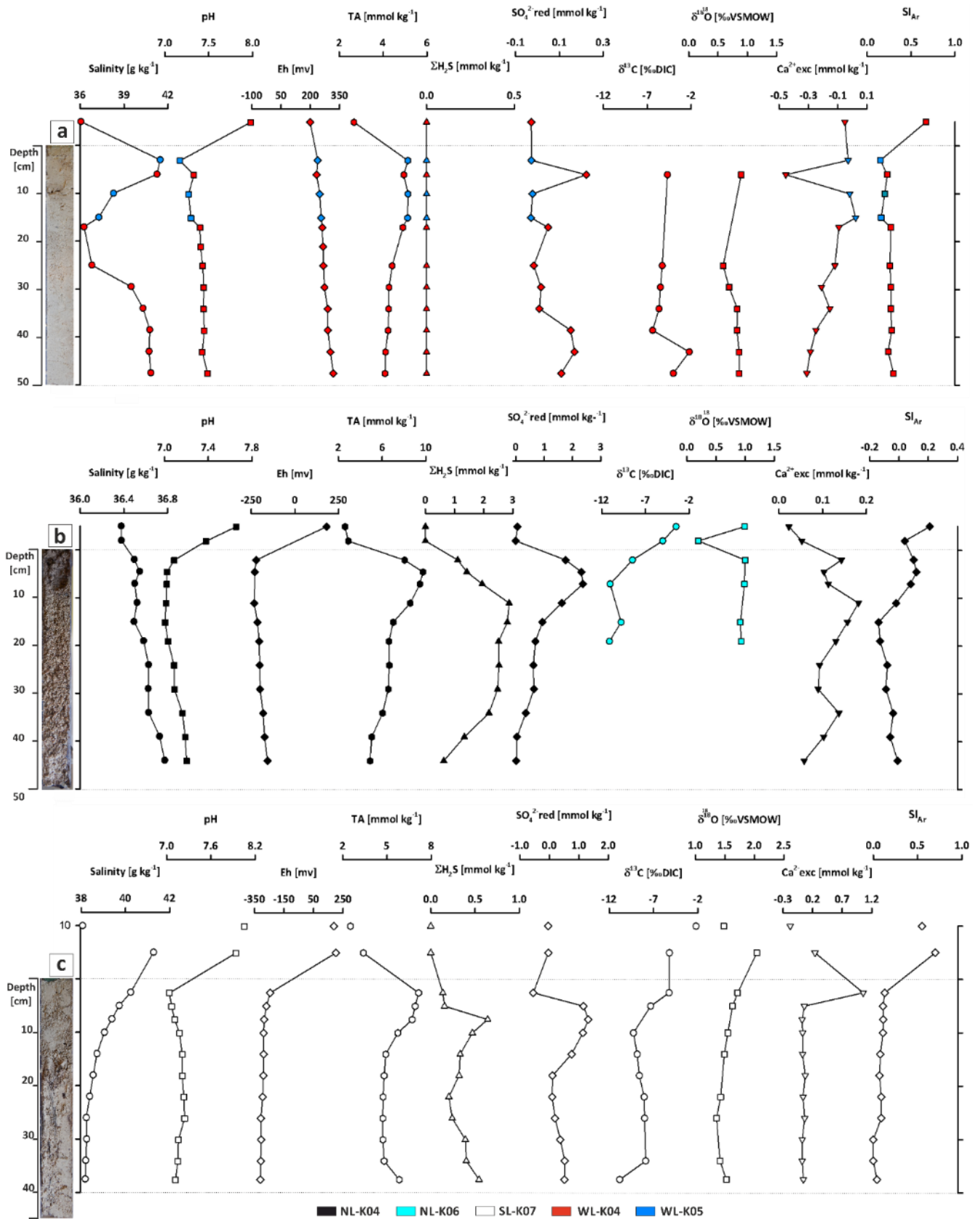


Figure 4.10: Physicochemical pore water parameters of west- (a), north- (b), and south lagoon cores (c). Diagrams (b) and (c) depict pore waters in an anoxic redox state, while (a) is characterized by oxic conditions.

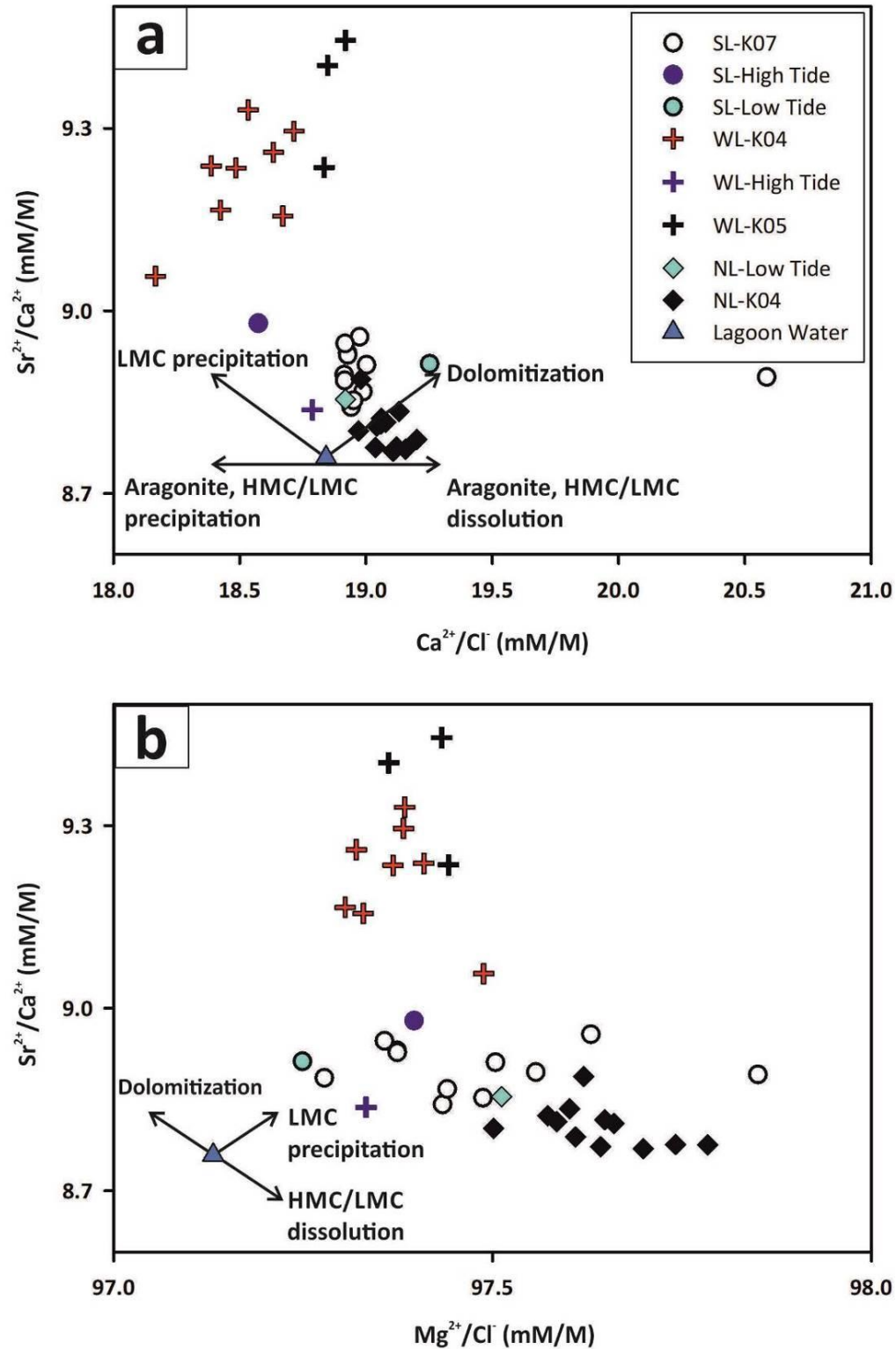


Figure 4.11: Crossplots of Sr^{2+}/Ca^{2+} versus Ca^{2+}/Cl^{-} (a), and Sr^{2+}/Ca^{2+} versus Mg^{2+}/Cl^{-} ratios (b) as diagenetic sensitive parameters. Briefly, the diagrams show the precipitation of small amounts of LMC/HMC/Ar in the west lagoon cores, while small quantities of Ar and HMC are dissolved and reprecipitated in the southern lagoon. In NL-K04, Ar and HMC dissolution are likely. Dolomitization can be excluded in all respective cases, as the Mg^{2+}/Cl^{-} ratio is not decreasing.

4.4.4 Bacterial community composition of sediment cores

Bacterial 16S rRNA gene analysis shows a diverse bacterial community, with a mean of 1286 (west lagoon), 1364 (north lagoon) and 2093 (south lagoon) amplicon sequence variants (ASVs; clustered at 100 % sequence identity) within the respective water columns (Figure 4.12). In the sediment of the west lagoon, ASV richness ranges between 1500 and 2000, with a decrease below 1000 between 17.5 and 22.5 cm. Within the north lagoon, 3449 ASVs were detected at 2.5 cm, which decrease to 1844 at 17.5 cm. The number of ASVs in the south lagoon shows a distinct boundary at a depth of 17.5 cm. Above, ASVs range between 1700 and 2080, whereas they drop below 500 from 17.5 to 37.5 cm (Figure 4.12).

The water column of the west lagoon is dominated by aerobic heterotrophic (relative abundance = 46 %) and facultative (an-)aerobic bacteria (40 %). Sulfate reducing bacteria (SRB), particularly of the genus *Desulfovibrionales* occur predominantly in the upper 5 cm of the core (13 %). Moreover, oxygenic phototrophs (*Cyanobacteriales*) are present at the sediment surface (2 %). With increasing depth, facultative (an-)aerobes (35-77 %) and aerobic heterotrophs (20-30 %) dominate the microbial community. This includes larger proportions of fermenting bacteria below a depth of 10 cm (22 %). Sulfur/sulfide oxidizing bacteria (SOX), of the order *Campylobacterales* (up to 36 % relative abundance) occur particularly in the water column of the north lagoon. Besides SOX bacteria, aerobic heterotrophs (15 %) and facultative (an-)aerobes (30-60 %) are the dominant metabolic groups. The sediment is dominated by SRB (*Desulfovibrionales*), which contribute up to 56 % of the total community at a depth of 17.5 cm, and fermenters (16-37 %) along the entire length of the core.

The water column of the south lagoon also harbors SOX bacteria (*Campylobacterales*; 7 %). The dominant metabolic groups are aerobic heterotrophs (37 %) and facultatives (33 %). Furthermore, SOX bacteria occur from the sediment surface to a depth of 2.5 cm with a relative abundance of 8 %. Below, SRB (*Desulfovibrionales*; 30 %) and fermenters (29 %) are the dominant groups. This trend changes alongside the mentioned decrease in species richness at 17.5 cm. Below this depth, facultative (an-) aerobes, particularly of the genus *Halomonas*, become the most abundant members of the bacterial community (relative abundance > 90 %).

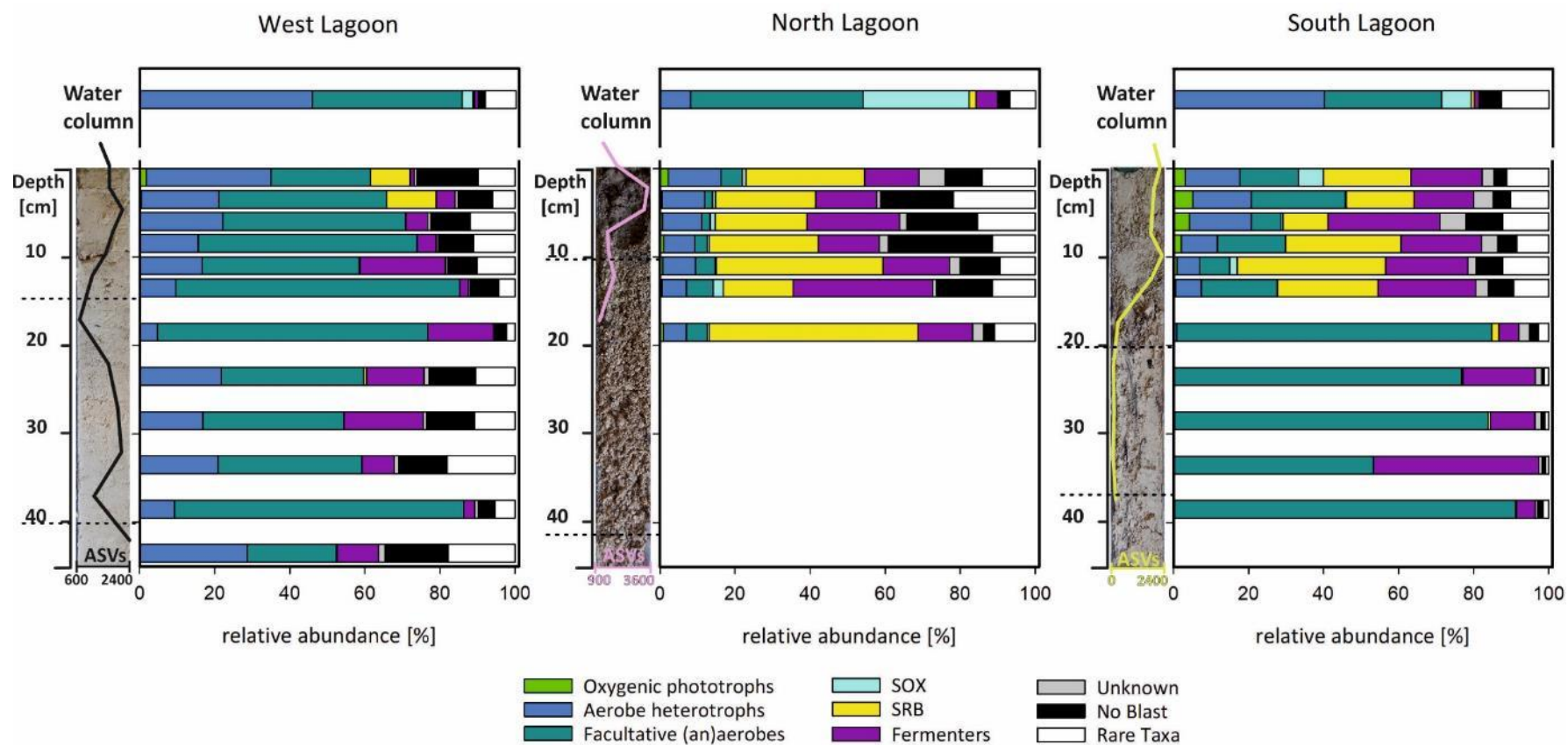


Figure 4.12: Total bacterial community grouped by metabolism at each site. The oxic west lagoon has a higher relative abundance of aerobic heterotrophic and facultative bacteria, in comparison to the anoxic northern and southern lagoon sediments with higher abundances of SOX bacteria, SRB and fermenters. The unknown taxa contain all organisms with a blast identity < 95 % and hit quality > 93 %, and the rare taxa contain all orders below 5 %. Lithological Units are indicated by dashed lines.

4.5 Discussion

4.5.1 Carbonate sediments within the lagoon of Aldabra

The lagoon of Aldabra has been proposed as pure lime mud depositing, recent analogue of Jurassic lagoons, which are well known for the deposition of fine-grained lithographic limestones (Gaillard et al., 1994; Bernier et al., 2014). Hence, the lagoon appears to be a suitable site to study the effects of early diagenesis on shallow marine mud. Indeed, a map of the benthic cover, based on referenced ground imaging, shows a wide distribution of carbonate sand, silt and mud at most of the inner shores of the lagoon (Hamylton et al., 2012; Hamylton et al., 2018). However, these works provide no information about the thickness of the sediments. Personal on-site investigations and coring now show that not all potentially suitable sites in the lagoon harbor a considerable sediment thickness (> 0.5 m). In contrast, most of the inner lagoon shore is characterized by the karstic, Pleistocene basement surface and contains only local patches of fine-grained sediments (Potts, 1977). The low accumulation of sediments arises from Aldabra's tectonic situation. Due to the fact that it is a raised atoll, tidal currents transport the lagoon sediments towards the open ocean (Stoddart et al., 1971). Nevertheless, we discovered bioclastic sand, which forms the tidal flats of the west lagoon, coarse shell debris and organic rich mud within karstic depressions in the north lagoon, and carbonate mud in current-protected areas of the south lagoon.

The west lagoon sampling site lies 4.5 km away from the western channels, which connect the lagoon to the ocean. Hence, high energetic tidal currents prevail and cause the deposition of a ca. 0.5 m thick succession of bioclastic sand on top of the Pleistocene basement. The cored intertidal sand is subdivided into 3 lithological units, according to the respective sorting of the grains. This is medium to well in WLU III (40-50 cm), poor in WLU II (15-40 cm), and medium in WLU I (0-15 cm). Biogenic carbonate mainly comprises fragments of coralline red algae and green algae of the order *Dasycladales*, which is typical for the shallow and warm water environment of the west lagoon (Barattolo, 1991).

The north lagoon represents a low-energy tidal flat, in which sediments accumulate in karstic depressions as coarse-grained shell detritus, topped by a thin layer (up to 10 cm) of organic rich mud. The sampled sediments are ca. 9 km away from the next connection to the open ocean. Although tropical cyclones are rare on Aldabra (Walsh, 1984), the succession of lithological units shows typical signs of swell lag deposits, which are characterized by the erosion or removal of fine grained- and the preservation of coarse-grained sediments by storm induced currents (Aigner, 1982). The organic rich mud of NLU I mirrors the current depositional environment, which is characterized by high C_{org} values (7-11 wt%) that decrease through decomposition towards NLU II ($C_{org} < 3\text{wt}\%$).

The south lagoon is also characterized by a low-energy tidal flat, which grades landwards into a mangrove swamp. Compared with the other two sites, it lies the farthest away from connections to the open ocean (9.5 km from Middle-, and 14.5 km from Gionnet Channel, Figure 4.1a). Fine grained carbonate sediments are trapped between mangrove shrubs and overlie the karstic basement up to 0.5 m.

SLU I (0-20 cm) is characterized by peloidal mud, foraminifera and ostracod shells, indicating a depositional environment devoid of currents and slightly elevated salinities (Greiner, 1974; Murray, 1973). SLU II (20-35 cm) shows mangrove rootage and bioturbated micrite, and SLU III (35-44 cm) depicts a higher abundance of skeletal particles (*Halimeda* and other green algae, coralline red algae, and shell detritus) compared to SLU I. The latter indicates a different depositional environment of SLU III compared to SLU I, possibly shaped by slightly enhanced currents.

Moreover, the available age data from the south (2293 ± 70 a, 1424 ± 64 a, and 771 ± 73 a) and west lagoon (2357 ± 70 a) indicate a late Holocene deposition of the sediments (< 2500 a). The inverted age pattern of SLU I points to redepositing or mixing by bioturbation of the unconsolidated sediments in the south lagoon.

4.5.2 Physicochemical pore water gradients and microbial effects as indicators of early diagenesis

The cores from three intertidal sites in the lagoon of Aldabra, exhibit three different pore water environments. The pore spaces of the west lagoon are oxic with high porosity, those of the north lagoon anoxic with high porosity, and those of the south lagoon are anoxic with low porosity.

The west lagoon lies close (4.5 km) to the western channels, which connect the lagoon with the open ocean. Hence salinity, $\delta^{13}\text{C}_{\text{DIC}}$, $\delta^{18}\text{O}_{\text{VSMOW}}$ and temperature match ocean values ($35 \text{ g}\cdot\text{kg}^{-1}$, -1.76 ‰ , 0.64 ‰ , 27.8 °C), and are slightly elevated during low tide. The cored intertidal flat is marked by complete dry fall during low tide. Strong tidal currents cause the deposition of bioclastic, porous sand. Due to its high porosity, the sediment receives regular input of lagoon water during the tides. This is mirrored by the salinity pore water profile, which shows higher values ($41.2\text{-}41.4 \text{ g}\cdot\text{kg}^{-1}$) at the sediment surface, due to evaporation during low tide coupled dry fall. Lower salinities are recorded between 10 and 25 cm ($36.8\text{-}38.2 \text{ g}\cdot\text{kg}^{-1}$), likely related to the onset of high tide currents. The lower parts of the core (25-50 cm) are once again characterized by dry fall affected water, possibly flowing from the supratidal hinterland towards the low water line with higher salinities ($>40 \text{ g}\cdot\text{kg}^{-1}$), $\delta^{18}\text{O}_{\text{VSMOW}}$ (0.8 ‰) and lower $\delta^{13}\text{C}_{\text{DIC}}$ (ca. -6 ‰). This salinity gradient fits a “skin- and body circulation” (Billerbeck et al., 2006), which describes the infiltration of the upper pore space by tidal water. Subsequently, the water percolates into deeper sediment layers and finally reaches the low waterline. Even though the pore space is completely oxic, the trend of SO_4^{2-} -red indicates that sulfate reduction occurs at a depth of 6 cm, coupled to a loss of Ca^{2+} within the pore water. The latter suggests the formation of carbonate minerals within the pore space, possibly related to the activity of *Desulfovibrionales* and *Cyanobacteriales*, which occur at similar depths (3-6 cm). This is further substantiated by the decreasing $\text{Ca}^{2+}/\text{Cl}^-$ and increasing $\text{Sr}^{2+}/\text{Ca}^{2+}$ ratio. However, as “fresh” pore water is provided with the tides, elemental ratios of $\text{Sr}^{2+}/\text{Ca}^{2+}$, $\text{Ca}^{2+}/\text{Cl}^-$, and $\text{Mg}^{2+}/\text{Cl}^-$ (Figure 4.11), provide just a snapshot of the associated mineral forming processes within the pore space.

Within the water column of the north lagoon, pH (7.6) and $\delta^{13}\text{C}_{\text{DIC}}$ (-3.5 ‰) are lower than the respective values of the open ocean (8.1 , -1.76 ‰). An effect which is likely induced by a high abundance of sulfur-oxidizing bacteria (SOX) of the order *Campylobacter* in the water column (Figure 4.12), which decrease pH values via sulfuric acid formation (Walter et al., 1993). Considerable sediment accumulations of mollusk detritus and mud are restricted to karstic depressions within the basement of the tidal flat, where water residues, despite tidal fluctuations. The redox potential decreases strongly within the upper part of the core and remains anoxic towards the bottom. This is accompanied by changes of $\Sigma\text{H}_2\text{S}$, SO_4^{2-} -red and TA, which show maxima within the mud of NLU I, indicating enhanced anaerobe bacterial activity and decomposition of OM. A finding that is further supported by low $\delta^{13}\text{C}_{\text{DIC}}$ (-8.5 ‰ to -11.0 ‰) of pore waters in this unit. The community composition shows SRB of the order *Desulfovibrionales* as the most abundant bacteria within the sediment, explaining the large amounts of sulfate reduction within NLU I and NLU II. SI_{Ar} scatters around zero throughout the core, but $\text{Ca}^{2+}/\text{Cl}^-$ and $\text{Mg}^{2+}/\text{Cl}^-$ show slightly elevated values in combination with constant $\text{Sr}^{2+}/\text{Ca}^{2+}$ ratios. This indicates low amounts of HMC and Ar dissolution, which concurs with high rates of SO_4^{2-} reduction. An indicator that sulfate reduction alone is not necessarily decisive with respect to carbonate precipitation.

The south lagoon lies farther away from the ocean than WL and NL (details in 5.1), which causes evaporation driven, increased salinity ($39 \text{ g}\cdot\text{kg}^{-1}$), temperature ($28.2 \text{ }^\circ\text{C}$), and $\delta^{18}\text{O}_{\text{VSMOW}}$ (1.48 ‰) in the water column. Low tide water, flowing from the mangrove covered hinterland towards the low stand water, shows a rise in these parameters ($42.5 \text{ g}\cdot\text{kg}^{-1}$, $36.1 \text{ }^\circ\text{C}$, 2.0 ‰). Aragonite saturation in the water column (high tide = 0.55; low tide = 0.7) is higher than in the WL (0.53) and NL (0.2), but remains below values required for authigenic Ar precipitation (De Choudens-Sanchez and Gonzalez, 2009 and references therein).

Within the sediment, the salinity decreases from low tide evaporation values of $>42 \text{ g}\cdot\text{kg}^{-1}$ at the top to $39 \text{ g}\cdot\text{kg}^{-1}$ at the bottom of the core. This indicates the long-term mean, as low porosity precludes large scale downward diffusion of more evaporated tidal waters. The redox potential shows the lowest values of all investigated sites (-243 to -309 mV), accounting for anaerobic microbial activity by SRB and fermenters, and further indicated by rising TA ($5\text{-}7 \text{ mmol}\cdot\text{kg}^{-1}$), $\delta^{13}\text{C}_{\text{DIC}}$ (-9 ‰), and SO_4^{2-} -red ($1.3 \text{ mmol}\cdot\text{kg}^{-1}$) in the upper 15 cm of the core. These values decrease (TA; SO_4^{2-} -red) or stabilize ($\delta^{13}\text{C}_{\text{DIC}}$) below 15 cm, accompanied by a constant $C_{\text{org}}/N_{\text{tot}}$ ratio (15-17), which indicates a stagnant or reduced microbial decomposition of OM (Kastner et al., 1990). The pH displays the lowest values at the sediment surface (7.0), alongside a drop of S_{Ar} from 0.7 to 0.2 and higher relative abundances of SOX bacteria. $\text{Ca}^{2+}/\text{Cl}^-$ and $\text{Mg}^{2+}/\text{Cl}^-$ ratios indicate Ar and HMC dissolution at the top of the core. This also indicates a decisive role of Campylobacteriales in influencing CaCO_3 dissolution through their pH lowering metabolic activity. A sharp shift in the bacterial community composition occurs below a depth of 15 cm. In the deeper core, SRB and SOX bacteria are virtually absent and are replaced by bacteria with versatile metabolisms, like the gammaproteobacteria *Halomonas*. This difference matches the stagnating $C_{\text{org}}/N_{\text{tot}}$ ratio and the division of lithological units. It implicates that the sediments traversed by mangrove roots (SLU II and III) yield organic compounds, which are harder to decompose (Benner et al., 1984).

4.5.3 Diagenetic signatures within Holocene lagoon sediments of Aldabra

Carbonate sediments within the lagoon of Aldabra originate from the disintegration of biogenic carbonate (i. e. algae, mollusks, and corals), whereas authigenic precipitation in the water column plays a minor role. A finding that is evident by the lack of fine-grained carbonate particles, carbonate mineral isotope values which are not in equilibrium with the respective water column, and low carbonate phase saturation. Diagenetic signatures are difficult to trace in the present study and solely recorded by cryptocrystalline CaCO_3 cements within the oxic pore space of the bioclastic sand in the west lagoon. The bulk isotope composition ($\delta^{13}\text{C}_{\text{carb}}$, $\delta^{18}\text{O}_{\text{carb}}$) remains unaffected by these changes, but two factors must be considered in this context: First, in order to detect diagenetic proxy changes, the isotope record of the precipitating fluid must be different compared to the pristine carbonate phase (Swart, 2015), which is evident in the present case. Second, the amount of cement is minor compared to abundant biogenic carbonate deposits, which compromises a detection of diagenetic isotope shift in the bulk record. This outcome concurs with observations made by Hover et al. (2001), who claimed that early diagenesis has usually minor effects on bulk geochemistry of carbonate sediments, due to mass effects. However, the formation of carbonate cements within WL sediments, has two main contributors. On the one hand, cement formation may be linked to the frequent input of “fresh” tidal lagoon water into the pore space. Thus, a constant ion supply, enhanced by evaporation during low tide, drives CaCO_3 supersaturation. On the other hand, the activity of microbes elevates pH values, particularly caused by the CO_2 consuming metabolism of photosynthetic *Cyanobacteriales*. Furthermore, sulfate reduction, which can occur in small anoxic niches within oxic

sediments (Jørgensen, 1977), rises alkalinity. Hence, both metabolic processes contribute to CaCO_3 supersaturation (Morse and Mackenzie, 1990). This point is supported by the chemical gradients of excess Ca^{2+} and the amount of SO_4^{2-} -red, which show a notable correspondence at a depth of 6 cm, in proximity to remnants of a microbial biofilm. However, the shape of the cements, which connect grains with each other, concurs with typical marine vadose cement types listed in Flügel (2004)

Sediments of the north- and south lagoon show typical anoxic microbial zones, including sulfate reduction (Jørgensen and Kasten, 2006), which cause lower pore water $\delta^{13}\text{C}_{\text{DIC}}$ values (-8.0 to -11.0 ‰). However, their effects are not directly visible in the bulk sediment isotope composition. The bulk is mainly controlled by the mineralogy and vital effects of biogenic carbonate, which shift the isotope equilibrium (Swart, 2015 and references therein). This explains the $\delta^{13}\text{C}_{\text{carb}}$ enrichment of aragonitic WL sediments compared to NL and SL deposits, which contain lower amounts of Ar. Pore water elemental ratios indicate only minor diagenetic changes, in form of dissolution of metastable carbonate (Ar and HMC) in the upper part of southern lagoon pore waters, connected to the activity of acidifying SOX bacteria (Campylobacteriales). In contrast to our observations, severe early diagenetic alteration of CaCO_3 related to OM degradation within anoxic environments is known from other studies (Pederson et al., 2019; Pederson et al., 2015). However, these results are not comparable to the present study, as the carbonate phases of these works were formed authigenic and in connection to microbial activity. These carbonate phases show a higher reactivity than non-microbial carbonate minerals, due to specific crystal morphologies, which include high intragranular porosities. In culture experiments with SRB, (Lange et al., 2018) detected Ar dissolution in *Arctica Islandica* shells in marine anoxic media within three months of incubation, but no re-precipitation of other carbonate minerals. These observations are consistent with our results from the north and south lagoon, in which anoxic conditions, including sulfate reduction, and only slightly elevated salinities prevail.

4.6 Conclusions

The present study provides an overview of the early diagenetic processes within oxic and anoxic pore spaces in Holocene carbonate sediments from the Aldabra Atoll. Unconsolidated, fine grained carbonate accumulations turned out to be scarce on this elevated coral atoll and were solely found in a protected bay at the inner shore of the south lagoon. Anoxic sediments of the north and south lagoon show no significant alterations of the bulk geochemistry by anoxic microbial processes, within the observed time scale of ca. 2,500 a. However, dissolution of metastable carbonate minerals is evident through changing elemental ratios of $\text{Sr}^{2+}/\text{Ca}^{2+}$ and $\text{Mg}^{2+}/\text{Cl}^-$ in the upper core of the south lagoon. These dissolution processes likely coincide with acidifying sulfur oxidation, caused by the presence of bacteria of the order Campylobacteriales. In contrast, the OM depleted, oxygenated diagenetic environment of the west lagoon favors the precipitation of typical marine vadose, cryptocrystalline CaCO_3 cements. Compared to abundant biogenic carbonate, the amount of cement is minor. Due to this mass effect, possible diagenetic isotope shifts of the cement are not traceable in the bulk record. The formation of the cements may be linked to the contemporaneous bacterial community of the sediment, which includes phototrophic *Cyanobacteriales* and SRB of the order *Desulfovibrionales*. A second contributor to the precipitation of cements is the supersaturation of pore waters with respect to carbonate due to evaporation. Our observations suggest that on short timescales (2,500 a), CaCO_3 precipitation within oxic pore spaces, has a higher early diagenetic effect on carbonate sediments than processes involving anoxic decomposition of OM.

4.7 Acknowledgements

We are very grateful to the staff of the Seychelles Island Foundation (SIF) for their unreserved support and hospitality on Aldabra. Special thanks to SIF ranger Ronny Marie for his extraordinary support in planning and continuous assistance in the field. We wish to thank the SIF project coordinators Nancy Bunbury, April Burt, and Frauke Fleischer-Dogley. Moreover, we acknowledge Wolfgang Dröse, Birgit Röring, Axel Hackmann, and Beate Gehnen for their support during lab work. We thank Anja Poehlein at the Göttingen Genomics laboratory for amplicon sequencing and initial sequence processing, supported by Melanie Heinemann and Sarah Schüßler. We also thank Adrian Immenhauser for insightful discussions. This study was funded by the German research foundation (DFG) within the framework of the “CHARON” research group (DA 374/11-1, AR 335/8-1). Further support was provided by the Open Access Publication Funds of the Georg-August-University of Göttingen.

4.8 References

- Aigner, T.: Calcareous tempestites: Storm-dominated stratification in upper muschelkalk limestones (middle trias, sw-germany), in: *Cyclic and event stratification*, Springer, 180-198, https://doi.org/10.1007/978-3-642-75829-4_13, 1982.
- Allan, J., and Matthews, R.: Isotope signatures associated with early meteoric diagenesis, *Sedimentology*, 29, 797-817, <https://doi.org/10.1111/j.1365-3091.1982.tb00085.x>, 1982.
- Andersen, K. S., Kirkegaard, R. H., Karst, S. M., and Albertsen, M.: Ampvis2: An r package to analyse and visualise 16s rRNA amplicon data, *BioRxiv*, 299537, <https://doi.org/10.1101/299537>, 2018.
- Banner, J. L., and Hanson, G. N.: Calculation of simultaneous isotopic and trace element variations during water-rock interaction with applications to carbonate diagenesis, *Geochimica et Cosmochimica Acta*, 54, 3123-3137, [https://doi.org/10.1016/0016-7037\(90\)90128-8](https://doi.org/10.1016/0016-7037(90)90128-8), 1990.
- Barattolo, F.: Mesozoic and cenozoic marine benthic calcareous algae with particular regard to mesozoic dasycladaleans, in: *Calcareous algae and stromatolites*, Springer, 504-540, https://doi.org/10.1007/978-3-642-52335-9_22, 1991.
- Bathurst, R. G.: Carbonate sediments and their diagenesis. Amsterdam, Development in sedimentology, Elsevier, <https://doi.org/10.1144/gsjgs.132.3.0342>, 1976.
- Benner, R., Maccubbin, A., and Hodson, R. E.: Anaerobic biodegradation of the lignin and polysaccharide components of lignocellulose and synthetic lignin by sediment microflora, *Applied and Environmental Microbiology*, 47, 998-1004, <https://doi.org/10.1128/aem.47.5.998-1004.1984>, 1984.
- Bernier, P.: For a reinstatement of "lithographic", a precise word to define a precise limestone, *Geobios*, 27, 307-311, [https://doi.org/10.1016/s0016-6995\(94\)80047-2](https://doi.org/10.1016/s0016-6995(94)80047-2), 1994.
- Bernier, P., Barale, G., Bourseau, J.-P., Buffetaut, E., Gaillard, C., Gall, J.-C., and Wenz, S.: The lithographic limestones of cerin (southern jura mountains, france). A synthetic approach and environmental interpretation, *Comptes Rendus Palevol*, 13, 383-402, <https://doi.org/10.1016/j.crpv.2014.01.006>, 2014.
- Billerbeck, M., Werner, U., Polerecky, L., Walpersdorf, E., DeBeer, D., and Huettel, M.: Surficial and deep pore water circulation governs spatial and temporal scales of nutrient recycling in intertidal sand flat sediment, *Marine Ecology Progress Series*, 326, 61-76, <https://doi.org/10.3354/meps326061>, 2006.
- Braithwaite, C.: Last interglacial changes in sea level on alibaba, western indian ocean, *Sedimentology*, <https://doi.org/10.1111/sed.12738>, 2020.
- Braithwaite, C. J., Taylor, J. D., and Kennedy, W. J.: The evolution of an atoll: The depositional and erosional history of alibaba, *Philosophical Transactions of the Royal Society of London. B, Biological Sciences*, 266, 307-340, <https://doi.org/10.1098/rstb.1973.0051>, 1973.
- Burdige, D.: 5.09 estuarine and coastal sediments—coupled biogeochemical cycling, *Treatise on Estuarine and Coastal Science*, 5, 279-308, <https://doi.org/10.1016/b978-0-12-374711-2.00511-8>, 2011.
- Burdige, D. J., Hu, X., and Zimmerman, R. C.: The widespread occurrence of coupled carbonate dissolution/precipitation in surface sediments on the bahamas bank, *American Journal of Science*, 310, 492-521, <https://doi.org/10.2475/06.2010.03>, 2010.

- Caporaso, J. G., Kuczynski, J., Stombaugh, J., Bittinger, K., Bushman, F. D., Costello, E. K., Fierer, N., Pena, A. G., Goodrich, J. K., and Gordon, J. I.: Qiime allows analysis of high-throughput community sequencing data, *Nature methods*, 7, 335-336, <https://doi.org/10.1038/nmeth.f.303>, 2010.
- Chen, L., Reeve, J., Zhang, L., Huang, S., Wang, X., and Chen, J.: Gmpr: A robust normalization method for zero-inflated count data with application to microbiome sequencing data, *PeerJ*, 6, e4600, <https://doi.org/10.7717/peerj.4600>, 2018a.
- Chen, S., Zhou, Y., Chen, Y., and Gu, J.: Fastp: An ultra-fast all-in-one fastq preprocessor, *Bioinformatics*, 34, i884-i890, <https://doi.org/10.1093/bioinformatics/bty560>, 2018b.
- Christ, N., Immenhauser, A., Wood, R. A., Darwich, K., and Niedermayr, A.: Petrography and environmental controls on the formation of phanerozoic marine carbonate hardgrounds, *Earth-Science Reviews*, 151, 176-226, <https://doi.org/10.1016/j.earscirev.2015.10.002>, 2015.
- De Choudens-Sanchez, V., and Gonzalez, L. A.: Calcite and aragonite precipitation under controlled instantaneous supersaturation: Elucidating the role of caco3 saturation state and mg/ca ratio on calcium carbonate polymorphism, *Journal of Sedimentary Research*, 79, 363-376, <https://doi.org/10.2110/jsr.2009.043>, 2009.
- Edgar, R. C.: Unoise2: Improved error-correction for illumina 16s and its amplicon sequencing, *BioRxiv*, 081257, <https://doi.org/10.1101/081257>, 2016.
- Elderfield, H., Yu, J., Anand, P., Kiefer, T., and Nyland, B.: Calibrations for benthic foraminiferal mg/ca paleothermometry and the carbonate ion hypothesis, *Earth and Planetary Science Letters*, 250, 633-649, <https://doi.org/10.1016/j.epsl.2006.07.041>, 2006.
- Farrow, G.: The climate of aldabra atoll, *Philosophical Transactions of the Royal Society of London. B, Biological Sciences*, 260, 67-91, <https://doi.org/10.1098/rstb.1971.0007>, 1971.
- Flügel, E.: *Microfacies of carbonate rocks: Analysis, interpretation and application*, Springer Science & Business Media, <https://doi.org/10.1007/978-3-662-08726-8>, 2004.
- Gaillard, C., Bernier, P., and Gruet, Y.: Le lagon d'aldabra (seychelles, océan indien), un modèle pour le paléoenvironnement de cerin (kimméridgien supérieur, jura méridional, france), *Geobios*, 27, 331-348, [https://doi.org/10.1016/s0016-6995\(94\)80050-2](https://doi.org/10.1016/s0016-6995(94)80050-2), 1994.
- Ge, Y., Pederson, C. L., Lokier, S. W., Traas, J. P., Nehrke, G., Neuser, R. D., Goetschl, K. E., and Immenhauser, A.: Late holocene to recent aragonite-cemented transgressive lag deposits in the abu dhabi lagoon and intertidal sabkha, *Sedimentology*, <https://doi.org/10.1111/sed.12707>, 2020.
- Gischler, E., and Lomando, A. J.: Holocene cemented beach deposits in belize, *Sedimentary Geology*, 110, 277-297, [https://doi.org/10.1016/s0037-0738\(96\)00088-7](https://doi.org/10.1016/s0037-0738(96)00088-7), 1997.
- Grasshoff, K., Kremling, K., and Ehrhardt, M.: *Methods of seawater analysis*, John Wiley & Sons, <https://doi.org/10.1002/9783527613984>, 2009.
- Greiner, G. O. G.: Environmental factors controlling the distribution of recent benthonic foraminifera, *Brevoria, Mus. Comp. Zool.*, 420, 1-35, <https://doi.org/10.1038/223168a0>, 1974.
- Groeneveld, J., Filipsson, H. L., Austin, W. E., Darling, K., McCarthy, D., Krupinski, N. B. Q., Bird, C., and Schweizer, M.: Assessing proxy signatures of temperature, salinity, and hypoxia in the baltic sea through foraminifera-based geochemistry and faunal assemblages, *Journal of Micropalaeontology*, <https://doi.org/10.5194/jm-37-403-2018>, 2018.
- Hamylton, S., Spencer, T., and Hagan, A.: Spatial modelling of benthic cover using remote sensing data in the aldabra lagoon, western indian ocean, *Marine Ecology Progress Series*, 460, 35-47, <https://doi.org/10.3354/meps09779>, 2012.

- Hamylton, S., Hagan, A., Bunbury, N., Fleischer-Dogley, F., and Spencer, T.: Mapping the lagoon at alibaba atoll, western indian ocean, 2018.
- Higgins, J. A., Blättler, C., Lundstrom, E., Santiago-Ramos, D., Akhtar, A., Ahm, A. C., Bialik, O., Holmden, C., Bradbury, H., and Murray, S.: Mineralogy, early marine diagenesis, and the chemistry of shallow-water carbonate sediments, *Geochimica et Cosmochimica Acta*, 220, 512-534, <https://doi.org/10.1016/j.gca.2017.09.046>, 2018.
- Hover, V. C., Walter, L. M., and Peacor, D. R.: Early marine diagenesis of biogenic aragonite and mg-calcite: New constraints from high-resolution stem and aem analyses of modern platform carbonates, *Chemical Geology*, 175, 221-248, [https://doi.org/10.1016/s0009-2541\(00\)00326-0](https://doi.org/10.1016/s0009-2541(00)00326-0), 2001.
- Jari Oksanen, F., Friendly, M., Kindt, R., Legendre, P., McGlinn, D., Minchin, P. R., O'Hara, R., Simpson, G. L., Solymos, P., and Stevens, M. H. H.: Vegan: Community ecology package, R package version, 2, 2018.
- Jørgensen, B.: Bacterial sulfate reduction within reduced microniches of oxidized marine sediments, *Marine Biology*, 41, 7-17, <https://doi.org/10.1007/bf00390576>, 1977.
- Jørgensen, B. B., and Kasten, S.: Sulfur cycling and methane oxidation, in: *Marine Geochemistry*, edited by Schulz, H. D. and Zabel, M., Springer, Berlin, 271-309, https://doi.org/10.1007/3-540-32144-6_8, 2006.
- Jourabchi, P., Van Cappellen, P., and Regnier, P.: Quantitative interpretation of ph distributions in aquatic sediments: A reaction-transport modeling approach, *American Journal of Science*, 305, 919-956, <https://doi.org/10.2475/ajs.305.9.919>, 2005.
- Kastner, M., Elderfield, H., Martin, J. B., Suess, E., Kvenvolden, K. A., and Garrison, R. E.: Diagenesis and interstitial-water chemistry at the peruvian continental margin—major constituents and strontium isotopes, Suess, E., von Huene, R., et al., *Proc. ODP, Sci. Results*, 413-440, <https://doi.org/10.2973/odp.proc.sr.112.144.1990>, 1990.
- Klindworth, A., Pruesse, E., Schweer, T., Peplies, J., Quast, C., Horn, M., and Glöckner, F. O.: Evaluation of general 16s ribosomal rna gene pcr primers for classical and next-generation sequencing-based diversity studies, *Nucleic acids research*, 41, e1-e1, <https://doi.org/10.1093/nar/gks808>, 2013.
- Lange, S. M., Krause, S., Ritter, A. C., Fichtner, V., Immenhauser, A., Strauss, H., and Treude, T.: Anaerobic microbial activity affects earliest diagenetic pathways of bivalve shells, *Sedimentology*, 65, 1390-1411, <https://doi.org/10.1111/sed.12428>, 2018.
- Mackenzie, F. T., Vink, S., Wollast, R., and Chou, L.: Comparative geochemistry of marine saline lakes, in: *Physics and chemistry of lakes*, Springer, 265-278, https://doi.org/10.1007/978-3-642-85132-2_9, 1995.
- Martin, M.: Cutadapt removes adapter sequences from high-throughput sequencing reads, *EMBnet journal*, 17, 10-12, <https://doi.org/10.14806/ej.17.1.200>, 2011.
- Meister, P.: Two opposing effects of sulfate reduction on carbonate precipitation in normal marine, hypersaline, and alkaline environments, *Geology*, 41, 499-502, <https://doi.org/10.1130/g34185.1>, 2013.
- Millero, F. J.: The physical chemistry of seawater, *Annual Review of Earth and Planetary Sciences*, 2, 101-150, <https://doi.org/10.1146/annurev.ea.02.050174.000533>, 1974.
- Morse, J. W., and Mackenzie, F. T.: *Geochemistry of sedimentary carbonates*, Elsevier, [https://doi.org/10.1016/s0070-4571\(08\)70329-7](https://doi.org/10.1016/s0070-4571(08)70329-7), 1990.

- Mucci, A., Sundby, B., Gehlen, M., Arakaki, T., Zhong, S., and Silverberg, N.: The fate of carbon in continental shelf sediments of eastern Canada: A case study, *Deep Sea Research Part II: Topical Studies in Oceanography*, 47, 733-760, [https://doi.org/10.1016/s0967-0645\(99\)00124-1](https://doi.org/10.1016/s0967-0645(99)00124-1), 2000.
- Murray, J. W.: Distribution and ecology of living benthic foraminiferids, <https://doi.org/10.4319/lo.1973.18.6.1011a>, 1973.
- Ni, S., Krupinski, N. Q., Groeneveld, J., Persson, P., Somogyi, A., Brinkmann, I., Knudsen, K., Seidenkrantz, M.-S., and Filipsson, H.: Early diagenesis of foraminiferal calcite under anoxic conditions: A case study from the landsort deep, Baltic Sea (IODP site M0063), *Chemical Geology*, 558, 119871, <https://doi.org/10.1016/j.chemgeo.2020.119871>, 2020.
- Parkhurst, D. L., and Appelo, C.: Description of input and examples for PHREEQC version 3: A computer program for speciation, batch-reaction, one-dimensional transport, and inverse geochemical calculations, US Geological Survey, 2328-7055, <https://doi.org/10.3133/tm6a43>, 2013.
- Pederson, C. L., McNeill, D. F., Klaus, J. S., and Swart, P. K.: Deposition and diagenesis of marine oncoids: Implications for development of carbonate porosity, *Journal of Sedimentary Research*, 85, 1323-1333, <https://doi.org/10.2110/jsr.2015.77>, 2015.
- Pederson, C. L., Klaus, J. S., Swart, P. K., and McNeill, D. F.: Deposition and early diagenesis of microbial mud in the Florida Everglades, *Sedimentology*, 66, 1989-2010, <https://doi.org/10.1111/sed.12569>, 2019.
- Potts, M.: Studies on blue-green algae and photosynthetic bacteria in the lagoon of Aldabra Atoll, Durham University, 1977.
- Quast, C., Pruesse, E., Yilmaz, P., Gerken, J., Schweer, T., Yarza, P., Peplies, J., and Glöckner, F. O.: The SILVA ribosomal RNA gene database project: Improved data processing and web-based tools, *Nucleic Acids Research*, 41, D590-D596, <https://doi.org/10.1093/nar/gks1219>, 2012.
- Rognes, T., Flouri, T., Nichols, B., Quince, C., and Mahé, F.: VSEARCH: A versatile open source tool for metagenomics, *PeerJ*, 4, e2584, <https://doi.org/10.7717/peerj.2584>, 2016.
- Rohling, E. J., Grant, K., Bolshaw, M., Roberts, A., Siddall, M., Hemleben, C., and Kucera, M.: Antarctic temperature and global sea level closely coupled over the past five glacial cycles, *Nature Geoscience*, 2, 500-504, <https://doi.org/10.1038/ngeo557>, 2009.
- Schweigert, G.: The decapod crustaceans of the upper Jurassic Solnhofen limestones: A historical review and some recent discoveries, *Neues Jahrbuch für Geologie und Paläontologie-Abhandlungen*, 260, 131-140, <https://doi.org/10.1127/0077-7749/2011/0162>, 2011.
- Siddall, M., Rohling, E. J., Almogi-Labin, A., Hemleben, C., Meischner, D., Schmelzer, I., and Smeed, D.: Sea-level fluctuations during the last glacial cycle, *Nature*, 423, 853-858, <https://doi.org/10.1038/nature01690>, 2003.
- Stoddart, D. R., Taylor, J., Fosberg, F., and Farrow, G.: Geomorphology of Aldabra Atoll, *Philosophical Transactions of the Royal Society of London. B, Biological Sciences*, 260, 31-66, <https://doi.org/10.1098/rstb.1971.0006>, 1971.
- Suess, E.: Mineral phases formed in anoxic sediments by microbial decomposition of organic matter, *Geochimica et Cosmochimica Acta*, 43, 339-352, [https://doi.org/10.1016/0016-7037\(79\)90199-6](https://doi.org/10.1016/0016-7037(79)90199-6), 1979.
- Swart, P. K., and Eberli, G.: The nature of the $\delta^{13}\text{C}$ of periplatform sediments: Implications for stratigraphy and the global carbon cycle, *Sedimentary Geology*, 175, 115-129, <https://doi.org/10.1016/j.sedgeo.2004.12.029>, 2005.

- Swart, P. K.: The geochemistry of carbonate diagenesis: The past, present and future, *Sedimentology*, 62, 1233-1304, <https://doi.org/10.1111/sed.12205>, 2015.
- Synal, H.-A., Stocker, M., and Suter, M.: Micadas: A new compact radiocarbon ams system, *Nuclear Instruments and Methods in Physics Research Section B: Beam Interactions with Materials and Atoms*, 259, 7-13, <https://doi.org/10.1016/j.nimb.2007.01.138>, 2007.
- Talbot, M., and Kelts, K.: Primary and diagenetic carbonates in the anoxic sediments of lake bosumtwi, ghana, *Geology*, 14, 912-916, [https://doi.org/10.1130/0091-7613\(1986\)14<912:padcit>2.0.co;2](https://doi.org/10.1130/0091-7613(1986)14<912:padcit>2.0.co;2), 1986.
- Team, R.: RStudio: integrated development for R.(RStudio, Inc., Boston, MA, USA), 2016.
- Team, R. C.: R: A language and environment for statistical computing, 2018.
- von Hoyningen-Huene, A. J. E., Schneider, D., Fussmann, D., Reimer, A., Arp, G., and Daniel, R.: Bacterial succession along a sediment porewater gradient at Lake Neusiedl in Austria, *Scientific data*, 6, 1-7, <https://doi.org/10.1038/s41597-019-0172-9>, 2019.
- Wacker, L., Bonani, G., Friedrich, M., Hajdas, I., Kromer, B., Němec, M., Ruff, M., Suter, M., Synal, H.-A., and Vockenhuber, C.: Micadas: Routine and high-precision radiocarbon dating, *Radiocarbon*, 52, 252-262, <https://doi.org/10.1017/s0033822200045288>, 2010a.
- Wacker, L., Christl, M., and Synal, H.-A.: Bats: A new tool for ams data reduction, *Nuclear Instruments and Methods in Physics Research Section B: Beam Interactions with Materials and Atoms*, 268, 976-979, <https://doi.org/10.1016/j.nimb.2009.10.078>, 2010b.
- Walsh, R.: *Climate of the seychelles, Biogeography and Ecology of the Seychelles Islands'* (Ed. DR Stoddart.) pp, 39-61, 1984.
- Walter, L. M., and Burton, E. A.: Dissolution of recent platform carbonate sediments in marine pore fluids, *American Journal of Science*, 290, 601-643, <https://doi.org/10.2475/ajs.290.6.601>, 1990.
- Walter, L. M., Bischof, S. A., Patterson, W. P., and Lyons, T. W.: Dissolution and recrystallization in modern shelf carbonates: Evidence from pore water and solid phase chemistry, *Philosophical Transactions of the Royal Society of London. Series A: Physical and Engineering Sciences*, 344, 27-36, <https://doi.org/10.1098/rsta.1993.0072>, 1993.
- Whitman, W. B.: *Bergey's manual of systematics of archaea and bacteria*, Wiley Online Library, <https://doi.org/10.1002/9781118960608.gbm01255>, 2015.
- Xu, H., Ai, L., Tan, L., and An, Z.: Stable isotopes in bulk carbonates and organic matter in recent sediments of lake qinghai and their climatic implications, *Chemical Geology*, 235, 262-275, <https://doi.org/10.1016/j.chemgeo.2006.07.005>, 2006.
- Zachos, J., Pagani, M., Sloan, L., Thomas, E., and Billups, K.: Trends, rhythms, and aberrations in global climate 65 ma to present, *science*, 292, 686-693, <https://doi.org/10.1126/science.1059412>, 2001.
- Zhang, J., Kobert, K., Flouri, T., and Stamatakis, A.: Pear: A fast and accurate illumina paired-end read merger, *Bioinformatics*, 30, 614-620, <https://doi.org/10.1093/bioinformatics/btt593>, 2014.

5. Decoupling of pore water chemistry, bacterial community profiles, and carbonate mud diagenesis in a land-locked pool on Aldabra (Seychelles, Indian Ocean)

Dario Fussmann, Avril J. E. von Hoyningen-Huene, Andreas Reimer, Dominik Schneider, Volker Karius, Sylvia Riechelmann, Chelsea Pederson, Peter K. Swart, Rolf Daniel and Gernot Arp

Manuscript in preparation, submitted to *Geomicrobiology Journal* (02/19/21), under review

Abstract. Comparative pore water-sediment studies are crucial to trace biogeochemical and early diagenetic interactions between mineral- and fluid phases. They are commonly conducted in stable environments with long-time diagenetic reactions between sediment and pore water. In contrast, this work presents a comparative study within the Cinq Cases pool system, a shallow and saline water body, with occasional marine influx and short-time diagenetic reactions between sediment and pore water. Cinq Cases is located on the Aldabra atoll in the western Indian Ocean. Sediments span ca. 3800 years and indicate three environmental stages: (i) An initial, at least temporary anoxic, palustrine environment, including meteoric diagenesis (Unit III), (ii) slow marine flooding, with cyanobacteria and sponge blooms (Unit II), and (iii) lagoon flooding, including oxic conditions within the sediment (Unit I). Such frequent changes in diagenetic environments of small water bodies can be retraced by three different proxies representing partially overlapping but different time scales: (i) sediments reflect ancient processes (ii) pore waters are influenced by recent processes, and (iii) bacterial communities reflect an overlay of ancient and recent processes.

5.1 Introduction

The fate of modern carbonate deposits is usually determined after their deposition at the sediment – water interface: Rapidly varying chemical conditions in pore fluids can result in different thermodynamic equilibria and favor geochemical alteration of primary carbonate phases (Pederson et al., 2020b; Swart, 2015 and references therein). Comparative pore water-sediment studies are crucial to retrace the biogeochemical influences on early diagenetic alteration, which has the potential to alter the geochemical record of carbonate archives (Allan and Matthews, 1982; Banner and Hanson, 1990; Bathurst, 1976; Higgins et al., 2018; Swart and Eberli, 2005). According to Fantle et al. (2010), a main driver of carbonate diagenetic reactivity is the degree of mineralogical and geochemical disequilibrium between solid and fluid, which is influenced by the stability of the depositional setting (Bathurst, 1983; Berner, 1980). Environments with long term stable conditions, e. g. pelagic marine basins, usually contain sediments in near steady-state conditions with the contemporaneous pore water and thus, lower reaction rates (Berner, 1980; Froelich et al., 1979). In contrast, shallow habitats with varying environmental conditions on short time scales, which possibly include subaerial exposure and a complete exchange of depositional water, create sharp geo- and hydrochemical gradients between pore water and sediment. Hence, non-steady-state conditions with higher reaction rates and rapid early diagenesis are favored (Deflandre et al., 2002; Dravis, 1996; Matsuda et al., 1995; Rassmann et al., 2016). Accordingly, non-steady state settings provide a time lapse effect on early diagenesis, which offers the chance to retrace the variety of carbon cycling and carbonate phase alterations in-situ. Such data can act as a helpful supplement to experimental studies (Goetschl et al., 2019; Pederson et al., 2020a; Lange et al., 2018; Ritter et al., 2017) These hydrochemical pore water gradients are further influenced by bacterial photo- and heterotrophic metabolic activity, well known from oxic and anoxic pore water environments (Dupraz et al., 2009; Fussmann et al., 2020; Jørgensen and Kasten, 2006; Pederson et al., 2019; von Hoyningen-Huene et al., 2019). Moreover, the metagenome of past microbial communities can be preserved in the sediment (Coolen et al., 2013; More et al., 2019; Orsi et al., 2017) and is referred to as the “paleome” (Inagaki et al., 2005), providing a proxy for ancient depositional (and diagenetic) environments. Hence, the paleome offers an opportunity to retrace non-steady-state conditions between sediment and contemporaneous pore water.

Such short scale fluctuations of hydrochemical pore water conditions can be observed in highly dynamic hydrologic and depositional settings such as shallow, evaporative water bodies with seasonal rainfall. The interplay of evaporative periods with occasional sediment exposure, and wetter periods with high rainfall causes sharp diffusion gradients between the water- and sediment column (Lee et al., 2008; Pederson et al., 2019; Porter et al., 2007). An example for such a dynamic hydrologic and carbonate depositional environment is provided by the interconnected pool chain of Cinq Cases, in the southeastern part of the Aldabra Atoll (Figure 5.1). Besides extreme seasonality, occasional flash floods within the lagoon provide an input of marine fluids, allochthone microbes, and carbonate grains. This environmental variation creates an interplay of freshwater-, marine-, and hypersaline conditions in a single, shallow water environment.

The objective of this study is to interpret the depositional and diagenetic conditions of fine-grained carbonate sediments and their contemporaneous pore water in a dynamic, non-steady-state environment. Two sediment cores from the pool system of Cinq Cases are documented and discussed here, by combining geo-, and hydrochemical datasets, with pore water 16S rRNA gene and transcript community data for a

detailed analysis of the state and conditions of carbonate phase alterations. The application of such a multi-proxy approach is crucial to ensure a robust data reproducibility and shall further emphasize the feasibility of 16S rRNA data to retrace diagenetic reaction paths.

5.2 Study area

The area of Cinq Cases lies in the south-eastern part of Aldabra (Figure 5.1a; 46°29'42.569"E, 9°25'46.338"S), a raised coral atoll in the western Indian Ocean, located ca. 420 km northwest of Madagascar and ca. 620 km east of the African continent. It belongs to the western peripheries of the Seychelles group and measures 34 km east to west and 14.5 km north to south. The atoll is located in the most arid sector of the western Indian Ocean (Farrow, 1971) with a distinct seasonality of rainfall. The majority of which occurs from December to April during the north-east monsoon, with an average of 970 mm/yr (value for the past 50 years; rain gauge data provided by the Seychelles Islands Foundation, SIF). During the south-west monsoon, from May to December, only minor rainfall is recorded. Aldabra is located northwest of the Indian Ocean belt of tropical cyclones and is rarely affected by severe storms.

Takamaka- ("Marine Isotope Stage"-MIS 7) and Aldabra-limestone (MIS 5) formations form a raised atoll rim up to 8 m above sea level, surrounding a shallow (up to 5 m in depth) lagoon, filled with unconsolidated Holocene sediment (Figure 5.1a; Braithwaite, 2020). The rim is dissected into 4 islands, namely Picard-, Polymnie-, Middle- (Île Malabar) and South Island (Grande Terre), which vary between 0.25 and 5 km in width. The lagoon is drained by three main channels: Grande Passe (between Polymnie and Île Picard), Passe Houareau (between Grande Terre and Île Malabar) and Passe Gionnet (between Polymnie and Île Malabar). A network of shallower channels between the lagoon and Open Ocean exists between Picard and Grand Terre, as well as Picard and Polymnie.

Braithwaite et al. (1973), provide a detailed depositional history of Aldabra, which includes phases of both, emergence and submergence during the Pleistocene. Those periods were accompanied by remarkable sea level fluctuations (e. g. in MIS 6, sea level is considered to be 90 ± 15 m lower than today; Siddall et al., 2003; Rohling et al., 2009) during glacial and interglacial phases, causing the highly karstified atoll rim and dense limestone surface seen today. As a result, rainfall usually accumulates in bigger karstic holes, forming superficial pools, which are not necessarily connected to tidal or oceanic influences (Braithwaite et al., 1989). The Aldabra lagoon formed between 4000 to 5000 years BP, when a slightly elevated sea-level (compared to present conditions), caused the flooding of the old reef platform (Braithwaite et al., 1973).

The pools of Cinq Cases form an interconnected chain, occasionally fed with lagoon water during flash floods via a branched lagoon channel system in the north-west, called Bras Cinq Cases (Figure 5.1). During fieldwork, at the end of dry season (November 2017), water level was 30-50 cm above sediment surface. The Cinq Cases pool system has a lag (up to a few hours) in tidal movements and a lower tidal altitude, making it only barely (subterranean) connected to marine waters (Braithwaite et al., 1989).

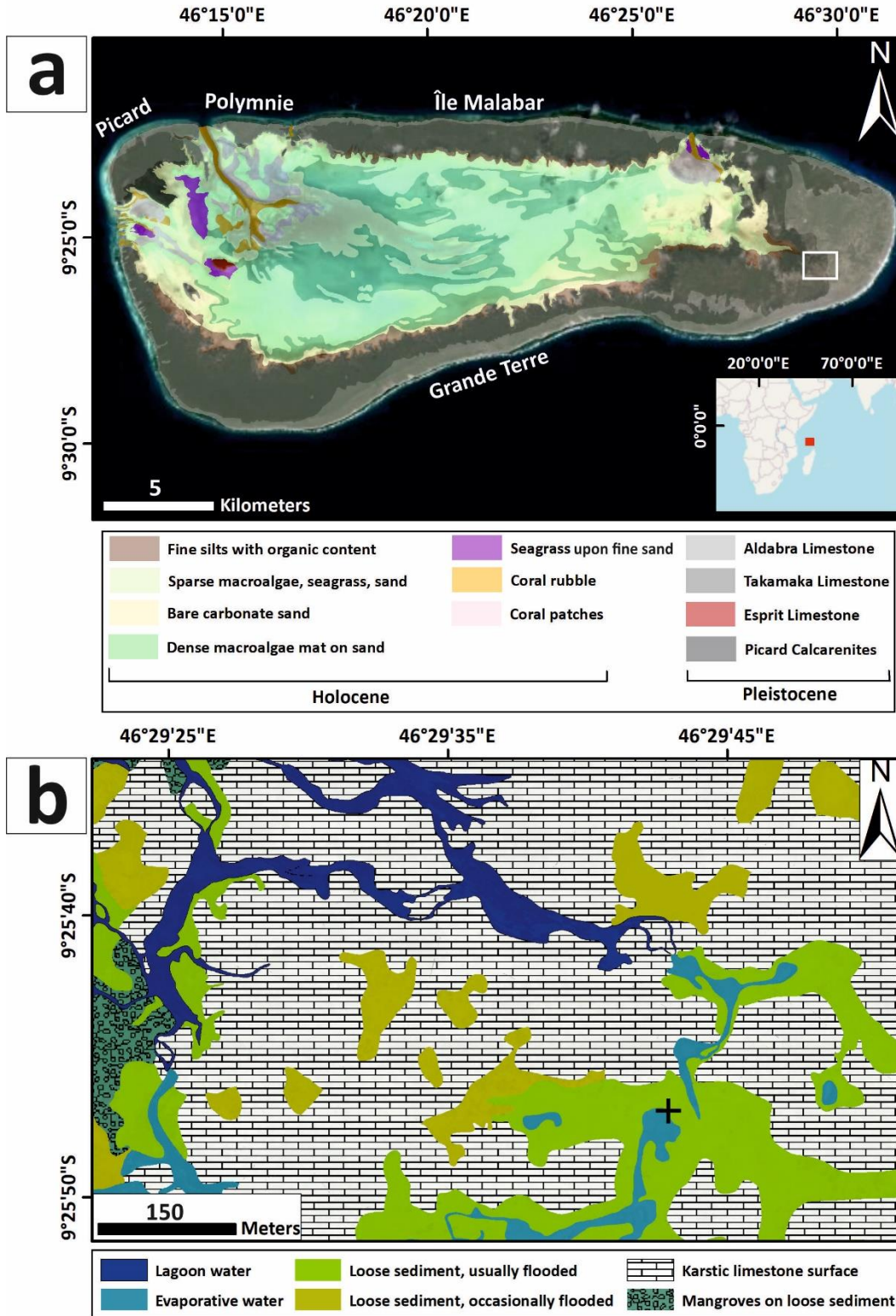


Figure 5.1a: Geography and deposits of Aldabra. The map is based upon ground sensing data from Hamylton et al. (2012), and on a geological map drawn by Braithwaite et al. (1973). The sampling area of Cinq Cases (white rectangle) was approached through the lagoon during low tide. Figure 1b shows a close up of the Cinq Cases pool area with self-classified ground types, based on a satellite image from 2013 (provided by the SIF). The area is connected to the lagoon at Bras Cinq Cases in the northwest of the image. The sampling area is indicated by a cross symbol.

5.3 Material and Methods

5.3.1 Sampling and field measurements

The sampling campaign at the Cinq Cases pool (46°29'45.558''E; 9°25'44.087''S) was performed in November 2017, at the end of the dry season. Physicochemical parameters of the water column were measured directly in the field using a WTW Multi 3630 device equipped with a WTW Tetracon conductivity probe, a WTW FDO 925 probe for dissolved O₂, and a WTW Sentix 940 electrode for temperature and pH (Xylem, Rye Brook, NY, USA). The pH probe has been calibrated against standard pH-buffers 7.010 and 10.010 (HI6007 and HI6010, Hanna Instruments, Woonsocket, RI, USA; standard deviation ≤ 2 %). Redox potential was measured with a WTW 340i device, equipped with a Pt61 probe (Schott, Mainz, Germany). Pool water was retrieved from a depth of 10 cm with a pre-rinsed 500 mL polyethylene (PE) bottle without headspace from which subsamples for anion, nutrient and total alkalinity (TA) determination were distributed into 100 mL PE and 250 mL Schott-Duran glass bottles (Schott, Mainz, Germany), respectively. For cation analysis, a 50 mL aliquot was filtered through membrane filters with a pore size of 0.8 μm (Roth, Karlsruhe, Germany) into a PE bottle and acidified with 100 μL HNO₃ (suprapur; Merck, Darmstadt, Germany). Total alkalinity was determined via titration within 24 hours after sampling using a hand-held titration device and 0.16 N H₂SO₄ cartridges (Hach Lange, Düsseldorf, Germany; standard deviation ≤ 1.5 %). Sediment cores were retrieved using PVC-tubes (6.3 cm in diameter) in approximately 30 cm lateral distance. Two cores, with an identical sedimentary sequence, and a length of 35 cm were used for sediment, pore water (CC-K04) and bacterial community profiling (CC-K01). Core CC-K01 was subsampled three times at every 2.5 cm of depth. The core supernatant was sampled by filtering 200 mL of water through a 3.0 μm PC (Merck, Darmstadt, Germany) and 0.2 μm PES filter sandwich (Sartorius, Göttingen, Germany) using a manual vacuum pump attached to a NALGENE filter holder with receiver (Thermo Fisher Scientific, Waltham, MA, USA). The RNA Protect Bacteria reagent (Qiagen, Hilden, Germany) was added immediately to preserve each sample for bacterial community profiling as described in von Hoyningen-Huene et al. (2019). Core CC-K04 was hermetically sealed after recovery and stored upright at temperatures close to its natural environment (30 ± 2 °C) for 24 hours. After redox sensitive measurements and pore water extraction, CC-K04 was opened and subsampled for hydro- and geochemical analyses with increments measuring 2.5 to 3.5 cm in width. Possible pressure differences are neglectable in the present case, because the cores were sampled just below the floor of a 30 to 50 cm high water column.

5.3.2 Petrographic, mineralogical and geochemical analyses

For bulk organic and inorganic carbon content detection, overall 11 subsamples were freeze dried, powdered with a ball mill, and measured by a LECO RC612 (Leco, St Joseph, MI, USA) multi-phase carbon and water determination device at the Georg-August-University Göttingen. For calibration, Leco synthetic carbon (1 and 4.98 carbon %) and Leco calcium carbonate (12 carbon %) were used. The same subsamples were utilized for CNS elemental detection, which was operated with a Euro EA 3000 Elemental Analyzer (Hekatech, Wegberg, Germany). 2.5-Bis (5-tert-benzoxazol-2-yl) thiophene BBOT and atropine sulfate monohydrate (IVA Analysetechnik, Meerbusch, Germany) were provided as reference material. Analytical accuracy of all analyses was better than 3 %. For bulk carbonate δ¹⁸O and δ¹³C (δ¹⁸O_{carb} and δ¹³C_{carb}) isotope analyses, duplicate ball milled subsamples were pre-rinsed with ultra-pure water and measured at the Ruhr-University-Bochum with a Thermo Finnegan-MAT 253 mass spectrometer, equipped with ConFloIV and GasBenchII interfaces (ThermoFisherScientific, Waltham, MA, USA). Internal standards were

corrected with certified IAEA-603 and NBS 18 reference materials and the 1σ -reproducibility was 0.05 ‰ for $\delta^{13}\text{C}$ and 0.06 ‰ for $\delta^{18}\text{O}$. Organic $\delta^{13}\text{C}$ and $\delta^{15}\text{N}$ ($\delta^{13}\text{C}_{\text{org}}$ and $\delta^{15}\text{N}_{\text{org}}$) isotopes were measured at the Rosenstiel School of Marine and Atmospheric Science, at the University of Miami. Twenty-five to 100 mg of sediment from each sample was dissolved with 10 % HCl overnight. The residue was filtered through glass microfibre filters and dried in a desiccator for a minimum of 48 h. The dry residue was packed in tin capsules and combusted using Dumas type combustion (Costech EA ECS 4010; Costech Analytical Technologies Inc., Valencia, Italy). Isotope data for carbon and nitrogen are reported relative to Vienna Pee Dee Belemnite (VPDB; $\delta^{13}\text{C}$) and atmospheric nitrogen ($\delta^{15}\text{N}$). The $\delta^{15}\text{N}$ values were measured on the non-acidified material and the $\delta^{13}\text{C}$ values discarded. The resultant CO_2 was analyzed using a continuous flow isotope-ratio mass spectrometer (Thermo Delta V Advantage; Thermo Fisher Scientific). Radiocarbon measurements were conducted for two organic-rich sediment samples at 22 to 25.5 and 32 to 35 cm depth from the top of the core. Measurements were performed at Beta Analytic testing laboratory (Miami, FL, USA), with a NEC accelerator mass spectrometer (National Electrostatics Corp., Middleton, WI, USA). Dates were measured relative to a modern reference standard, which was 95 % the ^{14}C signature of NIST SRM-4990C. Age calibrations were conducted via the High Probability Density Range Method (HPD; Ramsey, 2009) and the SHCAL13 database (Hogg et al., 2013).

X-ray-diffraction-analyses were performed with powdered sediment duplicate portions from the identical 11 increments as used for the bulk carbon detections, at the Department of Sedimentology and Environmental Geology in Göttingen by a PANanalytical (Almelo, Netherlands) Xpert MPD device (CuK α radiation, 2θ refraction range of 4-69.5°, step size 0.02°). Semi-quantitative phase composition analysis was performed with the Reference Intensity Ratio (RIR) of peaks by using Pananalytical's HighScore software (version 3.0.5). To correct for unidentifiable microcrystalline and amorphous phases, RIR results were normalized to inorganic carbon data retrieved from the aforementioned LECO RC612 device.

Another fraction from each sample increment was sub-sampled for thin sectioning and light microscopic observations. First, the soft sediment was dehydrated in an ethanol-series and treated with Sytox Green nucleic acid stain (Invitrogen, Carlsbad, CA, USA) to stain eukaryotic cell nuclei and prokaryotic cells for fluorescence microscopy. The stained samples were embedded in LR White resin (London Resin Company, Reading, United Kingdom) and cured in an oven for 24 hours at 60 °C. The hardened samples were cut, ground down to a thickness of 40 to 50 μm and capped with a glass cover. Petrographic observations were conducted with a petrographic and a laser-scanning microscope (Zeiss, Oberkochen, Germany, lsm excitation: 543 nm, 488 nm, 633 nm, laser unit: Argon/2, HeNe543, HeNe633). For electron-microprobe (EMP) measurements, non-capped, polished thin sections were carbon-vapored and analyzed by a JEOL JXA-8900 RL (Jeol, Tokyo, Japan) device. Samples were examined with an accelerating voltage of 15 kV and a beam diameter of 15 nm. Elemental analyses were conducted with 5 wavelength-dispersive spectrometers (WDS) equipped with an ArCH4 flow counter, a Xe counter and 14 analyzing crystals with 5 multilayers as detectors (standard deviation $\leq 0.07\%$). Further element mapping was conducted at non-capped, polished and carbon vapored thin sections, via energy-dispersive-X-ray spectroscopy (EDX) by a Gemini Leo 1530 SEM (Zeiss, Oberkochen, Germany) with a coupled INCA x-act (Oxford Instruments, Abingdon, United Kingdom) EDX detector.

5.3.3 Pore water analysis

Redox potential and pH gradients were measured directly in the sediment through newly drilled holes in the tube of core CC-K04. This procedure was conducted 24 hours after sampling with a portable WTW 340i

pH meter, equipped with an Inlab Solids Pro pH-electrode (Mettler Toledo, Columbus, OH, USA) and a Pt 5900 A redox electrode (SI Analytics, Mainz, Germany; standard deviation $\leq 2\%$). The boreholes were sealed, before pore water was extracted from the core with 5 cm CSS Rhizon samplers (Rhizosphere, Wageningen, Netherlands). Immediately after extraction, aliquots were fixed with Zn-acetate and HNO_3 (suprapur[®]) for determination of total sulfide ($\Sigma\text{H}_2\text{S}$) and major cations, respectively. Additionally, pore water for $\delta^{13}\text{C}_{\text{DIC}}$ analyses was filled into crimped vials without head space and poisoned with HgCl_2 to suppress organic activity. Pore water $\delta^{13}\text{C}_{\text{DIC}}$ was analyzed at the Ruhr-University-Bochum with a MAT 253 device with equipment, correspondent to 3.2 (1σ -reproducibility $\leq 0.19\%$). Pore water related $\delta^{13}\text{C}_{\text{DIC}}$ values are given relative to Vienna Pee-Dee Belemnite (VPDB). Pore water alkalinity was analyzed by a modified Hach titration method with 0.01 N HCl cartridges (Hach-Lange, Düsseldorf, Germany) as titrant. Concentrations of NH_4^+ , PO_4^{3-} , $\Sigma\text{H}_2\text{S}$ and dissolved silica ($\text{SiO}_{2(\text{aq})}$) were measured by photometric methods according to Grasshoff et al. (2009), using a SI Analytics Uviline 9400 spectrophotometer. Major cation (Ca^{2+} , Mg^{2+} , Na^+ , K^+ and Li^+) and anion (Cl^- , F^- , Br^- , SO_4^{2-} and NO_3^-) concentrations of pool and pore water samples (including the core supernatant) were analyzed by ion chromatography with suppressed and non-suppressed conductivity detection, respectively, at the Georg-August-University Göttingen (Metrohm 820 IC/Metrosep C3-250 analytical column, Metrohm 883 Basic IC/Metrohm ASupp5-250 analytical column, Metrohm, Herisau, Switzerland; standard deviation $\leq 1.5\%$). Inductively coupled plasma mass spectrometry (ICP-MS; ICAP-Q, ThermoFisherScientific, Waltham, MA, USA) was used to determine Sr, Ba, Fe, Mn, Rb and B, as control for the cation determination by ion chromatography (standard deviation $\leq 2\%$). Pore water $\delta^{18}\text{O}_{\text{Water}}$ was measured at Thermo Fisher Scientific GmbH in Bremen, with a Thermo Fisher™ Delta Ray™ Isotope Ratio Infrared Spectrometer (IRIS) coupled to an Universal Reference Interface (URI) Connect and Teledyne CETAC™ ASX-7100 Autosampler. Internal standards were corrected with certified USGS 48 reference material (standard deviation $\leq 0.07\%$). Pore water related $\delta^{18}\text{O}_{\text{Water}}$ values are reported relative to Vienna Standard Mean Ocean Water (VSMOW).

Measured data were processed with the PHREEQC software package (version 3; Parkhurst and Appelo, 2013). The implemented phreeqc.dat and wateqf4.dat databases were used to calculate ion activities of the water samples and compute mineral saturation states. Saturation indices are given as $\text{SI} = \log(\text{IAP}/K_{\text{sp}})$.

5.3.4 Bacterial community profiling

Before long-term storage at $-80\text{ }^\circ\text{C}$, the samples were centrifuged for 1 hour at $3150 \times g$ and the supernatant decanted. For bacterial community profiling, DNA and RNA were simultaneously extracted from all sediment and water samples using the PowerSoil Total RNA and DNA accessory kit (Qiagen, Hilden, Germany). Water samples were extracted from three independent filtration replicates and sediments were extracted three times per sampled depth. One gram of homogenized sediment or $\frac{1}{2}$ filter sandwich were extracted according to manufacturer's instructions. The final elution volume was reduced to $50\ \mu\text{L}$ of RNase free water (supplied by the manufacturer). DNA was frozen at $-20\text{ }^\circ\text{C}$ until use, while $1\ \mu\text{L}$ of RiboLock (Thermo Fisher Scientific, Waltham, MA, USA) was added to the RNA samples before storage at $-80\text{ }^\circ\text{C}$. Contaminant DNA was removed from all RNA samples by digestion with TurboDNase (Thermo Fisher Scientific, Waltham, MA, USA) according to manufacturer's instructions, including an additional incubation with $0.5\ \mu\text{L}$ of TurboDNase for 15 minutes at $37\text{ }^\circ\text{C}$ as described by (Schneider et al., 2017). To verify success of the DNA digest, $1\ \mu\text{L}$ of RNA was used as template in an amplicon PCR (described below). Decontaminated RNA was purified using the RNeasy MinElute kit (Qiagen, Hilden, Germany) and eluted twice in $14\ \mu\text{L}$ of RNase-free water. The purified RNA was reverse transcribed into cDNA with SuperScriptIV

reverse transcriptase (Thermo Fisher Scientific, Waltham, MA, USA) and manufacturer's instructions for gene-specific primers. RiboLock (Thermo Fisher Scientific, Waltham, MA, USA) was used as RNA protectant and the optional RNase H (Thermo Fisher Scientific, Waltham, MA, USA) step was included with 0.5 μ L of the enzyme and 20 minutes of incubation at 65 °C. The reverse primer S-D-Bact-0785-a-A-21 (Klindworth et al., 2013) was used to target the 16S subunit of the ribosomal RNA.

For the generation of amplicons, all DNA and cDNA samples were amplified by PCR in triplicate. A minimum of 25 ng or 7 μ L of template were used to amplify the total bacterial community from DNA and 1-3 μ L were used to amplify the potentially active community from the cDNA. The V3-V4 region of bacterial 16S rRNA genes and transcripts was amplified using Phusion DNA polymerase (Thermo Fisher Scientific, Waltham, MA, USA) with the SD-Bact-0341-b-S-17 forward and the S-D-Bact-0785-a-A-21 reverse primer (Klindworth et al., 2013) including MiSeq adapters. The 50 μ L PCR reaction mix and thermocycler protocol are described in von Hoyningen-Huene et al. (2019). After verification on an agarose gel (0.8 %), three PCR replicates per sample were pooled equimolar and purified using MagSi magnetic beads (Steinbrenner, Wiesenbach, Germany) with a Janus automated workstation (PerkinElmer, Downers Grove, IL, USA) according to manufacturer's instructions. PCR products were eluted in 28 μ L of EB buffer (Qiagen, Hilden, Germany).

Amplicons were sequenced using the Nextera XT kit with v3 chemistry on a MiSeq sequencer (both Illumina, San Diego, CA, USA). Sequences were demultiplexed and adapters removed before raw read quality filtering and processing. A detailed description of the bioinformatic pipeline used is given in Hoyningen-Huene et al. (2019). In short, sequences were quality-filtered, merged and trimmed using fastp (version 0.19.4; Chen et al., 2018), PEAR (version 0.9.11; Zhang et al., 2014), and cutadapt (version 1.18; Martin, 2011). Subsequently, merged 16S rRNA amplicons were dereplicated, chimeras removed and denoised into amplicon sequence variants (ASVs) at 100 % sequence identity using VSEARCH (version 2.9.1; Rognes et al., 2016). ASVs were taxonomically assigned using BLAST (Altschul et al., 1990) against the SILVA NR 138 database (Quast et al., 2012). Further processing and data manipulation were done in RStudio Version 1.3.959 using R version 3.5.2 (R Core Team, 2018). All ASVs below an identity of 95 % and a hit quality of \geq 93 % were categorized as unclassified taxa. Hit quality was determined as recommended by the SILVAngs user guide section 6 (SILVAngs, 2017). Extrinsic domains were removed from the ASV table. The ASV reads were normalized using gmpR and loaded into ampvis2 with a midpoint rooted tree (fasttree) and a FASTA file containing the ASV reference sequences. The three sequenced samples per sediment depth were merged for both the total (16S rRNA genes) and the active (16S rRNA transcripts) community by calculating gmpR-normalized mean ASV abundances. ASVs were then clustered on the taxonomic level of order and transformed into relative abundances. All samples with a relative abundance of \geq 1 % in at least one sample were used as a basis for the bar charts and plotted in SigmaPlot (version 11; Systat Software, San Jose, CA). The most abundant genera for each phylum were added to gain further information on the potential functional capabilities.

The 16S rRNA gene and transcript sequences were deposited in the National Centre for Biotechnology Information (NCBI) Sequence Read Archive (SRA) under BioProject accession number PRJNA611521.

5.4 Results

5.4.1 Petrography and geochemistry of sediments and organics

Based on macroscale color and grain size changes, the sediment core can be subdivided into three lithological units, with depths presented as cm below sediment top (Figure 5.2). Unit I extends from the sediment surface to 22 cm, Unit II from 22 to 28 cm, and Unit III from 28 to 35 cm.

Unit III (28-35 cm) shows a dark brown to black color and grain sizes between clay and fine silt, except for up to several sand sized bioclasts. The microfabric, which is darker in color than the matrix in the overlying Unit II and blackens under crossed polars. The matrix appears mottled, cracked and concentrates at voids filled with blocky low magnesium calcite (LMC) cement ($Mg \leq 0.6$ wt %; Figure 5.3c and d). Bioclasts consist of Gastropods and *Characea* oogonia (Figure 5.3e and f), complemented by highly altered *Halimeda*- and other coralline algae fragments. Additionally, up to a mm in size, macrophyte particles occur and small (up to 20 μm), opaque spots appear in lumps, often attached to cavities. The abundance of LMC cements decreases towards the bottom of Unit III. The blocky sparite is distributed unequally and occurs especially in bigger pore spaces. The cements exhibit a distinct zonation in the back-scatter-electron (BSE) images (Figure 5.4), dependent on their Fe, Mn and Ca content. Dark brown, peloidal aggregates occur in the vicinity of the LMC-crystals, which hold a higher concentration of Fe, Si and Al than the paler brown matrix parts (Figure 5.5). The overall content of $CaCO_3$ scatters around 30 wt %, of which 20 % are aragonite, 14 % HMC and 66 % LMC. The residing 70 wt % of bulk sediment consist of poorly crystalline Fe-Al-Si phases and organics. The C:N ratio and S_{tot} values increase to 20-25 and 1.5-2.3 wt % towards the bottom of Unit III. Organic $\delta^{15}N_{org}$ increases from 4.3 to 5.1 ‰ at the bottom of Unit III. Organic $\delta^{13}C_{org}$ increases to -23.9 ‰ in the 25.5 to 28 cm increment, before it stabilizes around -26 ‰ at the bottom of the section. Bulk $\delta^{18}O_{carb}$ slightly increases from -3.77 at the top to -3.42 ‰ at the bottom. In contrast, bulk $\delta^{13}C_{carb}$ decreases from -6.19 to -9.58 ‰ at the bottom of this Unit (Figure 2). The ^{14}C content of the organic sediment fraction discloses an age of 3760 ± 30 years BP for Unit III.

Unit II (22-28 cm) is characterized by a cohesive, light- to dark brown mud. Individual grains are difficult to trace, and can be classified as clay-sized. No internal structures are apparent. The microfabric consists of a homogenous, medium brown matrix, which blackens under crossed polars (Figure 5.3a, b). Silicic, up to several hundred μm long, sponge-needle-remnants are highly abundant. They make up ca. 30 % of the microfabric, whereas the residing 70 % consist of a medium brown matrix, made up of Fe-Al-Si bearing compounds with intercalated, dark brown aggregates of cyanobacteria colonies (Figure 5.6c-f). Bulk chemistry shows a decrease from 47 to 0 wt % carbonate in this section (Figure 5.2), whereas the C:N ratio scatters around 16 and S_{tot} averages 1.4 wt %. Organic $\delta^{13}C_{org}$ decreases to -26.5 ‰, whereas $\delta^{15}N_{org}$ remains at values around 4 ‰. The upper part of Unit II reveals bulk isotope values of -2.2 ‰ $\delta^{13}C_{carb}$ and -1.9 ‰ $\delta^{18}O_{carb}$. In addition, radiocarbon measurements date Unit II at 1370 ± 30 years BP.

Unit I is characterized by a thin microbial mat (approx. 5 mm thick) at the top, followed downwards by medium- to pale grey, carbonate silt to fine sand. The top of Unit I contains non-skeletal, micritic peloids of variable size (tens to hundreds of μm) and shape, embedded within a transparent, microcrystalline matrix (Figure 5.7a, b) and pale brown, cm sized microbial mat fragments with remnant coccoidal cyanobacteria (Figure 5.6a, b). Peloids compaction increases with depth and the transparent microcrystalline matrix is replaced by a brownish groundmass, which blackens under crossed polars. Mollusk and gastropod shell fragments occur occasionally throughout Unit I. Ostracod abundance decreases from 0 to 22 cm, whereas the abundance of foraminifera (*Rotaliida* and *Miliolida*) tests increases

towards the bottom of the unit. The CaCO_3 content in Unit I yields 64 wt % at the top, 74 wt % in the middle (15 cm) and 47 wt % at the bottom (22 cm). The carbonate fraction in Unit I distributes in ca. 75 % aragonite, 10 % high magnesium calcite (HMC) and 15 % low magnesium calcite (LMC). The residual bulk sediment contains poorly crystalline Fe-Al-Si phases and organic compounds. The C:N ratio of the organic material increases from 9 in the upper part of Unit I, to 22 at the bottom, whereas total sulfur content (S_{tot}) decreases from 1 wt % at 2.5 cm, to 0.5 wt % at 22 cm. Organic nitrogen ($\delta^{15}\text{N}_{\text{org}}$) varies between 3.5 and 4.2 ‰. Organic carbon ($\delta^{13}\text{C}_{\text{org}}$) values decrease from -18.5 at 2.5 cm, to -21.2 ‰ at the unit's bottom. Bulk $\delta^{13}\text{C}_{\text{carb}}$ values vary from -4.5 ‰ in the upper part of Unit I to -2.2 ‰ in the lower part, with $\delta^{18}\text{O}_{\text{carb}}$ values between -1.9 and -1.5 ‰.

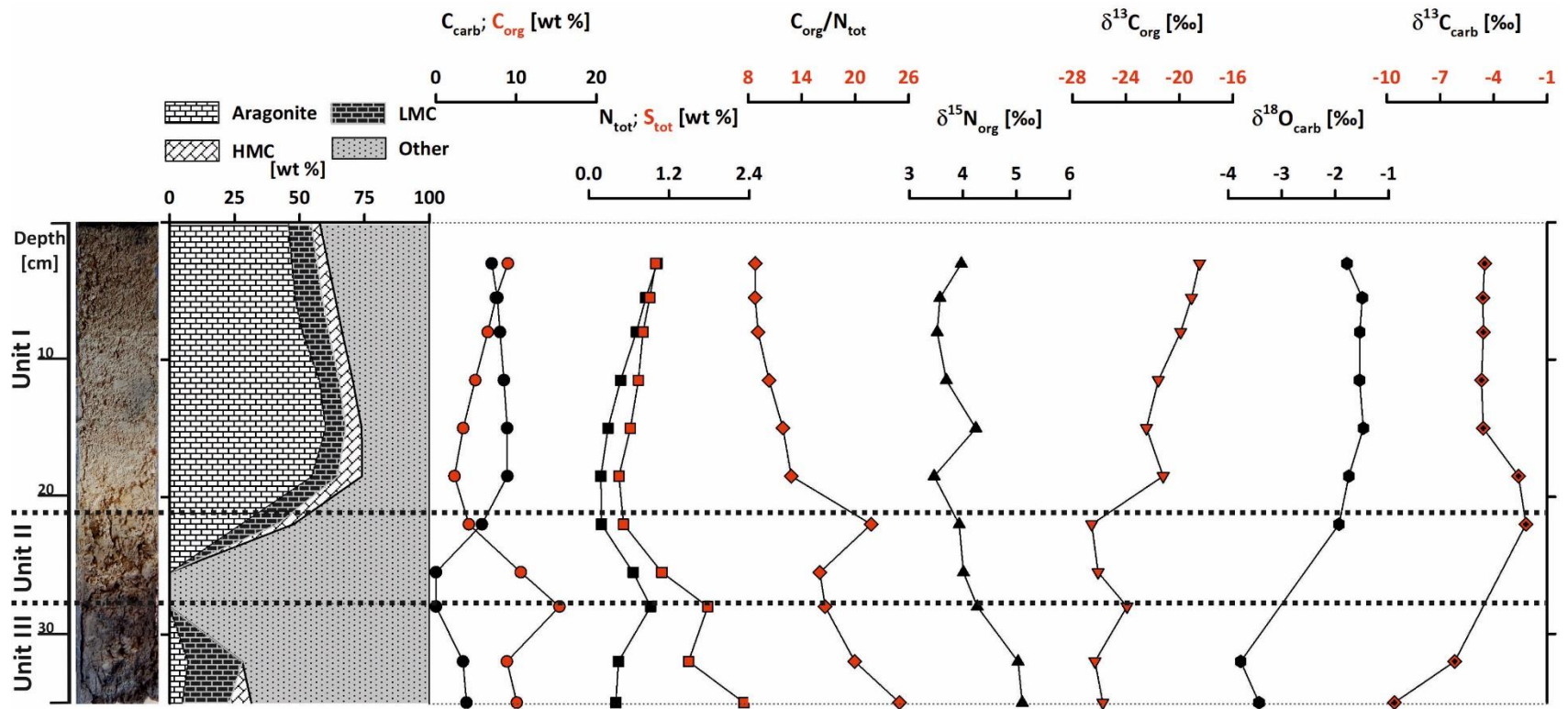


Figure 5.2: Bulk XRD-, CNS and stable isotope data of Core CC-K04. "Other Phases" consist of amorphous, Fe-Al-Si phases and organic compounds.

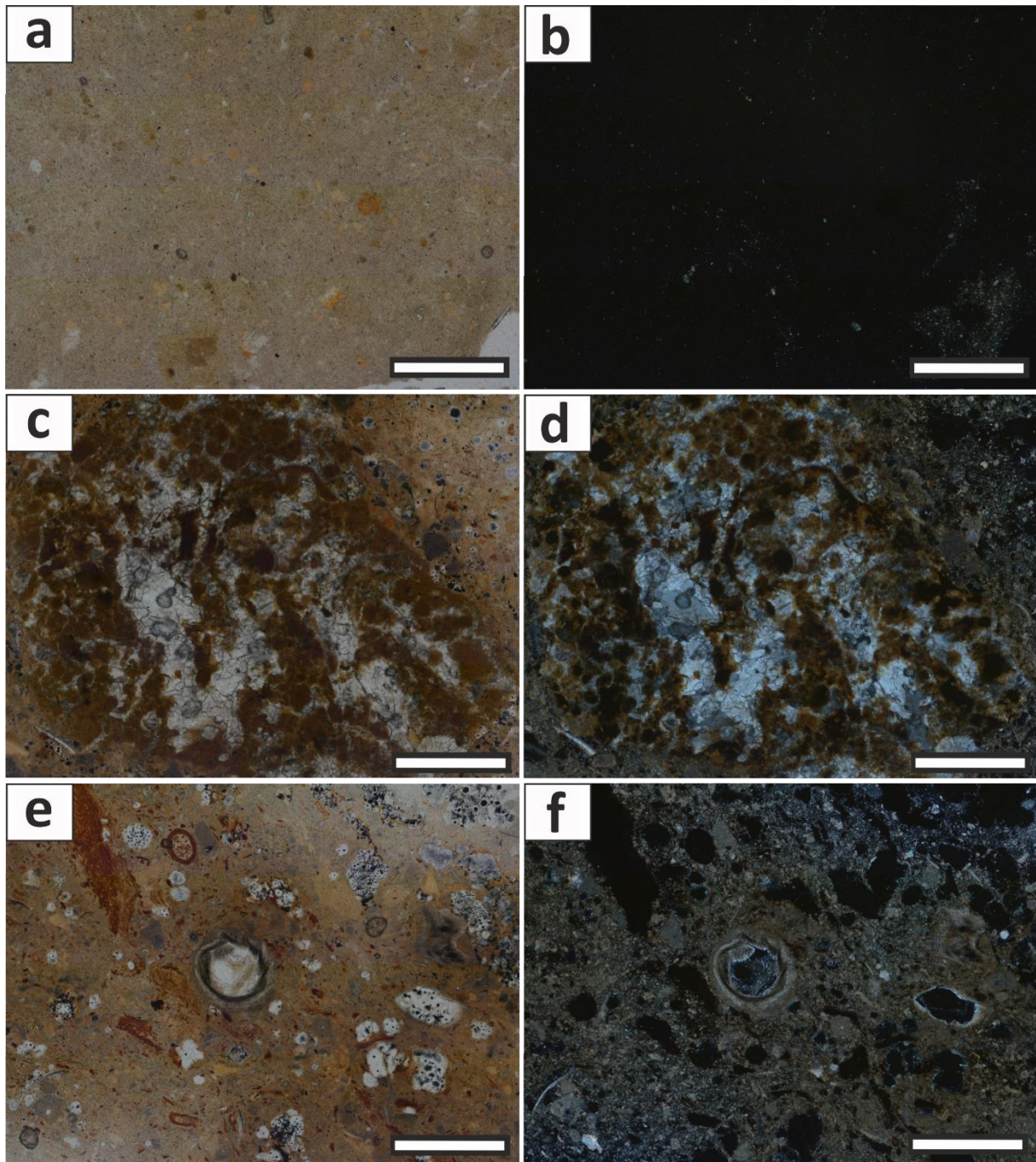


Figure 5.3: Characteristic microfabric features of Units II and III. (a) and (b) show the microfabric of Unit II in transmitted light (a) and under crossed polars (b). Carbonate is absent from this part of the unit. (c) and (d) illustrate carbonate cements in Unit III in transmitted light (c) and crossed polars (d). The matrix around the sparite (LMC) cements is notably darker. (e) and (f) show a microfabric overview at the bottom of Unit III, where the sparite cements decrease. Cross sectioned *Characea oogonia* occur in the image center. Scale bars measure 500 μm .

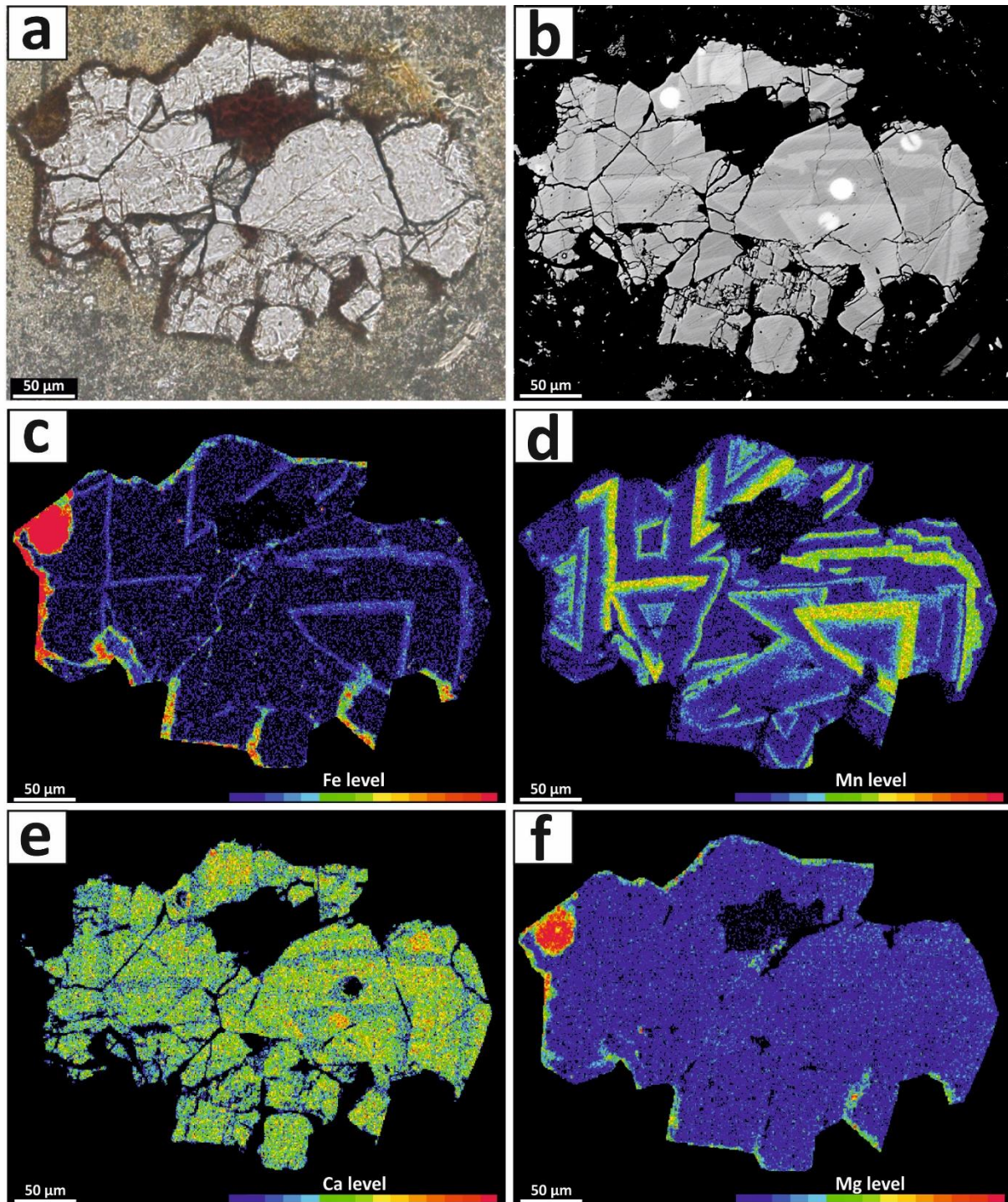


Figure 5.4: Close up images of a void in Unit III, filled with LMC cement. (a) shows the cement in transmitted light, whereas backscatter electron (BSE) image (b) depicts a clear zonation, derived from differences in Fe, Mn and Ca composition. This can be inferred from element maps (c), (d), and (e). In contrast to the zonation pattern, Mg is equally low in the blocky calcite crystals. According to the color scale, red indicates high element levels, whereas blue marks low levels. Elemental concentrations are reported in relative amounts.

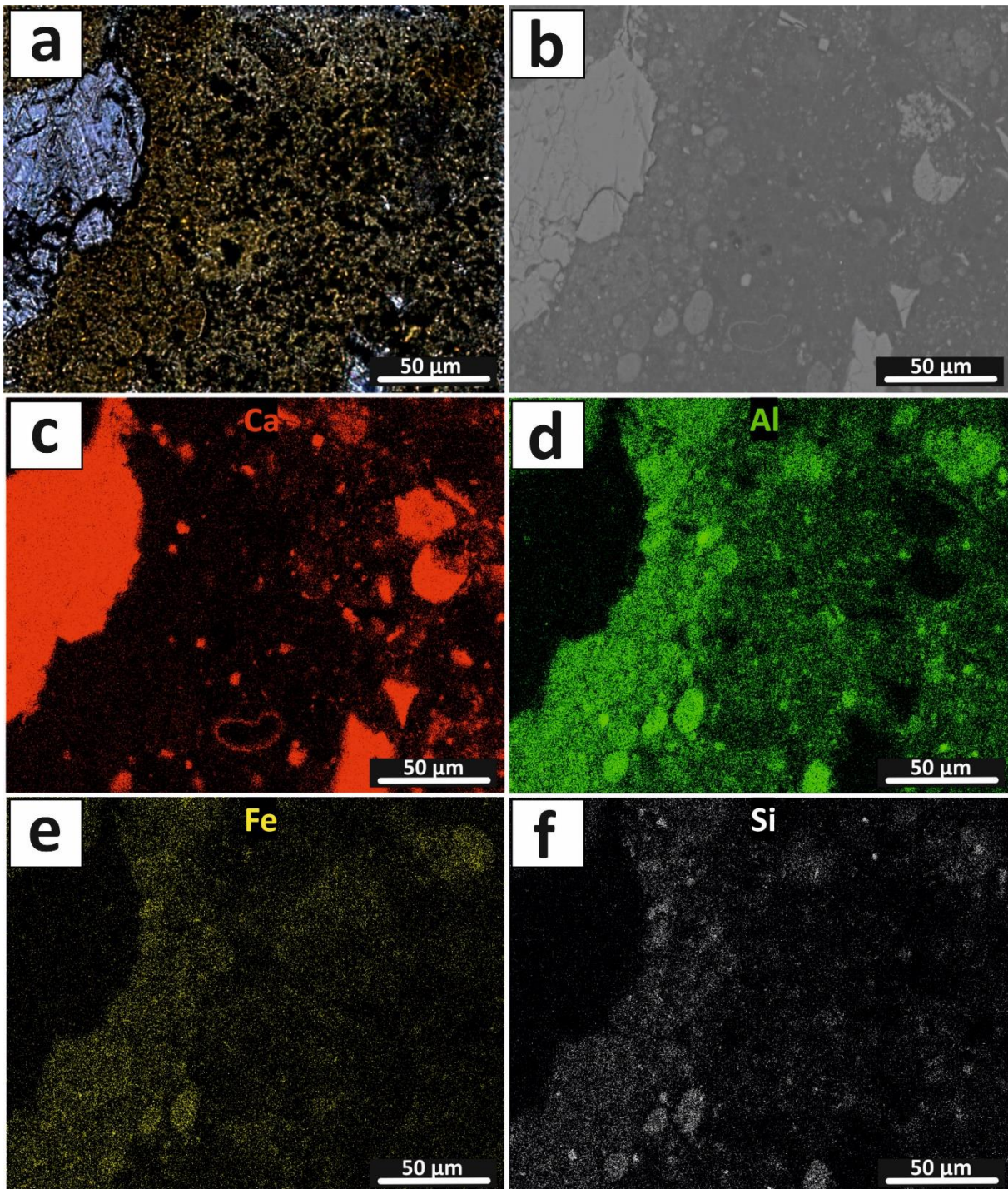


Figure 5.5: Distribution of major elements in the matrix of Unit III. Image (a) shows the analyzed sample area in transmitted light, whereas (b) shows the backscatter electron image of the identical sample part. EDX-based maps show the distribution of Ca (c), Al (d), Fe (e) and Si (f).

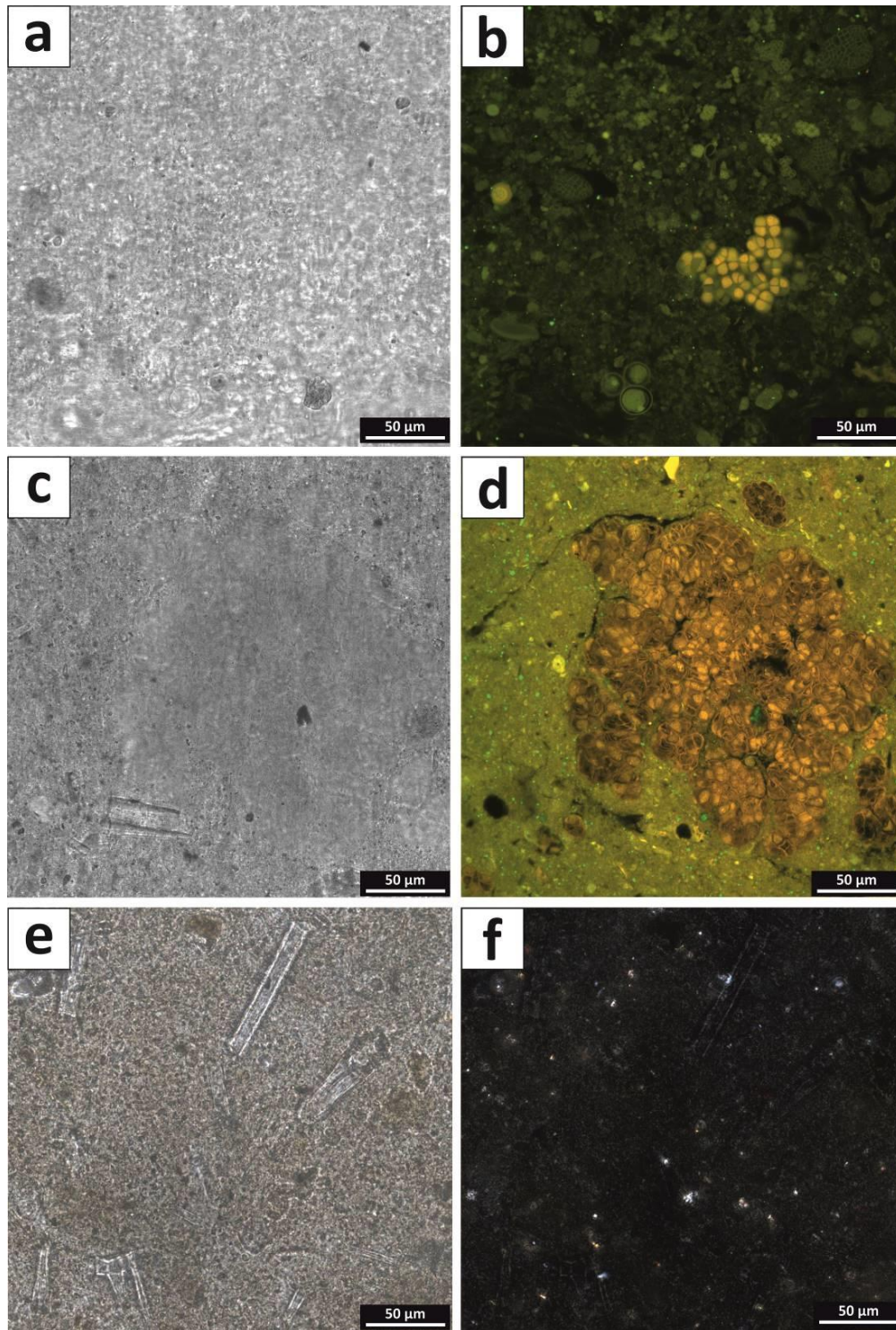


Figure 5.6: Close-up images of characteristic biological core features. Figures (a) and (b) show the microbial mat present in Unit I, in transmitted and fluorescent light (excitation 365 nm/emission 397-700 nm). Intact cyanobacteria cells are identifiable by their (chlorophyll related), yellow orange emitted fluorescence. Figure (c) and (d) illustrate cyanobacteria colonies found in Unit II in transmitted and fluorescent light. Compared to Unit I, most of the bacteria colonies are empty and compacted. Images (e) and (f) depict a close up of the sponge needles found in Unit II in transmitted light and under crossed polars.

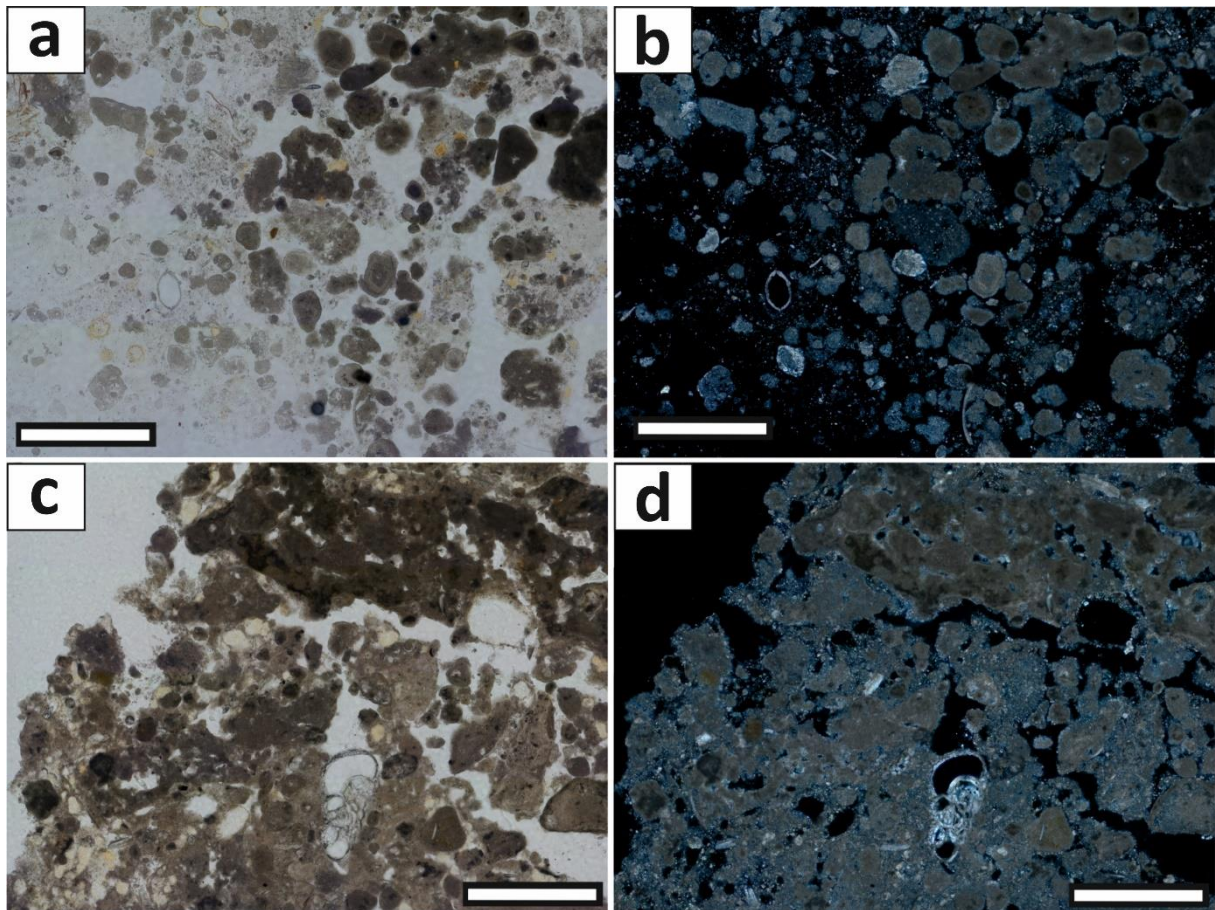


Figure 5.7: Microfabric overview of Unit I. Figure (a) and (b) show the upper part of Unit I (3-5.5 cm) in transmitted light and under crossed polars. Notable are the loose packing of micrite peloids and abundant ostracod tests. Figure (c) and (d) depict Unit I's compacted microfabric at a depth of 18 cm. In this section, the abundance of Miliolida and Rotiliida foraminifera is higher. Scale bars measure 500 μm .

5.4.2 Pore water chemistry

The water chemistry of the Cinq Cases pool (surface water overlying the core) is characterized by a salinity of $45.3 \text{ g}\cdot\text{kg}^{-1}$ and a pH of 8.5 (Figure 5.8a). Sodium (Na^+) and magnesium (Mg^{2+}) are the major cations, with concentrations of 604.5 and $68.6 \text{ mmol}\cdot\text{kg}^{-1}$, respectively. Calcium (Ca^{2+}) concentration is considerably lower, at $13.5 \text{ mmol}\cdot\text{kg}^{-1}$. Total alkalinity (TA) is $3.3 \text{ mmol}\cdot\text{kg}^{-1}$, whereas sulfate (SO_4^{2-}) and chloride (Cl^-) concentrations are 36.4 and $704 \text{ mmol}\cdot\text{kg}^{-1}$. Metabolite and nutrient concentrations (NH_4^+ , PO_4^{3-} , $\text{SiO}_{2(\text{aq})}$, $\Sigma\text{H}_2\text{S}$) are below $0.025 \text{ mmol}\cdot\text{kg}^{-1}$.

Pore water data significantly differ from those of the water column. At the sediment-water interface, the pH drops to 6.96, and further decreases to ca. 6.8 at the core bottom (30.5 cm depth; Figure 5.8a). Redox potential (Eh) suggests anoxic conditions at the core top (-41 mV), which change to oxic conditions (+85 mV) at 4.5 cm. Redox (Eh) values increase up to +151 mV at a depth of 20 cm and then slightly decrease to +146 mV at the core bottom. TA rises to $12.7 \text{ mmol}\cdot\text{kg}^{-1}$ at a depth of 2 cm, before decreasing to $6.7 \text{ mmol}\cdot\text{kg}^{-1}$ at 7 cm and stabilizing at values below $5 \text{ mmol}\cdot\text{kg}^{-1}$ with depth. Salinity increases almost linearly from $56.4 \text{ g}\cdot\text{kg}^{-1}$ at the core top, to $82.5 \text{ g}\cdot\text{kg}^{-1}$ at a depth of 16.5 cm, and remains constant to the bottom of the core. Mg^{2+} , Na^+ , K^+ and Cl^- show similar trends, increasing from the core top to 13 cm ($127.7 \text{ mmol}\cdot\text{kg}^{-1}$, $1099.2 \text{ mmol}\cdot\text{kg}^{-1}$, $22.3 \text{ mmol}\cdot\text{kg}^{-1}$ and $1280.7 \text{ mmol}\cdot\text{kg}^{-1}$), and remaining constant in the lower part of the core. Calcium concentrations are slightly higher at the core surface ($14.1 \text{ mmol}\cdot\text{kg}^{-1}$) in comparison to the water column ($13.5 \text{ mmol}\cdot\text{kg}^{-1}$). Dissolved hydrogen sulfide ($\Sigma\text{H}_2\text{S}$) only occurs in the uppermost pore water ($0.25 \text{ mmol}\cdot\text{kg}^{-1}$ at 2 cm; Figure 5.8b). Sulfate (SO_4^{2-}) shows a linear concentration trend from 2 to 13 cm, increasing from 53.7 to $66.7 \text{ mmol}\cdot\text{kg}^{-1}$. Sulfate then remains constant down to the bottom of the core, at concentrations of $64.6 \text{ mmol}\cdot\text{kg}^{-1}$. Additionally, the $\text{SO}_4^{2-}/\text{Cl}^-$ ratio increases from 0.135 at 2 cm to 0.144 at a depth of 4.5 cm, before stabilizing at values around 0.141 below 13 cm of depth. Ammonia (NH_4^+) concentrations are at $0.025 \text{ mmol}\cdot\text{kg}^{-1}$ in the water column. In the pore water, a maximum concentration of $0.43 \text{ mmol}\cdot\text{kg}^{-1}$ occurs at 2 cm, before slightly decreasing to $0.35 \text{ mmol}\cdot\text{kg}^{-1}$ at 7 cm, and $<0.07 \text{ mmol}\cdot\text{kg}^{-1}$ below 13 cm. The concentration of dissolved silica ($\text{SiO}_{2(\text{aq})}$) is $0.013 \text{ mmol}\cdot\text{kg}^{-1}$ in the water column and increases to $0.17 \text{ mmol}\cdot\text{kg}^{-1}$ in the upper pore water (2 cm). $\text{SiO}_{2(\text{aq})}$ concentration decreases to $<0.07 \text{ mmol}\cdot\text{kg}^{-1}$, at a depth of 10 cm. Subsequently, dissolved silica remains constant to the bottom of the core. Dissolved inorganic carbon isotopes (DIC; $\delta^{13}\text{C}_{\text{DIC}}$; Figure 5.8b) of waters are -9.37 ‰ within the water column, and increase to -5.54 in the pore water at 2 cm depth. The, $\delta^{13}\text{C}_{\text{DIC}}$ values then decrease to -8.53 at 16 cm, before a slight increase to -7.64 at 20 cm depth. In contrast, $\delta^{18}\text{O}_{\text{Water}}$ values are 2.17 in the water column and increase with depth, from 2.83 at the top to 3.1 at 20 cm.

A figure illustrating saturation indices (SI) of selected carbonates can be found in the supplementary material. All carbonate minerals are supersaturated in the water column ($\text{SI} \geq 1.1$), before their values dramatically decrease ($\text{SI} \geq 0.32$) in the pore water. However, calcite, protodolomite (dolomite (d)) and dolomite remain supersaturated throughout the core, whereas aragonite (SI vary between -0.05 and -0.07) is slightly undersaturated below a depth of 20 cm.

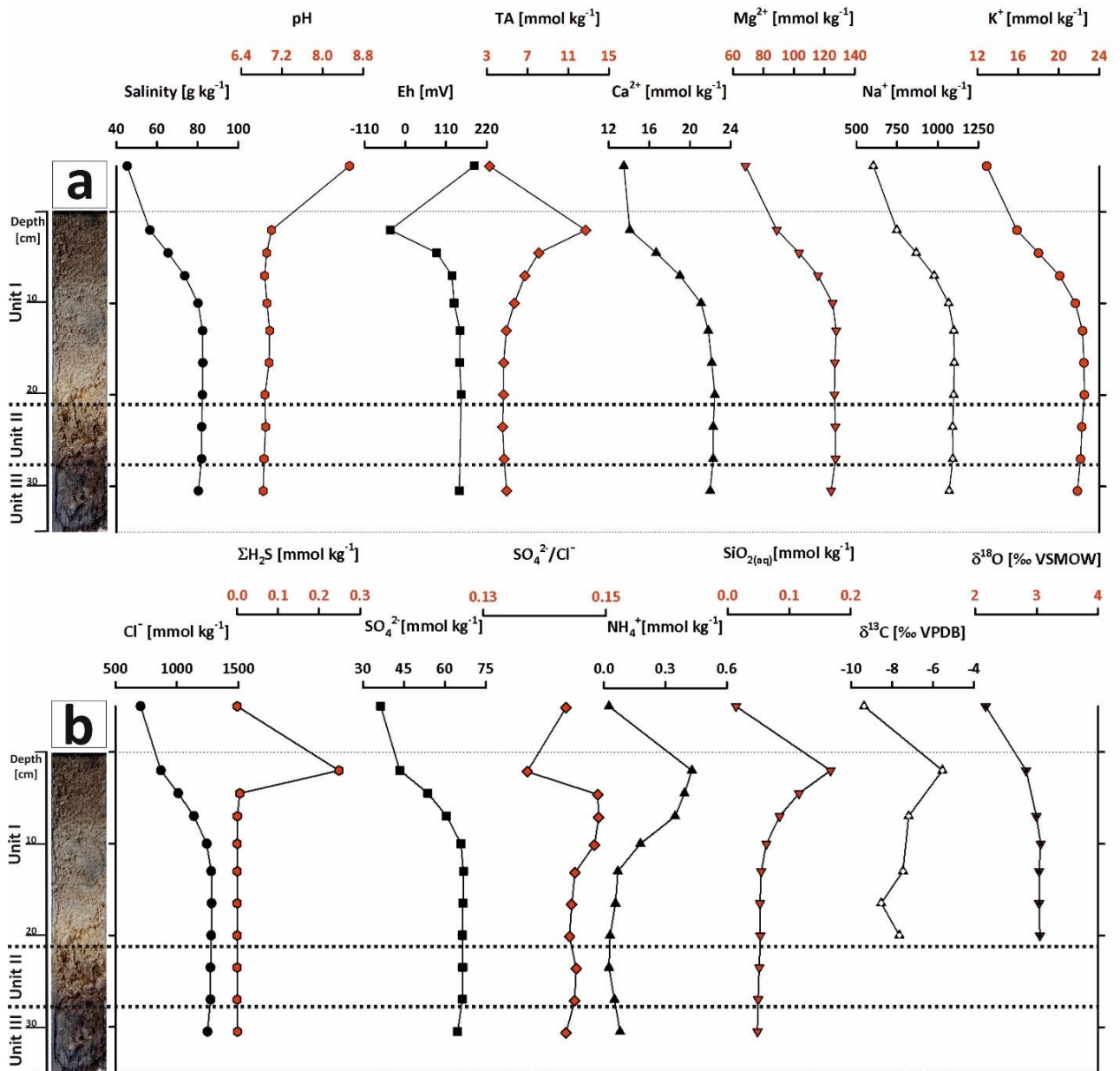


Figure 5.8: Hydrochemical properties in the water column and pore waters of the Cinq Cases pool. Note the increase of salinity (a), redox and decrease of pH with depth. Another notable detail is the increase of the Cl⁻/SO₄²⁻ ratio at 2.5 cm depth (b).

5.4.3 Bacterial community composition

Bacterial 16S rRNA gene analysis reveals the presence of a diverse bacterial community, with 2,407 amplicon sequence variants (ASVs; clustered at 100 % sequence identity) within the total and 1,953 ASVs within the active community of the water column. A mean of 2,540 ASVs are present in the total community of the top 22 cm (Unit I) of the core, whereas a mean of 1,612 ASVs is traceable in the respective active community. Overall, 1,902 total and 1,857 active community ASVs are observed at 22 to 28 cm depth (Unit II), and 1,566 ASVs in the total and 1,278 ASVs in the active community are detected from 28 to 35 cm (Unit III). 16S rRNA transcript analysis of abundant bacteria was conducted to detect taxa with potential metabolic activity, as suggested by (Blazewicz et al., 2013). RNA-based community analysis is commonly used as an estimation of the active fraction of a microbial community (DeAngelis et al., 2011; Hunt et al., 2013; Jones and Lennon, 2010; Simister et al., 2012). However, it should be noted that some cells are able to retain high ribosome content in a dormant state (Filion et al., 2009; Sukenik et al., 2012). Hence, 16S rRNA transcript data do not necessarily correspond to microbial metabolic activity, and must be evaluated with caution (Schwab et al., 2017). In the present study, we applied this approach to approximate the activity of key microbial groups, and to compare results to abundant physicochemical gradients and DNA-based taxonomic data. The different bacterial taxa were grouped at phylum (and in the case of Proteobacteria), class (Alpha-; Gammaproteobacteria) and genus (*Halomonas*) level (Figure 5.9). Metabolic properties of the different taxa were inferred from known metabolic processes from characterized relatives, listed in (Whitman, 2015 and additional literature; supplement, table S9).

The total community within the water column is dominated by aerobic heterotrophs, belonging to the Gammaproteobacteria class, and bacteria from the Actinobacteriota and Firmicutes. A sharp difference is notable between the abundance of Firmicutes in total and active community in the water column, which reflects the increased activity of the aerobic heterotrophic *Pontibacillus* in the active community.

The community compositions in the upper (carbonate rich) sediment section, from 0 to 22 cm (Unit I), can be divided into two parts (Figure 5.9): From 0 to 10 cm, there is an even distribution of Actinobacteriota, Proteobacteria and Chloroflexi. Phototrophic cyanobacteria occur from 0 to 10 cm, and sulfate reducing Desulfobacterota between 2.5 and 7.5 cm. A sharp difference between total and active community composition between 0 and 10 cm is observed. This is caused by a higher abundance of Firmicutes, in particular fermenting *Vallitalea* and lower abundance of aerobe thriving *Tropicimonas* (Alphaproteobacteria) at active community level. The deeper section (10 to 22.5 cm), does not contain cyanobacteria in the total community (below 15 cm), instead it has 22-37 % of Actinobacteria from 10 to 20 cm, which drop to 3 % at 22.5 cm. Another notable trend is the increase of Gammaproteobacteria with depth below 15 cm, particularly the genus *Halomonas*, which reaches its maximum abundance (43 %) at 22.5 cm. The potentially active community shows a similar trend, except for a higher abundance of Nitrospirota (18 % at 7.5 cm and 13 % at 17.5 cm).

From 22.5 to 27.5 cm, the total community shows an increase of Chloroflexi, from 7.8 % at 22.5 cm to 19.3 % at a depth of 25 cm, before slightly decreasing to 13.7 % at 27.5 cm. Firmicutes (19 % relative abundance), in particular the sulfate reducing *Fusibacter*, occur in increased relative abundance at a depth of 27.5 cm. Throughout the aforementioned section, the abundance of Alphaproteobacteria remains constant, whereas the content of Gammaproteobacteria decreases in the total community, from 43 % at 22.5 cm, to 16.2 % at 27.5 cm. The potentially active community shows a similar trend between 22.5 to 27.5 cm, with the exception that Firmicutes are almost absent from the lowest increment of this section (27.5 cm). At total and active bacterial community level, Desulfobacterota occur in notable amounts (up to 33.8 %) from 27.5 to 35 cm. In the same increment, the relative

abundance of Firmicutes increases to 53.7 %, which is related to an increase of the genus *Fusibacter*, while Chloroflexi decrease from 9.5 to 1.5 %. The bottom of the core (35-37.5 cm) contains a sharp decrease of Firmicutes (to 7.6 %) and Desulfobacterota (1.9 %), while the relative abundance of Gammaproteobacteria (especially *Halomonas*) and Chloroflexi increase to 33.9 % and 9.3 %, respectively. The RNA-derived data describe a comparable distribution in this section, apart from a higher abundance of Nitrospirota within the total community.

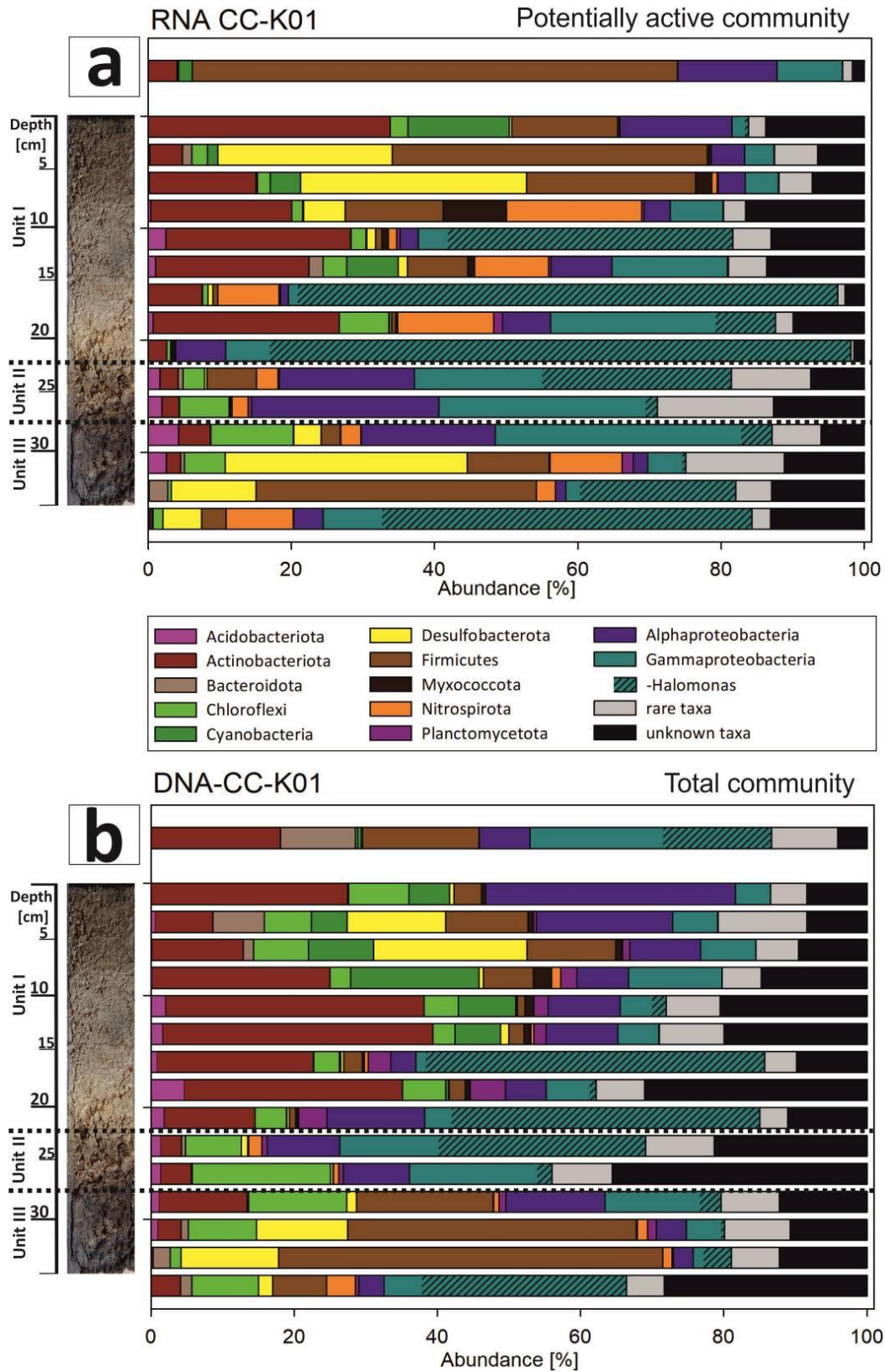


Figure 5.9: Potentially active (a) and total (b) bacterial community of core CC-K01, combined with the lithological Units of Core CC-K04. The unknown taxa contain all organisms with a blast identity < 95 % and hit quality > 93 %, and the rare taxa contain all orders below 1 % relative abundance. Notable are the high abundance of Halomonas at depths between 15 and 20 cm and Desulfobacterota in the upper (2.5-7.5 cm) and lower (30-35 cm) core. A photograph of core CC-K01 is provided in the supplement (Figure S51).

5.5 Discussion

5.5.1 Time and environment of carbonate deposition and diagenesis

The 35 cm sediment core from a pool at Cinq Cases shows a diverse sedimentary record. Three lithological units coincide with different environmental stages of the Cinq Cases “microbasin”: Unit III (28-35 cm) was deposited around 3800 years BP, and reveals signs of low salinity during deposition. Specifically, charophyte (*Characea*) oogonia, which generally occur in fresh- or brackish water (Wood, 1952; Wood and Imahori, 1959; Wray, 1977, halotolerant exceptions mentioned in Torn et al. (2014), and references therein) were observed in this section. Abundant plant detritus and $\delta^{13}\text{C}_{\text{org}}$ (-26.1 to -23.9 ‰) suggest an allochthone contribution of land-based C3-plants to the organic fraction. Enriched organic nitrogen values ($\delta^{15}\text{N}_{\text{org}}$ =+4.3 to +5.1 ‰) indicate a mixed signal of C3 plants and denitrification (Torres et al., 2012). Moreover, the microfacies of Unit III indicates a palustrine depositional setting: Dark brown, mottled areas with enhanced concentrations of iron (Fe) and aluminum (Al), suggest pedogenic remobilization in the carbonate mud (Figure 5.5e, d; Alonso-Zarza and Wright, 2010, and references therein). Areas of higher Fe and Al levels are often related to voids, filled with blocky, LMC cements, characteristic of meteoric diagenesis (Figure 5.4; Halley and Harris, 1979). These LMC cements make up most of the CaCO_3 fraction in this unit, with additional carbonate contributed by allochthone limestone fragments, autochthone charophyte oogonia, and gastropod shells. The LMC crystals have an unequal, spot-like distribution and distinct chemical zonation, related to varying Fe and Mn concentrations. This suggests varying redox conditions in the diagenetic pore fluid, which could coincide with changes in water level and possibly aerial exposure the Cinq Cases microbasin. The latter interpretation concurs with observations made by Kievman (1998) who reported increased Mn and Fe concentrations in LMC cements formed in the vadose zone below the soil horizon, hence, precluding ongoing LMC precipitation in the phreatic pore space of Unit III. Comparatively low $\delta^{13}\text{C}_{\text{carb}}$ (-9.58 to -6.19 ‰) and $\delta^{18}\text{O}_{\text{carb}}$ (-3.77 to -3.42 ‰) values suggest either a meteoric origin or alteration of the carbonate fraction by meteoric fluids (Allan and Matthews, 1982). However, the presently oxic Unit III must have at least temporarily experienced anoxic conditions, either during its deposition in a shallow lake or during pedogenesis and sulfidic diagenesis. This is further implied by high sulfur levels (up to 2.3 wt %) and opaque mineral phases, possibly iron sulfides (Hartmann and Nielsen, 1968; Strauss et al., 2012).

Unit II (22-28 cm) formed ca. 1370 years BP and is over 2400 years younger than Unit III. This significant age difference points towards a hiatus between the two units due to erosion and/or subaerial exposure. The sediment contains a pale or medium brown groundmass, consisting of amorphous, silicious Fe- and Al-phases, devoid of CaCO_3 . The clay to silt sized grains suggests a low energy environment, likely devoid of currents or tidal fluctuations. Remnant cyanobacteria and silicic sponge needles are abundant. Organic isotope measurements with constant $\delta^{13}\text{C}_{\text{org}}$ (-26 ‰) but slightly lower $\delta^{15}\text{N}_{\text{org}}$ values (+3.9 and +4.0 ‰) compared to Unit III, support the interpretation of an enhanced occurrence of nitrogen-fixing cyanobacteria, besides allochthone nitrogen sources, as these phototrophs discriminate against ^{13}C but not ^{15}N (Fogel and Cifuentes, 1993; Torres et al., 2012). The high abundance of silicic sponge needles further indicates a slow marine flooding, as no (siliceous) freshwater sponges are known from the Seychelles (Van Soest et al., 2018). Comparable “marine lakes” commonly show a colonization by single marine taxa such as *Placospongia* (Nichols and Barnes, 2005), *Protosuberites lacustris* and *Suberites sp.* (Pisera et al., 2010), hence, slow marine flooding of the Cinq Cases microbasin likely occurred during the deposition of Unit II.

Unit I, extending from the sediment water interface to 22 cm, shows a gradual facies change with depth: At the transition to Unit II (18-22 cm), CaCO_3 comprises 47 wt % of the sediment, and the

microfacies is characterized by a brown, Fe-Al-Si dominated groundmass, with loosely packed detrital peloids, angular shell detritus, and foraminifera tests (of the orders *Miliolina* and *Rotaliida*). Bulk $\delta^{13}\text{C}_{\text{carb}}$ values are relatively higher at the transition to Unit II (-2.2 to -2.6 ‰), which is possibly related to lower $^{13}\text{C}_{\text{org}}$ values (-26.5 ‰) of the associated organic matter. Slightly above this transition, the carbonate portion reaches 74 wt % CaCO_3 , with higher amounts of *Miliolida* and *Rotaliida* foraminifera, and shell detritus. This facies change indicates an increased marine influence on the Cinq Cases microbasin, likely caused by frequent (lagoon-) flooding events. From 15 to 22 cm, $\delta^{18}\text{O}_{\text{carb}}$ values are slightly depleted (-1.9 to -1.7 ‰; Swart, 2015 and references therein), which suggest either enhanced meteoric influence during deposition, or simply scatter due to CaCO_3 related component bias, as the values were measured on bulk CaCO_3 . As no diagenetic phases were observed in this segment, the latter is to be expected. From 0 to 10 cm, the percent CaCO_3 decreases to 64 wt %, as the organic sediment fraction increases up to 9 wt %. *Rotaliida* do not occur in this section and the abundance of *Miliolida*, which can adjust better to elevated salinities (Greiner, 1974; Murray, 1973), decreases to low numbers. In contrast, the abundance of ostracod tests increases, implying even harsher environmental conditions with higher evaporation rates, as they can tolerate salinities up to 18 ‰ (Bodergat, 1983; De Deckker, 1981). From 0 to 15 cm, $\delta^{13}\text{C}_{\text{carb}}$ and $\delta^{18}\text{O}_{\text{carb}}$ remain constant (-4.5 and -1.5 ‰, respectively), indicating the establishment of today's depositional and environmental conditions marked by high salinity (45-80 ‰), episodic rainfall and occasional marine flooding. $\delta^{13}\text{C}_{\text{org}}$ values increase from -21 (15 cm) to -18.5 ‰ (0 cm) towards the top of the core, suggesting photosynthetically derived organic matter, which is reworked by heterotrophic bacterial activity towards the bottom of this increment. $\delta^{15}\text{N}_{\text{org}}$ values (+4 to +3.5 ‰) are enriched compared to atmospheric nitrogen ($\delta^{15}\text{N} = 0$ ‰), explained again by a mixed signal of allochthonous C3 plants and denitrification (Torres et al., 2012). Active denitrification is further indicated by the increasing C:N ratio (from 8 to >21) towards the bottom of Unit I (Sarazin et al., 1992).

Summing up, the 35 cm core shows evidence of an initial palustrine environment in the Cinq Cases microbasin, followed by subaerial exposure, along with meteoric diagenesis (Unit III). Succeeding a depositional hiatus, the basin was slowly flooded by marine waters (Unit II). A final section (Unit I) reflects the establishment of the modern environment, characterized by elevated salinity, and by regular lagoon flooding, indicated by higher amounts of detrital shells at the Units bottom. Such lagoon flooding rarified over time, which is indicated by lower amounts of detrital carbonate particles (peloids, shell material) and higher abundances of organisms adapted to hypersaline conditions (ostracods and *Miliolida*).

5.5.2 Pore water gradients and their microbial and diagenetic implications

In the pore water profile, salinity increases from $45.3 \text{ g}\cdot\text{kg}^{-1}$ in the water column, to over $80 \text{ g}\cdot\text{kg}^{-1}$ below a depth of 12.5 cm. This evaporative trend is supported by increasing $\delta^{18}\text{O}_{\text{Water}}$ values, (from 2.1 to 3.0 ‰) and the conservative trends of Mg^{2+} , Na^+ , K^+ and Cl^- concentrations. These differences between the water column and pore waters may be related to the onset of rainfall at the end of dry season, whereas the higher salinity level at 12.5 cm (and below) reflects the actual dry season value. (Braithwaite et al., 1989), reported a higher salinity for the water column of Cinq Cases pools ($101.5 \text{ g}\cdot\text{kg}^{-1}$) in 1989, which suggests higher evaporation rates in the near past. The increasing salinity with depth contradicts the sedimentary facies, which indicates a change from hypersaline to brackish conditions.

The lack of shell detritus at the sediment-water interface and the presence of thin microbial mats refute recent lagoon flash floods, and indicate rainfall as main water input. Another notable difference is the sharp pH decrease from the water column (8.5) to the sediment (6.9 at 2.5 cm) and core bottom

(6.8 at 35 cm), which can be explained by the interaction of two major processes. First, the onset of bacterial activity in the microbial mat decreases the pH via metabolic input of CO_2 , and corresponding alkalinity increase (from 3.2 to 12.7 $\text{mmol}\cdot\text{kg}^{-1}$). Second, the positive redox value of the pore water causes oxidation of sulfide phases in deeper sediments, resulting in the genesis of sulfuric acid and lower pH (Schippers, 2004). Low alkalinity values (5 $\text{mmol}\cdot\text{kg}^{-1}$ at 12.5 cm) indicate decreasing bacterial metabolic activity with depth. Ammonia (NH_4^+), a potential metabolic end product of the bacterial metabolism (Smith and Macfarlane, 1997), indicates a similar trend in activity, with high values in the upper core part (0.4-0.2 $\text{mmol}\cdot\text{kg}^{-1}$ at 0-10 cm) and decreased values in the lower part (<0.08 $\text{mmol}\cdot\text{kg}^{-1}$ at 13-35 cm). The concentrations of hydrogen sulfide ($\Sigma\text{H}_2\text{S}$) and dissolved sulfate (SO_4^{2-}) can also be regarded in context with bacteria activity. The former is only observed directly below the microbial mat (0.25 $\text{mmol}\cdot\text{kg}^{-1}$ at 2 cm), where active bacterial sulfate reduction is to be expected, within the anoxic pore waters (Eh = -41 mV). In contrast, sulfate occurs in such high quantities (43- 66 $\text{mmol}\cdot\text{kg}^{-1}$) that the lowering effect of sulfate reduction on its concentration is only observable at 2.5 cm, indicated by a decreased value in a $\text{SO}_4^{2-}/\text{Cl}^-$ plot (Figure 5.8b). Moreover, the positive Eh values (+85 to +151 mV), from 4.5 cm to the bottom of the core, further contrast the sedimentary facies and bacterial community composition in the lower core part, which reflect anoxic redox conditions by its dark color, opaque minerals, high sulfide content, and (preferentially anoxic thriving) abundant taxa. This unusual redox profile can be explained by the formation of an “anoxic sandwich” (Figure 5.10), which is generated by oxygen diffusion via the karstified, irrigated Pleistocene basement below-, and the oxygenated water column above a zone of enhanced bacterial activity at the sediment top. An increase of pore water $\delta^{13}\text{C}_{\text{DIC}}$ values from -9.3 in the water column to -5.5 at the sediment water interface indicates an effect of phototropic activity. Heterotrophic activity in the core is evidenced by a $\delta^{13}\text{C}_{\text{DIC}}$ decrease with depth, despite the aforementioned evaporation trend. However, the disparate values of bulk carbonate $\delta^{13}\text{C}_{\text{carb}}$ and pore water DIC $\delta^{13}\text{C}_{\text{DIC}}$ indicate that no significant amount of carbonate minerals is being precipitated from the present pore water. This is further substantiated by the saturation indices of pore waters with respect to aragonite, calcite, and dolomite, which are over- or just slightly undersaturated, which is mainly controlled by the low pH (supplement, Figure S2).

Elemental and saturation trends are complemented by cross plots of various elemental ratios, useful for the identification of diagenetic processes (Figure 5.11; (Swart and Kramer, 1997)). Concentrations of Mg^{2+} and Ca^{2+} indicate a conservative behavior, whereas $\text{Sr}^{2+}/\text{Ca}^{2+}$ versus $\text{Ca}^{2+}/\text{Cl}^-$ and $\text{Sr}^{2+}/\text{Ca}^{2+}$ versus $\text{Mg}^{2+}/\text{Cl}^-$ diagrams show small scale differences in diagenetic conditions. In a $\text{Sr}^{2+}/\text{Ca}^{2+}$ versus $\text{Ca}^{2+}/\text{Cl}^-$ plot, aragonite precipitation in the water column, but dissolution in the pore water is mirrored by constant $\text{Sr}^{2+}/\text{Ca}^{2+}$ values, and decreasing $\text{Ca}^{2+}/\text{Cl}^-$ ratios, as aragonite is formed in the water column. Due to a subsequent dissolution of CaCO_3 , $\text{Ca}^{2+}/\text{Cl}^-$ ratios increase with depth. Increasing $\text{Mg}^{2+}/\text{Cl}^-$ ratios from the water column to the upper core also suggest potential dissolution of HMC. Below, $\text{Mg}^{2+}/\text{Cl}^-$ ratios decrease with depth, while $\text{Sr}^{2+}/\text{Ca}^{2+}$ ratios remain constant. This may be caused by either the absence of HMC for dissolution, or the formation of amorphous, precursor Mg-bearing clays at depth (Birsoy, 2002). The latter is indicated by a decrease of dissolved silica $\text{SiO}_{2(\text{aq})}$ from 0.17 $\text{mmol}\cdot\text{kg}^{-1}$ just below the sediment-water interface, to <0.07 $\text{mmol}\cdot\text{kg}^{-1}$ at 10 to 35 cm. The silica trend is possibly caused by the dissolution of diatom tests in the upper sediment, which can be induced solely by undersaturation (SI of amorphous $\text{SiO}_2 \leq -1.36$), or by biological processes. The enhanced silica release occurs at a depth with higher bacterial activity, wherein microbes may attack the organic matrix of diatom frustules and expose the silica-bearing skeleton to undersaturation (Bidle and Azam, 1999). The released SiO_2 is subsequently available for clay mineral precursor formation. Nevertheless, the differences in elemental ratios contain only very small amounts, compared with other studies (Swart

and Kramer, 1997; Pederson et al., 2019) and are, hence, only traceable by pore water gradients and not in the geochemical and mineralogical record.

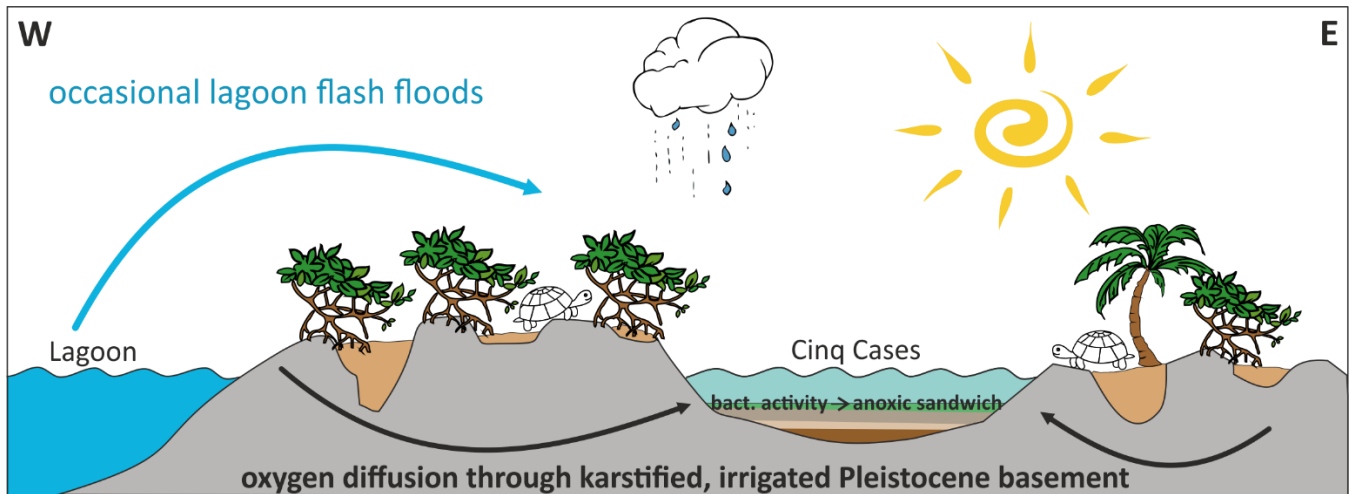


Figure 5.10: Schematic sketch of the Cinq Cases basin. The unusual redox profile of the pool sediment can be explained by an 'anoxic sandwich'. This is caused by an area of enhanced bacterial activity at the sediment top, which is affected by oxygen diffusion via the Pleistocene basement below- and the water column above the sediment.

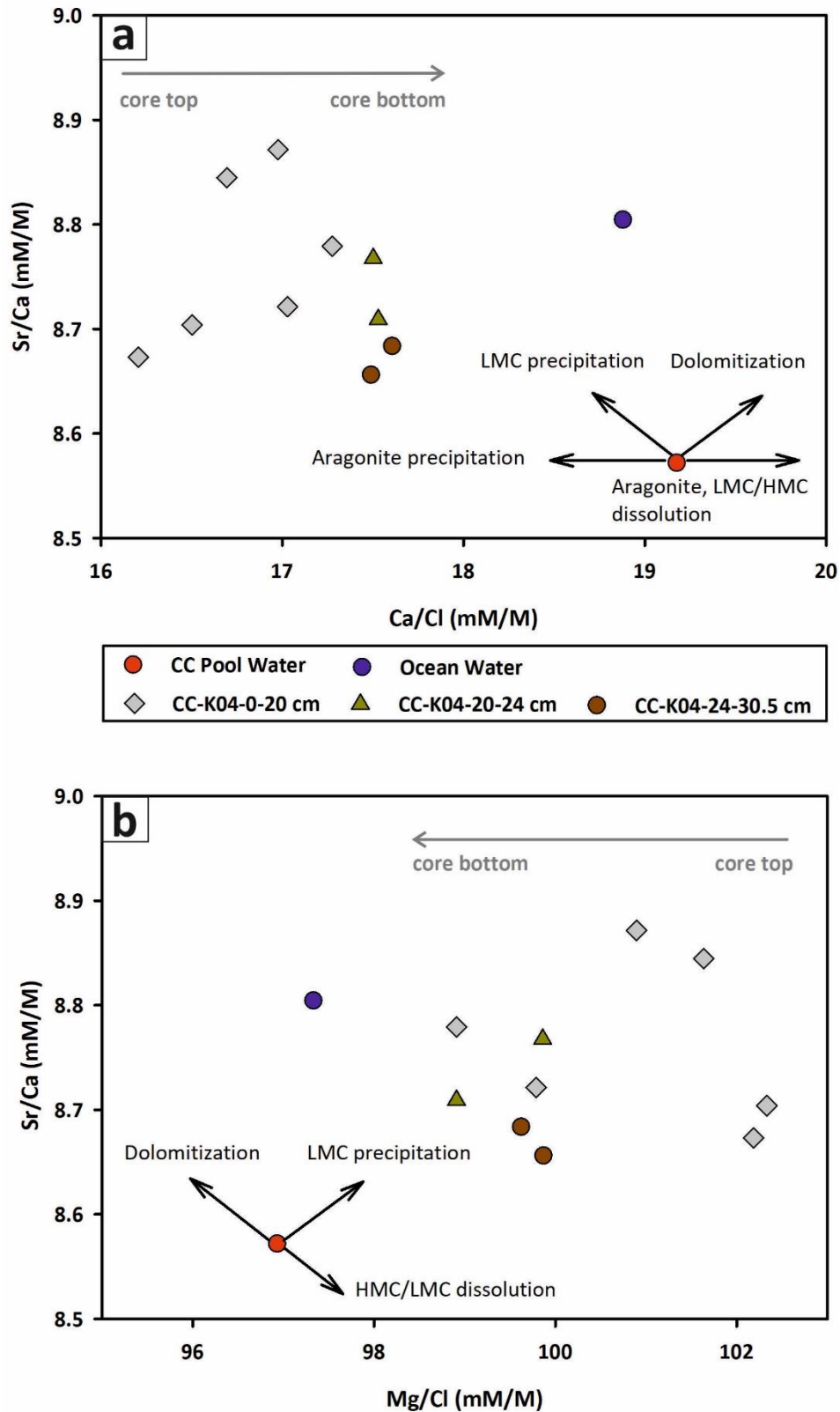


Figure 5.11: Sr/Ca versus Ca/Cl (a) and Sr/Ca versus Mg/Cl (b) plots, derived from pore water data of core CC-K04. Evident in a are aragonite precipitation in the water column and subsequent dissolution in the sediment. In contrast, b indicates HMC dissolution throughout the core section.

5.5.3 Bacterial abundance and its (partial) decoupling from current processes

The combination of DNA- and RNA-based 16S rRNA gene and transcript analysis offers the opportunity to study ancient- and recent bacterial activity within the water column and sediment of Cinq Cases. Higher salinities of the water column in the recent past, previously reported by Braithwaite et al., (1989), are supported by a high abundance of amplicon sequence variants (ASVs) of the halotolerant (to halophilic) bacteria *Halomonas* at total community level, although ASVs at RNA level are low. These bacteria tolerate salinities up to 32.5 ‰ and are well known for a versatile lifestyle, including aerobic and anaerobic metabolisms (Vreeland, 2015). In contrast, 16S rRNA genes from the less halotolerant *Pontibacillus* (optimum growth at 2-9 ‰ salinity; (Vos, 2015), which belongs to the Firmicutes phylum, are near absent in the total community of the water column, whereas present in high abundance at active community (>65 ‰) level. This suggests a thriving *Pontibacillus* population in the present Cinq Cases surface waters. The shift from *Halomonas* to *Pontibacillus* bacteria in the active community also points to reduced salinities in the present, compared to the recent past. This finding can be explained by cells seeding from the water column, followed by deposition in the sediment (Inagaki et al., 2005). Cyanobacterial ASVs are only present in the upper 15 cm, where complete cells were found in the thin sections. The ASVs are absent at greater depth, despite the abundance of compacted cyanobacteria colonies from 20 to 25 cm. This indicates that any extracellular DNA released by the damaged cyanobacterial cells has been degraded through biological processes and the sediment conditions, or not recovered by the extraction method. Any remnant DNA may, therefore, be too short or degraded for amplification and identification (Corinaldesi et al., 2008).

Furthermore, the high abundance (19-29 ‰) of *Actinomarinales*, which belong to the Actinobacteria phylum, from 10 and 20 cm is significant, as they typically thrive in surface waters of the open ocean. These bacteria are capable of a versatile heterotrophic lifestyle supported by actinorhodopsin-based photoheterotrophy, depending on the habitat. The occurrence of this ocean-derived allochthonous bacteria (*Actinomarinales*) from 10 to 20 cm supports the hypothesis of enhanced marine flooding of the Cinq Cases microbasin at the onset of deposition of Unit I. Due to their small size (cell volume ca. 0.013 μm^3) and adaptation to oligotrophic environments, *Actinomarinales* may be able to freely move through the pore space of the carbonate silt and scavenge nutrients (Ghai et al., 2013). The high abundance (81 to 27 ‰) of the salt tolerant *Halomonas* in both, the total and active community from 17.5 to 22.5 cm, may be enabled by the mentioned opportunistic lifestyle of bacteria belonging to this genus. It makes them capable of exploiting ecological niches, previously occupied by less versatile taxa. Recently, dormant *Halomonas* were isolated and revived from ca 100 million years old deep sea sediments (Morono et al., 2020), exemplifying the potential of this genus to survive in harsh habitats. *Halomonas* abundance decreases drastically below 22.5 cm, possibly caused by reduced pore space of the mud within Unit II, making it increasingly difficult to penetrate the deeper Unit III.

Typically anaerobic fermenters of the Chloroflexi (Anaerolineales, Dehalococcoida) and Firmicutes (Fusibacter, Vallitalea) phyla occur in the total community within the oxic sediments from 25.5 to 32.5 cm, overlapping with Units II and III. Since these clades are less abundant in the active community and redox values are positive, it is conceivable that they are not currently active in the Cinq Cases sediments and are in a dormant state. The dense sediment layer of Unit II may preclude bacterial migration to more shallow sections of the core, but it may also protect from competition by better adapted (aerobic heterotrophic) taxa. Hence, the anaerobic taxa may be remnants from former anoxic redox conditions and only be active in small microaerophilic to anaerobic niches. The same applies to sulfate reducing bacteria of the phylum Desulfobacterota, which occur in high abundances in redox positive sediments from 30 to 35 cm, where sulfate reduction should not be the preferential metabolism (Cypionka, 2000). However, sulfate is widely abundant at this depth, due to highly

evaporative pore waters, potentially enabling sulfate reduction. Due to the oxic sediments, the metabolic end product sulfide ($\Sigma\text{H}_2\text{S}$) is not observable at this depth. As sulfate reduction is not likely to be a high-energy yielding process in oxidizing environments (Dilling and Cypionka, 1990), the Desulfobacterota ASVs are also considered as remnants from a past anoxic period, which currently yield low metabolic activity. The 16S rRNA amplicon data illustrate a shift from past processes including anoxic phyla (Chloroflexi, Firmicutes and Desulfobacteriota) in the currently oxic environment of the deeper core, to presently active communities, including phototrophic cyanobacteria and aerobically thriving *Pontibacillus*, in the upper core and water column.

5.6 Conclusions

The sediments of Cinq Cases and their associated pore water represent different environmental stages of the Cinq Cases microbasin. The sedimentary facies develop from an anoxic- palustrine setting at the bottom of the core, to a suboxic to oxic, saline depositional environment at the top. In contrast, pore water indicates increasing salinity with depth. The differing environmental interpretation between these datasets is caused by a dynamic hydrologic setting, affected by evaporation, rainfall, and occasional lagoon flooding. Bacterial community composition and activity also lag behind the current hydrologic development, and represent an overlay of past and present processes, as indicated by the abundance of typically anoxic phyla, e. g. sulfate reducing Firmicutes and Desulfobacterota, in the active and total community within oxic sediments. In addition, the bacterial community data act as a convenient environmental proxy in this vigorous depositional environment. They support the sulfur bearing sediments of Unit III as deposits which experienced anoxic pore water conditions in the near past. The formation of blocky LMC cements and exceptionally low $\delta^{13}\text{C}_{\text{carb}}$ and $\delta^{18}\text{O}_{\text{carb}}$ values at depths between 28 to 32.5 cm in the core also relate to past, meteoric diagenesis. Pore water gradients further suggest present diagenetic pathways to include dissolution of aragonite and high-magnesium calcite in the upper sediment section. The combination of geo- and hydrochemical, as well as bacterial sequencing data, provides insight in an eventful depositional history, but due to short scale environmental changes, the data sets mirror different depositional stages. However, the evident decoupling of porewater, sediment, and gene data in the investigated pool on Aldabra underlines the necessity of multi-proxy studies in unstable and variable depositional settings to elucidate environmental history and early diagenetic alterations.

5.7 Acknowledgements

We thank the staff of the Seychelles Island Foundation (SIF) for their unreserved support and hospitality on Aldabra. In particular, we acknowledge SIF ranger Ronny Marie for his extraordinary support in planning and continuous assistance during sampling. Furthermore, we thank the SIF project coordinators Nancy Bunbury, April Burt, and Frauke Fleischer-Dogley. We express thanks to Wolfgang Dröse, Birgit Röring, Axel Hackmann, and Beate Gehnen for their support during lab work. We thank Anja Poehlein at the Göttingen Genomics laboratory for amplicon sequencing and initial sequence processing, supported by Melanie Heinemann and Sarah Schüßler. We also thank Adrian Immenhauser for insightful discussions. This study was funded by the German research foundation (DFG) within the framework of the “CHARON” research group (DA 374/11-1, AR 335/8-1). Further Support was provided by the Open Access Publication Funds of the Göttingen University

References

- Allan, J., and Matthews, R.: Isotope signatures associated with early meteoric diagenesis, *Sedimentology*, 29, 797-817, <https://doi.org/10.1111/j.1365-3091.1982.tb00085.x>, 1982.
- Alonso-Zarza, A. M., and Wright, V.: Palustrine carbonates, *Developments in Sedimentology*, 61, 103-131, [https://doi.org/10.1016/s0070-4571\(09\)06105-6](https://doi.org/10.1016/s0070-4571(09)06105-6), 2010.
- Altschul, S. F., Gish, W., Miller, W., Myers, E. W., and Lipman, D. J.: Basic local alignment search tool, *Journal of molecular biology*, 215, 403-410, [https://doi.org/10.1016/s0022-2836\(05\)80360-2](https://doi.org/10.1016/s0022-2836(05)80360-2), 1990.
- Banner, J. L., and Hanson, G. N.: Calculation of simultaneous isotopic and trace element variations during water-rock interaction with applications to carbonate diagenesis, *Geochimica et Cosmochimica Acta*, 54, 3123-3137, [https://doi.org/10.1016/0016-7037\(90\)90128-8](https://doi.org/10.1016/0016-7037(90)90128-8), 1990.
- Bathurst, R.: Carbonate sediments and their diagenesis (2d enlarged ed.), in, New York, Elsevier Publishing Co, https://doi.org/10.1007/978-94-009-7259-9_7, 1976.
- Bathurst, R.: Early diagenesis of carbonate sediments, in: *Sediment diagenesis*, Springer, 349-377, <https://doi.org/10.1144/gsjgs.132.3.0342>, 1983.
- Berner, R. A.: Early diagenesis: A theoretical approach, 1, Princeton University Press, <https://doi.org/10.1515/9780691209401>, 1980.
- Bidle, K. D., and Azam, F.: Accelerated dissolution of diatom silica by marine bacterial assemblages, *Nature*, 397, 508-512, <https://doi.org/10.1038/17351>, 1999.
- Birsoy, R.: Formation of sepiolite-palygorskite and related minerals from solution, *Clays and Clay Minerals*, 50, 736-745, <https://doi.org/10.1346/000986002762090263>, 2002.
- Blazewicz, S. J., Barnard, R. L., Daly, R. A., and Firestone, M. K.: Evaluating rrna as an indicator of microbial activity in environmental communities: Limitations and uses, *The ISME journal*, 7, 2061-2068, <https://doi.org/10.1038/ismej.2013.102>, 2013.
- Bodergat, A.-M.: Les ostracodes, témoins de leur environnement: Approche chimique et écologie en milieu lagunaire et océanique, 88, Département des sciences de la terre, Université Claude-Bernard, 1983.
- Braithwaite, C., Casanova, J., Frevert, T., and Whitton, B.: Recent stromatolites in landlocked pools on aldabra, western indian ocean, *Palaeogeography, palaeoclimatology, palaeoecology*, 69, 145-165, [https://doi.org/10.1016/0031-0182\(89\)90162-4](https://doi.org/10.1016/0031-0182(89)90162-4), 1989.
- Braithwaite, C.: Last interglacial changes in sea level on aldabra, western indian ocean, *Sedimentology*, <https://doi.org/10.1111/sed.12738>, 2020.
- Braithwaite, C. J., Taylor, J., and Kennedy, W. J.: The evolution of an atoll: The depositional and erosional history of aldabra, *Philosophical Transactions of the Royal Society of London. B, Biological Sciences*, 266, 307-340, <https://doi.org/10.1098/rstb.1973.0051>, 1973.
- Chen, S., Zhou, Y., Chen, Y., and Gu, J.: Fastp: An ultra-fast all-in-one fastq preprocessor, *Bioinformatics*, 34, i884-i890, <https://doi.org/10.1093/bioinformatics/bty560>, 2018.
- Coolen, M. J., Orsi, W. D., Balkema, C., Quince, C., Harris, K., Sylva, S. P., Filipova-Marinova, M., and Giosan, L.: Evolution of the plankton paleome in the black sea from the deglacial to anthropocene, *Proceedings of the National Academy of Sciences*, 110, 8609-8614, <https://doi.org/10.1073/pnas.1219283110>, 2013.
- Corinaldesi, C., Beolchini, F., and Dell'Anno, A.: Damage and degradation rates of extracellular DNA in marine sediments: Implications for the preservation of gene sequences, *Molecular Ecology*, 17, 3939-3951, <https://doi.org/10.1111/j.1365-294x.2008.03880.x>, 2008.

- Cypionka, H.: Oxygen respiration by desulfovibrio species, *Annual Reviews in Microbiology*, 54, 827-848, <https://doi.org/10.1146/annurev.micro.54.1.827>, 2000.
- De Deckker, P.: Ostracoda from australian inland waters—notes on taxonomy and ecology, *Proceedings of the royal Society of Victoria*, 93, 43-85, <https://doi.org/10.1111/j.1463-6409.1981.tb00483.x>, 1981.
- DeAngelis, K. M., Allgaier, M., Chavarria, Y., Fortney, J. L., Hugenholtz, P., Simmons, B., Sublette, K., Silver, W. L., and Hazen, T. C.: Characterization of trapped lignin-degrading microbes in tropical forest soil, *PloS one*, 6, e19306, <https://doi.org/10.1128/aem.05262-11>, 2011.
- Deflandre, B., Mucci, A., Gagné, J.-P., Guignard, C., and jørn Sundby, B.: Early diagenetic processes in coastal marine sediments disturbed by a catastrophic sedimentation event, *Geochimica et Cosmochimica Acta*, 66, 2547-2558, [https://doi.org/10.1016/s0016-7037\(02\)00861-x](https://doi.org/10.1016/s0016-7037(02)00861-x), 2002.
- Dilling, W., and Cypionka, H.: Aerobic respiration in sulfate-reducing bacteria, *FEMS Microbiology Letters*, 71, 123-127, <https://doi.org/10.1111/j.1574-6968.1990.tb03809.x>, 1990.
- Dravis, J. J.: Rapidity of freshwater calcite cementation—implications for carbonate diagenesis and sequence stratigraphy, *Sedimentary Geology*, 107, 1-10, [https://doi.org/10.1016/s0037-0738\(96\)00063-2](https://doi.org/10.1016/s0037-0738(96)00063-2), 1996.
- Dupraz, C., Reid, R. P., Braissant, O., Decho, A. W., Norman, R. S., and Visscher, P. T.: Processes of carbonate precipitation in modern microbial mats, *Earth-Science Reviews*, 96, 141-162, <https://doi.org/10.1016/j.earscirev.2008.10.005>, 2009.
- Fantle, M. S., Maher, K. M., and DePaolo, D.: Isotopic approaches for quantifying the rates of marine burial diagenesis, *Reviews of Geophysics*, 48, <https://doi.org/10.1029/2009rg000306>, 2010.
- Farrow, G.: The climate of alibaba atoll, *Philosophical Transactions of the Royal Society of London. B, Biological Sciences*, 260, 67-91, <https://doi.org/10.1098/rstb.1971.0007>, 1971.
- Filion, G., Laflamme, C., Turgeon, N., Ho, J., and Duchaine, C.: Permeabilization and hybridization protocols for rapid detection of bacillus spores using fluorescence in situ hybridization, *Journal of microbiological methods*, 77, 29-36, <https://doi.org/10.1016/j.mimet.2008.12.009>, 2009.
- Fogel, M. L., and Cifuentes, L. A.: Isotope fractionation during primary production, in: *Organic geochemistry*, Springer, 73-98, https://doi.org/10.1007/978-1-4615-2890-6_3, 1993.
- Froelich, P. N., Klinkhammer, G., Bender, M. L., Luedtke, N., Heath, G. R., Cullen, D., Dauphin, P., Hammond, D., Hartman, B., and Maynard, V.: Early oxidation of organic matter in pelagic sediments of the eastern equatorial atlantic: Suboxic diagenesis, *Geochimica et cosmochimica acta*, 43, 1075-1090, [https://doi.org/10.1016/0016-7037\(79\)90095-4](https://doi.org/10.1016/0016-7037(79)90095-4), 1979.
- Fussmann, D., von Hoyningen-Huene, A. J. E., Reimer, A., Schneider, D., Babková, H., Peticzka, R., Maier, A., Arp, G., Daniel, R., and Meister, P.: Authigenic formation of Ca-Mg carbonates in the shallow alkaline Lake Neusiedl, Austria, *Biogeosciences*, 17, 2085-2020, <https://doi.org/10.5194/bg-17-2085-2020>, 2020.
- Ghai, R., Mizuno, C. M., Picazo, A., Camacho, A., and Rodriguez-Valera, F.: Metagenomics uncovers a new group of low gc and ultra-small marine actinobacteria, *Scientific reports*, 3, 1-8, <https://doi.org/10.1038/srep02471>, 2013.
- Goetschl, K. E., Purgstaller, B., Dietzel, M., and Mavromatis, V.: Effect of sulfate on magnesium incorporation in low-magnesium calcite, *Geochimica et Cosmochimica Acta*, 265, 505-519, <https://doi.org/10.1016/j.gca.2019.07.024>, 2019.
- Grasshoff, K., Kremling, K., and Ehrhardt, M.: *Methods of seawater analysis*, John Wiley & Sons, <https://doi.org/10.1002/9783527613984>, 2009.
- Greiner, G. O. G.: Environmental factors controlling the distribution of recent benthonic foraminifera, *Brevoria, Mus. Comp. Zool.*, 420, 1-35, <https://doi.org/10.1038/223168a0>, 1974.

- Halley, R. B., and Harris, P. M.: Fresh-water cementation of a 1,000-year-old oolite, *Journal of Sedimentary Research*, 49, 969-987, 1979.
- Hamylton, S., Spencer, T., and Hagan, A.: Spatial modelling of benthic cover using remote sensing data in the aldabra lagoon, western Indian Ocean, *Marine Ecology Progress Series*, 460, 35-47, <https://doi.org/10.3354/meps09779>, 2012.
- Hartmann, M., and Nielsen, H.: Δ 34 s-werte in rezenten meeressedimenten und ihre deutung am beispiel einiger sedimentprofile aus der westlichen ostsee, *Geologische Rundschau*, 58, 621-655, <https://doi.org/10.1007/bf01820726>, 1968.
- Higgins, J. A., Blättler, C., Lundstrom, E., Santiago-Ramos, D., Akhtar, A., Ahm, A. C., Bialik, O., Holmden, C., Bradbury, H., and Murray, S.: Mineralogy, early marine diagenesis, and the chemistry of shallow-water carbonate sediments, *Geochimica et Cosmochimica Acta*, 220, 512-534, <https://doi.org/10.1016/j.gca.2017.09.046>, 2018.
- Hogg, A. G., Hua, Q., Blackwell, P. G., Niu, M., Buck, C. E., Guilderson, T. P., Heaton, T. J., Palmer, J. G., Reimer, P. J., and Reimer, R. W.: Shcal13 southern hemisphere calibration, 0–50,000 years cal bp, *Radiocarbon*, 55, 1889-1903, https://doi.org/10.2458/azu_js_rc.55.16783, 2013.
- Hunt, D. E., Lin, Y., Church, M. J., Karl, D. M., Tringe, S. G., Izzo, L. K., and Johnson, Z. I.: Relationship between abundance and specific activity of bacterioplankton in open ocean surface waters, *Applied and environmental microbiology*, 79, 177-184, <https://doi.org/10.1128/aem.02155-12>, 2013.
- Inagaki, F., Okada, H., Tsapin, A. I., and Nealson, K. H.: Microbial survival: The paleome: A sedimentary genetic record of past microbial communities, *Astrobiology*, 5, 141-153, <https://doi.org/10.1089/ast.2005.5.141>, 2005.
- Jones, S. E., and Lennon, J. T.: Dormancy contributes to the maintenance of microbial diversity, *Proceedings of the National Academy of Sciences*, 107, 5881-5886, <https://doi.org/10.1073/pnas.0912765107>, 2010.
- Jørgensen, B. B., and Kasten, S.: Sulfur cycling and methane oxidation, in: *Marine Geochemistry*, edited by Schulz, H. D. and Zabel, M., Springer, Berlin, 271-309, https://doi.org/10.1007/3-540-32144-6_8, 2006.
- Kievman, C. M.: Match between late pleistocene great bahama bank and deep-sea oxygen isotope records of sea level, *Geology*, 26, 635-638, [https://doi.org/10.1130/0091-7613\(1998\)026<0635:mblpbg>2.3.co;2](https://doi.org/10.1130/0091-7613(1998)026<0635:mblpbg>2.3.co;2), 1998.
- Klindworth, A., Pruesse, E., Schweer, T., Peplies, J., Quast, C., Horn, M., and Glöckner, F. O.: Evaluation of general 16s ribosomal rna gene pcr primers for classical and next-generation sequencing-based diversity studies, *Nucleic acids research*, 41, e1-e1, <https://doi.org/10.1093/nar/gks808>, 2013.
- Lange, S. M., Krause, S., Ritter, A. C., Fichtner, V., Immenhauser, A., Strauss, H., and Treude, T.: Anaerobic microbial activity affects earliest diagenetic pathways of bivalve shells, *Sedimentology*, 65, 1390-1411, <https://doi.org/10.1111/sed.12428>, 2018.
- Lee, R. Y., Porubsky, W. P., Feller, I. C., McKee, K. L., and Joye, S. B.: Porewater biogeochemistry and soil metabolism in dwarf red mangrove habitats (twin cays, belize), *Biogeochemistry*, 87, 181-198, <https://doi.org/10.1007/s10533-008-9176-9>, 2008.
- Martin, M.: Cutadapt removes adapter sequences from high-throughput sequencing reads, *EMBnet journal*, 17, 10-12, <https://doi.org/10.14806/ej.17.1.200>, 2011.
- Matsuda, H., Tsuji, Y., Honda, N., and Saotome, J.-i.: Early diagenesis of pleistocene carbonates from a hydrogeochemical point of view, irabu island, ryukyu islands: Porosity changes related to early carbonate diagenesis, 1995.

- More, K. D., Giosan, L., Grice, K., and Coolen, M. J.: Holocene paleodepositional changes reflected in the sedimentary microbiome of the black sea, *Geobiology*, 17, 436-448, <https://doi.org/10.1111/gbi.12338>, 2019.
- Morono, Y., Ito, M., Hoshino, T., Terada, T., Hori, T., Ikehara, M., D'Hondt, S., and Inagaki, F.: Aerobic microbial life persists in oxic marine sediment as old as 101.5 million years, *Nature communications*, 11, 1-9, <https://doi.org/10.1038/s41467-020-17330-1>, 2020.
- Murray, J. W.: Distribution and ecology of living benthic foraminiferids, <https://doi.org/10.4319/lo.1973.18.6.1011a>, 1973.
- Nichols, S. A., and Barnes, P. A.: A molecular phylogeny and historical biogeography of the marine sponge genus *placospongia* (phylum porifera) indicate low dispersal capabilities and widespread crypsis, *Journal of Experimental Marine Biology and Ecology*, 323, 1-15, <https://doi.org/10.1016/j.jembe.2005.02.012>, 2005.
- Orsi, W. D., Coolen, M. J., Wuchter, C., He, L., More, K. D., Irigoien, X., Chust, G., Johnson, C., Hemingway, J. D., and Lee, M.: Climate oscillations reflected within the microbiome of arabian sea sediments, *Scientific Reports*, 7, 1-12, <https://doi.org/10.1038/s41598-017-05590-9>, 2017.
- Parkhurst, D. L., and Appelo, C.: Description of input and examples for phreeqc version 3: A computer program for speciation, batch-reaction, one-dimensional transport, and inverse geochemical calculations, US Geological Survey, 2328-7055, <https://doi.org/10.3133/tm6a43>, 2013.
- Pederson, C., Mavromatis, V., Dietzel, M., Rollion-Bard, C., Breitenbach, S., Yu, D., Nehrke, G., and Immenhauser, A.: Variation in the diagenetic response of aragonite archives to hydrothermal alteration, *Sedimentary Geology*, 406, 105716, <https://doi.org/10.1016/j.sedgeo.2020.105716>, 2020.
- Pederson, C. L., Klaus, J. S., Swart, P. K., and McNeill, D. F.: Deposition and early diagenesis of microbial mud in the florida everglades, *Sedimentology*, 66, 1989-2010, <https://doi.org/10.1111/sed.12569>, 2019.
- Pisera, A., Rützler, K., Kaz'mierczak, J., and Kempe, S.: Sponges in an extreme environment: Suberitids from the quasi-marine satonda island crater lake (sumbawa, indonesia), *Marine Biological Association of the United Kingdom. Journal of the Marine Biological Association of the United Kingdom*, 90, 203, <https://doi.org/10.1017/s0025315409990968>, 2010.
- Porter, D., Roychoudhury, A. N., and Cowan, D.: Dissimilatory sulfate reduction in hypersaline coastal pans: Activity across a salinity gradient, *Geochimica et Cosmochimica Acta*, 71, 5102-5116, <https://doi.org/10.1016/j.gca.2007.08.023>, 2007.
- Quast, C., Pruesse, E., Yilmaz, P., Gerken, J., Schweer, T., Yarza, P., Peplies, J., and Glöckner, F. O.: The silva ribosomal rna gene database project: Improved data processing and web-based tools, *Nucleic acids research*, 41, D590-D596, <https://doi.org/10.1093/nar/gks1219>, 2012.
- Ramsey, CB.: Bayesian analysis of radiocarbon dates, *Radiocarbon*, 51, 337-360, <https://doi.org/10.1017/s0033822200033865>, 2009.
- Rassmann, J., Lansard, B., Pozzato, L., and Rabouille, C.: Carbonate chemistry in sediment porewaters of the rhône river delta driven by early diagenesis (northwestern mediterranean), <https://doi.org/10.5194/bg-13-5379-2016>, 2016.
- Ritter, A. C., Mavromatis, V., Dietzel, M., Kwiecien, O., Wiethoff, F., Griesshaber, E., Casella, L. A., Schmahl, W. W., Koelen, J., and Neuser, R. D.: Exploring the impact of diagenesis on (isotope) geochemical and microstructural alteration features in biogenic aragonite, *Sedimentology*, 64, 1354-1380, <https://doi.org/10.1111/sed.12356>, 2017.
- Rognes, T., Flouri, T., Nichols, B., Quince, C., and Mahé, F.: Vsearch: A versatile open source tool for metagenomics, *PeerJ*, 4, e2584, <https://doi.org/10.7717/peerj.2584>, 2016.

- Rohling, E. J., Grant, K., Bolshaw, M., Roberts, A., Siddall, M., Hemleben, C., and Kucera, M.: Antarctic temperature and global sea level closely coupled over the past five glacial cycles, *Nature Geoscience*, 2, 500-504, <https://doi.org/10.1038/ngeo557>, 2009.
- Sarazin, G., Michard, G., Al Gharib, I., and Bernat, M.: Sedimentation rate and early diagenesis of particulate organic nitrogen and carbon in aydat lake (puy de dôme, france), *Chemical Geology*, 98, 307-316, [https://doi.org/10.1016/0009-2541\(92\)90191-7](https://doi.org/10.1016/0009-2541(92)90191-7), 1992.
- Schippers, A.: Biogeochemistry of metal sulfide oxidation in mining environments, sediments, and soils, *Special Papers-Geological Society Of America*, 49-62, <https://doi.org/10.1130/0-8137-2379-5.49>, 2004.
- Schneider, D., Wemheuer, F., Pfeiffer, B., and Wemheuer, B.: Extraction of total DNA and rna from marine filter samples and generation of a cdna as universal template for marker gene studies, in: *Metagenomics*, Springer, 13-22, https://doi.org/10.1007/978-1-4939-6691-2_2, 2017.
- Schwab, V. F., Hermann, M., Roth, V.-N., Gleixner, G., Lehmann, R., Pohnert, G., Trumbore, S. E., Küsel, K., and Totsche, K.: Functional diversity of microbial communities in pristine aquifers inferred by plfa-and sequencing-based approaches, *Biogeosciences*, 14, 2697-2714, <https://doi.org/10.5194/bg-14-2697-2017>, 2017.
- Siddall, M., Rohling, E. J., Almogi-Labin, A., Hemleben, C., Meischner, D., Schmelzer, I., and Smeed, D.: Sea-level fluctuations during the last glacial cycle, *Nature*, 423, 853-858, <https://doi.org/10.1038/nature01690>, 2003.
- Simister, R., Taylor, M. W., Tsai, P., Fan, L., Bruxner, T. J., Crowe, M. L., and Webster, N.: Thermal stress responses in the bacterial biosphere of the great barrier reef sponge, *Environmental microbiology*, 14, 3232-3246, <https://doi.org/10.1111/1462-2920.12010>, 2012.
- Smith, E. A., and Macfarlane, G. T.: Formation of phenolic and indolic compounds by anaerobic bacteria in the human large intestine, *Microbial ecology*, 33, 180-188, <https://doi.org/10.1006/anae.1997.0121>, 1997.
- Strauss, H., Bast, R., Cording, A., Diekrup, D., Fugmann, A., Garbe-Schönberg, D., Lutter, A., Oeser, M., Rabe, K., and Reinke, D.: Sulphur diagenesis in the sediments of the kiel bight, sw baltic sea, as reflected by multiple stable sulphur isotopes, *Isotopes in environmental and health studies*, 48, 166-179, <https://doi.org/10.1080/10256016.2012.648930>, 2012.
- Sukenik, A., Kaplan-Levy, R. N., Welch, J. M., and Post, A. F.: Massive multiplication of genome and ribosomes in dormant cells (akinetes) of aphanizomenon ovalisporum (cyanobacteria), *The ISME Journal*, 6, 670-679, <https://doi.org/10.1038/ismej.2011.128>, 2012.
- Swart, P. K., and Kramer, P. A.: Geology of mud islands in florida bay, *Geology and hydrogeology of carbonate islands: developments in sedimentology*, 54, 249-274, [https://doi.org/10.1016/s0070-4571\(04\)80028-1](https://doi.org/10.1016/s0070-4571(04)80028-1), 1997.
- Swart, P. K., and Eberli, G.: The nature of the $\delta^{13}C$ of periplatform sediments: Implications for stratigraphy and the global carbon cycle, *Sedimentary Geology*, 175, 115-129, <https://doi.org/10.1016/j.sedgeo.2004.12.029>, 2005.
- Swart, P. K.: The geochemistry of carbonate diagenesis: The past, present and future, *Sedimentology*, 62, 1233-1304, <https://doi.org/10.1111/sed.12205>, 2015.
- Team, R.: RStudio: integrated development for R.(RStudio, Inc., Boston, MA, USA), 2016.
- Team, R. C.: R: A language and environment for statistical computing, 2018.
- Torn, K., Beilby, M. J., Casanova, M. T., and Al Khazaaly, S.: Formation of extracellular sulphated polysaccharide mucilage on the salt tolerant characeae lamprothamnium, *International review of hydrobiology*, 99, 326-334, <https://doi.org/10.1002/iroh.201301666>, 2014.

- Torres, I. C., Inglett, P. W., Brenner, M., Kenney, W. F., and Reddy, K. R.: Stable isotope ($\delta^{13}\text{C}$ and $\delta^{15}\text{N}$) values of sediment organic matter in subtropical lakes of different trophic status, *Journal of Paleolimnology*, 47, 693-706, <https://doi.org/10.1007/s10933-012-9593-6>, 2012.
- Van Soest, R., Boury-Esnault, N., Hooper, J., Rützler, K. d., De Voogd, N., Alvarez de Glasby, B., Hajdu, E., Pisera, A., Manconi, R., and Schoenberg, C.: World porifera database, The World Register of Marine Species (WoRMS). Available online: <http://www.marinespecies.org/porifera>, 2018.
- von Hoyningen-Huene, A. J. E., Schneider, D., Fussmann, D., Reimer, A., Arp, G., and Daniel, R.: Bacterial succession along a sediment porewater gradient at Lake Neusiedl in Austria, *Scientific data*, 6, 1-7, <https://doi.org/10.1038/s41597-019-0172-9>, 2019.
- Vos, P. D.: *Pontibacillus*, *Bergey's Manual of Systematics of Archaea and Bacteria*, 1-4, <https://doi.org/10.1002/9781118960608.gbm00541>, 2015.
- Vreeland, R. H.: *Halomonas*, *Bergey's Manual of Systematics of Archaea and Bacteria*, 1-19, <https://doi.org/10.1002/9781118960608.gbm01190>, 2015.
- Whitman, W. B.: *Bergey's Manual of Systematics of Archaea and Bacteria*, Wiley Online Library, <https://doi.org/10.1002/9781118960608.gbm01255>, 2015.
- Wood, R., and Imahori, K.: Geographical distribution of characeae, *Bulletin of the Torrey Botanical Club*, 86, 172-183, <https://doi.org/10.2307/2482517>, 1959.
- Wood, R. D.: The characeae, 1951, *The Botanical Review*, 18, 317-353, <https://doi.org/10.1007/bf02957549>, 1952.
- Wray, J.: Calcareous algae.—developments in paleontology and stratigraphy 4, 185 s., 170 abb, in, Elsevier-Verlag, Amsterdam—Oxford—New York, <https://doi.org/10.1016/c2009-0-19424-2>, 1977.
- Zhang, J., Kobert, K., Flouri, T., and Stamatakis, A.: Pear: A fast and accurate illumina paired-end read merger, *Bioinformatics*, 30, 614-620, <https://doi.org/10.1093/bioinformatics/btt593>, 2014.

6. Fine-grained carbonates exposed to changing pore water gradients

Diagenetic reactions in fine-grained carbonate sediments have the potential to alter geochemical proxy records (Allan and Matthews, 1982; Banner and Hanson, 1990; Swart and Eberli, 2005; Higgins et al., 2018) and significantly affect the global carbon cycle over geologic time scales ([Chapter 1.1](#)). Several proxies are suitable to trace diagenetic alterations ([Chapter 1.2](#)), of which $\delta^{18}\text{O}$ and $\delta^{13}\text{C}$ isotopes are commonly used, since their first application to alteration studies by Gross (1964). The vulnerability of both tracers ($\delta^{18}\text{O}$ and $\delta^{13}\text{C}$) to post-depositional alterations is well established (Berner, 1966; Walter et al., 1993; Patterson and Walter, 1994; Immenhauser et al., 2003), and comparative pore water studies have enabled inferences to the contemporaneous diagenetic environment (Froelich et al., 1979; Suess, 1979; Ku et al., 1999). However, pore water sampling techniques remained a limiting factor for the spatial resolution of such studies until the beginning of the 21st century, when Rhizon sampling was introduced to geological sciences by Seeberg-Elverfeldt et al. (2005). Moreover, microbial contributions to (early) diagenesis are recognized (Suess, 1979; Vasconcelos and McKenzie, 1997; Pederson et al., 2015), but the role of specific metabolisms or even organisms in carbonate mineral alteration processes is still under debate. This thesis aims at a detailed comparison of geochemical proxies in Holocene, fine-grained carbonate sediments with contemporaneous pore water. The precise, space-resolved pore water sampling technique, combined with bacterial gene data, represents a new comparative approach and a potential missing jigsaw piece to previous studies.

6.1 Boundary conditions of initial geochemical proxy values and their stability in modern, shallow marine carbonate sediments

The initial values of traditional isotope proxies such as $\delta^{13}\text{C}$ and $\delta^{18}\text{O}$, trace elements like Sr^{2+} , and major elements like Mg^{2+} in carbonate minerals are determined by various factors. These include mineralogy, precipitation mechanism (abiogenic/biogenic/microbial), and the chemistry of the abundant precipitating fluid ([Chapter 1.2](#)).

It is well-known that aragonite is enriched in $\delta^{13}\text{C}$ and $\delta^{18}\text{O}$ compared to LMC and HMC (Tarutani et al., 1969). This is also displayed by samples from the lagoon of Aldabra, which are presented in [Chapter 4](#). West lagoon (WL) samples are enriched in stable isotopes ($\delta^{13}\text{C}$, $\delta^{18}\text{O}$) and aragonite compared to samples of the north- and south lagoon (NL; SL). Furthermore, so called “vital effects” are visible in the lagoon samples. This is explained by the biogenic precipitation of most of the bulk carbonate in the lagoon of Aldabra. Vital effects describe the influence of certain carbonate precipitating organisms on the isotope record, as their secretion mechanism takes place out of isotopic equilibrium (McConnaughey, 1989; Adkins et al., 2003; McConnaughey, 2003). For example, aragonite, precipitated by green algae of the orders Dasycladales and Halimeda, likely contributes to the enriched $\delta^{13}\text{C}$ and $\delta^{18}\text{O}$ values of the WL (Wefer and Berger, 1981). In contrast, NL and SL gain most of their CaCO_3 from typical benthic, lagoonal organisms such as mollusks and foraminifera of the suborders Rotaliina and Miliolina. These organisms are renowned for precipitating in isotopic equilibrium (Wefer et al., 1981). Hence, the lower $\delta^{18}\text{O}$ and $\delta^{13}\text{C}$ signals of the SL and NL possibly reflect the availability of ambient mangrove rootage as depleted carbon source for the biogenic carbonate (Alfaro, 2008).

These initial stable isotope values can be affected by early diagenesis, which occurs in characteristic early diagenetic zones and includes certain alteration patterns of $\delta^{13}\text{C}$ and $\delta^{18}\text{O}$ (Swart, 2015 and references therein, Figure 6.1). During early marine diagenesis, the decay of organic matter (OM) and the concomitant release of CO_2 into the pore space of carbonate sediments, lower the pH value. This favors the dissolution of metastable CaCO_3 (aragonite, HMC) and its re-precipitation as the more stable LMC phase. The degradation process takes place under aerobic and anaerobic pore water conditions,

with SO_4^{2-} as the most important alternative oxidant, after oxygen is consumed ([Chapter 1.4](#); Froelich et al., 1979). This is rudimentarily visible in sediments of the SL ([Chapter 4](#), Figure 4.6), in which small amounts of aragonite dissolve in the uppermost sediment layer. As this process happens within the lagoon as a closed system, i. e. without the supply of significant amounts of other fluids than lagoon water, a change in bulk isotope composition of the potentially re-precipitating carbonate mineral is not expectable (Swart and Eberli, 2005). However, pore water and, hence, parts of the carbonate re-precipitating carbon pool are depleted in $\delta^{13}\text{C}$ ([Chapter 4](#), Figure 4.10). This is due to the decay of OM, but the dissolution potential of this process alone is not sufficient to affect the bulk isotope composition, which is determined by the limitation of oxidants, according to Swart (2015): He considers 1 g of aragonite (CaCO_3 ; $\rho = 2.9 \text{ g}\cdot\text{cm}^3$) with a porosity of 50 %, which would be exposed to $28 \text{ mmol}\cdot\text{kg}^{-1}$ of SO_4^{2-} in seawater. Overall, ca. $9.6\cdot 10^{-7}$ moles of SO_4^{2-} would be accessible for the oxidation of OM in the pore fluids. That chemical reaction would produce $19.2\cdot 10^{-7}$ moles of HCO_3^- , causing just a minimal impact on 0.01 moles of C in 1 g of aragonite. Hence, secondary carbonate mineral overgrowths might differ in mineralogy and isotopic composition compared to the initial phase, but they are only traceable by the application of high-resolution analytics and do not impact the bulk geochemistry (Hover et al., 2001).

This finding is consistent with observations from the WL (Aldabra) in [Chapter 4](#). Sediments from this locality consist of bioclastic carbonate sand, cemented by cryptocrystalline CaCO_3 . The cements precipitate in an oxic, marine vadose pore space. It is not entirely clear if they form abiogenic or by microbial contribution, which could lead to a significant $\delta^{13}\text{C}$ deviation compared to the substrate. However, the bulk signal (Figure 4.9) shows no distinct isotope shift. This further contributes to the hypothesis that the decay of OM alone, without any contribution of additional fluids (hence electron acceptors) is not sufficient to alter the bulk isotope record (Swart et al., 2002; Swart and Eberli, 2005; Swart, 2015).

The effects on early diagenetic alteration by external oxidants is illustrated by the study in [Chapter 5](#), which was conducted in a landlocked pool at Cinq Cases, in the southeast of Aldabra. The saline, shallow water body was subject to frequent environmental changes in the late Holocene, which have likely coincided with changes of depositional water. These variations included a palustrine setting (unit III; [Chapter 5](#)), which had been exposed to meteoric fluids, hence external oxidants, and anoxic diagenesis. This is indicated by the depleted bulk $\delta^{13}\text{C}$ and $\delta^{18}\text{O}$ record, and an iron (Fe^{2+}) and manganese (Mn^{2+}) related elemental zonation of diagenetic LMC crystals (Figure 5.4).

Summing up, the studies from Aldabra ([Chapter 4](#); [Chapter 5](#)) illustrate the variability of geochemical proxy stability in modern, shallow marine carbonate depositional settings. The bulk variation is not detectable in environments, which lack external input of oxidants. This causes only minor dissolution and re-precipitation of metastable carbonate phases. In contrast, the bulk geochemical record of Cinq Cases, a shallow water body with fluctuating input of external fluids, is highly variable. These findings basically confirm the present-day state of the science (Swart, 2015 and references therein) and conflict with the opinion of Walter et al. (1993), who stated that “analyses of altered components of ancient shelf carbonates may tell us more about the composition of pore water than ancient sea water”. Moreover, the studies in [Chapter 4](#) and [5](#) are the first detailed report of unconsolidated, Holocene sediments from Aldabra. Up to now, this atoll has been reported as a pure lime mud depositing environment, similar to famous lagoons of the Jurassic (Gaillard et al., 1994; Bernier et al., 2014). This view, however, should be adapted, according to the findings in [Chapter 4](#).

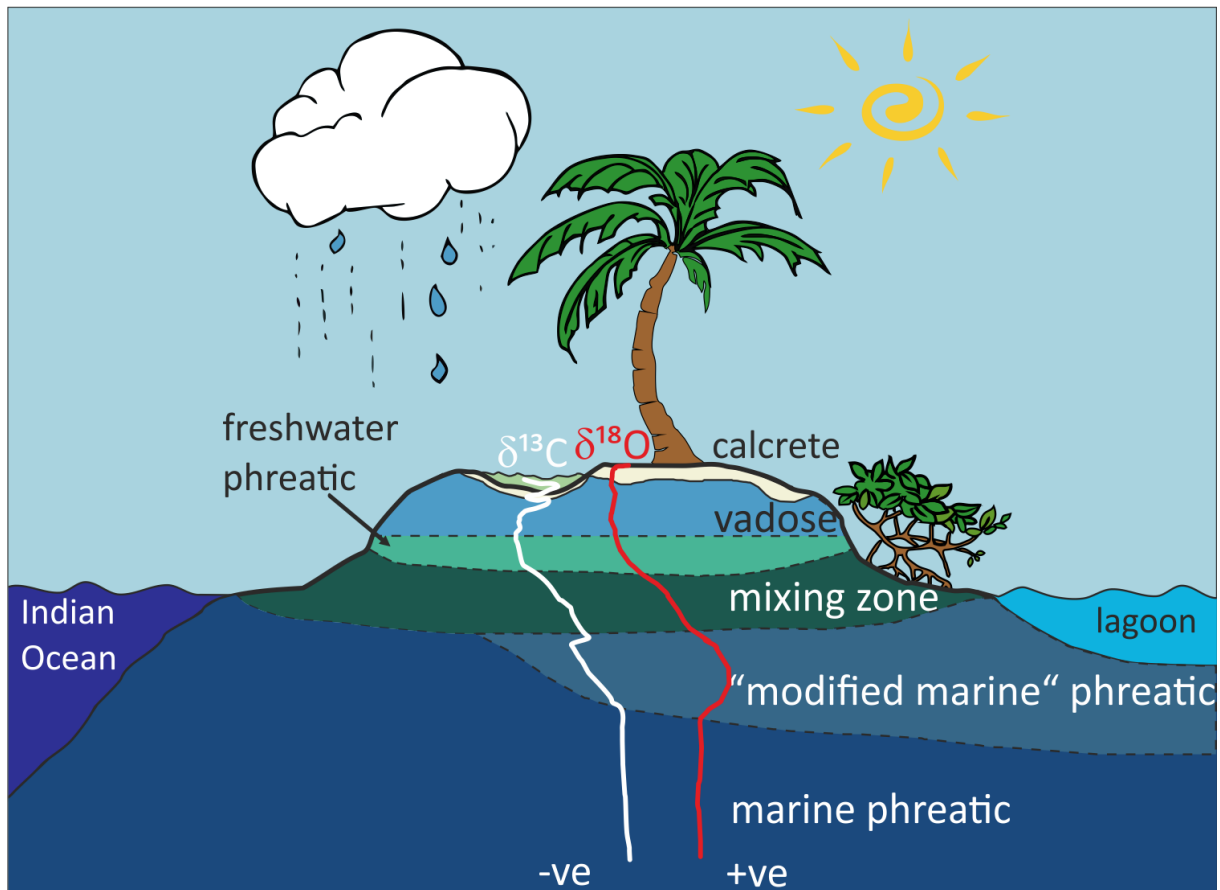


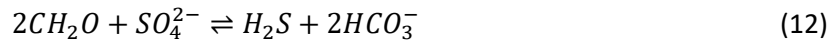
Figure 6.1: Characteristic early diagenetic zones on Aldabra. The drawing is changed after Swart (2015), whereas the stable isotope graphs and the “modified marine phreatic” zone are based on values obtained in the study in Chapter 4.

6.2 Impacts of bacterial activity on sediment geochemistry

Metabolic processes of microorganisms are the main driver of OM decomposition, which is coupled to the establishment of distinct physicochemical gradients in ambient pore water of carbonate sediments. The effects of these pore water gradient changes on the stability and geochemistry of carbonate phases were controversially discussed (Suess, 1979; Walter and Burton, 1990; Walter et al., 1993; Patterson and Walter, 1994; Swart and Eberli, 2005) and depend on a sufficient supply with electron acceptors (Swart, 2015).

After oxygen is depleted, physicochemical gradients within near surface sediments follow characteristic respiratory zones, which are established according to the energy yield of the respective electron acceptors (Chapter 1; Froelich et al., 1979; Jørgensen and Kasten, 2006). However, this characteristic succession is only valid for pelagic sediments, with low sedimentation rates and benthic productivity. Within shallow marine or lacustrine deposits that are presented in Chapters 2-5, this sequence of metabolic zones may be compromised by faunal bioturbation or traversing of plant rootage. Both processes increase the porosity and enhance diffusion between the metabolic zones. Nonetheless, the decay of OM goes hand in hand with metabolic CO_2 generation, which, when dissolved as carbonic acid in pore water, lowers the pH and potentially causes undersaturation of metastable CaCO_3 . When oxygen is depleted, several substitutional electron acceptors are available (Chapter 1) of which SO_4^{2-} is the most significant, as it is abundant in all marine settings. Organic matter degradation by dissimilatory sulfate reduction (SR) has two main effects: On the one hand, dissolved

inorganic carbon (DIC) is generated, which rises alkalinity and, thus, favors carbonate supersaturation (eq. 12, CH_2O represents OM; Jørgensen and Kasten, 2006).



The (in eq. 12) generated bicarbonate potentially dissociates into minor parts of carbonate ions (CO_3^{2-}), which increases the solubility product of CaCO_3 (Chapter 1.1, eq. 4). This chemical relationship has led authors to the assumption that SR possibly enhances carbonate saturation and eventually favors carbonate precipitation (Vasconcelos et al., 1995; Vasconcelos and McKenzie, 1997; Van Lith et al., 2002). On the other hand, OM oxidation by SR generates CO_2 . As mentioned before, this results in a decrease of pH, which lowers CaCO_3 saturation and eventually causes carbonate dissolution. However, as the end-products of SR also depend on the feeding substrate, it is under debate, if the net amounts of this metabolism have a significant impact on carbonate mineral stability (Meister, 2013; Gallagher et al., 2014). However, the studies from Lake Neusiedl (Chapters 2 and 3) and Aldabra (Chapter 4) suggest only minor effects of SR on carbonate mineral stability in near surface environments, as no pore water trend excursions of carbonate sensitive elements like Ca^{2+} , Mg^{2+} , and Sr^{2+} were observed in sediment sections with enhanced SR. However, SR also releases sulfide (eq. 12), which feeds sulfur-oxidizing bacteria (SOB). These SOB gain their energy from sulfur compounds ($\Sigma\text{H}_2\text{S}$), which produces protons (eq.13, Jørgensen and Kasten, 2006).



This metabolic process represents a second acid source, besides the carbonic acid generated by the oxidation of OM, and eventually favors CaCO_3 dissolution (Walter et al., 1993). This effect is evident in sediments from the SL (Chapter 4). In the upper section of the sediment core (SLU I), pore water gradients indicate the dissolution of metastable carbonate, associated with enhanced $\Sigma\text{H}_2\text{S}$ oxidation and the occurrence of SOB. Thus, OM oxidation by dissimilatory SR is not sufficient to significantly impact CaCO_3 saturation. However, if it is subsequently exposed to oxygen, hence coupled to sulfur oxidation, early diagenetic dissolution of carbonate minerals is favored. Moreover, the study in Chapter 4 is the first to associate the presence of SOB of the order Campylobacterales and the genus Malaciobacterales with this carbonate dissolution process.

All in all, the studies included in this thesis illustrate that bacterial activity during the earliest stages of diagenesis has only minor effects on the bulk geochemical composition of carbonate sediments in form of sulfur oxidation. If this process is not enhanced by the input of external oxidants, the diagenetic impact on stable bulk-isotope signatures in fine-grained carbonates remains insignificant.

6.3 Bacterial gene data as additional diagenetic proxy

Bacterial genes and their fragments have proven to survive several thousands of years (or even longer) in sediments if minor diagenetic alteration is provided. For example, bacterial DNA was extracted from Cretaceous black shales and deep sea sediments (Inagaki et al., 2005; Morono et al., 2020). As not all detectable DNA derives from active, but also from dormant or inactive cells, these organic compounds provide insights into past environmental conditions (Ciobanu et al., 2012; Inagaki et al., 2015). Hence, it is assumed that these cells have been present at the time of sediment deposition and form a genetic archive, referred to as “the Paleome” (Inagaki et al., 2005, Chapter 1).

Accordingly, bacterial DNA can settle from the water column and remain in the sediment, as demonstrated by a study from the black sea (More et al., 2019). These authors have found obligate aerobic DNA, in anoxic sediments, which enabled inferences to environmental conditions of the ancient water column. This finding is also documented in the studies of Chapters 2 and 3. In sediments of Lake Neusiedl, phototrophic Cyanobacteria DNA of the order Synechococcales was detected in anoxic sediments, at depths between 15 and 35 cm. At such light-depleted depths, the DNA represents relics

of an ancient water column as well, because it is impossible for Cyanobacteria to thrive under present conditions (Castenholz, 2015). In combination with ambient radiocarbon data, additional estimations of paleo-hydrochemical water column conditions of Lake Neusiedl would be possible. Bacterial RNA- and DNA based gene data were also used as paleo-environmental proxy in the study of Cinq Cases ([Chapter 5](#)). In sediments of the present-day oxic lower core part (Unit III), a high relative abundance of bacteria, which belong to the orders of Firmicutes and Desulfobacterota, was detected. The occurrence of these obligate anaerobe microorganisms indicates that the oxic deposits of Unit III have at least temporarily experienced anoxic conditions in the past. Summing up, bacterial gene data provide valuable paleoenvironmental information, if they are combined with geo- and hydrochemical datasets in multi-proxy studies.

References

- Adkins, J. F., Boyle, E. A., Curry, W., and Lutringer, A.: Stable isotopes in deep-sea corals and a new mechanism for “vital effects”, *Geochimica et Cosmochimica Acta*, 67, 1129-1143, [https://doi.org/10.1016/s0016-7037\(02\)01203-6](https://doi.org/10.1016/s0016-7037(02)01203-6), 2003.
- Alfaro, A. C.: Diet of *Littoraria scabra*, while vertically migrating on mangrove trees: Gut content, fatty acid, and stable isotope analyses, *Estuarine, Coastal and Shelf Science*, 79, 718-726, <https://doi.org/10.1016/j.ecss.2008.06.016>, 2008.
- Allan, J., and Matthews, R.: Isotope signatures associated with early meteoric diagenesis, *Sedimentology*, 29, 797-817, <https://doi.org/10.1111/j.1365-3091.1982.tb00085.x>, 1982.
- Banner, J. L., and Hanson, G. N.: Calculation of simultaneous isotopic and trace element variations during water-rock interaction with applications to carbonate diagenesis, *Geochimica et Cosmochimica Acta*, 54, 3123-3137, [https://doi.org/10.1016/0016-7037\(90\)90128-8](https://doi.org/10.1016/0016-7037(90)90128-8), 1990.
- Berner, R. A.: Chemical diagenesis of some modern carbonate sediments, *American Journal of Science*, 264, 1-36, <https://doi.org/10.2475/ajs.264.1.1>, 1966.
- Bernier, P., Barale, G., Bourseau, J.-P., Buffetaut, E., Gaillard, C., Gall, J.-C., and Wenz, S.: The lithographic limestones of cerin (southern jura mountains, france). A synthetic approach and environmental interpretation, *Comptes Rendus Palevol*, 13, 383-402, <https://doi.org/10.1016/j.crpv.2014.01.006>, 2014.
- Castenholz, R. W.: General characteristics of the cyanobacteria, *Bergey's Manual of Systematics of Archaea and Bacteria*, 1-23, <https://doi.org/10.1002/9781118960608.cbm00019>, 2015.
- Ciobanu, M.-C., Rabineau, M., Droz, L., Révillon, S., Ghiglione, J.-F., Dennielou, B., Jorry, S.-J., Kallmeyer, J., Etoubleau, J., and Pignet, P.: Sedimentological imprint on subseafloor microbial communities in western mediterranean sea quaternary sediments, *Biogeosciences*, 9, 3491-3512, <https://doi.org/10.5194/bg-9-3491-2012>, 2012.
- Froelich, P. N., Klinkhammer, G., Bender, M. L., Luedtke, N., Heath, G. R., Cullen, D., Dauphin, P., Hammond, D., Hartman, B., and Maynard, V.: Early oxidation of organic matter in pelagic sediments of the eastern equatorial atlantic: Suboxic diagenesis, *Geochimica et cosmochimica acta*, 43, 1075-1090, [https://doi.org/10.1016/0016-7037\(79\)90095-4](https://doi.org/10.1016/0016-7037(79)90095-4), 1979.
- Gaillard, C., Bernier, P., and Gruet, Y.: Le lagon d'aldabra (seychelles, océan indien), un modèle pour le paléoenvironnement de cerin (kimméridgien supérieur, jura méridional, france), *Geobios*, 27, 331-348, [https://doi.org/10.1016/s0016-6995\(94\)80050-2](https://doi.org/10.1016/s0016-6995(94)80050-2), 1994.
- Gallagher, K. L., Dupraz, C., and Visscher, P. T.: Two opposing effects of sulfate reduction on carbonate precipitation in normal marine, hypersaline, and alkaline environments: Comment, *Geology*, 42, e313-e314, <https://doi.org/10.1130/g34639c.1>, 2014.
- Gross, M. G.: Variations in the o18/o16 and c13/c12 ratios of diagenetically altered limestones in the bermuda islands, *The Journal of Geology*, 72, 170-194, <https://doi.org/10.1086/626975>, 1964.
- Higgins, J. A., Blättler, C., Lundstrom, E., Santiago-Ramos, D., Akhtar, A., Ahm, A. C., Bialik, O., Holmden, C., Bradbury, H., and Murray, S.: Mineralogy, early marine diagenesis, and the chemistry of shallow-water carbonate sediments, *Geochimica et Cosmochimica Acta*, 220, 512-534, <https://doi.org/10.1016/j.gca.2017.09.046>, 2018.
- Hover, V. C., Walter, L. M., and Peacor, D. R.: Early marine diagenesis of biogenic aragonite and mg-calcite: New constraints from high-resolution stem and aem analyses of modern platform carbonates, *Chemical Geology*, 175, 221-248, [https://doi.org/10.1016/s0009-2541\(00\)00326-0](https://doi.org/10.1016/s0009-2541(00)00326-0), 2001.

- Immenhauser, A., Della Porta, G., Kenter, J. A., and Bahamonde, J. R.: An alternative model for positive shifts in shallow-marine carbonate $\delta^{13}\text{C}$ and $\delta^{18}\text{O}$, *Sedimentology*, 50, 953-959, <https://doi.org/10.1046/j.1365-3091.2003.00590.x>, 2003.
- Inagaki, F., Okada, H., Tsapin, A. I., and Nealson, K. H.: Microbial survival: The paleome: A sedimentary genetic record of past microbial communities, *Astrobiology*, 5, 141-153, <https://doi.org/10.1089/ast.2005.5.141>, 2005.
- Inagaki, F., Hinrichs, K.-U., Kubo, Y., Bowles, M. W., Heuer, V. B., Hong, W.-L., Hoshino, T., Ijiri, A., Imachi, H., and Ito, M.: Exploring deep microbial life in coal-bearing sediment down to ~ 2.5 km below the ocean floor, *Science*, 349, 420-424, <https://doi.org/10.1126/science.aaa6882>, 2015.
- Jørgensen, B. B., and Kasten, S.: Sulfur cycling and methane oxidation, in: *Marine geochemistry*, Springer, 271-309, https://doi.org/10.1007/3-540-32144-6_8, 2006.
- Ku, T., Walter, L., Coleman, M., Blake, R., and Martini, A. M.: Coupling between sulfur recycling and syndepositional carbonate dissolution: Evidence from oxygen and sulfur isotope composition of pore water sulfate, south florida platform, USA, *Geochimica et Cosmochimica Acta*, 63, 2529-2546, [https://doi.org/10.1016/s0016-7037\(99\)00115-5](https://doi.org/10.1016/s0016-7037(99)00115-5), 1999.
- McConnaughey, T.: ^{13}C and ^{18}O isotopic disequilibrium in biological carbonates: I. Patterns, *Geochimica et Cosmochimica Acta*, 53, 151-162, [https://doi.org/10.1016/0016-7037\(89\)90282-2](https://doi.org/10.1016/0016-7037(89)90282-2), 1989.
- McConnaughey, T.: Sub-equilibrium oxygen-18 and carbon-13 levels in biological carbonates: Carbonate and kinetic models, *Coral reefs*, 22, 316-327, <https://doi.org/10.1007/s00338-003-0325-2>, 2003.
- Meister, P.: Two opposing effects of sulfate reduction on carbonate precipitation in normal marine, hypersaline, and alkaline environments, *Geology*, 41, 499-502, <https://doi.org/10.1130/g34185.1>, 2013.
- More, K. D., Giosan, L., Grice, K., and Coolen, M. J.: Holocene paleodepositional changes reflected in the sedimentary microbiome of the black sea, *Geobiology*, 17, 436-448, <https://doi.org/10.1111/gbi.12338>, 2019.
- Morono, Y., Ito, M., Hoshino, T., Terada, T., Hori, T., Ikehara, M., D'Hondt, S., and Inagaki, F.: Aerobic microbial life persists in oxic marine sediment as old as 101.5 million years, *Nature communications*, 11, 1-9, <https://doi.org/10.1038/s41467-020-17330-1>, 2020.
- Patterson, W. P., and Walter, L. M.: Syndepositional diagenesis of modern platform carbonates: Evidence from isotopic and minor element data, *Geology*, 22, 127-130, [https://doi.org/10.1130/0091-7613\(1994\)022<0127:sdompc>2.3.co;2](https://doi.org/10.1130/0091-7613(1994)022<0127:sdompc>2.3.co;2), 1994.
- Pederson, C. L., McNeill, D. F., Klaus, J. S., and Swart, P. K.: Deposition and diagenesis of marine oncoids: Implications for development of carbonate porosity, *Journal of Sedimentary Research*, 85, 1323-1333, <https://doi.org/10.2110/jsr.2015.77>, 2015.
- Seeberg-Elverfeldt, J., Schlüter, M., Feseker, T., and Kölling, M.: Rhizon sampling of porewaters near the sediment-water interface of aquatic systems, *Limnology and oceanography: Methods*, 3, 361-371, <https://doi.org/10.4319/lom.2005.3.361>, 2005.
- Suess, E.: Mineral phases formed in anoxic sediments by microbial decomposition of organic matter, *Geochimica et Cosmochimica Acta*, 43, 339-352, [https://doi.org/10.1016/0016-7037\(79\)90199-6](https://doi.org/10.1016/0016-7037(79)90199-6), 1979.
- Swart, P. K., James, N. P., Mallinson, D., Malone, M. J., Matsuda, H., and Simo, T.: 10. Data report: Carbonate mineralogy of sites drilled during leg 182, <https://doi.org/10.2973/odp.proc.sr.182.010.2002>, 2002.

- Swart, P. K., and Eberli, G.: The nature of the $\delta^{13}\text{C}$ of periplatform sediments: Implications for stratigraphy and the global carbon cycle, *Sedimentary Geology*, 175, 115-129, <https://doi.org/10.1016/j.sedgeo.2004.12.029>, 2005.
- Swart, P. K.: The geochemistry of carbonate diagenesis: The past, present and future, *Sedimentology*, 62, 1233-1304, <https://doi.org/10.1111/sed.12205>, 2015.
- Tarutani, T., Clayton, R. N., and Mayeda, T. K.: The effect of polymorphism and magnesium substitution on oxygen isotope fractionation between calcium carbonate and water, *Geochimica et Cosmochimica Acta*, 33, 987-996, [https://doi.org/10.1016/0016-7037\(69\)90108-2](https://doi.org/10.1016/0016-7037(69)90108-2), 1969.
- Van Lith, Y., Vasconcelos, C., Warthmann, R., Martins, J., and McKenzie, J.: Bacterial sulfate reduction and salinity: Two controls on dolomite precipitation in lagoa vermelha and brejo do espinho (brazil), *Hydrobiologia*, 485, 35-49, <https://doi.org/10.1007/s00792-005-0441-8>, 2002.
- Vasconcelos, C., McKenzie, J. A., Bernasconi, S., Grujic, D., and Tiens, A. J.: Microbial mediation as a possible mechanism for natural dolomite formation at low temperatures, *Nature*, 377, 220-222, <https://doi.org/10.1038/377220a0>, 1995.
- Vasconcelos, C., and McKenzie, J. A.: Microbial mediation of modern dolomite precipitation and diagenesis under anoxic conditions (lagoa vermelha, rio de janeiro, brazil), *Journal of sedimentary Research*, 67, 378-390, <https://doi.org/10.1306/d4268577-2b26-11d7-8648000102c1865d>, 1997.
- Walter, L. M., and Burton, E. A.: Dissolution of recent platform carbonate sediments in marine pore fluids, *American Journal of Science*, 290, 601-643, <https://doi.org/10.2475/ajs.290.6.601>, 1990.
- Walter, L. M., Bischof, S. A., Patterson, W. P., and Lyons, T. W.: Dissolution and recrystallization in modern shelf carbonates: Evidence from pore water and solid phase chemistry, *Philosophical Transactions of the Royal Society of London. Series A: Physical and Engineering Sciences*, 344, 27-36, <https://doi.org/10.1098/rsta.1993.0072>, 1993.
- Wefer, G., and Berger, W. H.: Stable isotope composition of benthic calcareous algae from Bermuda, *Journal of Sedimentary Research*, 51, 459-465, <https://doi.org/10.1306/212f7cac-2b24-11d7-8648000102c1865d>, 1981.
- Wefer, G., Killingley, J. S., and Lutze, G. F.: Stable isotopes in recent larger foraminifera, *Palaeogeography, Palaeoclimatology, Palaeoecology*, 33, 253-270, [https://doi.org/10.1016/0031-0182\(81\)90042-0](https://doi.org/10.1016/0031-0182(81)90042-0), 1981.

7. Summary, conclusions, and outlook

7.1 Summary and conclusions

Isotope- and trace element signals, derived from carbonates of the fossil record, are used as standard proxies to reconstruct paleoenvironmental conditions. The main goal of the “DFG-Forschergruppe 1644 Charon” is to evaluate the vulnerability of these proxies to diagenetic alterations. This thesis was part of the “Charon subproject 7”, which had the primary aim to retrace microbial effects on the early diagenesis of fine-grained carbonate sediments. This was addressed by the application of multi-proxy studies, which consisted of sediment geochemical-, pore water-, and bacterial 16S rRNA gene data. Geochemical measurements comprised bulk analytics (LECO-CNS, Isotope-Mass-Spectrometry), thin sectioning and light optical observations, as well as high-resolution optics (SEM-EDX, EPM-WDX). Pore water analytics included IC, ICP-MS, and photometrical methods. Bacterial genes were retrieved via 16S rRNA gene sequencing. The present thesis contributes to the evaluation of microbial effects on traditional isotope and trace element signals in the fossil record by addressing the following questions:

- i. What are the effects of hydrochemical pore water gradients on contemporary, fine-grained carbonate phases during the earliest stages of diagenesis?
- ii. Which impacts does the nearby environment have on carbonate mineralogy, stable isotope- and elemental concentrations? Such impacts include OM supply and physicochemistry of the overlying water body.
- iii. Which role do specific bacteria play in the establishment of hydrochemical pore water gradients and how do they affect the stability of carbonate phases?
- iv. Are geomicrobiological multi-proxy studies, consisting of sediment-geochemical-, pore water-, and bacterial 16S rRNA datasets suitable to tackle these questions?

The studies in [Chapters 2 and 3](#) focus on anoxic carbonate mud deposits of Lake Neusiedl (eastern Austria), which are primarily made up of authigenic HMC and protodolomite. The results indicated that bulk bacterial metabolic effects keep the pore water pH and the saturation of carbonate minerals low ($SI \leq 0$) within the sediment. Crystals of authigenic phases decrease in size with depth, and re-precipitation of other phases is not detectable. Furthermore, the Mg-content and the HMC/protodolomite ratio remain stable throughout the core. The bacterial community harbors a significant abundance of Cyanobacteria of the order Synechococcales in the water column and changes towards fermenting taxa (primarily Chloroflexi) with increasing sediment depth. These observations indicate a dissolution of authigenic HMC and protodolomite and changes of the organic substrate with depth. The carbonate precipitation possibly takes place in the aerobic, alkaline, and well-mixed water column. This process may be associated with CO₂ sequestration by Cyanobacteriales, which rises carbonate saturation (e.g. Thompson and Ferris, 1990). However, these studies ([Chapters 2 and 3](#)) do not suggest diagenetic changes of the bulk geochemical record of carbonate sediments from such an alkaline, lacustrine setting.

The study presented in [Chapter 4](#), provides an overview of diagenetic processes within oxic and anoxic pore spaces in Holocene sediments from the Aldabra Atoll (western Indian Ocean). This raised coral atoll was previously described as a recent analogue of Jurassic limestones (Gaillard et al., 1994; Bernier et al., 2014) with extensive deposition of fine-grained carbonate mud. These observations could not be confirmed by this study, as most of the sampling sites harbored only a thin sediment cover. However, three localities were approached and sampled (west lagoon-WL, north lagoon-NL, south lagoon-SL), which

exhibit three different sedimentary and pore water environments. Oxygenated, porous bioclastic sand is found in the WL, anoxic, porous shell debris, topped by organic-rich carbonate mud in the NL, and anoxic, non-permeable carbonate mud, traversed by mangrove roots in the SL. Overall, diagenetic features were solely detected in the WL, where carbonate particles are cemented by layers of cryptocrystalline HMC. No significant diagenetic alterations are notable in the bulk isotope- and elemental record. This absence of diagenetic changes in the bulk record, despite obvious cementation, can be explained by mass effects. Another valid point for the lack of alteration, is the chemistry of the precipitating fluid, which is possibly similar to that of the biogenic host carbonate (Swart, 2015). The formation of the cements may be linked to the contemporaneous bacterial community of the sediment, which includes phototrophic Cyanobacteriales and SRB of the order Desulfovibrionales. A second contributor to the precipitation of the diagenetic carbonate is possibly the CaCO_3 supersaturation of pore waters due to evaporation. In contrast, pore water gradients reveal aragonite dissolution at the sediment top of the SL, evident through changing elemental ratios of $\text{Sr}^{2+}/\text{Ca}^{2+}$ and $\text{Mg}^{2+}/\text{Cl}^-$. This dissolution process coincides with acidifying sulfur oxidation coupled to the presence of bacteria of the order Campylobacteriales. Overall, our observations suggest that within geologically short time scales (2357 ± 70 a), CaCO_3 precipitation within oxic pore spaces (observed in the WL) has a higher early diagenetic effect on carbonate sediments than processes involving anoxic decomposition of OM (evident in the NL and SL).

Chapter 5 deals with carbonate sediment, sampled from a saline water body in the Cinq Cases pool system, which is located in the eastern part of Aldabra. The sedimentary sequence evolves from a palustrine facies, characterized by a dark brown matrix and Characean oogonia at the bottom of the core (Unit III) to a slightly hypersaline facies, which consists of micrite peloids and milliolid foraminifera at the sediment top (Unit I). Furthermore, Unit III harbors anoxic features, such as opaque mineral phases and a high total sulfur content. In addition, blocky LMC cements are notable in Unit III. They concentrate at voids and show depleted stable isotope values ($\delta^{13}\text{C}$ and $\delta^{18}\text{O}$). In contrast, the pore water salinity within the entirely oxygenated sediment column increases with depth and conflicts with the palustrine, anoxic sedimentary facies and the meteoric LMC cements at the bottom. Abundant 16S rRNA genes of sulfate reducers within Unit III further confirm that the sediment at the bottom was (at least) temporary exposed to anoxic conditions. Overall, the sediments of Cinq Cases and their associated pore water represent different environmental stages of the Cinq Cases pool system. The apparently differing environmental interpretation between these datasets is caused by a dynamic hydrologic setting, affected by evaporation, rainfall, and occasional lagoon flooding. Such a decoupling of pore water, sediment-, and gene data underlines the necessity of multi-proxy studies in unstable and variable depositional settings to elucidate the environmental history and the time scale of early diagenetic alterations.

The final discussion in Chapter 6 integrates the results of Chapters 2-5 and evaluates potential pore water and environmental impacts on carbonate phases during early diagenesis. Such diagenetic effects are usually associated with anoxic, heterotrophic OM degradation (Suess, 1979; Walter and Burton, 1990; Walter et al., 1993; Patterson and Walter, 1994). However, the outcomes of Chapters 2-5 indicated that bulk metabolic effects cause only minor alteration of carbonate phases, which is often represented by the dissolution of metastable minerals. Those metabolic effects can be solely enhanced by the addition of external oxidants, such as sulfate (Swart, 2015). The main driver of CaCO_3 dissolution is the generation of a second acid source besides H_2CO_3 , which is represented by H_2SO_4 (Walter et al., 1993). This is a metabolic end product of SOX-bacteria, which are represented by the order Campylobacter in the previous studies.

7.2 Outlook

The outcomes of this thesis point to a minor microbial impact on the bulk geochemical record during early diagenesis. Alterations in anoxic sediments occur as dissolution of metastable carbonate minerals and can be enhanced by the input of external fluids. However, several questions of the case studies require further investigation.

First of all, the formation mechanism and origin of authigenic carbonate in Lake Neusiedl (Chapters 2 and 3) is not completely understood. This would require sampling of sediment filtrates from the water column of the shallow alkaline lake. Stable isotope data ($\delta^{13}\text{C}$ and $\delta^{18}\text{O}$) and high-resolution optics (SEM) could clarify whether carbonate precipitation in this lake involves a microbial contribution. Additionally, seasonal sampling could elucidate, if fluctuating temperature conditions cause the preferential formation of protodolomite. This is indicated by increased Ca^{2+} concentrations in the water column of Lake Neusiedl during the winter months (Wolfram and Herzig, 2013).

With respect to diagenetic studies on Aldabra (Chapter 4), a specific analysis of cryptocrystalline cements from west lagoon sediments could clarify their formation mechanism. Up to now, it is unclear, if contemporaneous sulfate reducers and/or phototrophic bacteria play a significant role in this process. The retrieval of $\delta^{13}\text{C}$ isotope data from available thin sections, e. g. via secondary-ion mass spectrometry, could solve this issue. In addition, cultivation of SOX-bacteria (of the order Campylobacter) could quantify the carbonate dissolution effects, induced by these organisms.

The study of a saline water body at Cinq Cases (Chapter 5) also leaves some questions unanswered. A crucial point is the sampling of just one set of cores (one core for bacterial gene- and one for geoscientific data) at the end of the dry season. This represents a limitation of the lateral extend of the sediments, and time frame of diagenesis. Hence, it would be interesting to gather information about the change of pore water and water column physicochemistry during different seasons. This could be achieved via repeated measurements at Cinq Cases and would, additionally, enable more precise statements about the hydrologic environment.

References

- Bernier, P., Barale, G., Bourseau, J.-P., Buffetaut, E., Gaillard, C., Gall, J.-C., and Wenz, S.: The lithographic limestones of cerin (southern jura mountains, france). A synthetic approach and environmental interpretation, *Comptes Rendus Palevol*, 13, 383-402, <https://doi.org/10.1016/j.crpv.2014.01.006>, 2014.
- Gaillard, C., Bernier, P., and Gruet, Y.: Le lagon d'aldabra (seychelles, océan indien), un modèle pour le paléoenvironnement de cerin (kimméridgien supérieur, jura méridional, france), *Geobios*, 27, 331-348, [https://doi.org/10.1016/s0016-6995\(94\)80050-2](https://doi.org/10.1016/s0016-6995(94)80050-2), 1994.
- Patterson, W. P., and Walter, L. M.: Syndepositional diagenesis of modern platform carbonates: Evidence from isotopic and minor element data, *Geology*, 22, 127-130, [https://doi.org/10.1130/0091-7613\(1994\)022<0127:sdompc>2.3.co;2](https://doi.org/10.1130/0091-7613(1994)022<0127:sdompc>2.3.co;2), 1994.
- Suess, E.: Mineral phases formed in anoxic sediments by microbial decomposition of organic matter, *Geochimica et Cosmochimica Acta*, 43, 339-352, [https://doi.org/10.1016/0016-7037\(79\)90199-6](https://doi.org/10.1016/0016-7037(79)90199-6), 1979.
- Swart, P. K.: The geochemistry of carbonate diagenesis: The past, present and future, *Sedimentology*, 62, 1233-1304, <https://doi.org/10.1111/sed.12205>, 2015.
- Thompson, J., and Ferris, F.: Cyanobacterial precipitation of gypsum, calcite, and magnesite from natural alkaline lake water, *Geology*, 18, 995-998, [https://doi.org/10.1130/0091-7613\(1990\)018<0995:cpogca>2.3.co;2](https://doi.org/10.1130/0091-7613(1990)018<0995:cpogca>2.3.co;2), 1990.
- Walter, L. M., and Burton, E. A.: Dissolution of recent platform carbonate sediments in marine pore fluids, *American Journal of Science*, 290, 601-643, <https://doi.org/10.2475/ajs.290.6.601>, 1990.
- Walter, L. M., Bischof, S. A., Patterson, W. P., and Lyons, T. W.: Dissolution and recrystallization in modern shelf carbonates: Evidence from pore water and solid phase chemistry, *Philosophical Transactions of the Royal Society of London. Series A: Physical and Engineering Sciences*, 344, 27-36, <https://doi.org/10.1098/rsta.1993.0072>, 1993.
- Wolfram, G., and Herzig, A.: Nährstoffbilanz Neusiedler See, *Wiener Mitteilungen*, 228, 317-338, 2013.

Appendices

Appendix A

Supplementary information for Chapters 2 and 3:

Authigenic formation of Ca-Mg carbonates in the shallow alkaline Lake Neusiedl, Austria

Dario Fussmann, Avril Jean Elisabeth von Hoyningen-Huene, Andreas Reimer, Dominik Schneider, Hana Babková, Robert Peticzka, Andreas Maier, Gernot Arp, Rolf Daniel, and Patrick Meister

Bacterial succession along a pore water gradient at Lake Neusiedl in Austria

Avril Jean Elisabeth von Hoyningen-Huene, Dominik Schneider, Dario Fussmann, Andreas Reimer, Gernot Arp, and Rolf Daniel

Table A1: data plotted in Figure 2.3

Depth [LN-K04; cm b.s.]	Porosity	C _{org} :N _{tot}	C _{org} [weight %]	C _{carb} [weight %]	S _{tot} [weight %]
1.00	0.72				
2.50		9.80	2.01	7.20	0.12
5.00	0.66	9.40	2.20	7.03	0.13
7.50		9.71	2.04	7.20	0.13
10.00	0.62	9.58	2.05	7.54	0.13
12.50		9.95	2.17	7.26	0.12
15.00	0.65	9.69	1.87	7.23	0.12
17.50		10.58	2.00	7.10	0.15
20.00	0.63	11.34	1.95	6.38	0.15
22.50		11.60	2.10	5.96	0.18
25.00	0.65	12.03	2.85	5.68	0.24
27.50		12.71	3.70	5.77	0.24
30.00	0.62	13.18	4.02	5.56	0.28

Table A2: data plotted in Figure 2.7

Depth [K04; cm b.s.]	Calcite [wt %]	HMC [wt %]	Protodolomite [wt %]	Muscovite [wt %]	Feldspar [wt %]	Quartz [wt %]	Clay [wt %]
2.5	5.1	33.3	21.7	18.1	6.0	12.0	3.6
5.0	5.7	34.1	18.8	12.9	6.5	13.9	6.3
7.5	5.7	31.9	22.4	21.9	5.6	11.1	4.5
10.0	5.7	34.4	22.8	17.0	4.3	10.3	4.4
12.5	7.1	29.8	23.6	13.9	8.2	11.2	6.1
15.0	5.0	35.6	19.7	13.2	6.2	13.8	6.2
17.5	5.6	32.5	21.0	19.8	8.0	12.2	4.5
20.0	7.4	26.0	19.7	18.5	7.1	14.3	4.9
22.5	6.5	24.4	18.8	14.6	9.2	18.3	6.7
25.0	7.6	21.0	18.7	19.4	10.9	18.0	5.6
27.5	8.6	23.7	15.8	17.3	9.9	16.1	7.5
30.0	7.4	23.7	15.3	21.7	10.6	15.6	6.6
32.5	8.6	21.0	17.2	22.5	9.7	13.9	6.5

Table A3: data plotted in Figure 2.8

Depth [K04; cm b.s.]	HMC [Mg/(Ca+Mg)]	Protod. [Mg/(Ca+Mg)]	(HMC+Protod.)/CC	HMC/Protod.
2.50	16.65	44.51	10.84	1.54
5.00	17.14	47.42	9.34	1.81
7.50	18.41	46.52	9.56	1.42
10.00	18.45	47.40	10.10	1.51
12.50	17.28	47.89	7.54	1.26
15.00	15.85	49.12	11.17	1.81
17.50	15.46	48.90	9.58	1.55
20.00	14.77	43.70	6.18	1.32
22.50	17.02	48.65	6.69	1.30
25.00	18.14	49.04	5.23	1.12
27.50	17.19	47.83	4.60	1.50
30.00	16.39	49.18	5.29	1.55
32.50	20.37	49.13	4.47	1.22

Table A4: data plotted in Figure 2.10

Depth [cm b. s.]	SI _{Aragonite} [log IAP/KT]	SI _{Calcite} [log IAP/KT]	SI _{Protodolomite} [log IAP/KT]	SI _{Dolomite} [log IAP/KT]
-5.00	0.95	1.09	2.92	3.49
-1.00	0.70	0.84	2.40	2.97
2.00	-0.46	-0.32	-0.05	0.52
4.50	-0.33	-0.18	0.15	0.72
7.00	-0.13	0.02	0.42	0.99
10.00	-0.06	0.09	0.54	1.11
13.00	-0.06	0.09	0.55	1.12
16.00	-0.01	0.13	0.65	1.23
19.00	0.02	0.16	0.73	1.30
22.00	0.01	0.16	0.73	1.30
25.00	-0.01	0.14	0.71	1.28
27.50	0.01	0.16	0.74	1.31

Table A5: data plotted in Figure 2.9

Depth [cm b. s.]	TA [meq L ⁻¹]	pH	SiO ₂ [mmol L ⁻¹]	Ca ²⁺ [mmol L ⁻¹]	Mg ²⁺ [mmol L ⁻¹]	Na ⁺ [mmol L ⁻¹]	K ⁺ [mmol L ⁻¹]	Cl ⁻ [mmol L ⁻¹]	Eh [mV]
-5.00	11.18	9.02	3.95	0.33	5.13	14.35	0.87	7.08	
-1.00	11.18	8.67	3.95	0.33	5.09	14.34	0.87	7.08	423.00
2.00	11.25	7.31	3.88	0.42	4.99	14.30	0.90	7.09	-234.30
4.50	11.81	7.37	3.60	0.48	4.88	14.23	0.91	7.13	-219.60
7.00	12.56	7.46	2.80	0.58	4.46	14.18	0.92	7.17	
10.00	14.06	7.49	1.84	0.59	4.25	14.32	0.91	7.24	-214.20
13.00	14.81	7.51	1.45	0.54	4.06	14.68	0.93	7.37	
16.00	15.75	7.54	1.34	0.53	4.07	15.34	0.95	7.47	-214.10
19.00	16.00	7.59	1.54	0.51	4.02	16.15	0.96	7.70	
22.00	16.13	7.60	1.76	0.49	3.94	17.02	1.01	7.97	-186.40
25.00	16.31	7.60	1.95	0.46	3.84	18.43	1.08	8.31	-109.30
27.50	16.75	7.60	2.41	0.48	3.99	19.92	1.06	8.78	-121.10

NH ₄ ⁺ [mmol L ⁻¹]	NO ₂ ⁻ [μmol L ⁻¹]	Fe ²⁺ [μmol L ⁻¹]	Mn ²⁺ [μmol L ⁻¹]	PO ₄ ³⁻ [mmol L ⁻¹]	ΣH ₂ S [mmol L ⁻¹]	SO ₄ ²⁻ [mmol L ⁻¹]	CH ₄ [μmol L ⁻¹]	DIC [mmol L ⁻¹]
0.00	0.05	0.18	0.01	0.00	1.96	3.95	64.12	
0.03	0.13	0.24	0.02	0.00	0.04	3.95	14.74	11.71
0.03	0.86	1.35	0.02	0.00	0.00	3.88	157.33	13.59
0.13	0.22	0.50	0.04	0.01	0.03	3.60	210.67	15.37
0.22	0.19	0.35	0.04	0.01	0.25	2.80	227.79	14.94
0.33	0.00	0.22	0.04	0.01	0.89	1.84		17.33
0.36	0.00	0.47	0.04	0.01	0.93	1.45		18.01
0.37	0.00	0.25	0.07	0.02	0.83	1.34		
0.37	0.00	0.28	0.07	0.02	0.85	1.54		
0.36	0.00	0.17	0.07	0.01	0.72	1.76		
0.36	0.00	0.25	0.04	0.01	0.50	1.95		
0.36	0.00	0.31	0.07	0.01	0.88	2.41		

Table A6: data plotted in Figure 2.11

Depth [LN-K01; cm]	Acidobacteria [abundance %]	Actinobacteria	Bacteroidetes	Chloroflexi	Cyanobacteria	Proteobacteria-Alpha	Proteobacteria-Delta	Proteobacteria-Gamma	rare taxa
10.000	0.787	42.018	8.302	2.548	1.870	21.747	0.671	9.624	8.846
0.000	10.045	6.905	6.710	15.093	2.300	2.228	6.075	17.359	23.315
-5.000	8.065	4.026	1.520	10.020	0.244	1.413	9.690	36.554	21.293
-10.000	9.663	3.438	1.476	12.872	0.139	1.273	10.073	30.411	22.514
-15.000	9.858	4.357	0.906	15.268	0.118	1.195	10.072	29.819	23.008
-20.000	11.390	3.433	1.004	24.294	0.048	1.603	11.576	17.684	22.453
-25.000	17.477	3.983	0.984	35.435	0.012	1.822	5.369	14.076	18.104
-30.000	14.053	1.811	2.098	46.851	0.007	1.220	8.465	6.332	14.627
-35.000	14.421	5.538	2.389	38.433	0.004	1.070	9.434	6.813	16.138

Depth [LN-K02; cm]	Acidobacteria [abundance %]	Actinobacteria	Bacteroidetes	Chloroflexi	Cyanobacteria	Proteobacteria-Alpha	Proteobacteria-Delta	Proteobacteria-Gamma	rare taxa
10.000	0.777	46.238	7.043	3.078	1.763	19.742	0.668	7.923	8.933
0.000	8.326	7.472	6.231	17.785	2.012	1.965	5.309	14.930	25.962
-5.000	9.337	6.540	4.918	16.497	0.323	2.433	9.161	18.043	24.160
-10.000	8.639	5.425	4.038	16.015	0.868	2.188	10.102	20.102	25.083
-15.000	8.980	5.685	2.027	12.790	0.867	1.800	11.316	21.631	28.133
-17.500	10.866	2.006	0.097	10.267	1.563	0.719	2.520	50.563	20.659
-20.000	13.455	2.029	1.812	46.252	0.085	1.397	8.315	9.973	13.361
-22.500	11.247	2.293	3.277	45.635	0.600	1.854	9.157	6.136	15.198
-25.000	11.092	1.658	2.841	48.791	0.016	1.394	9.626	5.915	12.578
-27.500	11.888	3.848	2.257	44.475	0.128	1.273	9.156	6.600	15.846
-30.000	9.312	2.662	1.665	36.904	0.233	1.104	8.458	22.832	13.037
-32.500	8.395	5.544	1.024	28.052	0.614	0.699	4.735	35.350	12.714

Table A7: data plotted in Figure 2.11

Depth	aerobic	anaerobic	facultative	unknown
[LN-K01; cm]	[abundance %]			
10.00	65.72	7.83	17.97	8.48
0.00	18.49	28.78	29.64	23.09
-5.00	8.21	57.00	15.85	18.94
-10.00	6.86	58.80	14.57	19.77
-15.00	7.05	63.66	9.51	19.77
-20.00	6.83	57.60	15.98	19.60
-25.00	7.10	70.50	6.20	16.21
-30.00	3.67	76.03	7.84	12.45
-35.00	4.35	74.06	8.55	13.04

Depth	aerobic	anaerobic	facultative	unknown
[LN-K02; cm]	[abundance %]			
10.00	67.43	9.10	14.88	8.59
0.00	16.56	30.80	27.58	25.07
-5.00	13.51	36.81	27.43	22.26
-10.00	12.40	39.69	25.40	22.51
-15.00	12.18	41.43	21.53	24.87
-17.50	4.57	62.14	14.25	19.04
-20.00	3.88	71.84	12.05	12.22
-22.50	4.61	72.39	9.05	13.95
-25.00	3.99	77.58	6.86	11.56
-27.50	3.83	76.71	5.36	14.10
-30.00	3.36	70.75	15.33	10.56
-32.50	3.69	65.23	21.63	9.46

Appendix B

Supplementary information for Chapter 4:

Tracing early diagenesis: Pore water gradients and bacterial communities within Holocene carbonate sediments in the lagoon of Aldabra (Seychelles)

Dario Fussmann, Avril Jean Elisabeth von Hoyningen-Huene, Andreas Reimer, Dominik Schneider, Volker Karius, Sylvia Riechelmann, Volker Liebetrau, Torben Gentz, Rolf Daniel, and Gernot Arp

Table B1: data plotted in Figure 4.8

Sample (core-depth)	Calcite (CaCO ₃ , wt%)	Aragonite (CaCO ₃ , wt%)	Mg-Calcite (Mg _{0.1} Ca _{0.9} CO ₃ , wt%)	Other phases
WL-K04-0-5	17.3	65.2	13.4	4.1
WL-K04-5-10	17.1	63.8	15.2	3.8
WL-K04-10-15	22.1	62.5	11.5	3.9
WL-K04-15-20	16.4	63.6	16.4	3.7
WL-K04-20-25	16.3	64.3	15.3	4.1
WL-K04-25-30	16.3	68.2	11.5	4.0
WL-K04-30-35	17.3	66.2	12.5	4.0
WL-K04-35-40	22.8	57.0	16.1	4.1
WL-K04-40-45	20.4	62.0	13.5	4.1
WL-K04-45-50	9.6	73.0	13.5	3.9
NL-K04-0-3	22.7	42.3	4.5	30.5
NL-K04-3-6	21.4	51.8	3.3	23.5
NL-K04-6-8	23.3	40.1	5.8	30.8
NL-K04-8-10	21.8	50.7	3.9	23.6
NL-K04-10-12	28.0	53.3	5.4	13.3
NL-K04-12-17	29.1	57.3	4.7	8.9
NL-K04-17-22.5	30.3	59.6	2.9	7.3
NL-K04-22.5-26.5	30.8	55.0	5.6	8.7
NL-K04-26.5-31.5	32.8	58.9	2.9	5.3
NL-K04-31.5-36.5	29.3	62.5	3.9	4.3
NL-K04-36.5-42.5	44.9	47.9	2.9	4.3
NL-K04-42.5-46	30.9	56.9	5.8	6.4
NL-K04-46-49.5	29.4	53.4	5.5	11.8
SL-K04-0-5	33.6	54.1	5.6	6.7
SL-K04-5-10	28.4	57.8	6.6	7.1
SL-K04-10-15	28.6	59.1	4.7	7.5
SL-K04-15-20	32.0	56.5	3.8	7.7
SL-K04-20-25	27.2	60.0	4.7	8.2
SL-K04-25-30	31.1	55.6	5.7	7.6
SL-K04-30-35	38.1	48.6	6.7	6.7
SL-K04-35-40	27.0	60.8	6.8	5.4
SL-K04-40-44	29.6	57.3	6.7	6.4

Table B2: data plotted in Figure 4.9

Sample [core-depth]	C _{tot} [wt %]	C _{org} [wt %]	C _{karb} [wt %]	CaCO ₃ [wt %]	N _{tot} [wt %]	S _{tot} [wt %]	δ ¹³ C[‰ VPDB]	δ ¹⁸ O[‰ VPDB]
WL-K04-0-5	11.95	0.44	11.51	95.91	0.047	0.12	1.25	-2.43
WL-K04-5-10	11.94	0.4	11.54	96.16	0.043	0.09	1.42	-2.37
WL-K04-10-15	11.97	0.44	11.53	96.08	0.044	0.12	0.85	-2.32
WL-K04-15-20	11.96	0.4	11.56	96.33	0.04	0.13	1.59	-2.18
WL-K04-20-25	11.98	0.47	11.51	95.91	0.042	0.11	1.41	-2.37
WL-K04-25-30	11.94	0.42	11.52	96.00	0.041	0.14		
WL-K04-30-35	11.93	0.41	11.52	96.00	0.041	0.13	1.60	-2.32
WL-K04-35-40	11.91	0.4	11.51	95.91	0.039	0.14	1.55	-2.41
WL-K04-40-45	11.89	0.38	11.51	95.91	0.037	0.14	2.02	-2.14
WL-K04-45-50	11.89	0.36	11.53	96.08	0.033	0.14		
NL-K04-0-3	19.43	11.09	8.34	69.50	0.581	1.04	-0.79	-3.28
NL-K04-3-6	16.49	7.29	9.2	76.66	0.434	0.73	-0.77	-3.24
NL-K04-6-8	18.96	10.65	8.31	69.25	0.596	0.89	-0.71	-3.18
NL-K04-8-10	17.44	8.27	9.17	76.41	0.406	0.64	-1.08	-2.84
NL-K04-10-12	13.43	3.03	10.4	86.66	0.167	0.37	-0.82	-2.91
NL-K04-12-17	12.34	1.41	10.93	91.08	0.089	0.2	-1.80	-2.40
NL-K04-17-22.5	12.4	1.27	11.13	92.75	0.067	0.17	-0.59	-2.02
NL-K04-22.5-26.5	12.48	1.52	10.96	91.33	0.087	0.21	-1.10	-2.52
NL-K04-26.5-31.5	12.05	0.69	11.36	94.66	0.05	0.13	-2.75	-2.96
NL-K04-31.5-36.5	12.17	0.68	11.49	95.75	0.042	0.14	-1.81	-2.42
NL-K04-36.5-42.5	12.13	0.64	11.49	95.75	0.04	0.12	-1.22	-2.03
NL-K04-42.5-46	12.47	1.24	11.23	93.58	0.067	0.26	-0.35	-2.02
NL-K04-46-49.5	13.81	3.22	10.59	88.25	0.19	0.39	-1.00	-2.81
SL-K04-0-5	12.36	1.16	11.20	93.3	0.095	0.18	0.07	-2.81
SL-K04-5-10	12.39	1.24	11.15	92.9	0.093	0.21	0.14	-2.66
SL-K04-10-15	12.67	1.57	11.10	92.5	0.092	0.22	0.07	-2.74
SL-K04-15-20	12.70	1.62	11.08	92.3	0.094	0.24	0.20	-2.86
SL-K04-20-25	12.46	1.44	11.02	91.8	0.092	0.25	0.11	-2.83
SL-K04-25-30	12.42	1.33	11.09	92.4	0.084	0.24	0.00	-2.75
SL-K04-30-35	12.23	1.03	11.20	93.3	0.063	0.16	-0.16	-2.71
SL-K04-35-40	12.07	0.72	11.35	94.6	0.048	0.14	-0.38	-2.43
SL-K04-40-44	12.26	1.03	11.23	93.6	0.062	0.15	-0.59	-2.74

Table B3: data plotted in Figure 4.11

Sample [core-nr]	Salinity [g kg ⁻¹]	pH	Eh [mV]	TA [mmol kg ⁻¹]	ΣH ₂ S [mmol kg ⁻¹]	SO ₄ ²⁻ _{red} [mmol kg ⁻¹]	δ ¹³ C [‰ VPDB]	δ ¹⁸ O [‰ VSMOW]	Ca ²⁺ _{exc} [mmol kg ⁻¹]	SI _{Ar} [log IAP/KT]
ALD_WL	36.05	7.98	199	2.67	0	-0.03			-0.05	0.67
WL_K05_01	41.46	7.17	238	5.12	0	-0.03			-0.03	0.15
WL_K04_02	41.26	7.33	233	4.94	0	0.22	-4.69	0.9	-0.45	0.23
WL_K05_03	38.28	7.27	248	5.14	0	-0.02			-0.02	0.2
WL_K05_04	37.28	7.3	256	5.12	0	-0.03			0.02	0.16
WL_K04_05	36.27	7.4	261	4.9	0	0.05			-0.09	0.27
WL_K04_06		7.41	265							
WL_K04_07	36.81	7.43	268	4.41	0	-0.02	-5.29	0.59	-0.12	0.26
WL_K04_08	39.48	7.44	272	4.27	0	0.02	-5.49	0.69	-0.21	0.27
WL_K04_09	40.3	7.44	289	4.25	0	0.01	-5.65	0.83	-0.15	0.27
WL_K04_10	40.76	7.45	290	4.23	0	0.15	-6.38	0.82	-0.25	0.28
WL_K04_11	40.71	7.43	303	4.11	0	0.17	-2.21	0.86	-0.29	0.24
WL_K04_12	40.83	7.49	318	4.08	0	0.11	-4.03	0.86	-0.31	0.3
ALD_NL	36.38	7.65	180	2.61	0	0.05	-3.5	0.99	0.02	0.21
NL_K04_T	36.38	7.38		2.9	0	-0.01	-5.02	0.2	0.05	0.04
NL_K04_02	36.49	7.09	-222	8.04	1.11	1.76	-8.47	1	0.14	0.1
NL_K04_03	36.54	7.02	-229	9.72	1.42	2.32			0.1	0.12
NL_K04_04	36.5	7.02		9.44	1.94	2.37	-11.02	0.99	0.11	0.08
NL_K04_05	36.52	7.01	-233	8.57	2.87	1.62			0.18	-0.02
NL_K04_06	36.49	7.01	-214	7.01	2.81	0.94	-9.77	0.92	0.16	-0.14
NL_K04_07	36.58	7.03	-204	6.62	2.51	0.69	-11.11	0.93	0.13	-0.13
NL_K04_08	36.63	7.09	-202	6.65	2.52	0.62			0.09	-0.08
NL_K04_09	36.62	7.09	-199	6.56	2.48	0.64			0.09	-0.09
NL_K04_10	36.63	7.17	-182	6.04	2.18	0.35			0.14	-0.04
NL_K04_11	36.73	7.19	-173	5.04	1.33	0.03			0.1	-0.06
NL_K04_12	36.77	7.2	-157	4.9	0.63	0.01			0.06	-0.01
ALD_SL_01	38.07	8.05	187.8	2.53	0	-0.04	-2.2	1.48	-0.18	0.55
ALD_SL_02	41.27	7.94	201.5	3.4	0	-0.04	-5.2	2.04	0.24	0.7
SL-K07_01	40.24	7.04	-243	7.15	0.14	-0.55	-5.24	1.72	1.06	0.13
SL-K07_02	39.72	7.07	-269	6.91	0.16	1.15	-7.31	1.63	0.06	0.11
SL-K07_03	39.39	7.11	-283	6.7	0.64	1.32			0.02	0.11
SL-K07_04	39.05	7.18	-288	5.73	0.47	1.14	-9.26	1.55	0.03	0.11
SL-K07_05	38.71	7.21	-286	4.92	0.33	0.75	-8.83	1.49	0.03	0.08
SL-K07_06	38.54	7.21	-289	4.81	0.32	0.11	-8.59		0.07	0.07
SL-K07_07	38.38	7.23	-294	4.73	0.2	0.09	-8.05	1.43	0.04	0.09
SL-K07_08	38.23	7.24	-306	4.71	0.24	0.19	-8.01	1.36	0.06	0.09
SL-K07_09	38.25	7.16	-304	4.72	0.39	0.37			0.02	0
SL-K07_10	38.2	7.15	-307	4.81	0.4	0.52	-7.88	1.42	0.02	0
SL-K07_11	38.19	7.12	-309	5.83	0.54	0.51	-10.8	1.52	0.04	0.04

Table B4: data plotted in Figure 4.11; WC = water column

Sample [rel abundance %]	depth [cm]	Oxygenic phototroph	Aerobic heterotroph	facultative	SOX	SRB	Fermenters	unknown	no blast	rare
WL-0	WC	0.14	45.88	39.85	2.88	0.41	0.80	0.13	1.80	8.10
WL-1	0.00	1.74	33.32	26.43	0.01	10.53	1.16	0.72	16.36	9.74
WL-2	2.50	0.41	20.68	44.77	0.00	13.14	5.03	0.80	9.12	6.03
WL-3	5.00	0.01	22.13	48.69	0.00	0.08	5.78	0.84	10.54	11.93
WL-4	7.50	0.00	15.55	58.30	0.00	0.04	5.16	0.62	9.38	10.95
WL-5	10.00	0.00	16.77	41.68	0.00	0.23	22.76	0.66	7.75	10.15
WL-6	12.50	0.00	9.61	75.59	0.00	0.03	2.36	0.44	7.57	4.39
WL-7	17.50	0.00	4.75	71.95	0.00	0.04	17.59	0.20	3.23	2.24
WL-8	22.50	0.01	21.71	38.05	0.00	0.67	15.28	1.48	12.30	10.51
WL-9	22.50	0.00	16.84	37.53	0.00	0.13	21.09	0.86	12.69	10.87
WL-10	27.50	0.00	20.86	38.31	0.00	0.09	8.53	1.17	13.04	18.00
WL-11	37.50	0.00	9.30	77.03	0.00	0.04	2.93	0.80	4.54	5.37
WL-12	42.50	0.00	28.67	23.72	0.00	0.24	11.02	1.62	16.85	17.87
NL-0	WC	0.02	8.16	45.91	28.25	1.76	5.81	0.15	3.15	6.78
NL-1	0.00	2.20	14.10	5.61	1.04	31.65	14.30	7.09	9.87	14.14
NL-2	2.50	0.57	11.37	2.08	0.88	26.56	16.25	1.11	19.28	21.90
NL-3	5.00	0.67	10.54	2.21	1.26	24.46	24.68	2.01	18.78	15.39
NL-4	7.50	1.04	8.31	3.26	0.52	29.08	16.30	2.44	27.69	11.36
NL-5	10.00	0.80	8.62	5.29	0.34	44.41	17.74	2.79	10.61	9.41
NL-6	12.50	0.54	6.52	7.21	2.73	18.51	37.19	0.99	14.98	11.33
NL-7	17.50	0.96	6.09	5.65	0.45	55.54	14.58	2.86	3.04	10.83
SL-0	WC	0.02	8.16	45.91	28.25	1.76	5.81	0.15	3.15	6.78
SL-1	0.00	3.13	14.62	15.65	6.58	23.30	18.96	3.22	3.41	11.14
SL-2	2.50	5.19	15.52	25.11	0.28	18.06	15.81	5.21	4.57	10.25
SL-3	5.00	4.34	16.45	7.90	0.50	12.01	29.73	7.06	9.71	12.28
SL-4	7.50	2.14	9.62	18.04	0.17	30.65	21.49	4.29	5.06	8.53
SL-5	10.00	0.96	5.98	8.13	1.87	39.68	21.87	2.10	7.13	12.28
SL-6	12.50	0.58	6.85	20.20	0.06	26.75	26.11	3.23	6.91	9.31
SL-7	17.50	0.01	0.88	83.89	0.01	1.91	5.31	2.84	2.40	2.74
SL-8	22.50	0.00	0.28	76.43	0.00	0.41	19.28	1.71	0.63	1.27
SL-9	27.50	0.01	0.39	83.42	0.00	0.62	11.90	1.57	1.04	1.05
SL-10	32.50	0.00	0.20	53.04	0.00	0.05	44.05	0.94	0.89	0.83
SL-11	37.50	0.00	0.43	90.78	0.00	0.13	5.04	0.76	1.26	1.60

Table B5: data plotted in Figure 4.12, HT = High Tide, LT = Low Tide

Sample [core-depth]	depth [cm]	Sr/Ca [mM/m]	Ca/Cl [mM/m]	Mg/Cl [mM/m]
ALD_WL	WC	8.8	18.8	97.3
WL_K05_01	3.0	9.2	18.8	97.4
WL_K04_02	6.0	9.1	18.2	97.5
WL_K05_03	9.0	9.4	18.8	97.4
WL_K05_04	13.0	9.4	18.9	97.4
WL_K04_05	17.0	9.3	18.7	97.4
WL_K04_06	21.0			
WL_K04_07	25.0	9.2	18.7	97.3
WL_K04_08	29.5	9.3	18.5	97.4
WL_K04_09	34.0	9.3	18.6	97.3
WL_K04_10	38.5	9.2	18.5	97.4
WL_K04_11	43.0	9.2	18.4	97.3
WL_K04_12	47.5	9.2	18.4	97.4
ALD_NL	WC	8.9	18.9	97.5
NL_K04_T	0.0	8.8	19.0	97.5
NL_K04_02	2.0	8.8	19.1	97.6
NL_K04_03	4.5	8.8	19.1	97.6
NL_K04_04	7.0	8.8	19.1	97.6
NL_K04_05	11.0	8.8	19.2	97.6
NL_K04_06	15.0	8.8	19.2	97.6
NL_K04_07	19.0	8.8	19.1	97.7
NL_K04_08	24.0	8.8	19.0	97.7
NL_K04_09	29.0	8.8	19.0	97.8
NL_K04_10	34.0	8.8	19.1	97.7
NL_K04_11	39.0	8.8	19.1	97.6
NL_K04_12	44.0	8.9	19.0	97.6
ALD_SL_01	WC-HT	9.0	18.6	97.4
ALD_SL_02	WC-LT	8.9	19.3	97.2
SL-K07_01	2.5	8.9	20.6	97.9
SL-K07_02	5	9.0	19.0	97.6
SL-K07_03	7.5	8.9	18.9	97.6
SL-K07_04	10	8.9	18.9	97.4
SL-K07_05	14	8.9	18.9	97.4
SL-K07_06	18	8.9	19.0	97.5
SL-K07_07	22	8.8	18.9	97.4
SL-K07_08	26	8.9	19.0	97.4
SL-K07_09	30	8.9	18.9	97.4
SL-K07_10	34	8.9	18.9	97.3
SL-K07_11	37.5	8.9	19.0	97.5

Appendix C

Supplementary information for Chapter 5:

Decoupling of pore water chemistry, bacterial community profiles, and carbonate mud diagenesis in a land-locked pool on Aldabra (Seychelles, Indian Ocean)

Dario Fussmann, Avril J. E. von Hoyningen-Huene, Andreas Reimer, Dominik Schneider, Volker Karius, Sylvia Riechelmann, Chelsea Pederson, Peter K. Swart, Rolf Daniel and Gernot Arp

Table C1: data plotted in Figure 5.2

Sample	Depth [cm bsf]	C _{org} [wt%]	C _{carb} [wt%]	CaCO ₃ [wt%]	N _{tot} [wt%]	S _{tot} [wt %]	C _{org} /N _{tot}	δ ¹³ C _{carb} [VPDB‰]	δ ¹⁸ O _{carb} [VPDB‰]	δ ¹³ C _{org} [VPDB‰]	δ ¹⁵ N _{tot} [ATM‰]
CC-K04-0-3	3.00	8.97	6.96	57.99	1.02	1.00	8.77	-4.51	-1.77	-18.49	3.97
CC-K04-3-5.5	5.50	7.48	7.67	63.91	0.85	0.91	8.76	-4.61	-1.49	-19.09	3.57
CC-K04-5.5-8	8.00	6.46	7.99	66.58	0.71	0.81	9.09	-4.58	-1.53	-19.9	3.52
CC-K04-8-11.5	11.50	4.9	8.48	70.67	0.47	0.74	10.33	-4.68	-1.54	-21.56	3.69
CC-K04-11.5-15	15.00	3.4	8.89	74.08	0.28	0.62	11.88	-4.58	-1.47	-22.46	4.24
CC-K04-15-18.5	18.50	2.31	8.90	74.17	0.18	0.45	12.83	-2.60	-1.74	-21.21	3.46
CC-K04-18.5-22	22.00	4.10	5.74	47.83	0.18	0.52	21.80	-2.19	-1.92	-26.56	3.93
CC-K04-22-25.5	25.50	10.57	0.00	0.00	0.65	1.09	16.03			-26.08	4.01
CC-K04-25.5-28.5	28.50	15.40	0.00	0.00	0.92	1.78	16.63			-23.92	4.27
CC-K04-28.5-32	32.00	8.84	3.38	28.16	0.44	1.49	19.95	-6.19	-3.76	-26.32	5.03
CC-K04-32-35	35.00	10.09	3.80	31.67	0.40	2.32	24.97	-9.58	-3.42	-25.72	5.11

Table C2: data plotted in Figure 5.2

Sample	Depth [cm bsf]	Aragonite [wt%]	Calcite [wt%]	HMC [wt%]	Other Phases [%]
CC-K04-0-3	3.00	45.75	9.02	3.22	42.00
CC-K04-3-5.5	5.50	48.29	10.65	4.97	36.08
CC-K04-5.5-8	8.00	51.22	10.24	5.12	33.42
CC-K04-8-11.5	11.50	57.74	7.76	5.17	29.33
CC-K04-11.5-15	15.00	59.97	7.94	6.17	25.92
CC-K04-15-18.5	18.50	54.70	10.20	9.27	25.84
CC-K04-18.5-22	22.00	27.26	14.35	6.22	52.17
CC-K04-22-25.5	25.50	0.00	0.00	0.00	100.00
CC-K04-25.5-28.5	28.50	0.00	0.00	0.00	100.00
CC-K04-28.5-32	32.00	7.14	21.03	0.00	71.83
CC-K04-32-35	35.00	4.91	18.29	8.47	68.33

Table C3: data plotted in Figure 5.8

Sample	Depth [cm bsf]	Salinity [g kg ⁻¹]	pH	Eh [mV]	TA [mmol kg ⁻¹]	Ca ²⁺ [mmol kg ⁻¹]	Mg ²⁺ [mmol kg ⁻¹]	Na ⁺ [mmol kg ⁻¹]	K ⁺ [mmol kg ⁻¹]	Cl ⁻ [mmol kg ⁻¹]
ALD_CC_02	WC	45.37	8.53	186.60	3.26	13.50	68.26	604.54	12.91	704.18
CC_K04_01	2.0	56.47	7.00	-41.00	12.72	14.09	88.84	748.62	15.89	869.41
CC_K04_02	4.5	65.49	6.90	85.00	8.10	16.68	103.42	868.18	18.01	1010.62
CC_K04_03	7.0	73.65	6.86	126.00	6.75	19.02	115.78	978.50	20.09	1139.16
CC_K04_04	10.0	80.20	6.91	132.00	5.69	21.10	125.40	1067.08	21.63	1242.87
CC_K04_05	13.0	82.43	6.96	148.00	4.91	21.81	127.80	1099.27	22.33	1280.68
CC_K04_06	16.5	82.53	6.95	147.00	4.64	22.16	126.88	1101.53	22.48	1282.74
CC_K04_07	20.0	82.37	6.87	151.00	4.63	22.45	126.65	1098.66	22.52	1280.46
CC_K04_08	23.5	81.98	6.88		4.54	22.30	127.24	1091.60	22.28	1274.19
CC_K04_09	27.0	82.01	6.85		4.69	22.29	127.27	1092.58	22.15	1274.41
CC_K04_10	30.5	80.38	6.83	146.00	4.93	22.00	124.48	1070.91	21.84	1249.55

$\Sigma\text{H}_2\text{S}$ [mmol kg ⁻¹]	SO_4^{2-} [mmol kg ⁻¹]	$\text{Cl}^- / \text{SO}_4^{2-}$	NH_4^+ [mmol kg ⁻¹]	SiO_2 [mmol kg ⁻¹]	$\delta^{13}\text{C}$ [VPDB‰]	$\delta^{18}\text{O}$ [VSMOW‰]
0.00	36.42	7.14	0.02	0.01	-9.37	2.17
0.25	43.43	7.39	0.43	0.17	-5.54	2.82
0.01	53.71	6.94	0.39	0.12		
0.00	60.58	6.94	0.35	0.08	-7.19	2.99
0.00	65.86	6.96	0.18	0.06		3.06
0.00	66.74	7.08	0.07	0.05	-7.46	3.04
0.00	66.66	7.10	0.06	0.05	-8.53	3.04
0.00	66.41	7.12	0.03	0.05	-7.64	3.05
0.00	66.48	7.07	0.02	0.05		
0.00	66.39	7.08	0.05	0.05		
0.00	64.61	7.14	0.08	0.05		

Table C4: data plotted in Figure 5.9a

Depth [cm bsf]	Acidobacteria [%]	Actinobacteria [%]	Bacterioidetes [%]	Chloroflexi [%]	Cyanobacteria [%]	Desulfobacterota [%]	Firmicutes [%]	Myxococcota [%]
WC	0.00	4.01	0.19	0.02	1.92	0.01	67.79	0.01
0	0.01	33.76	0.06	2.45	14.15	0.37	14.78	0.33
2.5	0.18	4.62	1.30	2.14	1.48	24.37	43.98	0.49
5	0.13	14.93	0.18	1.77	4.25	31.52	23.63	2.25
7.5	0.33	19.72	0.01	1.51	0.09	5.83	13.69	8.86
10	2.43	25.84	0.04	2.09	0.10	1.24	0.91	0.88
12.5	1.04	21.39	2.00	3.26	7.21	1.30	8.42	0.98
15	0.07	7.48	0.01	0.75	0.02	0.66	0.69	0.04
17.5	0.69	25.98	0.01	6.88	0.15	0.30	0.51	0.30
20	0.10	2.52	0.00	0.51	0.00	0.23	0.13	0.01
22.5	1.62	2.57	0.66	3.00	0.02	0.34	6.89	0.04
25	1.95	2.34	0.11	6.85	0.00	0.22	0.10	0.09
27.5	4.24	4.48	0.04	11.51	0.02	3.88	2.67	0.08
30	2.49	2.02	0.53	5.67	0.01	33.81	11.44	0.14
32.5	0.06	0.04	2.66	0.44	0.00	11.85	39.16	0.01
35	0.22	0.32	0.09	1.42	0.00	5.39	3.45	0.00

Nitrospirae [%]	Planctomycetota [%]	Alphaproteobacteria [%]	Gammaproteobacteria [%]	Halomonas [%]	rare taxa [%]	unknown taxa [%]
0.00	0.00	13.85	8.85	0.33	1.38	1.65
0.01	0.00	15.58	1.77	0.56	2.44	13.74
0.03	0.07	4.62	4.14	0.04	6.04	6.50
0.77	0.13	3.78	4.65	0.05	4.71	7.23
18.88	0.35	3.60	7.42	0.02	3.13	16.55
1.20	0.47	2.53	4.08	39.88	5.34	13.00
10.33	0.35	8.46	16.19	0.09	5.39	13.60
8.55	0.23	1.07	1.15	75.56	1.04	2.68
13.42	1.26	6.71	22.91	8.49	2.46	9.93
0.21	0.12	6.98	5.99	81.36	0.40	1.44
2.97	0.25	18.79	17.75	26.51	11.14	7.46
2.31	0.49	26.14	28.69	1.80	16.24	12.67
2.76	0.07	18.68	34.24	4.41	6.87	6.03
10.05	1.59	1.97	4.74	0.62	13.77	11.17
2.65	0.02	1.40	1.86	21.90	5.00	12.94
9.35	0.03	4.14	8.07	51.84	2.56	13.10

Table C5: data plotted in Figure 5.9b

Depth [cm bsf]	Acidobacteria [%]	Actinobacteria [%]	Bacterioidetes [%]	Chloroflexi [%]	Cyanobacteria [%]	Desulfobacterota [%]	Firmicutes [%]	Myxococcota [%]
WC	0.00	18.09	10.48	0.30	0.55	0.07	16.34	0.00
0	0.00	27.45	0.14	8.42	5.69	0.62	3.87	0.58
2.5	0.62	8.01	7.21	6.55	5.02	13.76	11.48	0.76
5	0.24	12.68	1.39	7.67	9.11	21.44	12.40	0.83
7.5	0.27	24.73	0.01	2.86	17.96	0.60	7.00	2.53
10	2.10	36.02	0.03	4.78	8.02	0.22	1.08	1.14
12.5	1.68	37.67	0.07	3.07	6.38	1.11	2.12	1.00
15	0.89	21.82	0.04	3.56	0.20	0.44	2.63	0.22
17.5	4.67	30.47	0.01	6.06	0.38	0.09	2.26	0.56
20	1.91	12.61	0.05	4.39	0.02	0.35	0.90	0.30
22.5	1.39	2.86	0.59	7.80	0.01	0.89	0.06	0.04
25	1.43	4.22	0.10	19.31	0.00	0.33	0.09	0.03
27.5	1.17	12.30	0.18	13.67	0.01	1.40	19.09	0.03
30	0.97	3.27	1.00	9.53	0.01	12.73	40.28	0.13
32.5	0.11	0.23	2.35	1.51	0.00	13.59	53.70	0.01
35	0.07	4.07	1.61	9.30	0.01	1.92	7.55	0.00

Nitrospirae [%]	Planctomycetota [%]	Alphaproteobacteria [%]	Gammaproteobacteria [%]	Halomonas [%]	rare taxa [%]	unknown taxa [%]
0.00	0.04	7.04	18.54	15.25	9.20	4.10
0.00	0.04	34.80	4.66	0.26	5.08	8.38
0.00	0.46	18.96	6.32	0.05	12.44	8.37
0.09	1.06	9.87	7.70	0.02	5.95	9.54
1.31	2.22	7.19	13.04	0.01	5.51	14.74
0.08	2.02	10.02	4.33	2.10	7.54	20.52
0.41	1.67	9.98	5.76	0.07	9.02	19.98
0.60	3.11	3.52	1.25	47.48	4.41	9.84
0.08	4.92	5.73	5.91	1.07	6.74	31.05
0.08	3.99	13.62	3.66	43.17	3.89	11.06
1.86	0.77	10.11	13.71	29.01	9.60	21.31
0.72	0.61	9.31	17.67	2.24	8.37	35.58
0.79	0.97	13.81	13.07	3.17	8.11	12.24
1.50	1.24	4.17	4.69	0.60	9.19	10.72
1.27	0.19	2.76	1.28	4.05	6.72	12.21
4.07	0.42	3.49	5.20	28.69	5.29	28.31

Table C6: data plotted in Figure 5.11

Sample	Depth [cm bsf]	Sr/Ca [mM/m]	Ca/Cl [mM/m]	Mg/Cl [mM/m]
ALD_CC_02	WC	19.2	96.9	3.07
CC_K04_01	2.0	8.7	16.2	102.2
CC_K04_02	4.5	8.7	16.5	102.3
CC_K04_03	7.0	8.8	16.7	101.6
CC_K04_04	10.0	8.9	17.0	100.9
CC_K04_05	13.0	8.7	17.0	99.8
CC_K04_06	16.5	8.8	17.3	98.9
CC_K04_07	20.0	8.7	17.5	98.9
CC_K04_08	23.5	8.8	17.5	99.9
CC_K04_09	27.0	8.7	17.5	99.9
CC_K04_10	30.5	8.7	17.6	99.6

Curriculum Vitae

Dario Fußmann

Date of birth: June 21st, 1990

Place of birth: Trier

Education

- | | |
|--------------|-----------------------------------------------------------------------------------------------------------------------------------------------------------------------------------------------------------------------------------------------------------------------------------------------------------------------------------------------------|
| 2017-present | PhD Geosciences (Georg-August-University Göttingen)
<u>Thesis title:</u> <i>“Microbial alteration of geochemical proxies in fine-grained carbonate sediments during early diagenesis”</i>
<u>Supervisors:</u> Prof. Dr. Gernot Arp, Prof. Dr. Andreas Pack |
| 2013-2016 | MSc Geosciences (University of Bremen)
<u>Overall grade:</u> 1.5 (good)
<u>Thesis title:</u> <i>“Mineral precipitation and fluid compositions in selected alkaline springs of the Wadi Tayin Block, Oman Ophiolite: structural and geochemical controls”</i>
<u>Supervisors:</u> Prof. Dr. Wolfgang Bach, Prof. Dr. Simone Kasemann |
| 2010-2013 | BSc Geosciences (Friedrich-Schiller-University Jena)
<u>Overall grade:</u> 1.8 (good)
<u>Thesis title:</u> <i>“Strukturelle, geochemische sowie mineralogische Untersuchung lakustriner Mikrobialithe des Tangra Yumco Seesystems, Tibetplateau“</i>
<u>Supervisors:</u> Dr. Peter Frenzel, Prof. Dr. Reinhard Gaupp |
| 2009 | Abitur (Gymnasium Konz)
<u>Overall grade:</u> 2.7 (satisfactory) |

Conference contributions

Fußmann, D., von Hoyningen-Huene, A., Schneider, D., Reimer, A., Daniel, R. and Arp, G. (2019): *Early microbial impact on carbonate diagenesis in lagoon sediments on Aldabra, Western Indian Ocean*, GeoMünster, Münster, Germany (**talk**).

Fußmann, D., von Hoyningen-Huene, A., Schneider, D., Reimer, A., Daniel, R. and Arp, G.: (2019): *Early microbial impact on carbonate diagenesis in lagoon sediments on Aldabra, Western Indian Ocean*, Goldschmidt conference, Barcelona, Spain (**poster**).

Fussmann, D., von Hoyningen-Huene, A., Schneider, D., Reimer, A., Arp, G. and Daniel, R. (2018): *Early microbial impact on carbonate diagenesis in lagoon sediments on Aldabra, Western Indian Ocean*, European Geosciences Union General Assembly, Vienna, Austria (**talk**).

Fussmann, D., von Hoyningen-Huene, A., Schneider, D., Reimer, A., Daniel, R., Arp, G. and Meister, P. (2018): *Authigenic carbonate formation in Lake Neusiedl - biotic and abiotic contributions*, GeoBonn, Bonn, Germany (**talk**).

Publications

(*=corresponding author)

Fussmann, D.*, von Hoyningen-Huene, A. J. E., Reimer, A., Schneider, D., Babková, H., Peticzka, R., Maier, A., Arp, G., Daniel, R., and Meister, P.: Authigenic formation of Ca-Mg carbonates in the shallow alkaline Lake Neusiedl, Austria, *Biogeosciences*, 17, 2085-2020, <https://doi.org/10.5194/bg-17-2085-2020>, 2020.

von Hoyningen-Huene, A. J. E., Schneider, D., Fussmann, D., Reimer, A., Arp, G., and Daniel, R.*: Bacterial succession along a sediment porewater gradient at Lake Neusiedl in Austria, *Scientific Data*, 6, 1-7, <https://doi.org/10.1038/s41597-019-0172-9>, 2019.